

University of Alberta

**Phase Behavior and Thermophysical Properties of Athabasca Bitumen
and Athabasca Bitumen + Toluene Mixtures in Near-critical Water**

by

Mohammad Javad Amani

A thesis submitted to the Faculty of Graduate Studies and Research
in partial fulfillment of the requirements for the degree of

Doctor of Philosophy

in

Chemical Engineering

Department of Chemical and Materials Engineering

©Mohammad Javad Amani

Spring 2014

Edmonton, Alberta

Permission is hereby granted to the University of Alberta Libraries to reproduce single copies of this thesis and to lend or sell such copies for private, scholarly or scientific research purposes only. Where the thesis is converted to, or otherwise made available in digital form, the University of Alberta will advise potential users of the thesis of these terms.

The author reserves all other publication and other rights in association with the copyright in the thesis and, except as herein before provided, neither the thesis nor any substantial portion thereof may be printed or otherwise reproduced in any material form whatsoever without the author's prior written permission.

Abstract

The phase behavior and thermophysical properties of heavy hydrocarbons + water at elevated temperatures underpins development and implementation of coordinated production and refining processes, where for example, bitumen is produced by a SAGD method (steam assisted gravity drainage) and the resulting bitumen + water mixtures are then upgraded directly. Supercritical water is an effective solvent for hydrocarbons at high temperatures and reduces coke formation when present during upgrading. In this work, the thermophysical properties and phase behavior of Athabasca bitumen + solvent + water mixtures are investigated and the results are compared to large molecule size hydrocarbons + water binaries available in the literature. Experiments were conducted using a variable-volume X-ray view cell in the broad range of temperature and pressure up to 644 K and 26.2 MPa near the critical point of water. The P-x and PT phase diagrams for pseudo-binaries and pseudo-ternaries of bitumen + solvent + water are constructed and single phase bitumen-rich regions are identified. The solubility of water in the hydrocarbon-rich phase, a key parameter in the design of water-based upgrading reactors, is evaluated to provide a reliable reference for solubility of water in high-molar-mass hydrocarbons. The accuracy of water solubility in the hydrocarbon-rich phase and phase behavior boundaries were validated by reproducing pressure-composition diagrams at fixed temperature and pressure-temperature diagrams for 1-methylnaphthalene + water and toluene + water binaries presented in the literature. Impacts of toluene addition on solubility of water in Athabasca bitumen + water mixtures are described. Furthermore, the

density of bitumen phase and the impact of water solubility on the volume of mixing for the bitumen-rich liquid phase are discussed. A simple and robust model is developed to predict solubility of water in ill-defined hydrocarbons below their upper critical end point. An empirical model is also proposed to extend the solubility data to higher temperatures (> 673 K) where the mixtures are reactive. This body of work including phase diagrams, solubility and density data and models are expected to provide essential data to define promising regimes of temperature, pressure and composition for the application of water in hydrocarbon resource processing.

Acknowledgments

I express my sincere gratitude and appreciation to my advisors, Professor John M. Shaw for providing me with the great opportunity to work in the research area of petroleum thermodynamics, for his deep knowledge, expert guidance, mentorship, huge encouragement and support at all levels.

I thank Professor Murray R. Gray, my co-supervisor, for offering valuable and constructive comments. His unique feedback and suggestion on my research are highly appreciated.

In addition, I am very grateful to Professor Marco Satyro, for his worthy help and patient guidance during my project. I can't say thank you enough to him for his enthusiasm and encouragement.

I thank Professor Arno de Klerk for his helpful discussions and comments.

I take this opportunity to express my gratitude to all of my colleagues in petroleum thermodynamics research group who have been instrumental in the successful completion of this project. I particularly appreciate Keivan Khaleghi for his kind guidance to understand the basics and operation of the X-ray view cell. I am grateful to Mildred Becerra, the lab manager of Petroleum Thermodynamic Research Lab, for providing a safe working environment, assistance and technical support, especially during the two laboratory moves we endured, and equipment, and samples as needed. I appreciate Slava Fedossenکو for his help in laboratory move.

I also thank ; Office Support, Computer Support, Machine Shop, and Instrument Shop staff in the Chemical and Materials Engineering Department at U of A for their help and assistance.

My gratitude goes to my friends; Ali A., Ali Sh., Amin, Ata, Ehsan, Farzad, Hesam, Kasra, Keivan Kh., Keivan N., Milad, Mohtada, Mojtaba, Nafiseh, Nasseh, Nima, Parastoo, Reza, Robert, Roohi, Roya, Sajjad, Saman, Somayeh and all other beloved friends who helped me and create many wonderful times in Edmonton.

My sincere appreciation goes to my mother and father for their unconditional love, care and support. I will never truly be able to express my deepest appreciation to both of you. I love you and owe all my success in life to you forever.

Funding provided by the Centre for Oil Sands Innovation (COSI) and the sponsors of the NSERC Industrial Research Chair in Petroleum Thermodynamics (Natural Sciences and Engineering Research Council of Canada (NSERC), Alberta Innovates Energy and Environment Solutions, British Petroleum, ConocoPhillips Canada, Halliburton Energy Services, KBR Energy and Chemical, Imperial Oil Resources, Nexen Inc., Shell Canada Ltd., Total E&P Canada Ltd., Virtual Materials Group) is gratefully acknowledged.

Contents

CHAPTER 1. INTRODUCTION.....	1
1.1 BACKGROUND AND THESIS OUTLINE	1
1.2 MOTIVATION OF THE RESEARCH	3
1.2.1 <i>Surface bitumen upgrading</i>	3
1.2.2 <i>In-situ bitumen combination SAGD</i>	4
1.3 REVIEW ON OTHER PROCESSES INCLUDING HYDROCARBONS AND WATER AT HIGH TEMPERATURES	5
1.3.1 <i>Supercritical extraction of oil shale and heavy fractions</i>	5
1.3.2 <i>Contaminated soils remediation</i>	6
1.3.3 <i>Oxidation and thermal reaction of hydrocarbons in water</i>	6
1.4 REVIEW ON THERMOPHYSICAL PROPERTIES AND PHASE BEHAVIOR OF HYDROCARBON + WATER MIXTURES	
7	
1.4.1 <i>Phase behavior basics</i>	7
1.4.2 <i>Phase equilibria of water + hydrocarbon mixtures</i>	9
1.4.2.1 Water + n-Alkanes binary mixture data at high pressure and temperature	10
1.4.2.2 Water + aromatics binary mixtures at elevated temperatures and pressures	11
1.4.2.3 Water + heavy oil and multi-component hydrocarbon mixtures	11
1.4.3 <i>Solubility of water in hydrocarbons</i>	12
1.4.4 <i>Volumetric behavior of hydrocarbons + water mixtures</i>	15
1.4.5 <i>Water + hydrocarbons phase behavior modeling</i>	15
1.4.5.1 Application of cubic equations of state to calculate water + hydrocarbon phase equilibria	16
1.4.5.2 Advanced non-cubic equations of state	17
1.4.5.3 Empirical and semi-empirical approach	19
1.5 OBJECTIVES	20
1.6 OVERVIEW OF THE RESEARCH METHODOLOGY	21
1.7 REFERENCES	25
CHAPTER 2. PHASE BEHAVIOR OF ATHABASCA BITUMEN + WATER MIXTURES AT HIGH	
TEMPERATURE AND PRESSURE.....	34
2.1 INTRODUCTION	34
2.2 MATERIALS AND METHODS	36
2.2.1 <i>Experimental apparatus</i>	36
2.2.2 <i>Experimental method validation measurements</i>	39
2.2.2.1 1-Methylnaphthalene + water mixtures.....	39
2.2.2.2 Toluene + water mixtures.....	42

2.2.3	<i>Phase diagram construction</i>	45
2.3	RESULTS AND DISCUSSION	46
2.4	CONCLUSION	58
2.5	REFERENCES	59
CHAPTER 3. VOLUME OF MIXING AND SOLUBILITY OF WATER IN ATHABASCA BITUMEN AT HIGH TEMPERATURE AND PRESSURE.....		63
3.1	INTRODUCTION	63
3.2	EXPERIMENTS AND METHODOLOGY	66
3.2.1	<i>Water solubility measurement validation</i>	67
3.2.2	<i>Liquid density measurement validation</i>	69
3.3	RESULTS AND DISCUSSION	71
3.3.1	<i>Solubility of water in bitumen</i>	71
3.3.2	<i>Excess volume of the Athabasca bitumen-rich liquid phase</i>	79
3.4	CONCLUSION	84
3.5	REFERENCES	84
CHAPTER 4. THE PHASE BEHAVIOR OF ATHABASCA BITUMEN + TOLUENE + WATER TERNARY MIXTURES 91		
4.1	INTRODUCTION	91
4.1.1	<i>Solubility of water in hydrocarbons</i>	92
4.1.2	<i>Phase behavior of hydrocarbon + water mixtures</i>	93
4.2	EXPERIMENTAL SET-UP AND METHODOLOGY	93
4.3	RESULTS AND DISCUSSION	95
4.3.1	<i>Phase Diagrams for Bitumen + Toluene + Water Mixtures</i>	95
4.3.2	<i>Water solubility in bitumen + toluene mixtures at high temperatures</i>	103
4.3.3	<i>Density of water-rich and hydrocarbon-rich liquid phases</i>	105
4.3.4	<i>Density differences between the water-rich and hydrocarbon-rich liquid phases</i>	108
4.3.5	<i>Phase behavior type transition</i>	110
4.4	CONCLUSIONS	114
4.5	REFERENCES	114
CHAPTER 5. CORRELATIONS FOR CALCULATING THE SOLUBILITY OF WATER IN ILL-DEFINED HYDROCARBONS.....		118
5.1	INTRODUCTION	118
5.2	MODEL DEVELOPMENT	121

5.2.1	<i>Model A: solubility of water in hydrocarbons below the UCEP of hydrocarbon + water mixtures</i>	121
5.2.2	<i>Model B: solubility of water in hydrocarbon-rich liquids above the UCEP of hydrocarbon + water mixtures</i>	125
5.3	RESULTS AND DISCUSSION	131
5.3.1	<i>Model A</i>	131
5.3.1.1	<i>Model A Fitting Results</i>	131
5.3.1.2	<i>Model A Testing and Evaluation</i>	133
5.3.1.3	<i>Impact of input parameter uncertainty on predicted water solubility outcomes</i>	141
5.3.2	<i>Model B – Water Solubility in hydrocarbons above the UCEP</i>	143
5.4	CONCLUSION	146
5.5	REFERENCES	146
CHAPTER 6. CONCLUSIONS AND REMARKS		151
6.1	FUTURE WORKS AND RECOMMENDATIONS	154
APPENDIX 1. STANDARD OPERATING PROCEDURES OF THE X-RAY VIEW CELL		155
APPENDIX 2. SUPPLEMENTARY DATA		174
APPENDIX 3. IMAGE PROCESSING CODE IN MATLAB		190

List of Tables

<i>Table 1.1. Available literature data for solubility of water in pure hydrocarbons above 373.2 K...</i>	13
<i>Table 1.2. Solubility of water in reservoir fluids and petroleum fractions.</i>	15
<i>Table 2.1. Properties for Athabasca bitumen [21].....</i>	37
<i>Table 2.2. Experimental phase behavior data for 1-methylnaphthalene + water mixtures at 573 K.</i>	41
<i>Table 2.3. Observed L=V critical points for toluene + water binary mixtures.</i>	43
<i>Table 2.4. LLV three-phase pressure for toluene + water mixtures.....</i>	44
<i>Table 2.5. LLV/LL and L₂V/L phase boundaries for Athabasca bitumen + water mixtures</i>	54
<i>Table 3.1. Water solubility in toluene (wt %).....</i>	69
<i>Table 3.2. Water solubility in 1-methylnaphthalene (wt %).....</i>	69
<i>Table 3.3. Saturated density of liquid 1-methylnaphthalene (kg/m³).....</i>	71
<i>Table 3.4. Solubility of water in the bitumen-rich liquid phase.</i>	78
<i>Table 3.5. Density of Athabasca bitumen</i>	78
<i>Table 3.6. Bitumen-rich phase density and excess specific volume data.....</i>	83
<i>Table 4.1. LLV/LL and L₂V/L₂ boundaries of {(1-w) bitumen + (w) toluene} + water mixtures at a weight fraction of w=0.443.....</i>	100
<i>Table 4.2. LLV/LL and L₂V/L₂ boundaries of {(1-w) bitumen + (w) toluene} + water mixtures at a weight fraction of w=0.668.....</i>	102
<i>Table 4.3. Solubility of water in {(1-w) bitumen + (w) toluene} blends at w=0.443 and 0.668. Water solubility is reported in weight fraction.....</i>	104
<i>Table 4.4. Density of water-saturated toluene.....</i>	107
<i>Table 4.5. Density of water-saturated 1-methylnaphthalene vs. predicted ideal mixing density. .</i>	107
<i>Table 4.6. Density of (1-w) bitumen + (w) toluene at w=0.667 weight fraction.....</i>	112
<i>Table 4.7. Density of water saturated bitumen-rich phase for {(1-w) bitumen + (w) toluene} + water mixtures at w=0.448 and 0.667.....</i>	113
<i>Table 5.1. List of substances and their properties used fit parameters for Model A (equation 5-4)</i>	128
<i>Table 5.2. Parameters for Model A (equation 5-4).....</i>	130
<i>Table 5.3. Overview of Model A performance</i>	130
<i>Table 5.4. Properties of heavy oils used to test Model A, and to obtain coefficients for Model B</i>	143

Table 5.5. Solubility of water in Athabasca bitumen Chapter 3 [35] and experimentally derived K values..... 145

List of Figures

Figure 1.1. Operating conditions for some current bitumen production and upgrading processes. .5	5
Figure 1.2. Characteristics of binary phase behavior by Type according to the van Konynenburg and Scott classification scheme.9	9
Figure 1.3. Types II and III (a and b) binary phase behavior projections. Pure component vapor pressure curves are shown on pressure–temperature (P–T) diagrams by dashed lines, solid lines represent both liquid–gas (LV) and liquid–liquid (LL) critical curves and three-phase lines (LLV lines) are represented by dotted-dashed. Dark circles and open circles stand for pure component critical points and upper critical end points (UCEP) respectively [29]..... 10	10
Figure 1.4. An illustration for X-ray transmission image. 22	22
Figure 1.5. Athabasca bitumen + 49.9% water at 573 K and 8.8 MPa 23	23
Figure 2.1. Schematic pressure-temperature projections for Type II, IIIa and IIIb phase behavior. Pure component vapor pressure curves (), liquid-gas (LV) and liquid-liquid (LL) critical loci (), liquid-liquid vapor lines (), pure component critical points () and critical end points ()..... 35	35
Figure 2.2. X-ray view cell apparatus schematic..... 38	38
Figure 2.3. Vapor phase volume trends adjacent to LV/L and LLV/LL boundaries for 1-methylnaphthalene + water mixtures at 573 K. Data: LLV/LL: 78.9 wt % 1-methylnaphthalene (), LV/L: 78.3 wt % 1-methylnaphthalene () and LV/L: 96.3 wt % 1-methylnaphthalene (). Linear extrapolation of experimental volume data (). Trends computed using the Peng-Robinson equation of state [35] with $K_{ij}=0.26$ ()..... 40	40
Figure 2.4. Pressure-composition diagram for the 1- methylnaphthalene + water binary at 573 K. Phase behavior boundaries identified by Christensen [17] (). Phase behavior and phase behavior boundaries identified in this work: LV data (), LV/L boundary values (), and LLV/LL boundary value ()..... 41	41
Figure 2.5. Typical x-ray images for the toluene (88.4 wt %) + water binary. The vapor phase (V) has a low intensity. The toluene-rich liquid (L_1) has an intermediate intensity (light liquid) and the water rich liquid (L_2) has a low intensity (dense liquid) . The magnetic stirrer (black sphere at the base of the cell) and the bellows (black cylinder at the top of the cell) are visible in some of the images. L_1/L_2 () and L_1/V () interfaces are shown in the images where present..... 43	43
Figure 2.6. Pressure-temperature projection for the toluene + water binary (Type IIIa). The solid curves () are the water and toluene vapor pressures [27]. The solid triangles, Brunner [19], () and the open diamonds, this work, () are points on the L=V critical locus. Solid squares, Brunner	

[19], (), crosses, Anderson [28], (x), open triangles, Chandler [29], () and stars, this work, () are LLV three-phase points..... 45

Figure 2.7. Typical x-ray images for Athabasca bitumen (AB) + water mixtures at 613.5 K. liquid/liquid() and liquid/vapor () interfaces are shown in the images where present..... 46

Figure 2.8. Pressure-temperature diagrams for Athabasca bitumen + water mixtures at fixed Athabasca bitumen wt %: a) 9.2 wt %, b) 55.9 wt %, c) 66.3 wt %, d) 73.3 wt %, e) 78.3 wt %, f) 87.7 wt % wt %, g) 88.7 wt %, h) 96.6 wt %. The water vapor pressure curve is shown in each figure as a dotted curve () terminating at a critical point designated with a solid circle (). Liquid-vapor and liquid-liquid-vapor equilibrium data, are shown as open circles () and open triangles () respectively. Points on LV/L and LLV/LL boundaries are shown as solid squares () and (), and solid curves () trace the LLV/LL and LV/L boundaries. Boundaries designated with a dash-dot lines () are illustrative and were not identified experimentally..... 51

Figure 2.9. Pressure-composition diagrams for Athabasca bitumen + water at fixed temperature: a) 583.2 K, b) 623.2 K, c) 644 K. Measured liquid-vapor () and liquid-liquid-vapor () equilibrium data are shown. The vapor pressure of water obtained from [27]. Solid lines () show the LL/LLV and L₂V/ L₂ boundaries where points on these boundaries are designated with () and (), respectively, and the L₂V/LLV boundary defined by the vapor pressure of water (). Boundaries designated with a dash-dot lines () are illustrative and were not identified experimentally..... 53

Figure 2.10. Schematic pressure-temperature projection and pressure-composition at fixed temperature phase diagrams for the Athabasca bitumen + water pseudo binary mixture. Pure component vapor pressure curves (), liquid-gas (L=V) and liquid-liquid (L=L) critical loci (), liquid-liquid vapor curve (), L=V and L=L critical points () and K-point (). 57

Figure 2.11. Thermal reaction rates for 9.2 () and 66.3 () wt % Athabasca bitumen + water mixtures..... 58

Figure 3.1. Type IIIb pressure-temperature projection for water + hydrocarbon binary mixtures. () critical points for the water and the hydrocarbon, and () the UCEP for the mixture. () and () are the critical locus and LLV three-phase curve respectively and () denotes vapor/bubble pressure curves (Chapter 2)..... 65

Figure 3.2. The X-ray view cell schematic. The view-cell is equipped with a variable volume bellows and a magnetic stirrer. 67

Figure 3.3. P-x diagrams for tetralin + water at 573.2 K: (a) mass-based and (b) mole-based. The experimental data () and the three-phase line () are from Christensen [37] and () is the estimated composition of the saturated tetralin-rich liquid..... 68

Figure 3.4. The solubility of water in: a) toluene (this work (), Anderson et al. [32] (), Brown et al. [24] (), Chandler et al. [31] (), Jou et al. [65] () and Neely et al. [34] (+)) and in b) 1-methylnaphthalene (this work (), Economou et al. [26] (), Christensen et al. [37] (), and compilation of the former data by Shaw et al. [21] ())..... 70

Figure 3.5. Pressure-composition diagrams for Athabasca bitumen + water at fixed temperature: (a) 523.0 K (b) 548.2 K, (c) 573.1 K, (d) 583.2 K, (e) 593.1 K, (f) 603.5 K, (g) 613.4 K, (h) 623.2 K, (i) 633.8 K, (j) 644. Measured liquid-vapor () and liquid-liquid-vapor () equilibrium data are shown. The vapor pressure of water obtained from [59]. Solid lines () show the LL/LLV and L₂V/L₂ boundaries where points on these boundaries are designated with () and (), respectively, and the L₂V/LLV boundary defined by the vapor pressure of water (). Boundaries designated with a dash-dot lines () are illustrative and were not identified experimentally..... 76

Figure 3.6. Solubility of water in Athabasca bitumen, this work (), and in other hydrocarbons: a) all available hydrocarbons; b) high molar mass compounds and heavy oils, and equation 3-1 () . Symbols: toluene () [24, 31, 32], ethylbenzene () [27], m-xylene (+) [32], ethylcyclohexane (-) [27], n-octane () [27], tetralin () [26], 1,2,3,4-Tetrahydroquinoline [33], thianaphthene () [33], cis-decalin () [26], 1-butylcyclohexane () [26], decane () [26], 1-methylnaphthalene () [26], 1-ethylnaphthalene () [26], 1,4-diisopropylbenzene () [26], 9,10-dihydrophenanthrene () [33], naphtha (, Mw = 147) [60], kerosene(x, Mw = 173) [60], lubricating oil (, Mw = 425) [60], gross oil mixtures (, Mw = 425) [63], Coalinga crude oil (, Mw = 439) [61], Huntington Beach crude oil (, Mw = 442) [61], Peace River crude oil (, Mw = 571) [61] Cat Canyon crude oil (, Mw = 627) [61] 77

Figure 3.7. A typical volume of mixing for heavy hydrocarbon + water at temperatures lower than the upper critical end point..... 80

Figure 3.8. Excess volume () for the Athabasca bitumen-rich phase at saturation. The line segments, (-----) represent the excess volumes of unsaturated Athabasca bitumen. Temperature is a parameter..... 81

Figure 3.9. The derivative of excess volume with water mass fraction obtained by analyzing excess volume data for benzene () [46, 47], toluene () [46, 49], ethylbenzene () [46, 49], n-hexane () [50], n-decane () [50], and for Athabasca bitumen () this work..... 82

Figure 4.1. P-x diagrams of {(1-w) bitumen +(w) toluene} + water mixture for w=0.443 wt fraction at 493.1 (a), 513.1 (b), 533.1 (c), 553.1 (d), 573.2 K (e). Measured liquid-vapor () and liquid-liquid-vapor () equilibrium data are shown. The vapor pressure of water () obtained from [32]. Solid lines () show the LLV/LL and L₂V/L₂ boundaries where points on these boundaries are designated with () and (), respectively, and the LLV/L₂V boundary defined by the vapor pressure

of water (). Boundaries designated with a dash-dot lines () are illustrative and were not identified experimentally. Bubble pressure of Athabasca bitumen + 0.448 toluene () is also shown..... 97

Figure 4.2. P-x diagrams of {(1-w) bitumen +(w) toluene} + water mixture for w=0.668 wt fraction at 492.7 (a), 512.8 (b), 532.6 (c), 553.2 (d), 563.2 (e), 573.3 K (f). Measured liquid-vapor () and liquid-liquid-vapor () equilibrium data are shown. The vapor pressure of water () obtained from [32]. Solid lines () show the LLV/LL and L₂V/L₂ boundaries where points on these boundaries are designated with () and (), respectively, and the LLV/L₂V boundary defined by the vapor pressure of water (). Boundaries designated with a dash-dot lines () are illustrative and were not identified experimentally. Bubble pressure of Athabasca bitumen + 0.667 toluene () is also shown..... 99

Figure 4.3. Solubility of water in {(1-w) bitumen +(w) toluene} mixtures for w = 0.0 i.e.: Athabasca bitumen () Chapter 3, w=0.443 () and 0.668 (), this work, and w = 1.0 i.e.: toluene () [14, 16-19]. Computed weight fraction averaged water solubilities in bitumen + toluene mixtures based on smoothed data: w=0.443 () and 0.668 () weight fraction (equation 4-4)..... 104

Figure 4.4. Experimental density of water-saturated toluene at the LLV/LL boundary pressure (). The predicted density of the toluene-rich phase at the LL/LLV boundary pressure is based on water and toluene densities at the LLV/LL boundary pressure, and ideal mixing (equation 4-5) () using smoothed water solubility experimental data [20]. 106

Figure 4.5. Experimental density of water saturated 1-methylnaphthalene at the LLV/LL boundary pressure (). The predicted density of the 1-methylnaphthalene-rich liquid phase is based water density at the LLV/LL boundary pressure and 1 methylnaphthalene at its vapor pressure and ideal mixing equation 4-5 () using smoothed water solubility experimental data [21]..... 106

Figure 4.6. Computed density of saturated {(1-w) bitumen + (w) toluene} mixtures at: w= 0.170 (), 0.448 (), and 0.667 () weight fraction toluene at the LLV/LL boundary pressure (equation 4-5). Densities for Athabasca bitumen () Chapter 3, and water () [32] are shown for completeness. Experimental data for water saturated bitumen + toluene phase at w= 0.448 () and 0.667 () are also shown. 109

Figure 4.7. Approximate density inversion boundary for {(1-w) bitumen +(w) toluene} + water () mixtures at the LLV/LL boundary pressure. 109

Figure 4.8. Experimental density of (1-w) Athabasca bitumen + (w) toluene at w= 0.667 vs temperature (). The predicted density of toluene + bitumen mixtures at the saturation pressure based on ideal mixing (). 110

Figure 4.9. Schematic showing the transition from Type IIIa to Type IIIb phase behavior as the composition of bitumen in the bitumen + toluene + water mixtures increases, from Figure (a) to (c). The LLV curve (), LV and LL critical locus (), the saturation curve of water and hydrocarbons () are shown. The upper critical end point of the mixture is represented by (), while the critical point of water and hydrocarbons are represented by (). 112

Figure 5.1. Solubility of water in pure hydrocarbons and reservoir fluids at temperatures above 373 K. Solubility of water in Athabasca bitumen () Chapter 3 [35], Athabasca bitumen + 0.443 toluene () Chapter 4 [50], Athabasca bitumen + 0.668 toluene () Chapter 4 [50], toluene () [5, 33, 34], ethylbenzene () [6], m-xylene (+) [6], ethylcyclohexane (-) [7], tetralin () [9], thianaphthene () [52], cis-decalin () [9], 1-butylcyclohexane () [9], decane () [9], 1-methylnaphthalene () [10], 1-ethylnaphthalene () [10], 1,4-diisopropylbenzene () [10], 9,10-dihydrophenanthrene () [52], naphtha (, Mw = 147) [47], kerosene(x, Mw = 173) [47], lubricating oil (, Mw = 425) [47], gross oil mixtures (, Mw = 425) [46], Coalinga crude oil (, Mw = 439) [48], Huntington Beach crude oil (, Mw = 442) [48], Peace River crude oil (, Mw = 571) [48] and Cat Canyon crude oil (, Mw = 627) [48]. 122

Figure 5.2. Solubility of water in paraffins (), olefins () and naphthenes () at 293.2 ± 1 K as a function of normal boiling point [1-12]. 123

Figure 5.3. Solubility of water in aromatic hydrocarbons a) as a function of boiling temperature at 293.2 ± 1 K () and 373.2 () and 477.6 (); b) as a function of hydrogen weight fraction 293.2 ± 1 K () and 373.2 () and 473.2 () [1-12]. 125

Figure 5.4. P-x diagrams of Athabasca bitumen + water (a) 623.2 K and (b) 644 K. Measured liquid-vapor () and liquid-liquid-vapor () equilibrium data are shown. The vapor pressure of water obtained from [39]. Solid lines () show the LL/LLV and L_2V/L_2 boundaries where points on these boundaries are designated with () and (), respectively, and the L_2V/LLV boundary defined by the vapor pressure of water (). Boundaries designated with a dash-dot lines () are illustrative and were not identified experimentally (Chapter 3). 127

Figure 5.5. Calculated solubility of water in cyclohexane equation 5-4 (), experimental data [40] () and tentative experimental data [3] (). 132

Figure 5.6. Error dispersion between calculated values for the solubility of water in pure hydrocarbons and Athabasca bitumen Model A (equation 5-4) and experimental data (Table 5.1). The $\pm 30\%$ deviations () are also shown. 133

Figure 5.7. Calculated solubility of water in Athabasca bitumen () using: Model A (training set), () low temperature solubility model (test set) [28], () API recommended model (test set) [32] and experimental data () Chapter 3 [35]. 133

Figure 5.8. Calculated solubility of water in: (a) gasoline G10 - molecular weight 82 g/mole and an average boiling point 58.9 oC () [41, 42], (b) kerosene () and paraffinic oil () [43]. The predicted values using Model A () and a low-temperature NRTL based solubility model () [28] are shown..... 135

Figure 5.9. Solubility of water in hydrocarbons predicted by Model A () and () low temperature solubility model (kerosene) [28] compared to experimental data: (a) naphtha () [47], (b) kerosene () [47], (c) lubricating oil () [47] and (d) fuel mixtures () [46]..... 137

Figure 5.10. Predicted solubility of water in oils using Model A (), fitted NRTL based solubility model () [28], and the corresponding experimental data [48]: (a) Coalinga (), (b) Huntington Beach (), (c) Peace River () and (d) Cat Canyon crude()..... 139

Figure 5.11. Predicted solubility of water in ((1-w) Athabasca bitumen + (w) toluene) + water. Model A: w = 0.668 () and 0.443 (); NRTL based approach: w = 0.668 () and 0.443 () [28, 51]. Experimental data in Chapter 4 w = 0.668 () and 0.443 ()..... 140

Figure 5.12. 10% variation in inputs (a) average normal boiling point and (b) hydrogen weight fraction. Predicted solubility of water in ((1-w) Athabasca bitumen + (w) toluene) + water: w = 0.668 () and 0.443 () Model A, and experimental data in Chapter 4 w = 0.668 () and 0.443 ()..... 142

Figure 5.13. Estimating K for Athabasca bitumen () (evaluated based on equation 5-7 and 5-8) using Model A (equation 5-4) + the NIST water vapor pressure equation () and the LLV/LL phase boundary pressure (), and Model B, equation 5-11 ()..... 145

List of Abbreviations and Symbols

Symbol	Unit	Description
1-MN		1-Methylnaphthalene
AB		Athabasca bitumen
H	<i>MPa/mole fraction</i>	Henry's constant
H_{wt}	<i>wt fraction</i>	Elemental Hydrogen content
K	<i>MPa/wt fraction</i>	Semi-Henry's constant
L		Liquid phase
L_1		Less dense liquid
L_2		More dense liquid
L_2V		More dense liquid-vapor
L_2V/L		Boundary which separates liquid-vapor and liquid regions
LL		Liquid-liquid
LLV		Liquid- Liquid –Vapor
LLV/LV		Boundary which separates LLV and LV regions
LV		Liquid- Vapor
P	<i>MPa</i>	Pressure
PAHs		Polycyclic Aromatic Hydrocarbons
PT		Pressure-Temperature
P-x		Pressure-Composition
RTD		Resistance Temperature Detector
S	<i>wt fraction</i>	Solubility
T	<i>K</i>	Temperature
T_b	<i>°C</i>	Average normal boiling point
V		Vapor
w	<i>wt fraction</i>	Weight fraction composition
X	<i>mole fraction</i>	Mole fraction composition

Chapter 1. Introduction

1.1 Background and thesis outline

Water as a solvent plays a significant role in many industrial processes. Beside the normal properties of water at low temperatures, water presents different and interesting properties in its critical region. The properties of near-critical and supercritical water are used in the design and operation of processes worldwide. Oil extraction, secondary/tertiary oil recovery methods, supercritical extraction, oxidative reactions, municipal and industrial wastes destruction, hydrothermal synthesis and hydrolysis reactions are important instances that involve hydrocarbon + water mixtures at elevated temperatures. One of the possible applications of high temperature water is in heavy oil/bitumen extraction and upgrading. The use of water in bitumen production and upgrading processes may provide a significant advantage over current practice due to the possible elimination of asphaltene precipitation effects.

Asphaltenes, comprising up to 30 wt % of vacuum residues, pose serious problems in oil production, transport and upgrading processes. A detailed understanding of their structure and behavior are essential to control/avoid possible problems particularly in heavy oil and bitumen production and refining processes. Many questions about the nature of bitumen/asphaltene behavior and their characteristics are still unanswered and the economic impact of this uncertainty is significant. Water has the potential to be used as an effective solvent for controlling asphaltene aggregation and reactions. The use of water would modify the current technologies for extraction, upgrading and refining. Having good knowledge of phase equilibria of water + bitumen and heavy oil mixtures near the critical point of water is a first step toward the development of possible process designs.

Understanding and interpretation of the phase behavior of water + hydrocarbon mixtures and evaluation of their thermodynamic properties such as phase composition and density are indispensable inputs for designing and development of processes. Water + hydrocarbons mixtures are highly non-ideal and exhibit complex phase behaviors. Detection and prediction of such complex phase behaviors has received extensive attention since the 1980s. During the past few decades, scholars have determined the phase behavior of water mixtures with numerous low molecular weight hydrocarbons at

temperatures near the critical point of water. However, experimental data for mixtures which include heavy hydrocarbons and industrially relevant mixtures (resids, boiling range cuts, SARA fractions) remain scarce due to difficulties of measuring thermodynamic properties and observing phase boundaries and phase changes at high temperatures and pressures.

The goal of this project is to provide basic and process knowledge related to the potential use of water to enhance the extraction and upgrading of bitumen by improving the quality of the bitumen product. Bitumen (from paraffinic froth treatment) is used as the initial reference material for phase behavior measurements and reaction studies. The phase behavior, thermophysical and transport properties of bitumen + water mixtures and bitumen + solvent + water under extreme conditions are determined in this research.

This thesis is prepared in a mixed format. It comprises a General Introduction (Chapter 1), four chapters addressing specific research topics (Chapters 2-5) presented in a self-contained paper-format, each one including an introduction, a research methodology, results, discussion, conclusions and references, followed by a General Conclusions and Remarks chapter (Chapters 6).

Chapter 1 provides the motivation for the thesis work, an overall introduction to the research topic and a literature review. This is followed by a description of the scope of the research and experimental methodologies used to tackle the research objectives. Chapter 2 explores the phase behavior of Athabasca bitumen + water mixtures. The details of the phase behavior identified in Chapter 2, are elucidated in Chapter 3, where the topics include: the solubility of water in Athabasca bitumen, the density of the bitumen-rich phase, excess volume data. The phase behavior of Athabasca bitumen + water + toluene mixtures is explored in Chapter 4. Models for predicting the solubility of water in the hydrocarbon-rich liquid are described and best practices discussed in Chapter 5. The general conclusions and recommendation are presented in Chapter 6. The appendices comprise supplementary data, computer programming code and an operating procedure for the X-ray view cell.

1.2 Motivation of the research

1.2.1 Surface bitumen upgrading

The use of water as a solvent at high temperature and pressure offers new insights into the phase behavior and aggregation of asphaltenes, and may open new directions for upgrading technology. Water could offer a unique medium for controlling asphaltene aggregation and reactions. Several publications are available that address the effects of near critical or super critical water on heavy hydrocarbon upgrading [1-14]. The role of water in thermal upgrading reaction as chemical agent is still controversial, but all the researchers suggest that using water can provide valuable advantages over current practice.

Watanabe et al. [1] evaluated Canadian oil sand bitumen upgrading in supercritical water at 723 K with a feed comprising 90% maltene and 10% of hexane asphaltenes. density of water were 100 and 200 kg/m³. The reactions were performed for up to 30 minutes under an Ar atmosphere. In order to determine the mechanism of coke formation, Scanning Electron Microscope (SEM) was employed to scan the coke produced. For neat pyrolysis (in the absence of water), the coke formed by agglomeration of smaller coke particles, while the produced coke in the presence of water comprised a porous medium. Watanabe et al. [1] suggested that the coke formed in high-density water cases formed from a liquid phase that can dissolve some of the asphaltenes. They also speculated on the reaction mechanism in water by suggesting that there are two liquid phases and two lighter and heavier fractions for asphaltene. The lighter fraction is dissolved by super critical water and is present at low concentration along with light hydrocarbons. The heavier asphaltene fraction is present at an elevated concentration and undergoes condensation reactions to form coke. Using this framework, they also modified phase separation kinetic (PSK) method to describe the reactions mechanism.

Sato [2] et al. reported on the effects water and supercritical water partial oxidation of asphalt at (673 K) and 20.0 to 37.0 MPa under both air and argon atmospheres. As a negligible amount of coke was formed during their experiments they treated all solids present at the end of an experiment as unreacted asphaltenes. They concluded that increasing temperature resulted in higher conversion of asphalt to gaseous products and heavier components, however large error of measurements may cast doubt on the conclusions. Sulfur tended to escape as H₂S or be converted to toluene insolubles.

Han et al. [3, 4] performed coal-tar pitch upgrading in water in temperature range of 673 to 753 K at 25 to 38 MPa under nitrogen. The residence time for samples was between 1 and 80 minutes. The products of water upgrading and pyrolysis in the absence of water were compared to determine the effect of water. Product yields and asphaltene conversion increase with temperature for all cases and more asphaltenes are converted in water than in nitrogen.

Morimoto et al. [5] investigated impacts of water on bitumen upgrading reactions. They conducted experiments using oil sand, obtained from Steam Assisted Gravity Drainage (SAGD) process, in nitrogen, water and toluene media at 420 to 450 °C and 20 to 30 MPa. According to their reported results of converted distillate fractions in water and nitrogen media, they concluded water doesn't participate as chemical agent in upgrading reactions. They noted dispersion effect by water, results in lower coke formation rather than high-pressure nitrogen medium. Liu and co-workers [6] also confirm the presence of water phase led to more amount of light cracked products and lower coke formation, however they suggest that thermal reactions are dominated by the free radical mechanism.

1.2.2 In-situ bitumen combination SAGD

The SAGD recovery process is one of the preferred production methods for Canadian oil sand reservoirs. The SAGD concept was originally developed by Butler and co-workers [15, 16] and was successfully tested for the first time in Alberta, Canada. The conventional SAGD process consists of two parallel horizontal wells including injector and producer through oil sand reservoir. The injector well normally is located a few meters above the producer well that is placed at the bottom of the bitumen-rich layer to increase the efficiency of production. Steam, in the temperature range of 423 to 543 K, is injected through the injector well into the reservoir to decrease the viscosity of bitumen. Then, the heated mobile bitumen and condensed steam flow down into the producer well by pressure gradient and gravity forces. As water and bitumen are contacted during the SAGD process, the thermophysical properties of bitumen + water at high temperature can be used to predict and development of such processes.

The viscosity of the produced bitumen using SAGD process is too high to easily transport and is either diluted for long distance transport or it is subjected to an upgrading process to improve transport properties. Development of on-site or in-situ upgrading combined

with SAGD, where hot bitumen + water mixtures at high pressures are already present may prove to be a viable solution [5, 8].

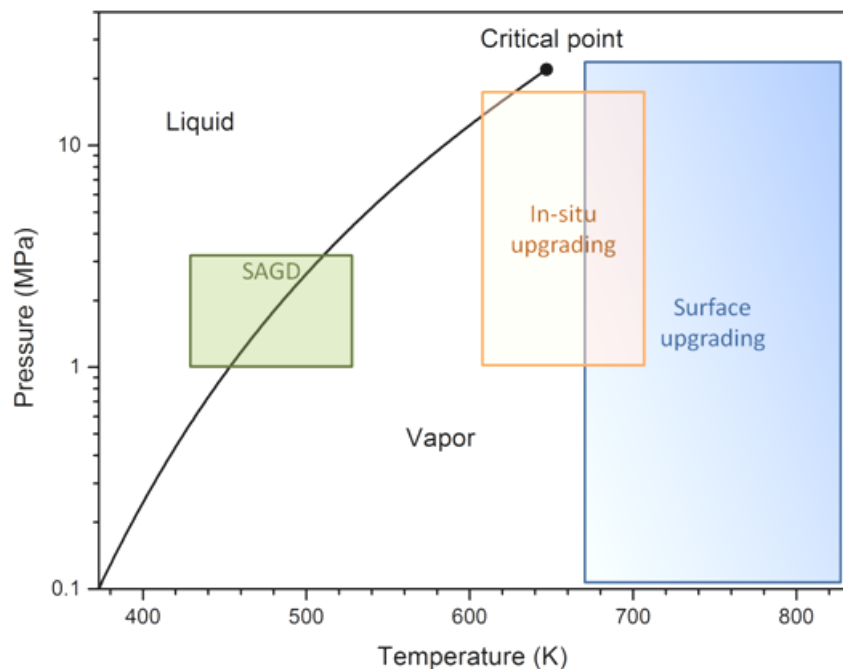


Figure 1.1. Operating conditions for some current bitumen production and upgrading processes.

The preferred operating conditions for the SAGD process, and in-situ and surface upgrading processes are shown in Figure 1.1. The goal of this research is to investigate the phase behavior and properties of bitumen + water mixtures in support of the development of these production and upgrading processes. The experimental results of this research are obtained in the temperature range 523 to 644 K for bitumen + water mixtures and 473 to 573 K for ternary mixtures of bitumen + toluene + water.

1.3 Review on other processes including hydrocarbons and water at high temperatures

Applications can be found where water only acts as a solvent to those where water also participates chemical reaction. This breadth of application is presented in this section.

1.3.1 Supercritical extraction of oil shale and heavy fractions

Oil shale is a fine-grained sedimentary rock that contains oil. Hu et al. [17] investigated exploiting supercritical fluid extraction with water using Huadian oil shale, (Jilin province, China). They conducted several experiments in order to compare supercritical

fluid extraction with water and toluene at 30 MPa and 673 K. Their investigations showed that extraction with water was more effective than with toluene. They Also reported that extraction process pressure influenced the extraction yield and oil composition as well as the extraction rate, and recommended using super critical water for this application over sub critical water. Their results are in agreement with later work available in the literature [18]. A detailed study by El Harfi et al. [19] showed that both the temperature and the extraction process time affect the oil yield and composition. They varied the extraction temperature from 653 to 673 K and observed that the oil yield increased while the fractions of paraffins and aromatics increased and the fractions of asphaltenes decreased. Increasing residence time had a similar impact. Oil yield increased while the amount of asphaltenes and polars decreased.

1.3.2 Contaminated soils remediation

Hawthorne et al. [20] studied the extraction of organic pollutants from soils with subcritical and supercritical water, with a focus on the impact of water polarity variation with temperature on outcomes. They recommended specific temperature ranges in the interval 323 to 673 K for extraction of highly polar organics e.g. chlorophenols to non-polar pollutants e.g. large molecule n-alkanes that exploit the decrease in water polarity with temperature. Knowledge of the solubility of hydrocarbons in water is key to the development of water-based remediation processes.

1.3.3 Oxidation and thermal reaction of hydrocarbons in water

The treatment of industrial waste-water (containing high concentrations of organics) is another application for water at high temperatures. Harmful wastes are destroyed and hydrogen and light hydrocarbons are produced. These processes are based on hydrothermal reactions that occur in supercritical water. For example, Jarana et al. [21] investigated supercritical water gasification, of such wastes in the temperature range of 723 to 823 K at 25 MPa. They investigated the effects of oxidants and catalyst addition, temperature and oxygen concentration on the yields of principal products and noted that not all organics are converted to useful products. Tar and char are also produced.

Brunner [22] published an excellent review on applications of supercritical water oxidation (SCWO). SCWO is an effective method for the destruction of anthropogenic waste materials. As the oxidative reactions are exothermic, they produce the required amount of energy for the reactions. For example, water + 2% (w/w) n-hexane is self-

sustaining without heat addition. However, technical difficulties remain due to the highly corrosive reaction medium, supercritical water, and the precipitation of salt [23-26]. Marrone et al. [25] reviewed the methods of corrosion control in SCWO and gasification processes. They concluded that there is not a single construction material that can handle the effects of all feed types under all conditions, but for a given application, corrosion can be controlled by a combination of material selection, chemistry control, mechanical design and process design.

Hydrothermal and hydrolysis reactions have attracted much attention. Brunner [27] reviewed hydrolysis and hydrothermal reactions in sub-and supercritical water. Water is highly active and can participate in reactions which are generally called “hydrolysis reactions”. Hydrolysis reactions can also be catalyzed by acids including carbon dioxide. Examples include decomposition of glycerol and formaldehyde, degradation of phenanthrene and naphthalene and hydrolysis of diphenylether in near critical and supercritical water.

1.4 Review on Thermophysical Properties and Phase Behavior of Hydrocarbon + Water Mixtures

1.4.1 Phase behavior basics

The study of the phase behavior of binary mixtures deepens the understanding of complicated phase behavior of multi-components in practical engineering processes. The phase behavior of binary mixtures have been classified by van Konynenburg and Scott [28]. Their classification scheme is based on the shape and unique features of critical curves in the P-T projections of each case. Figure 1.2 illustrates the main characteristics of Types of binary phase behavior. The LLV region is represented as a curve on PT phase diagrams due to degree of freedom for the binary mixture. As the number of components increases, the LLV curve expands to an area on PT diagrams.

For type I phase behavior a continuous liquid-vapor critical locus connects the critical point of the light component and the critical point of the heavy component. Type I often occurs for binary mixtures of two chemically similar materials possessing similar critical temperatures and pressures.

For Type II phase behavior, a continuous liquid-vapor critical locus starts from one of the pure component critical point and ends at the other pure component critical point. This aspect of the phase behavior is similar to Type I. Another important feature for Type II, is the presence of an LL immiscible region at low temperature. In this Type of phase behavior, a second critical curve which represents the locus of liquid-liquid critical points is present. This critical curve intersects the three-phase line (LLV line) at low temperature and pressure at a point called an Upper Critical End Point (UCEP).

For binary mixtures with higher immiscibility, Type III can be observed. In contrast to Type II, The critical points of components are not connected with a continuous critical locus. For Type III binaries, the three phase line extends from low temperature and pressure to intersect the liquid-vapor critical locus extended from the critical point of light component. The other liquid-vapor critical locus starts from the critical point of heavy component, and after passing through a minimum pressure, continues to higher pressure and lower temperature.

As shown in Figure 1.2, Type IV phase behavior exhibits LLV behavior at low temperature up to the first UCEP similar to Type II at low temperatures. Above the first UCEP, the components are miscible. As temperature rises further, another immiscible region forms which confines by second UCEP and a Lower Critical End Point (LCEP). The liquid-vapor critical point locus originating from the critical point of the light component joins the second LLV line at LCEP, while the other liquid-vapor critical point locus (extended from heavy component) intersects the LLV line at the second UCEP.

In Type V phase behavior, the components are miscible at low temperature, but the mixture behaves similar to Type IV at the high temperature. Type V retains high temperature LLV line including the UCEP and LCEP from Type IV phase behavior.

Type VI phase behavior is rare in nature. Similar to Type I, a continuous liquid-vapor critical point locus connects the critical points of the pure components. In addition to this behavior, a small immiscible region limited to UCEP and LCEP is observed at lower temperatures. A continuous liquid-liquid critical curve starts from LCEP and ends at UCEP.

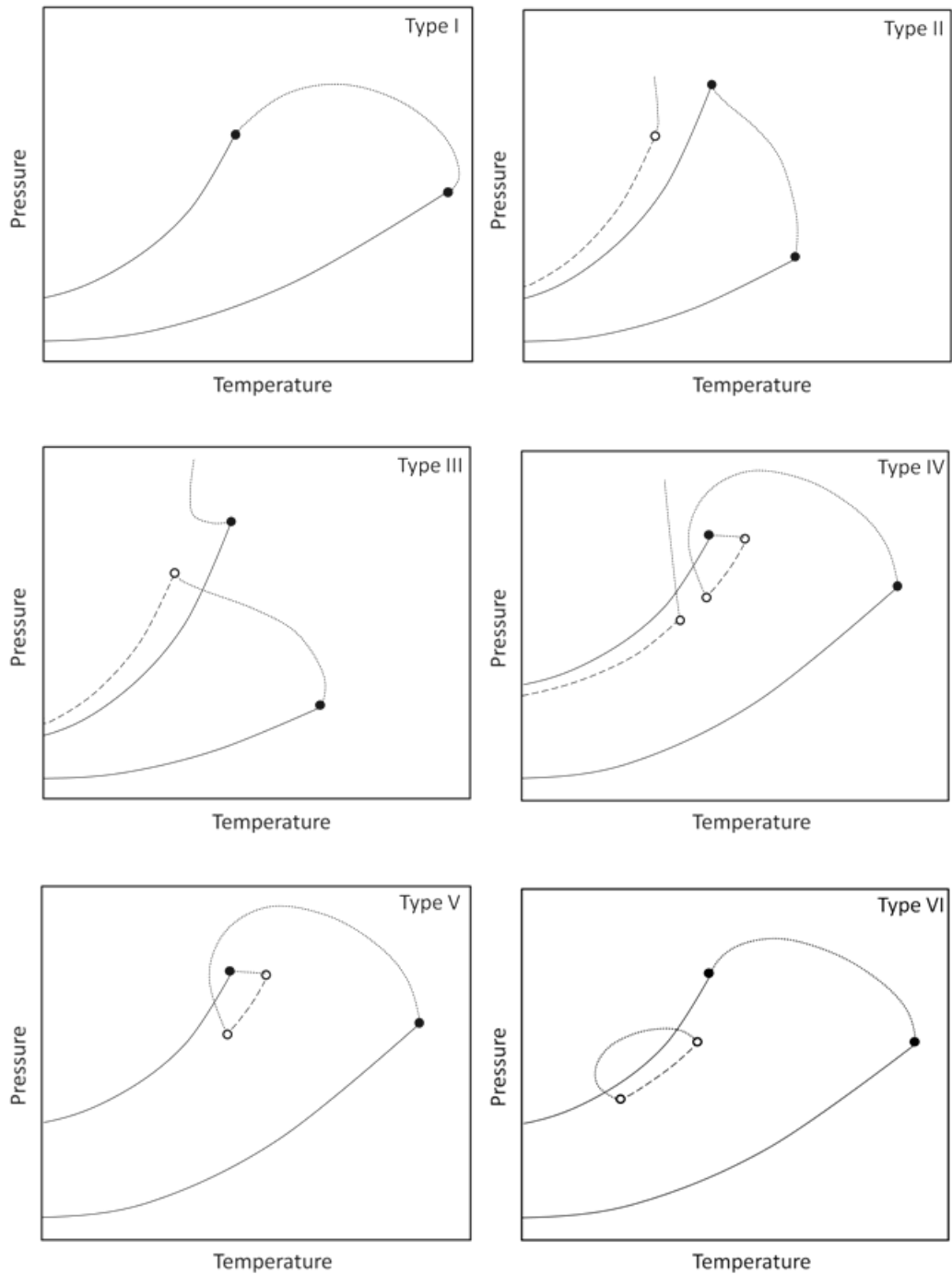


Figure 1.2. Characteristics of binary phase behavior by Type according to the van Konynenburg and Scott classification scheme.

1.4.2 Phase equilibria of water + hydrocarbon mixtures

Based on van Konynenburg and Scott classification, the observed phase behavior Types for water + hydrocarbon binary mixtures are Type II or III. Type III phase behavior has two important sub categories Type IIIa and Type IIIb [29]. However both types are

frequently referred to as Type III in the literature. The main difference between Type IIIa and IIIb is whether the three-phase line that extends from low temperature and pressure intersects the liquid-vapor critical locus close to the water critical point or the hydrocarbon critical point. Type IIIa corresponds to a wide variety of water + hydrocarbon binary mixtures where the molar mass of the hydrocarbon is low such as the lower n-alkanes [30] and aromatics with lower critical points than that of water [29]. Type IIIb corresponds to cases where the critical temperature of the hydrocarbon is greater than that of water, e.g.: n-C₁₈ [30]. A few water + aromatics mixtures where the critical temperature of the aromatic is greater than the critical temperature of water exhibit Type II phase behavior. Examples include 1-methyl-naphthalene and tetralin [31], and naphthalene and biphenyl [29].

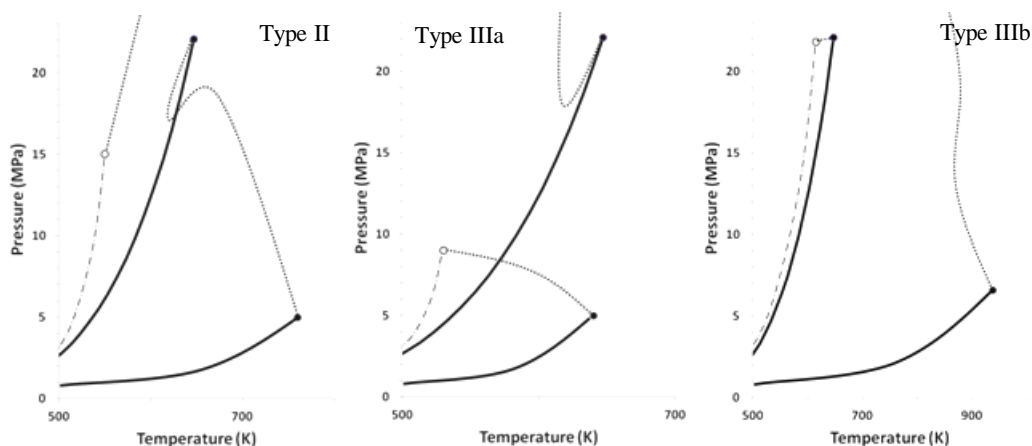


Figure 1.3. Types II and III (a and b) binary phase behavior projections. Pure component vapor pressure curves are shown on pressure–temperature (P–T) diagrams by dashed lines, solid lines represent both liquid–gas (LV) and liquid–liquid (LL) critical curves and three-phase lines (LLV lines) are represented by dotted-dashed. Dark circles and open circles stand for pure component critical points and upper critical end points (UCEP) respectively [29].

1.4.2.1 Water + n-Alkanes binary mixture data at high pressure and temperature

De Loos and co-workers [32-34] obtained high temperature and pressure phase equilibria for water + propane [32], n-hexane [33], n-pentane and n-heptane [34]. The water+ n-decane binary was investigated by Wang et al. [35], who suggested that water + n-decane mixtures are Type III. Phase equilibrium data for water + n-butane and n-hexane were reported by Yiling et al. [36]. A continuous-flow apparatus was used by Stevenson et al.

[37] to measure equilibrium compositions and critical points for water + sequalane and dodecane mixtures in a range 600 to 660 K. It was found that both binary mixtures show Type IIIa phase behavior. Brunner's research [30] in the field of phase behavior detection of water + n-alkanes mixtures are very valuable. Brunner employed an optical view cell to investigate phase behavior of mixtures over a broad range of temperatures and pressures. Binary mixtures of water and n-alkanes with carbon numbers less than 26 ($< C_{26}$) exhibit Type IIIa phase behavior. Critical points of C_{26} + n-alkanes exceed that of water and they exhibit Type IIIb phase behavior. For low carbon number n-alkanes, L_2V is confined by an UCEP and the critical point of hydrocarbon. As the carbon number on n-alkanes rises, the surrounded region by $LLV + L_2V$ and UCEP move towards $LL+L_1V$ critical curve and touch this curve. The point that LLV , L_2V , L_1V and LL meet each other simultaneously is referred as three-critical end point (TCEP). As the carbon number increases further, L_2V and LL establish a continuous curve and leave TCEP.

1.4.2.2 Water + aromatics binary mixtures at elevated temperatures and pressures

Brunner also investigated the phase equilibria and critical phenomena for water + 26 aromatic and alkyl aromatic binary mixtures [29]. Water + alkyl-substituted benzenes and decalin exhibit Type IIIa phase behavior while water + polycyclic aromatic hydrocarbons (PAHs) with up to 4 rings exhibit Type II phase behavior. Water + indene exhibits Type IIIb phase behavior. Transitions among phase behavior types arise for "families" of aromatic compounds. Phase behavior type for binaries with water is dependent on the specific critical temperature, molecular size, and structure of the hydrocarbon.

Phase equilibrium measurements for water + tetralin and 1-methylnaphthalene, up to the critical temperatures of the mixtures, are available [31]. These mixtures exhibit Type II phase behavior. Rabezki [38] et al. reports PVTx properties of water + toluene mixtures, along with Krichevskii parameter, partial molar volume and molar volume values. Furutaka et al. [39] report water compositions and densities of hydrocarbon-rich phases at equilibrium for water + toluene and ethylbenzene mixtures.

1.4.2.3 Water + heavy oil and multi-component hydrocarbon mixtures

There are few papers reporting experimental data near the critical point of water for mixtures of water with multi-component hydrocarbons or heavy oil. Brunner et al. [40]

investigated the phase equilibrium of ternary mixtures of water, toluene, n-hexane and n-hexadecane at 573 K. At this condition, well below the critical temperature of water, liquid-liquid phase behavior was observed as one would expect. Shimoyama [41] and co-workers studied of water + hexane + hexadecane, water + toluene + decane, and water + toluene + ethylbenzene ternary mixtures at 500 to 573 K and only observed LL phase behavior as expected. Rasulov et al. [42] measured PVT_x properties for ternaries with specific compositions of water, n-propanol and n-hexane in the temperature range 309.3 to 678.8 K. They reported liquid–liquid and liquid–vapor phase equilibrium curves.

Brunner [29] also studied phase equilibria of ternary mixtures of water + decalin + tetralin at elevated temperatures. In the experiments, the ratio of decalin to tetralin was a constant value. The results are for ternary mixtures of water + ((decalin (x) + tetralin (1-x)) at x = 1 (a), 0.5 (b), 0.25 (c) and 0.0 (d). As the mole fraction of decalin decreases, the phase behavior of the mixture undergoes a transition from Type III to Type II. Binary mixtures of decalin + water exhibit Type III phase behavior (x = 1). Between x = 0.25 and x = 0 the phase behavior transitions to Type II. The point of these illustrations is to show that the phase behavior of show ternary mixtures can interpreted from the perspective of binary mixture equilibrium data.

Other researchers investigated upgrading of heavy hydrocarbons by SCW, but they only reported final compositions and effects of different parameters on oil yield and did not report phase behavior data for their mixtures systematically. For example, Watanabe et al. [1], note that water and heavy hydrocarbons are not miscible, but they have not published phase diagrams.

1.4.3 Solubility of water in hydrocarbons

Experimental measurements for mutual solubility of hydrocarbons and water are very challenging both at room temperature where the solubilities are low and at high temperature and pressure due to the extreme conditions. Accurate and reliable data on hydrocarbons and water solubility are essential to develop a robust thermodynamic model to predict phase equilibria for such complex mixtures. Many Authors have investigated the mutual solubility of pure hydrocarbons + water over a broad range of temperatures. Maczynski et al. [43-47] and Shaw et al. [48-54] have provided extensive and critically evaluated mutual solubility data in the literature based on reviews up to 2006. The data are compiled in a consistent way and the works provide mutual solubility data as a

function of temperature for different types of pure hydrocarbons from C₅ to C₃₆. The elaboration of experimental data and measurement technique for all these solubility data is beyond the scope of this thesis. As water solubility in the hydrocarbon-rich phase is the focus here, only water solubility data in pure hydrocarbons at temperatures above 373.2 K are presented in Table 1.1:

Table 1.1. Available literature data for solubility of water in pure hydrocarbons above 373.2 K.

Component name	Formula	Mw	T min.(K)	T max.(K)	References
Benzene	C ₆ H ₆	78.11	276.2	523.2	Anderson et al. [55] Burd et al. [56] Tsonopoulos et al. [57] Thompson et al. [58] Chandler [59]
Cyclohexane	C ₆ H ₁₂	84.16	283.2	473.2	Tsonopoulos et al. [57] Burd et al. [56] Plenkina et al. [60]
Hexane	C ₆ H ₁₄	86.17	273.2	477.6	Tsonopoulos et al. [57] Burd et al. [56]
Toluene	C ₇ H ₈	93.14	273.2	548.2	Anderson et al. [55] Brown et al. [61] Chandler et al. [59] Jou et al. [62] Neely et al. [63]
eEthylbenzene	C ₈ H ₁₀	106.17	273.2	568.1	Chen et al. [64] Guseva et al. [65] Heidman et al. [66]
M-xylene	C ₈ H ₁₀	106.17	273.2	473.4	Anderson et al. [55]
m-Cresol	C ₇ H ₈ O	108.14	293.5	412.1	Leet et al. [67]
Ethylcyclohexane	C ₈ H ₁₆	112.21	310.9	561.4	Heidman et al. [66]
1-octene	C ₈ H ₁₆	112.21	310.9	549.8	Economou et al. [68]
n-octane	C ₈ H ₁₈	114.23	273.2	550.4	Heidman et al. [66] Miller et al. [69] Price et al. [70]
Indoline	C ₈ H ₉ N	119.16	293.5	490.3	Leet et al. [67]
Quinoline	C ₉ H ₇ N	129.16	293.5	498.2	Leet et al. [67]
1,2,3,4-	C ₁₀ H ₁₂	132.20	424.7	595.9	Economou et al. [68]

tetrahydronaphthalene					Christensen et al. [31]
1,2,3,4-Tetrahydroquinoline	$C_9H_{11}N$	133.19	293.5	501.6	Leet et al. [67]
Thianaphthene	C_8H_6S	134.20	332.2	490.5	Leet et al. [67]
1,3-diethylbenzene	$C_{10}H_{14}$	134.22	310.9	582.5	Economou et al. [68]
Cis-decalin	$C_{10}H_{18}$	138.25	374.1	599.1	Economou et al. [68]
Butylcyclohexane	$C_{10}H_{20}$	140.27	310.9	584.3	Economou et al. [68]
1-decene	$C_{10}H_{20}$	140.27	374.2	475.2	Economou et al. [68]
Decane	$C_{10}H_{22}$	142.28	298.2	576.2	Economou et al. [68]
					Namiot et al. [71]
1-methylnaphthalene	$C_{11}H_{10}$	142.20	273.2	589.4	Christensen et al. [31] Economou et al. [68]
1-ethylnaphthalene	$C_{12}H_{12}$	156.22	366.5	594.4	Economou et al. [68]
1,4-diisopropylbenzene	$C_{12}H_{18}$	162.27	310.9	590.0	Economou et al. [68]
9,10-Dihydrophenanthrene	$C_{14}H_{12}$	180.25	333.7	493.8	Leet et al. [67]

Mutual solubility data for water + heavy petroleum products is scarce in the open literature, even though there is a significant demand for them. Table 1.2 presents published water solubility in reservoir fluids and petroleum fractions.

Pedersen et al. [72] studied the mutual solubility of water and a light reservoir fluid at 308.2, 373.2 and 473.2 K. Water concentration was measured by solvent extraction from the oil phase, followed by gas chromatography analysis. Nelson [73] reported solubility of water in oil products such as gasoline, jet fuels, kerosenes and oils with average molecular weight of 425. He clearly noted that these data are approximate, but the method of measurement was not mentioned. Griswold et al. [74] used the cloud point measurement method to determine the solubility of water in naphtha, kerosene and lubricating oil. In another study, Glandt et al. [75] investigated the impact of water solubility on four crude oils at elevated temperature. They used Karl Fischer titration to determine water content in the oil-rich phase.

Table 1.2. Solubility of water in reservoir fluids and petroleum fractions.

Petroleum fraction	Mw	T min. (K)	T max. (K)	Reference
Gas condensate mixture	35	308.2	473.2	Pedersen et. al. [72]
Naphtha	147	432.2	495.2	Griswold et al. [74]
Kerosene	173	385.2	537.2	Griswold et al. [74]
Lubricating oil	425	397.2	554.2	Griswold et al. [74]
Gross oil mixtures	425	443.2	554.2	Nelson [73]
Coalinga crude oil	439	450.6	557.0	Glandt et al. [75]
Huntington Beach crude oil	442	413.3	560.3	Glandt et al. [75]
Peace River crude oil	571	450.6	556.0	Glandt et al. [75]
Cat Canyon crude oil	627	432.5	561.3	Glandt et al. [75]

1.4.4 Volumetric behavior of hydrocarbons + water mixtures

Kamilov et al. [76] measured C_p and PVT properties of water + n-hexane binary mixtures. Abdulagatov and co-workers [77-79] conducted experiments to measure PVTx properties of water + n-heptane, n-octane, benzene and dilute solutions of n-hexane. Haruki et al. [80] investigated the phase behavior of water + decane/toluene binary mixtures near the critical point of water and evaluated the application of a modified Soave Redlich-Kwong (MSRK) equation of state to calculate PVTx properties. Tian et al. [81] studied the phase behavior of water + iso-butane and n-butane in great detail and evaluated the excess molar volumes and excess molar Gibbs free energies for water + n-butane mixtures. Rasulov and co-workers [82-84] studied the PVT properties and phase equilibria for binary mixtures of water + n-hexane and n-heptane using a constant-volume piezometer and provided a relationship between pressure and temperature at constant density and composition. These studies show that the expected behavior is for the water-rich and hydrocarbon-rich phases to possess positive volumes of mixing over broad ranges of conditions.

1.4.5 Water + hydrocarbons phase behavior modeling

Phase behavior prediction for water + hydrocarbon mixture presents numerous challenges that appear linked to the variability of water properties, the extreme variability of phase compositions with temperature and pressure and the impact of minor differences in hydrocarbon molecular structure on phase behavior outcomes. Another big challenge is for mixtures containing water + bitumen/heavy oil is that bitumen and heavy oil are not

well-defined mixtures. Defining heavy oils is challenging due to the large number of different molecules present in their fractions. Previous efforts [85, 86] in our research group suggest that the group contribution theory, which is proven to be an appropriate method to estimate critical properties of heavy components, can improve the quality of phase behavior calculations. However, the unknown and complicated molecular structure of bitumen, and a lack of reliable experimental phase behavior data make the development of a general thermodynamic model unlikely.

The identity of chemical potentials, or equivalently fugacities, of molecular species in all co-existing phases is the key relation in phase equilibrium calculations:

$$\mu_{i,\text{water}} = \mu_{i,\text{hydrocarbon}} = \mu_{i,\text{vapor}} = \dots \quad (1-1)$$

or:

$$f_{i,\text{water}} = f_{i,\text{hydrocarbon}} = f_{i,\text{vapor}} = \dots \quad (1-2)$$

both sets of equations can be calculated using equations of state or activity coefficient models.

1.4.5.1 Application of cubic equations of state to calculate water + hydrocarbon phase equilibria

Cubic equations of state are the most common thermodynamic models in the petroleum industry because of their simplicity and accuracy. Their application to water + hydrocarbon mixtures has been less successful.

Early on Kabadi et al. [87] suggested modifying mixing rules for water + hydrocarbon mixtures using the Soave-Redlich-Kwong equation of state. They suggested an asymmetric mixing rule that is a function of composition. Michel and co-workers [88] investigated the application of cubic equations of state in calculations of mutual solubilities of water and hydrocarbons. They stated that conventional mixing rules for cubic equation did not lead to reliable results for engineering calculations. Daridon et al. [89] developed a model for water + n-alkanes with a modified binary interaction parameter in terms of composition and reduced temperature. Eubank et al. [90] suggested a correlation for K_{ij} , used with the Peng-Robinson equation, which considers both temperature and carbon number impacts to predicts the solubility of water in n-alkanes. Soreide et al. [91] and Dhima et al. [92] used two sets of binary interaction parameters for

aqueous and non-aqueous phases. They also proposed a composition-based for $\alpha(T_r)$ in the Peng-Robinson equation to consider impacts of salts in the aqueous phase. Huraki and co-workers [80, 93] proposed an exponent-type mixing rule for the energy parameter in SRK equation. They adjusted the binary parameters to give precise fits to the experimental data. None of these approaches has proven to be generalizable.

Huron and Vidal [94] developed a combinatorial model of equation of state and Gibbs excess model to predict phase equilibria of polar components at high pressures. This model used the standard mixing rule for co-volume parameter, but the mixing rule of the energy parameter was based on an activity coefficient model e.g. NRTL. Tsonopoulos et al. [95] studied the application of the Huron–Vidal mixing rule with the PR EOS on the 1-hexene + water mixture. They stated that the Huron–Vidal mixing rule led to much better results compared to conventional van der Waals mixing rules. Li et al. [96] coupled a modified Huron–Vidal mixing rule with the UNIFAC method to predict solubility and phase equilibria for light hydrocarbon + water mixtures.

1.4.5.2 Advanced non-cubic equations of state

With the recent evolution in thermodynamic models, a large number of authors consider taking into account the self-associating character of water. As these models are generally complicated, and are not superior in their prediction of properties of mixtures containing water over the cubic equations, they have not displaced them for chemical engineering calculations.

Kiselev et al. [97] performed measurements and simulations to obtain phase and thermodynamic properties of dilute mixtures of water + toluene. A crossover Helmholtz free-energy model was applied to simulate a dilute aqueous toluene solution at a fixed mole fraction of toluene ($x = 0.0287$). The results are valid over narrow ranges of temperatures and densities but can be applied to a wider range by extrapolation. Abdulagatov et al. [98] studied the thermodynamic properties of dilute aqueous n-hexane solutions at high temperatures using the same crossover equation of state.

Errington et al. [99] attempted to use molecular simulation to predict water + methane and water + ethane phase equilibria at temperatures up to the water critical point and over a broad range of pressures. They reported Henry's constants for hydrocarbons in water

(dilute conditions), but failed to predict phase diagrams using molecular simulation or an equation of state for associating fluids.

Neichel et al. [100] investigated a perturbation type equation of state to calculate critical curves for water + n-alkanes near the critical point of water. They used repulsion and attraction terms in their equation that are based on the square-well potential model. They obtained promising results but did not present critical loci or other phenomena for a full range of compositions. Other researchers [95, 101] suggested including association effects due to hydrogen bonding in hydrocarbon + water mixtures.

As cubic equations of state do not correlate phase equilibria for mixtures containing highly polar and associating compounds, Kontogeorgis and co-workers [102] coupled the SRK EOS with an association term, similar to that of SAFT. More generally, in order to consider the effects of hydrogen bonding and intermolecular associating forces, and also to retain the simplicity of the model, the association term is added to classical cubic equations of state e.g. PR and SRK. Applications of Cubic plus Association (CPA) models for complex mixtures comprising polar/associating components like water, alcohols, glycols and organic acid are widely studied by Kontogeorgis et al. [103-106]. Yan et al. [107] successfully applied the CPA model to mixtures of reservoir fluids + water. Their correlations were combined with other petroleum characterization methods.

Voutsas et al. [108] used both CPA and the statistical associating fluid theory (SAFT) to predict the phase equilibrium of mixtures of pure hydrocarbons + water. The SAFT model did not offer an advantage over CPA in the examined cases. Aparicio-Martinez and Hall [109] compared four equations of state in the modeling of the phase behavior of water + N₂, + CO₂ and + n-alkane binaries. The CPA with Soave-Redlich-Kwong (SRK) and Peng-Robinson (PR), SAFT and the perturbed-chain SAFT (PC-SAFT) equations of state were evaluated. They compared calculated values with the available experimental data at low and high temperatures to show the accuracy of the models. They indicated that the predicted results are in good qualitative agreement with the experimental data but the results are not quantitative in general. The correctness of global phase diagrams and n-alkane mole fraction at 298.1 K were their target variables.

1.4.5.3 Empirical and semi-empirical approach

In the absence of a general modeling approach for predicting the phase behavior and phase compositions of hydrocarbon + water mixtures even with well defined binary mixtures, a few authors have tried to develop simple empirical expressions to describe thermophysical properties of these mixtures e.g. mutual solubilities for well-defined and ill-defined hydrocarbons alike. These expressions correlate the mixture properties with temperature and a molecular feature of hydrocarbons. Tsionopoulos et al. [57, 66, 68] has been active in this area.

From classical thermodynamics, the solubility of a solute is related to heat of solution:

$$\partial \ln(x_i) / \partial T \cong \frac{\Delta h_i^{\text{sol}}}{RT^2} \quad (1-3)$$

where x_i is the mole fraction of component i , and Δh_i^{sol} is given by:

$$\Delta h_i^{\text{sol}} = \bar{h}_i - h_i \quad (1-4)$$

\bar{h}_i and h_i are the enthalpy of component (i) in the solution and as a pure liquid. Assuming Δh_i^{sol} is a linear function of temperature, the equation above can be integrated to obtain:

$$\ln(x_i) = A + BT + C \ln(T) \quad (1-5)$$

where A,B and C are fitting parameters determined from experimental data. Tsionopoulos et al. [57, 66, 68] showed that equation (1-5) fits the solubility data of hydrocarbons in water. In order to correlate water solubility in hydrocarbons, they reasoned that the heat of solution for water in hydrocarbons near the upper critical end point goes to infinity:

$$\lim_{T \rightarrow T_{\text{UCEP}}} \frac{\partial \ln(x_w)}{\partial T} \cong \lim_{T \rightarrow T_{\text{UCEP}}} \frac{\Delta h_i^{\text{sol}}}{RT^2} \rightarrow \infty \quad (1-6)$$

and proposed an empirical expression that reproduces this behavior:

$$\ln(x_w) = A + B\left(\frac{1}{T_r} - 1\right) + C(1 - T_r)^{\frac{1}{3}} + D(1 - T_r) \quad (1-7)$$

Tsionopoulos [110, 111], correlated mutual solubilities and heats of solution for normal alkanes, normal alkylcyclohexanes, linear 1-alkenes, and normal alkylbenzenes + water near room temperature and found that the solubility of water in a hydrocarbon-rich phase

is a function of the carbon number (CN) for each hydrocarbon family at room temperature:

$$\ln(x_w) = \frac{A+B.CN}{C+CN} \quad (1-8)$$

The fitting parameters A, B, C for each family are reported [110].

Neely et al. [63] used the empirical equation to represent the solubility of water in benzene, toluene, and 3-methylpentane :

$$\ln(x_w) = A + B.\ln(T_{r,w}) \quad (1-9)$$

where $T_{r,w}$ is defined as absolute temperature over the critical temperature of water.

Ruelle et al. [112, 113] studied general predictive expressions to estimate the mutual solubility of hydrocarbons + water at room temperature. They used molar volume of the hydrocarbon as a variable parameter in these equations. They also confirm the solubility of water in hydrocarbons is much less dependent on the hydrocarbon size comparing with that of hydrocarbon in water. Amovilli and co-workers [114] combined a mobile order theory with the polarizable continuum model to predict solubility of water in hydrocarbons at 293 K. Yaws [115-117] also developed a general empirical model to estimate mutual solubility as a function of temperature.

1.5 Objectives

The phase behavior of water + bitumen/heavy hydrocarbon + low molar mass hydrocarbon mixtures is complex and variable. Consequently, the thermophysical properties and phase compositions are uncertain. For example, from the literature review, if water + bitumen/ heavy hydrocarbon mixtures are treated as pseudo binary mixtures, the phase behavior Type may be Type II or IIIb. As water + low molar mass hydrocarbon binary mixtures may exhibit Type II or Type IIIa phase behavior and bitumen/heavy oil + low molar mass hydrocarbon pseudo binary mixtures may exhibit Type I or Type III phase behavior, transitions in phase behavior type must occur in pseudo ternary phase diagrams including water, bitumen/heavy oil, and low molar mass hydrocarbons. Providing greater clarity concerning the properties and nature of this phase space through an illustrative example is a key theoretical and conceptual goal of this thesis.

From a quantitative perspective, the main objective of this work is to probe the thermophysical properties of bitumen + solvent + water so that the basic and process knowledge related to the extraction and upgrading of oil sands bitumen relative to current practice is improved. Questions such as do water + hydrocarbon mixtures exhibit single-phase behavior and if so under what conditions, and how does the aggregation of asphaltenes vary with the nature of the phase behavior and mass fraction of water in single-phase regions are either addressed or recommended for follow up study.

The following specific objectives are foci of interest:

- Construct the phase diagrams of Athabasca bitumen + water in the form of pressure-temperature and pressure-composition phase diagram and projections
- Identify single phase regions for water + bitumen/heavy oil mixtures at elevated temperatures
- Measure solubility of water in bitumen-rich liquid phase and the excess volume of bitumen-rich liquid
- Investigate impacts of solvent addition on the phase behavior and properties of bitumen + solvent + water
- Develop an efficient and accurate thermodynamic model to predict thermophysical properties of ill-defined heavy hydrocarbons + water mixtures
- Provide a reliable basis to extrapolate properties of interest to upgrading reaction conditions where experimental measurements are not possible in practice

1.6 Overview of the Research methodology

Experimental and procedural details related to specific topics are addressed in Chapters 2-4. In this section an overview of the experimental approach is provided. Observation and quantification of phase behaviors and phase compositions is nontrivial given the opacity of the phases to visible light.

Athabasca bitumen, obtained from Syncrude is the base material for the phase behavior and related studies reported in this work. This material, derived from mined bitumen, was subjected to warm water extraction plus naphtha dilution, and naphtha recovery by distillation at 523-623 K.

Since heavy hydrocarbons/bitumen and asphaltenes are opaque to visible light, their phase behavior cannot be observed using conventional phase detection methods and a specialized X-ray transmission tomography method, developed by our research group is used to observe the phase behavior of mixtures containing heavy hydrocarbons.

The principles of the X-ray transmission tomography technique and the experimental set-up can be found elsewhere (Abedi et al. 1999). In brief, the apparatus consists of a variable-volume beryllium view cell that is transparent to X-rays. The intensity of the transmitted X-ray beam, after passing through the cell walls and the sample, depends on the density and composition of phases present. The number of phases and their corresponding volumes, densities and compositions can be obtained through careful calibration, over a broad range of temperatures and pressures as illustrated in 1.4, using an image of a CO₂ + Maya crude sample at 60 °C and 8.27 MPa. Liquid-liquid-vapor phase behavior is readily observed.

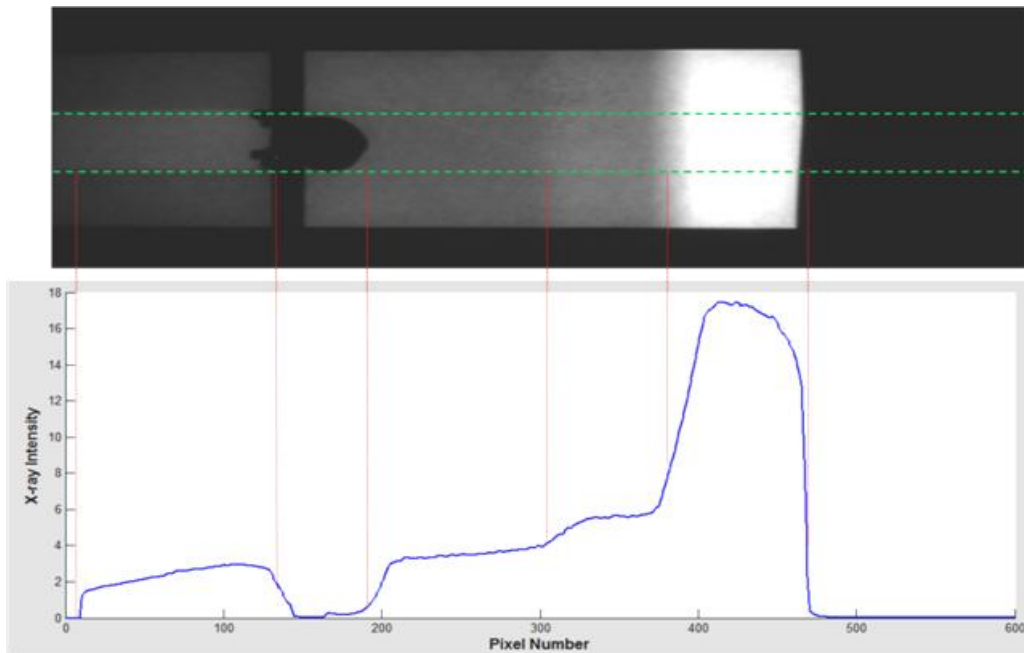


Figure 1.4. An illustration for X-ray transmission image.

Phase diagrams for Athabasca bitumen + water and Athabasca bitumen + toluene + water will be constructed using the synthetic method. This comprises systematic measurement of the phase behavior of mixtures with fixed composition over a broad range of temperatures and pressures. In each experiment, fixed amounts of water, low molar mass hydrocarbon, and bitumen are injected into the view-cell and phase volumes and densities

are recorded at set pressures and temperatures. Pressure-temperature diagrams at fixed compositions, pressure-temperature projections and pressure-composition phase diagrams at fixed temperature are then constructed as composites from experimental results obtained from ten or more trials [118]. Figure 1.5 presents a single X-ray image for Athabasca bitumen + 49.9% water at 573 K and 8.8 MPa. Based on such X-ray images, the number of phases, the density and volumes of each phase at specified experimental conditions can be determined. Systematic analysis of a series of images at different temperatures and pressures makes it possible to plot phase boundaries such as LL/LLV, LV/L or LV critical curves and to detect the phase behavior type of mixtures. Since only limited number of conditions can be probed, it is only possible to construct parts of phase diagrams with a focus on the pressure, temperature and composition ranges of greatest interest.

In addition to phase diagrams, phase volumes and phase densities and phase compositions are determined by detailed processing of images such as those shown in Figures 1.4 and 1.5, and from interpretation of the intersections of phase behavior boundaries in composite phase diagrams, e.g.: saturated water content in hydrocarbon-rich phases is determined from the intersection of the single phase liquid region with the two phase liquid region.

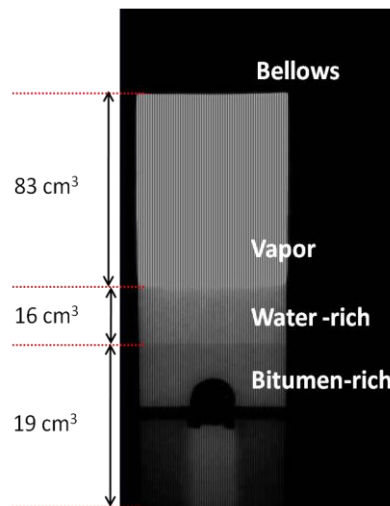


Figure 1.5. Athabasca bitumen + 49.9% water at 573 K and 8.8 MPa

Density and excess volume for bitumen-rich phase are evaluated based on two approaches: mass balance and measurements of bitumen phase volumes and X-ray intensity difference between water and hydrocarbons-rich liquid phases.

In the later case, calibration of x-ray intensity and the intensity difference between the water-rich and hydrocarbon-rich phases provides individual phase densities and information regarding the relative density of the two phases. From basic theory, the intensity of an x-ray beam transmitted through a layer of material with thickness x and density ρ is expressed as:

$$I = I_0 \exp(-\mu\rho x) \quad (1-10)$$

where I_0 is the initial X-ray intensity of the beam, and μ is the element specific mass attenuation coefficient. Mass attenuation coefficients for elements as a function of photon energy (keV) are available at NIST [120] and the mass attenuation coefficients for compounds or mixtures are obtained by summing element contributions:

$$\mu = \sum_i w_i \mu_i \quad (1-11)$$

where w_i is the weight fraction of the atomic constituents of a compound.

The X-ray intensity difference between the water-rich and hydrocarbon-rich phases can be related to the density difference between coexisted phases. As the thickness of materials and the initial X-ray intensity are the same for both phases, the relation between transmitted X-ray intensity and density of phases at fixed elevation can be expressed as:

$$\alpha \ln \left(\frac{I_{hc}}{I_w} \right) = -\mu_w \rho_w + \mu_{hc} \rho_{hc} \quad (1-12)$$

subscripts w and hc represent water and hydrocarbon-rich phase respectively. The coefficient α , a machine constant, known from the apparatus geometry and from calibration using a single-phase fluid, is needed because the distance from the point x-ray source to the detector varies with elevation within the cell. To improve the precision of the water-saturated hydrocarbon phase density measurements, the water-rich phase comprising essentially only water is used as an internal reference and the impact of water content on the X-ray attenuation coefficient of hydrocarbon-rich phase, a secondary effect, is captured with equation 1-11. The water content in the hydrocarbon-rich phase is obtained from experimental data whether in the current work, or from the literature. As water density is a precisely known function of temperature and pressure, and the mass attenuation coefficients are known accurately, the error of the hydrocarbon-rich liquid phase density measurements is small.

1.7 References

- [1] M. Watanabe, S.-n. Kato, S. Ishizeki, H. Inomata, and R. L. Smith Jr, "Heavy oil upgrading in the presence of high density water: Basic study," *The Journal of Supercritical Fluids*, vol. 53, pp. 48-52, 2010.
- [2] T. Sato, T. Adschiri, K. Arai, G. L. Rempel, and F. T. T. Ng, "Upgrading of asphalt with and without partial oxidation in supercritical water," *Fuel*, vol. 82, pp. 1231-1239, Jul 2003.
- [3] L.-n. Han, R. Zhang, and J.-c. Bi, "Upgrading of coal-tar pitch in supercritical water," *Journal of Fuel Chemistry and Technology*, vol. 36, pp. 1-5, 2008.
- [4] L. N. Han, R. Zhang, and J. C. Bi, "Experimental investigation of high-temperature coal tar upgrading in supercritical water," *Fuel Processing Technology*, vol. 90, pp. 292-300, Feb 2009.
- [5] M. Morimoto, Y. Sugimoto, Y. Saotome, S. Sato, and T. Takanohashi, "Effect of supercritical water on upgrading reaction of oil sand bitumen," *The Journal of Supercritical Fluids*, vol. 55, pp. 223-231, 2010.
- [6] Y. Liu, F. Bai, C. C. Zhu, P. Q. Yuan, Z. M. Cheng, and W. K. Yuan, "Upgrading of residual oil in sub- and supercritical water: An experimental study," *Fuel Processing Technology*, vol. 106, pp. 281-288, Feb 2013.
- [7] S. Kokubo, K. Nishida, A. Hayashi, H. Takahashi, O. Yokota, and S. Inage, "Effective Demetalization and Suppression of Coke Formation Using Supercritical Water Technology for Heavy Oil Upgrading," *Journal of the Japan Petroleum Institute*, vol. 51, pp. 309-314, Sep 2008.
- [8] H. Kamimura, S. Takahashi, A. Kishita, H. ChengXie, and H. Enomoto, "Upgrading of bitumen with supercritical water for a system combined with sagd," *Abstracts of Papers of the American Chemical Society*, vol. 216, pp. U879-U879, Aug 1998.
- [9] Z. M. Cheng, Y. Ding, L. Q. Zhao, P. Q. Yuan, and W. K. Yuan, "Effects of Supercritical Water in Vacuum Residue Upgrading," *Energy & Fuels*, vol. 23, pp. 3178-3183, May-Jun 2009.
- [10] W. Wahyudiono, T. Shiraishi, M. Sasaki, and M. Goto, "Bitumen upgrading under solvothermal/hydrothermal conditions," *Research on Chemical Intermediates*, vol. 37, pp. 375-381, 2011.
- [11] T. Adschiri, "Supercritical water up-grading of heavy oils," *Nihon Enerugi Gakkaishi/Journal of the Japan Institute of Energy*, vol. 88, pp. 172-175, 2009.
- [12] C. Xu and J. Donald, "Upgrading peat to gas and liquid fuels in supercritical water with catalysts," *Fuel*, vol. In Press, Corrected Proof.
- [13] B. M. Vogelaar, M. Makkee, and J. A. Moulijn, "Applicability of supercritical water as a reaction medium for desulfurisation and demetallisation of gasoil," *Fuel Processing Technology*, vol. 61, pp. 265-277, 1999.
- [14] S. C. Pasppek, "upgrading heavy hydrocarbons with supercritical water and light olefins," USA Patent, 1984.
- [15] R. M. Butler, G. S. McNab, and H. Y. Lo, "THEORETICAL-STUDIES ON THE GRAVITY DRAINAGE OF HEAVY OIL DURING INSITU STEAM HEATING," *Canadian Journal of Chemical Engineering*, vol. 59, pp. 455-460, 1981.
- [16] R. M. Butler and D. J. Stephens, "THE GRAVITY DRAINAGE OF STEAM-HEATED HEAVY OIL TO PARALLEL HORIZONTAL WELLS," *Journal of Canadian Petroleum Technology*, vol. 20, pp. 90-96, 1981.

- [17] H. Hu, J. Zhang, S. Guo, and G. Chen, "Extraction of Huadian oil shale with water in sub- and supercritical states," *Fuel*, vol. 78, pp. 645-651, 1999.
- [18] J. Yanik, M. Yüksel, M. Saglam, N. Olukçu, K. Bartle, and B. Frere, "Characterization of the oil fractions of shale oil obtained by pyrolysis and supercritical water extraction," *Fuel*, vol. 74, pp. 46-50, 1995.
- [19] K. El Harfi, C. Bennouna, A. Mokhlisse, M. Ben Chanaa, L. Lemee, J. Joffre, et al., "Supercritical fluid extraction of Moroccan (Timahdit) oil shale with water," *Journal of Analytical and Applied Pyrolysis*, vol. 50, pp. 163-174, 1999.
- [20] S. B. Hawthorne, Y. Yang, and D. J. Miller, "Extraction of organic pollutants from environmental solids with sub- and supercritical water," *Analytical Chemistry*, vol. 66, pp. 2912-2920, 1994.
- [21] M. B. García Jarana, J. Sánchez-Oneto, J. R. Portela, E. Nebot Sanz, and E. J. Martínez de la Ossa, "Supercritical water gasification of industrial organic wastes," *The Journal of Supercritical Fluids*, vol. 46, pp. 329-334, 2008.
- [22] G. Brunner, "Near and supercritical water. Part II: Oxidative processes," *The Journal of Supercritical Fluids*, vol. 47, pp. 382-390, 2009.
- [23] M. Schubert, J. W. Regler, and F. Vogel, "Continuous salt precipitation and separation from supercritical water. Part 2. Type 2 salts and mixtures of two salts," *The Journal of Supercritical Fluids*, vol. In Press, Corrected Proof.
- [24] M. Schubert, J. W. Regler, and F. Vogel, "Continuous salt precipitation and separation from supercritical water. Part 1: Type 1 salts," *The Journal of Supercritical Fluids*, vol. In Press, Corrected Proof.
- [25] P. A. Marrone and G. T. Hong, "Corrosion control methods in supercritical water oxidation and gasification processes," *The Journal of Supercritical Fluids*, vol. 51, pp. 83-103, 2009.
- [26] P. Kritzer, "Corrosion in high-temperature and supercritical water and aqueous solutions: a review," *The Journal of Supercritical Fluids*, vol. 29, pp. 1-29, 2004.
- [27] G. Brunner, "Near critical and supercritical water. Part I. Hydrolytic and hydrothermal processes," *The Journal of Supercritical Fluids*, vol. 47, pp. 373-381, 2009.
- [28] P. H. Vankonynenburg and R. L. Scott, "Critical Lines and Phase-Equilibria in Binary Vanderwaals Mixtures," *Philosophical Transactions of the Royal Society of London Series a-Mathematical Physical and Engineering Sciences*, vol. 298, pp. 495-540, 1980.
- [29] E. Brunner, M. C. Thies, and G. M. Schneider, "Fluid mixtures at high pressures: Phase behavior and critical phenomena for binary mixtures of water with aromatic hydrocarbons," *The Journal of Supercritical Fluids*, vol. 39, pp. 160-173, 2006.
- [30] E. Brunner, "Fluid mixtures at high pressures IX. Phase separation and critical phenomena in 23 (n-alkane + water) mixtures," *The Journal of Chemical Thermodynamics*, vol. 22, pp. 335-353, 1990.
- [31] S. P. Christensen and M. E. Paulaitis, "Phase equilibria for tetralin-water and 1-methylnaphthalene-water mixtures at elevated temperatures and pressures," *Fluid Phase Equilibria*, vol. 71, pp. 63-83, 1992.
- [32] T. W. De Loos, A. J. M. Wijen, and G. A. M. Diepen, "Phase equilibria and critical phenomena in fluid (propane + water) at high pressures and temperatures," *The Journal of Chemical Thermodynamics*, vol. 12, pp. 193-204, 1980.
- [33] T. W. De Loos, W. G. Penders, and R. N. Lichtenthaler, "Phase equilibria and critical phenomena in fluid (n-hexane + water) at high pressures and

- temperatures," *The Journal of Chemical Thermodynamics*, vol. 14, pp. 83-91, 1982.
- [34] T. W. De Loos, J. H. van Dorp, and R. N. Lichtenthaler, "Phase equilibria and critical phenomena in fluid (n-alkane + water) systems at high pressures and temperatures," *Fluid Phase Equilibria*, vol. 10, pp. 279-287, 1983.
- [35] Q. Wang and K.-C. Chao, "vapor-liquid and liquid-liquid equilibria and critical states of water + n-decane mixtures," *Fluid Phase Equilibria*, vol. 59, pp. 207-215, 1990.
- [36] T. Yiling, T. Michelberger, and E. U. Franck, "High-pressure phase equilibria and critical curves of (water + n-butane) and (water + n-hexane) at temperatures to 700 K and pressures to 300 MPa," *The Journal of Chemical Thermodynamics*, vol. 23, pp. 105-112, 1991.
- [37] R. L. Stevenson, D. S. LaBracio, T. A. Beaton, and M. C. Thies, "Fluid Phase Equilibria and critical phenomena for the dodecane-water and squalane-water systems at elevated temperatures and pressures," *Fluid Phase Equilibria*, vol. 93, pp. 317-336, 1994.
- [38] M. G. Rabezkii, A. R. Bazaev, I. M. Abdulagatov, J. W. Magee, and E. A. Bazaev, "PVTx measurements for water + toluene mixtures in the near-critical and supercritical regions," *Journal of Chemical and Engineering Data*, vol. 46, pp. 1610-1618, 2001.
- [39] S. Furutaka and S. Ikawa, "Volume expansion behavior of water-hydrocarbon mixtures at high temperatures and pressures as studied by infrared spectroscopy," *Fluid Phase Equilibria*, vol. 217, pp. 181-188, Mar 2004.
- [40] G. Brunner, A. Steffen, and R. Dohrn, "high-pressure liquid-liquid equilibria in ternary-systems containing water, benzene, toluene, n-hexane and n-hexadecane," *Fluid Phase Equilibria*, vol. 82, pp. 165-172, Feb 1993.
- [41] Y. Shimoyama, M. Haruki, Y. Iwai, and Y. Arai, "Measurement and prediction of liquid-liquid equilibria for water + hexane + hexadecane, water + toluene + decane, and water + toluene + ethylbenzene ternary systems at high temperatures and pressures," *Journal of Chemical and Engineering Data*, vol. 47, pp. 1232-1236, 2002.
- [42] S. M. Rasulov and A. R. Rasulov, "Phase equilibrium and PVT-properties of 0.7223H₂O+0.1242 n-C₆H₁₄+0.1535 n-C₃H₇OH ternary system," *High Temperature*, vol. 43, pp. 45-50, Jan-Feb 2005.
- [43] A. Maczynski, D. G. Shaw, M. Goral, B. Wisniewska-Gocłowska, A. Skrzecz, Z. Maczynska, et al., "IUPAC-NIST solubility data series. 81. Hydrocarbons with water and seawater - Revised and updated part 1. C-5 hydrocarbons with water," *Journal of Physical and Chemical Reference Data*, vol. 34, pp. 441-476, Jun 2005.
- [44] A. Maczynski, D. G. Shaw, M. Goral, B. Wisniewska-Gocłowska, A. Skrzecz, I. Owczarek, et al., "IUPAC-NIST solubility data series. 81. Hydrocarbons with water and seawater - Revised and updated. Part 2. Benzene with water and heavy water," *Journal of Physical and Chemical Reference Data*, vol. 34, pp. 477-552, Jun 2005.
- [45] A. Maczynski, D. G. Shaw, M. Goral, B. Wisniewska-Gocłowska, A. Skrzecz, I. Owczarek, et al., "IUPAC-NIST solubility data series. 81. Hydrocarbons with water and seawater - Revised and updated. Part 3. C₆H₈-C₆H₁₂ hydrocarbons with water and heavy water," *Journal of Physical and Chemical Reference Data*, vol. 34, pp. 657-708, Jun 2005.
- [46] A. Maczynski, D. G. Shaw, M. Goral, B. Wisniewska-Gocłowska, A. Skrzecz, I. Owczarek, et al., "IUPAC-NIST solubility data series. 81. Hydrocarbons with

- water and seawater-revised and updated. Part 4. C₆H₁₄ hydrocarbons with water," *Journal of Physical and Chemical Reference Data*, vol. 34, pp. 709-753, Jun 2005.
- [47] A. Maczynski, D. G. Shaw, M. Goral, B. Wisniewska-Gocłowska, A. Skrzecz, I. Owczarek, et al., "IUPAC-NIST Solubility Data Series. 81. Hydrocarbons with water and seawater-revised and updated. Part 5. C-7 hydrocarbons with water and heavy water," *Journal of Physical and Chemical Reference Data*, vol. 34, pp. 1399-1487, 2005.
- [48] D. G. Shaw, A. Maczynski, M. Goral, B. Wisniewska-Gocłowska, A. Skrzecz, I. Owczarek, et al., "IUPAC-NIST Solubility Data Series. 81. Hydrocarbons with water and seawater-revised and updated. Part 6. C₈H₈-C₈H₁₀ hydrocarbons with water," *Journal of Physical and Chemical Reference Data*, vol. 34, pp. 1489-1553, 2005.
- [49] D. G. Shaw, A. Maczynski, M. Goral, B. Wisniewska-Gocłowska, A. Skrzecz, L. Owczarek, et al., "IUPAC-NIST solubility data series. 81. Hydrocarbons with water and seawater revised and updated. Part 7. C₈H₁₂-C₈H₁₈ hydrocarbons with water," *Journal of Physical and Chemical Reference Data*, vol. 34, pp. 2261-2298, Dec 2005.
- [50] D. G. Shaw, A. Maczynski, M. Goral, B. Wisniewska-Gocłowska, A. Skrzecz, I. Owczarek, et al., "IUPAC-NIST solubility data series. 81. Hydrocarbons with water and seawater - Revised and updated. Part 8. C-9 hydrocarbons with water," *Journal of Physical and Chemical Reference Data*, vol. 34, pp. 2299-2345, Dec 2005.
- [51] D. G. Shaw, A. Maczynski, M. Goral, B. Wisniewska-Gocłowska, A. Skrzecz, I. Owczarek, et al., "IUPAC-NIST solubility data series. 81. Hydrocarbons with water and seawater-revised and updated. Part 9. C-10 hydrocarbons with water," *Journal of Physical and Chemical Reference Data*, vol. 35, pp. 93-151, Mar 2006.
- [52] D. G. Shaw, A. Maczynski, M. Goral, B. Wisniewska-Gocłowska, A. Skrzecz, I. Owczarek, et al., "IUPAC-NIST solubility data series. 81. Hydrocarbons with water and seawater-revised and updated. Part 10. C-11 and C-12 hydrocarbons with water," *Journal of Physical and Chemical Reference Data*, vol. 35, pp. 153-203, Mar 2006.
- [53] D. G. Shaw, A. Maczynski, M. Goral, B. Wisniewska-Gocłowska, A. Skrzecz, I. Owczarek, et al., "IUPAC-NIST solubility data series. 81. Hydrocarbons with water and seawater-revised and updated. Part 11. C-13-C-36 hydrocarbons with water," *Journal of Physical and Chemical Reference Data*, vol. 35, pp. 687-784, Jun 2006.
- [54] D. G. Shaw, A. Maczynski, G. T. Hefter, M. Kleinschmidt, D. Mackay, P. A. Meyers, et al., "IUPAC-NIST solubility data series. 81. Hydrocarbons with water and seawater-revised and updated part 12. C-5-C-26 hydrocarbons with seawater," *Journal of Physical and Chemical Reference Data*, vol. 35, pp. 785-838, Jun 2006.
- [55] F. E. Anderson and J. M. Prausnitz, "Mutual solubilities and vapor-pressures for binary and ternary aqueous systems containing benzene, toluene, meta-xylene, thiophene and pyridine in the region 100-200-degrees-c," *Fluid Phase Equilibria*, vol. 32, pp. 63-76, Dec 1986.
- [56] S. D. Burd, J. Braun, and W. G. Braun, vol. 48, ed: *Proc. Am. Pet. Inst., Div. Refin.*, 1968, p. 464.
- [57] C. Tsonopoulos and G. M. Wilson, "high-temperature mutual solubilities of hydrocarbons and water .1. benzene, cyclohexane and normal-hexane," *Aiche Journal*, vol. 29, pp. 990-999, 1983.

- [58] W. H. Thompson and J. R. Snyder, "Mutual Solubilities of Benzene and Water. Equilibria in the Two Phase Liquid - Liquid Region," *Journal of Chemical & Engineering Data*, vol. 9, pp. 516-520, 1964/10/01 1964.
- [59] K. Chandler, B. Eason, C. L. Liotta, and C. A. Eckert, "Phase equilibria for binary aqueous systems from a near-critical water reaction apparatus," *Industrial & Engineering Chemistry Research*, vol. 37, pp. 3515-3518, Aug 1998.
- [60] R. M. Plenkina, G. D. Efremova, and Pryaniko.Ro, "CRITICAL PHENOMENA IN CYCLOHEXANE-AMMONIA SYSTEM," *Zhurnal Fizicheskoi Khimii*, vol. 46, pp. 271-&, 1972.
- [61] J. S. Brown, J. P. Hallett, D. Bush, and C. A. Eckert, "Liquid-liquid equilibria for binary mixtures of water plus acetophenone, plus 1-octanol, plus anisole, and plus toluene from 370 K to 550 K," *Journal of Chemical and Engineering Data*, vol. 45, pp. 846-850, Sep-Oct 2000.
- [62] F. Y. Jou and A. E. Mather, "Liquid-liquid equilibria for binary mixtures of water plus benzene, water plus toluene, and water plus p-xylene from 273 K to 458 K," *Journal of Chemical and Engineering Data*, vol. 48, pp. 750-752, May-Jun 2003.
- [63] B. J. Neely, J. Wagner, R. L. Robinson, and K. A. M. Gasem, "Mutual solubility measurements of hydrocarbon-water systems containing benzene, toluene, and 3-methylpentane," *Journal of Chemical and Engineering Data*, vol. 53, pp. 165-174, Jan 2008.
- [64] H. P. Chen and J. Wagner, "mutual solubilities of alkylbenzene plus water-systems at temperatures from 303 to 373-k - ethylbenzene, p-xylene, 1,3,5-trimethylbenzene and butylbenzene," *Journal of Chemical and Engineering Data*, vol. 39, pp. 679-684, Oct 1994.
- [65] A. N. Guseva and E. I. Parnov, "isothermal sections of the binary systems monocyclic arenes-water at 25-degrees, 100-degrees and 200-degrees-c," *Zhurnal Fizicheskoi Khimii*, vol. 38, pp. 805-806, 1964.
- [66] J. L. Heidman, C. Tsonopoulos, C. J. Brady, and G. M. Wilson, "High-temperature mutual solubilities of hydrocarbons and water .2. Ethylbenzene, ethylcyclohexane, and normal-octane," *Aiche Journal*, vol. 31, pp. 376-384, 1985.
- [67] W. A. Leet, H. M. Lin, and K. C. Chao, "Mutual solubilities in 6 binary-mixtures of water + a heavy hydrocarbon or a derivative," *Journal of Chemical and Engineering Data*, vol. 32, pp. 37-40, Jan 1987.
- [68] I. G. Economou, J. L. Heidman, C. Tsonopoulos, and G. M. Wilson, "Mutual solubilities of hydrocarbons and water .3. 1-hexene, 1-octene, C-10-C-12 hydrocarbons," *Aiche Journal*, vol. 43, pp. 535-546, Feb 1997.
- [69] D. J. Miller and S. B. Hawthorne, "Solubility of liquid organics of environmental interest in subcritical (hot/liquid) water from 298 K to 473 K," *Journal of Chemical and Engineering Data*, vol. 45, pp. 78-81, Jan-Feb 2000.
- [70] L. C. Price, "Aqueous solubility of petroleum as applied to its origin and primary migration," *AAPG Bulletin*, vol. 60, pp. 213-244, 1976.
- [71] A. Y. Namiot, V. G. Skripka, G. F. Gubkina, and O. A. Boksha, "utilization of 2-parametric equations of state for a description of phase behavior of mixtures of water and nonpolar substances," *Zhurnal Fizicheskoi Khimii*, vol. 50, pp. 854-858, 1976.
- [72] K. S. Pedersen, J. Milter, and C. P. Rasmussen, "Mutual solubility of water and a reservoir fluid at high temperatures and pressures: Experimental and simulated data," *Fluid Phase Equilibria*, vol. 189, pp. 85-97, 2001.
- [73] W. L. Nelson, "Solubility of water in oil," *oil & gas journal*, p. 140, April 1956.

- [74] J. Griswold and J. E. Kasch, "Hydrocarbon-water Solubilities at elevated temperatures and pressures," *Industrial and Engineering Chemistry*, vol. 34, pp. 804-806, 1942.
- [75] C. A. Glandt and W. G. Chapman, "Effect of water dissolution on oil viscosity," *Spe Reservoir Engineering*, vol. 10, pp. 59-64, Feb 1995.
- [76] I. K. Kamilov, L. V. Malysheva, A. R. Rasulov, K. A. Shakbanov, and G. V. Stepanov, "The experimental investigation of $C_{v,x}$, P , V , T properties and the equation of state of the n-hexane-water system," *Fluid Phase Equilibria*, vol. 125, pp. 177-184, 1996.
- [77] I. M. Abdulagatov, A. R. Bazaev, R. K. Gasanov, E. A. Bazaev, and A. E. Ramazanova, "Measurement of the PVT_x properties of n-heptane in supercritical water," *The Journal of Supercritical Fluids*, vol. 10, pp. 149-173, 1997.
- [78] I. M. Abdulagatov, A. R. Bazaev, E. A. Bazaev, M. B. Saidakhmedova, and A. E. Ramazanova, "PVT_x measurements and partial molar volumes for water-hydrocarbon mixtures in the near-critical and supercritical conditions," *Fluid Phase Equilibria*, vol. 150-151, pp. 537-547, 1998.
- [79] I. M. Abdulagatov, E. A. Bazaev, A. R. Bazev, and M. G. Rabezki, "PVT_x measurements for dilute water+n-hexane mixtures in the near-critical and supercritical regions," *The Journal of Supercritical Fluids*, vol. 19, pp. 219-237, 2001.
- [80] M. Haruki, Y. Iwai, S. Nagao, Y. Yahiro, and Y. Arai, "Measurement and correlation of phase equilibria for water + hydrocarbon systems near the critical temperature and pressure of water," *Industrial and Engineering Chemistry Research*, vol. 39, pp. 4516-4520, 2000.
- [81] Y. Tian, X. Zhao, L. Chen, H. Zhu, and H. Fu, "High pressure phase equilibria and critical phenomena of water + iso-butane and water + n-butane systems to 695 K and 306 MPa," *The Journal of Supercritical Fluids*, vol. 30, pp. 145-153, 2004.
- [82] S. M. Rasulov and I. A. Isaev, "Phase equilibrium of a water-n-hexane system in the region of lower locus of critical points," *Teplofizika Vysokikh Temperatur*, vol. 40, pp. 344-347, 2002.
- [83] S. M. Rasulov and I. A. Isaev, "Phase equilibrium and critical lines in n-pentane + water and n-hexane + water systems," *High Temperature*, vol. 44, pp. 838-842, 2006.
- [84] S. M. Rasulov and A. R. Rasulov, "The pVT properties and phase equilibria in the n-pentane-water binary system," *Russian Journal of Physical Chemistry A*, vol. 83, pp. 756-759, 2009.
- [85] N. Saber and J. M. Shaw, "Rapid and robust phase behaviour stability analysis using global optimization," *Fluid Phase Equilibria*, vol. 264, pp. 137-146, 2008.
- [86] N. Saber and J. M. Shaw, "Toward multiphase equilibrium prediction for ill-defined asymmetric hydrocarbon mixtures," *Fluid Phase Equilibria*, vol. 285, pp. 73-82, Nov 2009.
- [87] V. N. Kabadi and R. P. Danner, "A MODIFIED SOAVE-REDLICH-KWONG EQUATION OF STATE FOR WATER HYDROCARBON PHASE-EQUILIBRIA," *Industrial & Engineering Chemistry Process Design and Development*, vol. 24, pp. 537-541, 1985.
- [88] S. Michel, H. H. Hooper, and J. M. Prausnitz, "Mutual solubilities of water and hydrocarbons from an equation of state - need for an unconventional mixing rule," *Fluid Phase Equilibria*, vol. 45, pp. 173-189, Apr 1989.
- [89] J. L. Daridon, B. Lagourette, H. Saintguirons, and P. Xans, "A cubic equation of state model for phase-equilibrium calculation of alkane plus carbon-dioxide plus

- water using a group-contribution Kij," *Fluid Phase Equilibria*, vol. 91, pp. 31-54, Nov 1993.
- [90] P. T. Eubank, C. H. Wu, J. F. J. Alvarado, A. Forero, and M. K. Beladi, "MEASUREMENT AND PREDICTION OF 3-PHASE WATER/HYDROCARBON EQUILIBRIA," *Fluid Phase Equilibria*, vol. 102, pp. 181-203, Dec 1994.
- [91] I. Soreide and C. H. Whitson, "PENG-ROBINSON PREDICTIONS FOR HYDROCARBONS, CO₂, N₂, AND H₂S WITH PURE WATER AND NaCl BRINE," *Fluid Phase Equilibria*, vol. 77, pp. 217-240, Sep 1992.
- [92] A. Dhima, J. C. de Hemptinne, and G. Moracchini, "Solubility of light hydrocarbons and their mixtures in pure water under high pressure," *Fluid Phase Equilibria*, vol. 145, pp. 129-150, Mar 1998.
- [93] M. Haruki, Y. Iwai, S. Nagao, and Y. Arai, "Measurement and correlation of liquid-liquid equilibria for water + aromatic hydrocarbon binary systems at high temperatures and pressures," *Journal of Chemical and Engineering Data*, vol. 46, pp. 950-953, 2001.
- [94] M. J. Huron and J. Vidal, "NEW MIXING RULES IN SIMPLE EQUATIONS OF STATE FOR REPRESENTING VAPOR-LIQUID-EQUILIBRIA OF STRONGLY NON-IDEAL MIXTURES," *Fluid Phase Equilibria*, vol. 3, pp. 255-271, 1979.
- [95] I. G. Economou and C. Tsonopoulos, "Associating models and mixing rules in equations of state for water/hydrocarbon mixtures," *Chemical Engineering Science*, vol. 52, pp. 511-525, Feb 1997.
- [96] J. D. Li, I. Vanderbeken, S. Y. Ye, H. Carrier, and P. Xans, "Prediction of the solubility and gas-liquid equilibria for gas-water and light hydrocarbon-water systems at high temperatures and pressures with a group contribution equation of state," *Fluid Phase Equilibria*, vol. 131, pp. 107-118, May 1997.
- [97] S. B. Kiselev, J. F. Ely, M. Abdulagatov, A. R. Bazaev, and J. W. Magee, "Equation of state and thermodynamic properties of pure toluene and dilute aqueous toluene solutions in the critical and supercritical regions," *Industrial and Engineering Chemistry Research*, vol. 41, pp. 1000-1016, 2002.
- [98] I. M. Abdulagatov, A. R. Bazaev, J. W. Magee, S. B. Kiselev, and J. F. Ely, "PVT_x measurements and crossover equation of state of pure n-hexane and dilute aqueous n-hexane solutions in the critical and supercritical regions," *Industrial and Engineering Chemistry Research*, vol. 44, pp. 1967-1984, 2005.
- [99] J. R. Errington, G. C. Boulougouris, I. G. Economou, A. Z. Panagiotopoulos, and D. N. Theodorou, "Molecular simulation of phase equilibria for water-methane and water-ethane mixtures," *Journal of Physical Chemistry B*, vol. 102, pp. 8865-8873, 1998.
- [100] M. Neichel and E. U. Franck, "Critical curves and phase equilibria of water-n-alkane binary systems to high pressures and temperatures," *Journal of Supercritical Fluids*, vol. 9, pp. 69-74, Jun 1996.
- [101] J. Z. Wu and J. M. Prausnitz, "Phase equilibria for systems containing hydrocarbons, water, and salt: An extended Peng-Robinson equation of state," *Industrial & Engineering Chemistry Research*, vol. 37, pp. 1634-1643, May 1998.
- [102] G. M. Kontogeorgis, E. C. Voutsas, I. V. Yakoumis, and D. P. Tassios, "An equation of state for associating fluids," *Industrial & Engineering Chemistry Research*, vol. 35, pp. 4310-4318, Nov 1996.
- [103] G. M. Kontogeorgis, M. L. Michelsen, G. K. Folas, S. Derawi, N. von Solms, and E. H. Stenby, "Ten years with the CPA (Cubic-Plus-Association) equation of

- state. Part 2. Cross-associating and multicomponent systems," *Industrial & Engineering Chemistry Research*, vol. 45, pp. 4869-4878, Jul 2006.
- [104] G. M. Kontogeorgis, M. L. Michelsen, G. K. Folas, S. Derawi, N. von Solms, and E. H. Stenby, "Ten years with the CPA (Cubic-Plus-Association) equation of state. Part 1. Pure compounds and self-associating systems," *Industrial & Engineering Chemistry Research*, vol. 45, pp. 4855-4868, Jul 2006.
- [105] G. K. F. Georgios M. Kontogeorgis, *Thermodynamic Models for Industrial Applications*, First ed.: Wiley Ltd., 2010.
- [106] G. K. Folas, G. M. Kontogeorgis, M. L. Michelsen, and E. H. Stenby, "Application of the cubic-plus-association (CPA) equation of state to complex mixtures with aromatic hydrocarbons," *Industrial & Engineering Chemistry Research*, vol. 45, pp. 1527-1538, Feb 2006.
- [107] W. Yan, G. M. Kontogeorgis, and E. H. Stenby, "Application of the CPA equation of state to reservoir fluids in presence of water and polar chemicals," *Fluid Phase Equilibria*, vol. 276, pp. 75-85, 2009.
- [108] E. C. Voutsas, G. C. Boulougouris, I. G. Economou, and D. P. Tassios, "Water/hydrocarbon phase equilibria using the thermodynamic perturbation theory," *Industrial & Engineering Chemistry Research*, vol. 39, pp. 797-804, Mar 2000.
- [109] S. Aparicio-Martínez and K. R. Hall, "Phase equilibria in water containing binary systems from molecular based equations of state," *Fluid Phase Equilibria*, vol. 254, pp. 112-125, 2007.
- [110] C. Tsonopoulos, "Thermodynamic analysis of the mutual solubilities of hydrocarbons and water," *Fluid Phase Equilibria*, vol. 186, pp. 185-206, Aug 2001.
- [111] C. Tsonopoulos, "Thermodynamic analysis of the mutual solubilities of normal alkanes and water," *Fluid Phase Equilibria*, vol. 156, pp. 21-33, Mar 1999.
- [112] P. Ruelle and U. W. Kesselring, "Aqueous solubility prediction of environmentally important chemicals from the mobile order thermodynamics," *Chemosphere*, vol. 34, pp. 275-298, Jan 1997.
- [113] P. Ruelle and U. W. Kesselring, "Nonlinear dependence of the solubility of water in hydrocarbons on the molar volume of the hydrocarbon," *Journal of Solution Chemistry*, vol. 25, pp. 657-665, Jul 1996.
- [114] C. Amovilli and F. M. Floris, "Solubility of water in liquid hydrocarbons: a bridge between the polarizable continuum model and the mobile order theory," *Physical Chemistry Chemical Physics*, vol. 5, pp. 363-368, 2003.
- [115] C. L. Yaws and U. Yadav, "How temp. affects H₂O solubility in cycloalkanes," *Oil & Gas Journal*, vol. 110, pp. 96-+, Jan 2012.
- [116] C. L. Yaws, P. Rane, and V. Nigam, "Solubility of Water in Benzenes As a Function of Temperature," *Chemical Engineering*, vol. 118, pp. 42-46, Dec 2011.
- [117] C. L. Yaws and P. M. Rane, "How temp. affects H₂O solubility in alkanes," *Oil & Gas Journal*, vol. 108, pp. 130-133, Dec 2010.
- [118] X. Y. Zou, X. H. Zhang, and J. M. Shaw, "Phase behavior of Athabasca vacuum bottoms plus n-alkane mixtures," *Spe Production & Operations*, vol. 22, pp. 265-272, May 2007.
- [119] X. H. Zhang, "The impact of multiphase behavior on coke deposition in heavy oil hydroprocessing catalysts," Ph.D, University of Alberta, Edmonton, 2006.
- [120] E. W. Lemmon, M. O. McLinden, and D. G. Friend, "Thermophysical Properties of Fluid Systems," in *NIST Chemistry WebBook*, NIST Standard Reference Database Number 69, P. J. Linstrom and W. G. Mallard, Eds., ed Gaithersburg

MD, <http://webbook.nist.gov>: National Institute of Standards and Technology, 2012.

Chapter 2. Phase behavior of Athabasca bitumen + water mixtures at high temperature and pressure¹

2.1 Introduction

Water, a polar solvent at room temperature, becomes a nonpolar solvent at high temperatures as a consequence of a significant decrease its dielectric constant [1,2]. This unusual property makes water a promising medium to use in the design and operation of novel high-temperature processes for hydrocarbon production and refining. For example, the application of near critical and super-critical water in heavy oil and bitumen extraction and upgrading processes [3–9], has received much attention in the recent years. The use of water in refining processes may provide significant advantages over current practice due to the possible elimination of asphaltene precipitation effects, and a reduction in coke formation [3–9]. Having a good knowledge of phase equilibria arising in water + bitumen and heavy oil mixtures is a first step toward the development and optimization of possible upgrading process designs [10].

Detection and evaluation of the phase behavior of hydrocarbon + water mixtures has received extensive attention since the 1980s using static and flow apparatus. De Loos and co-workers obtained high temperature and pressure phase equilibria for water + propane [11], n-hexane [12], n-pentane and n-heptane [13]. Phase equilibrium data for water + n-butane and n-hexane were reported by Yiling et al. [14]. The water + n-decane binary was investigated by Wang et al. [15]. Stevenson et al. [16] measured equilibria and critical points for water + sequalane and dodecane mixtures in the range of 600–660 K using a flow apparatus. Phase equilibrium measurements for water + tetralin and 1-methylnaphthalene, up to critical temperatures of mixtures, are also available [17]. Brunner [18] investigated the phase behavior of water + n-alkane mixtures from carbon number 1–36 systematically over a broad range of temperatures and pressures. Brunner also investigated the phase equilibria and critical phenomena for water + 26 aromatic and alkyl aromatic binary mixtures [19].

¹ This chapter with minor modifications has been published in *The Journal of Supercritical Fluids*: M. J. Amani, M. R. Gray, and J. M. Shaw, *The Journal of Supercritical Fluids*, vol. 77, pp. 142-152, 2013.

The phase behavior of binary mixtures was classified by van Konynenburg and Scott [20]. Their classification scheme is based on the unique features of critical loci and critical points in the PT projections. According to the van Konynenburg and Scott classification scheme, water + hydrocarbon binary mixtures fall within the Type II or Type III phase behavior classes illustrated in Figure 2.1.

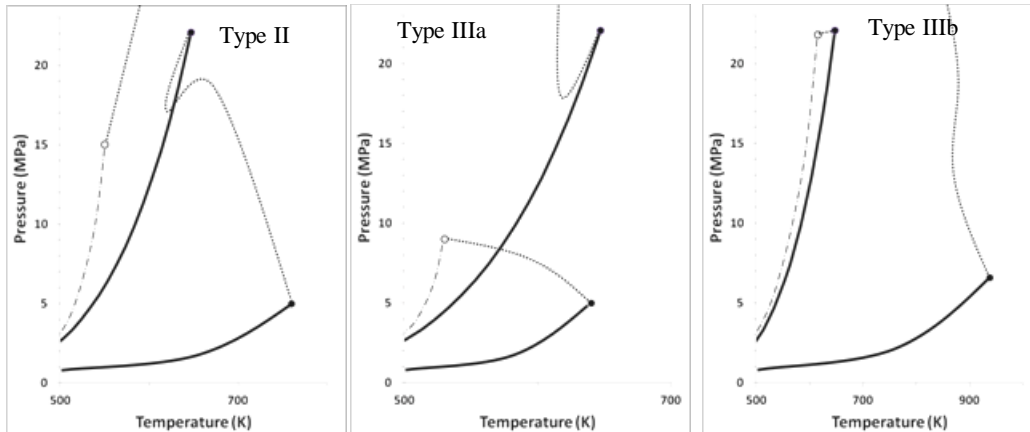


Figure 2.1. Schematic pressure-temperature projections for Type II, IIIa and IIIb phase behavior. Pure component vapor pressure curves (—), liquid-gas (LV) and liquid-liquid (LL) critical loci (.....), liquid-liquid vapor lines (---), pure component critical points (●) and critical end points (○).

Type II has no subcategories while Type III phase behavior can be divided into two sub categories Type IIIa and Type IIIb [18,19]. For Type II phase behavior, a continuous liquid–vapor critical locus connects the pure component critical points. Thus at high temperatures, only liquid, vapor or liquid–vapor phase behavior is observed in the Type II projection. At low temperatures, liquid, vapor, liquid–liquid vapor, and liquid–liquid phase behavior arises and consequently a second critical locus is present in the Type II projection. The liquid-liquid critical locus, present in Type II phase behavior, intersects the liquid–liquid–vapor three-phase line at an upper critical end point (UCEP) where two liquids become critically identical in the presence of a vapor. In Type III phase behavior, the liquid–vapor critical locus is discontinuous. One segment extends from one of the pure components to high pressure (water Type IIIa, hydrocarbon Type IIIb) depending on the relative critical temperatures of the components. The second critical locus segment extends from the other component (hydrocarbon Type IIIa, water Type IIIb) and intersects liquid–liquid–vapor three-phase line at a K-point where one of the liquids and the vapor become critically identical in the presence of the second liquid. For Type II, Type IIIa and Type IIIb phase behavior, the LLV curve arises at pressures exceeding the

vapor pressure of water. This is a key characteristic of water + hydrocarbon phase behavior and a feature exploited in the construction of pressure–composition diagrams at fixed temperature in this work.

Type IIIa phase behavior arises in a wide variety of water + hydrocarbon binary mixtures where the molar mass of the hydrocarbon is low, such as the lower n-alkanes (water + propane [11], n-butane [14], n-hexane [12,14], n-pentane [13], n-heptane [13], n-C₂₅ and below [18]) and one ring aromatics (water + benzene, toluene, o-xylene, p-xylene, and 1,3,5- trimethylbenzene [19]). Type IIIb and Type II phase behaviors arise where the critical temperature of the hydrocarbon is greater than that of water. Water + polycyclic aromatic hydrocarbons with up to 4 rings mixtures exhibit Type II phase behavior, examples include water + 1-methylnaphthalene and tetralin [17,19], naphthalene and biphenyl [19]. By contrast, water + large n-alkanes and aromatics hydrocarbon where the critical temperature of the hydrocarbon is much greater than the critical temperature of water typically exhibit Type IIIb phase behavior, e.g.: water + n-C₂₆ and above [18], and indene [19].

High-temperature experimental phase behavior data for mixtures which include heavy hydrocarbons and industrially relevant mixtures (resids, boiling range cuts, SARA fractions) remain scarce due to difficulties associated with observing phase changes and measuring equilibrium properties with opaque mixtures compounded at high-temperature and high-pressure conditions by the possible impacts of thermolysis and other chemical reactions on results. In this preliminary work, the phase behavior of Athabasca bitumen + water is explored. Identification of the nature of mixture phase behavior type, either Type II or Type IIIb, is a particular focus.

2.2 Materials and methods

2.2.1 Experimental apparatus

Athabasca bitumen, provided by Syncrude Canada Ltd., Alberta, Canada was produced by a commercial froth treatment process. The elemental and SARA analyses for the sample of Athabasca bitumen used in this work are presented in Table 2.1 [21]. Analyses for similar samples of Athabasca bitumen are available in the literature [22,23]. Deionised water (99.99 wt % pure) HPLC grade was provided by Sigma–Aldrich. 1-methylnaphthalene (99.0 wt %) used for validation experiments provided by Acros

Organics. The equipment was washed with toluene (99.9 wt % purity) provided by Fischer Scientific, before and after each experiment.

The phase equilibrium experiments were performed using an X-ray view cell. A schematic is shown in Figure 2.2. Detailed descriptions of the construction and operation of the equipment can be found elsewhere [24–26]. Only a brief summary is provided here. The view cell consists of an open-ended cylinder with an approximate internal volume of 200 cm³. The upper end cap includes a variable volume bellows. The internal volume of the cell is varied inflating or deflating the bellows using high-pressure nitrogen. While the lower end cap is fixed, the minimum volume of the cell, >10 cm³, is dictated by the presence of internals, such as a stirrer resting on the lower end cap, and feed lines that facilitate gas and liquid injection and air removal once the cell is assembled.

Table 2.1. Properties for Athabasca bitumen [21]

Elemental composition	wt %
Carbon	83.2 ± 0.9
Hydrogen	9.7 ± 0.4
Nitrogen	0.4 ± 0.2
Sulphur	5.3 ± 0.2
Oxygen	1.7 ± 0.3
SARA analysis	wt %
saturates	16.1 ± 2.1
aromatics	48.5 ± 2.3
resins	16.8 ± 1.2
asphaltene (C ₅)	18.6 ± 1.8

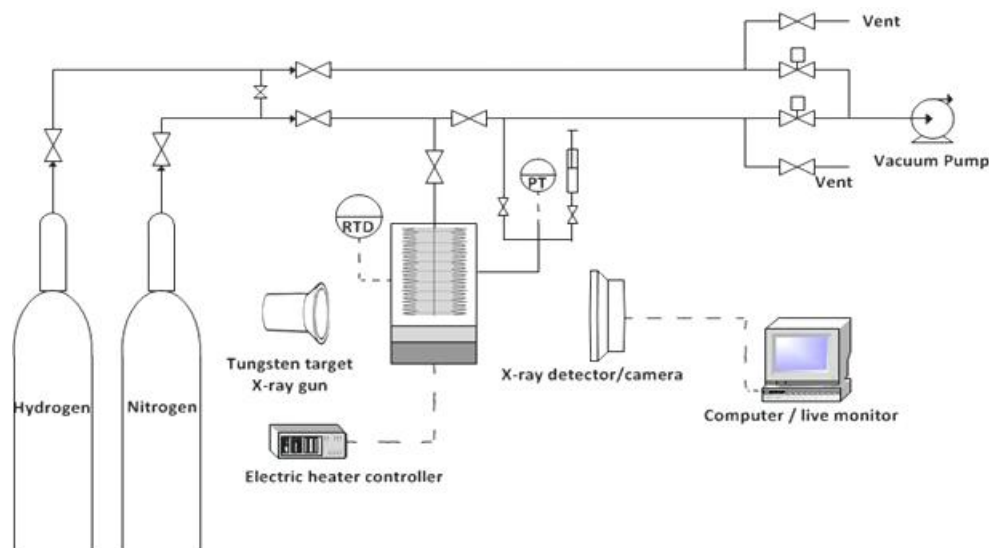


Figure 2.2. X-ray view cell apparatus schematic

A polychromatic X-ray beam, emitted from a point source tungsten-target, is transmitted through parallel slots in the insulation surrounding the view cell. The transmitted X-rays are then captured by an X-ray sensitive image intensifier (Siemens 11 and 28 cm dual field cesium iodide) in line with a video camera (Pulnix tm-9710 with a 35 mm imaging lens) and converted to digital images. The images are monitored and recorded using an on line computer. The heating system comprises two electric heating jackets connected to a PID (proportional, integral, derivative) controller. The interior temperature of the cell is monitored and controlled using a RTD (resistance temperature detector). Three K-type thermocouples were used to monitor the exterior wall temperature of the cell. For these measurements, the pressure within the view cell and the variable volume bellows were measured using pressure transducers with an operating range of 0–27.6 MPa. All experimental measurements fall within the operating range of transducers. Phase boundaries arising at higher pressures are interpreted based on experimental measurements at lower pressure. Air was purged from the view cell and connecting tubing by reducing the pressure in the cell to 14 kPa and purging twice with nitrogen and dropping the pressure to below 14 kPa after each purge. The view cell was leak tested with hydrogen at 10.5 MPa for one hour at room temperature. The criterion for a successful leak test was a pressure drop of less than 0.02 MPa in one hour.

The equipment was calibrated for temperature, pressure and volume using pure liquids (water, toluene, 1-methylnaphthalene and n-dodecane) for which properties are well

established. For example, near the critical point of water (647.1 K and 22.1 MPa [27]) the pressure measurement reproducibility is within ± 0.07 MPa. The cross section area at the bottom of the cell was reduced in order to increase volume measurement accuracy, for small volumes, and to facilitate detection of possible asphaltene deposits. Volume measurement error is less than ± 0.05 cm³ (for volumes less than 4.8 cm³) and ± 0.2 cm³ (for volumes greater than 4.8 cm³). At lower temperatures pressure reproducibility is within ± 0.03 MPa. Temperature was controlled to within ± 0.1 K. Volume calibrations performed with pure components revealed that 5 cm³ of water and toluene became trapped in unheated tubing and in the pressure transducer housing at temperatures greater than 403 K. Less-volatile components 1-methylnaphthalene, n-dodecane and bitumen were not subject to this phenomenon at temperatures up to more than 573 K. Mixture compositions were adjusted to reflect the impact of this effect, by subtracting the trapped mass. This correction was validated by reproducing phase diagrams for toluene + water and 1-methylnaphthalene + water binaries as described below.

2.2.2 Experimental method validation measurements

Validation experiments were performed to illustrate the accuracy and precision of the indirect LLV/LL and LV/L phase behavior boundary identification technique, and to illustrate the effectiveness of the calibration technique for addressing the impact of constituent volatility on phase compositions in the view cell.

2.2.2.1 1-Methylnaphthalene + water mixtures

Direct detection of (LV/L or V, and LLV/LV or LL) phase behavior boundaries with 1-methylnaphthalene + water mixtures is challenging due to the broad range of volumes required, particularly at elevated temperatures. However, pressures for these phase behavior boundaries can be determined indirectly based on vapor volume variations arising from cell volume variations at fixed feed mass and composition. If the vapor phase volume fraction is small, pressure and vapor phase volume become linearly related, as exemplified in Figure 2.3 for 1-methylnaphthalene + water mixtures at 573 K. For small vapor volumes both experimental data, and computations based on the same mixture compositions and masses using the Peng-Robinson equation of state show the same trend. As the phase boundary is approached the pressure-phase volume relationship becomes linear. Remote from the phase boundary the expected curvature in the relationship becomes evident, as is observed for the model. The equation of state model

was not fit to the vapor volume data. The water-1-methylnaphthalene interaction parameter, $K_{ij} = 0.26$, was fit to the data for water solubility in 1-methylnaphthalene over same temperature range. It is only the trend that is important. The estimation of boundaries by linear extrapolation over vapor phase volume makes it possible to prepare pressure–composition diagrams. One such phase diagram, for 1-methylnaphthalene + water at 573 K, is shown in Figure 2.4. The LV/L and LLV/LL boundaries evaluated by extrapolation agree with direct observations [17] to within measurement error as noted in Table 2.2. Differences in LV/L and LLV/LL phase boundary pressures obtained using these two approaches are less than 3%.

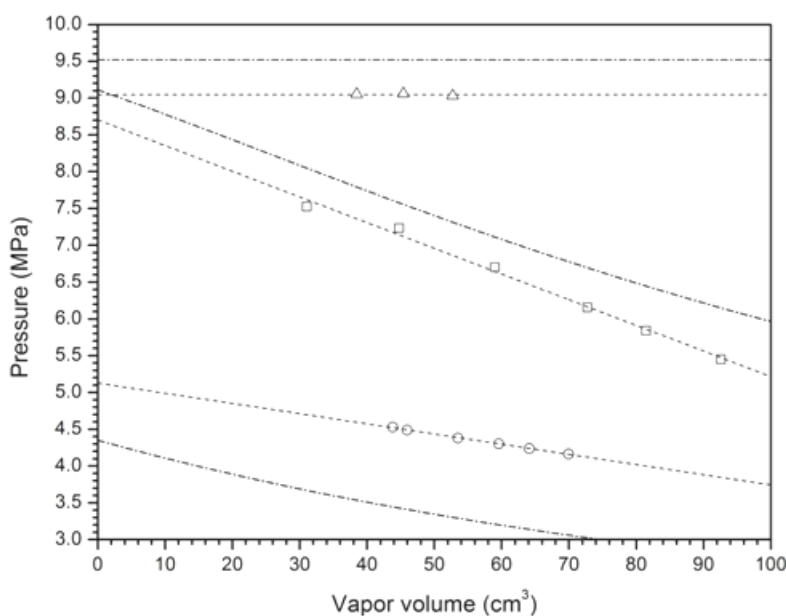


Figure 2.3. Vapor phase volume trends adjacent to LV/L and LLV/LL boundaries for 1-methylnaphthalene + water mixtures at 573 K. Data: LLV/LL: 78.9 wt % 1-methylnaphthalene (Δ), LV/L: 78.3 wt % 1-methylnaphthalene (\square) and LV/L: 96.3 wt % 1-methylnaphthalene (\circ). Linear extrapolation of experimental volume data (---). Trends computed using the Peng-Robinson equation of state [35] with $K_{ij} = 0.26$ (-.-.-).

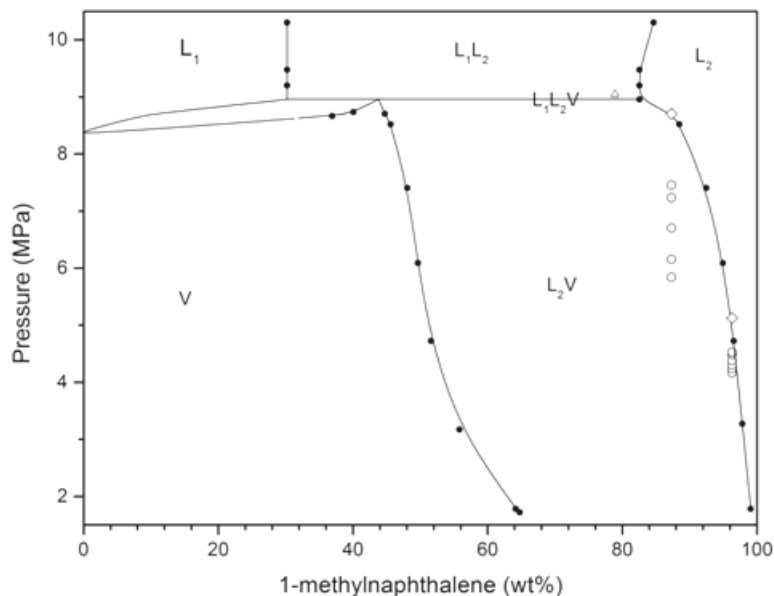


Figure 2.4. Pressure-composition diagram for the 1- methylnaphthalene + water binary at 573 K. Phase behavior boundaries identified by Christensen [17] (●). Phase behavior and phase behavior boundaries identified in this work: LV data (○), LV/L boundary values (◇), and LLV/LL boundary value (Δ).

Table 2.2. Experimental phase behavior data for 1-methylnaphthalene + water mixtures at 573 K.

1-MN concentration (wt %) ± 0.1	Pressure (MPa) ± 0.07	Temperature ($^{\circ}\text{C}$) ± 0.1	Vapor phase volume (cm^3) ± 0.2	Phases	Experimental data (MPa) [17]
96.3	4.16	300.1	69.9	LV	
96.3	4.24	300.1	64.1	LV	
96.3	4.30	300.0	59.6	LV	
96.3	4.38	299.9	53.5	LV	
96.3	4.49	300.0	45.9	LV	
96.3	4.53	300.0	43.8	LV	
96.3	5.13*	300.0		LV/L	4.96**
87.3	5.45	300.0	92.6	LV	
87.3	5.84	300.0	81.4	LV	
87.3	6.16	300.0	72.7	LV	

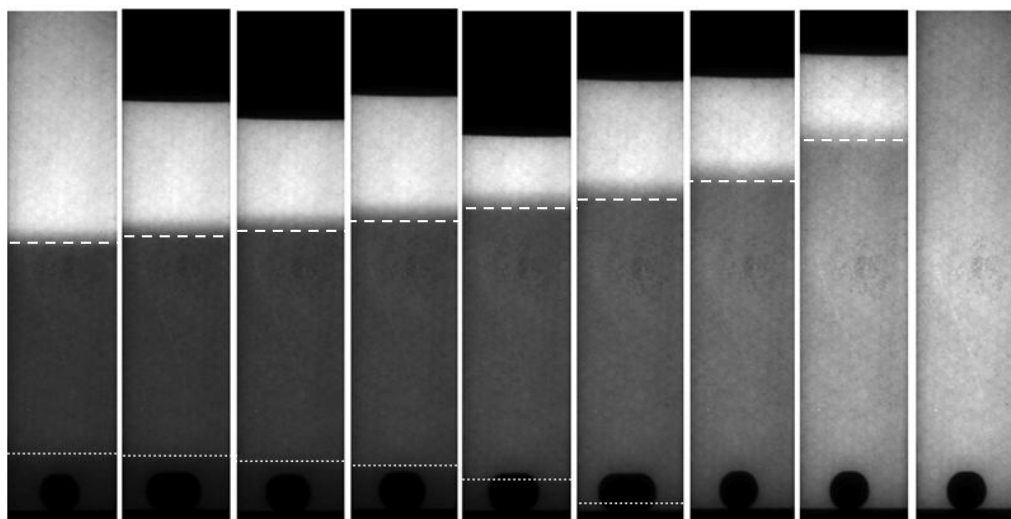
87.3	6.70	300.0	59.0	LV	
87.3	7.23	299.9	44.8	LV	
87.3	7.52	299.9	31.0	LV	
87.3	8.70*	300.0		LV/L	8.75**
78.9	9.03	300.0	52.7	LLV	
78.9	9.06	300.1	45.4	LLV	
78.9	9.05	300.0	38.4	LLV	
78.9	9.05*	300.0		LLV/LL	8.96**

*-Value obtained by extrapolation.

**-Value obtained by interpolation of direct experimental observations available in the literature [17].

2.2.2.2 Toluene + water mixtures

Validation experiments were performed with toluene + water binaries to evaluate the accuracy of phase behavior boundary results obtained where both constituents condense at temperatures above 323 K. Figure 2.5 shows typical X-ray images for toluene (88.4 wt %) + water phase behavior. The number of phases, phase volumes, interfaces, and the relative density associated with each phase are clearly visible. For the experimental conditions shown, the water-rich liquid phase (L_2) shrinks as temperature is increased, and is absent from the image at 533.1 K. The toluene-rich phase (L_1) expands and becomes less dense with increasing temperature. No interface was observed at 573.2 K, a temperature above the critical temperature of the mixture (565 K). The results for LLV three-phase points, Table 2.3, and critical points identified by direct observation in this work, which possess larger uncertainties, Table 2.4, are both in good agreement with data from Burner [19], Anderson [28] and Chandler [29], as illustrated in Figure 2.6. Toluene + water mixtures were also used to illustrate phase behavior measurement reproducibility. For binary mixtures, LLV pressures are composition independent at fixed temperature. Thus, LLV/LL phase behavior boundary pressures identified using water + 40.7, 83, 86.5, and 88.4 wt % toluene mixtures comprise a reproducibility data set. These phase behavior boundary pressures, identified indirectly, are reproducible to within the measurement uncertainty on average, and agree to within 3% of smoothed data from the literature on average, as also noted in Table 2.3.



413.0 K	432.1 K	453.0 K	472.1 K	492.9 K	513.2 K	533.1 K	553.2 K	573.2 K
0.59 MPa	0.99 MPa	1.61 MPa	2.39 MPa	3.53 MPa	5.13 MPa	6.78 MPa	8.08 MPa	9.40 MPa

Figure 2.5. Typical x-ray images for the toluene (88.4 wt %) + water binary. The vapor phase (V) has a low intensity. The toluene-rich liquid (L_1) has an intermediate intensity (light liquid) and the water rich liquid (L_2) has a low intensity (dense liquid). The magnetic stirrer (black sphere at the base of the cell) and the bellows (black cylinder at the top of the cell) are visible in some of the images. L_1/L_2 (.....) and L_1/V (- - -) interfaces are shown in the images where present.

Table 2.3. Observed L=V critical points for toluene + water binary mixtures.

Toluene composition (wt %) ± 0.1	Temperature (K) ± 2.0	Pressure (MPa) ± 0.50
92.5	578.5	7.31
90.3	573.3	8.11
88.4	563.2	8.81

Table 2.4. LLV three-phase pressure for toluene + water mixtures.

Temperature (K)± 0.1	Toluene(wt %) ± 0.1	LLV pressure (MPa) ± 0.07	LLV/LL boundary Pressure (MPa)	LLV/LL boundary pressure (smoothed literature data) (MPa)*
432	83	0.99	1.01 ± 0.02	1.03
432	88.4	0.99		
432.2	86.5	1.03		
452.4	40.7	1.58	1.57 ± 0.04	1.61
452.9	83	1.53		
453	88.4	1.61		
453.4	86.5	1.6		
471.8	40.7	2.31	2.37 ± 0.05	2.38
472.7	88.4	2.39		
473	86.5	2.42		
473.1	83	2.34		
492.8	83	3.61	3.51 ± 0.07	3.48
493	40.7	3.43		
493	88.4	3.52		
493.1	86.5	3.58		
512.7	83	5.04	5.04 ± 0.09	4.95
513	40.7	4.97		
513	86.5	5.03		
513.2	88.4	5.13		
532.8	83	7.01	7.08 ± 0.07	6.89
532.9	40.7	7.11		
533.1	86.5	7.15		
552.9	83	9.23	9.36 ± 0.14	9.49
553	40.7	9.5		

*smoothed values based on data from Burner [19], Anderson [28], and Chandler [29].

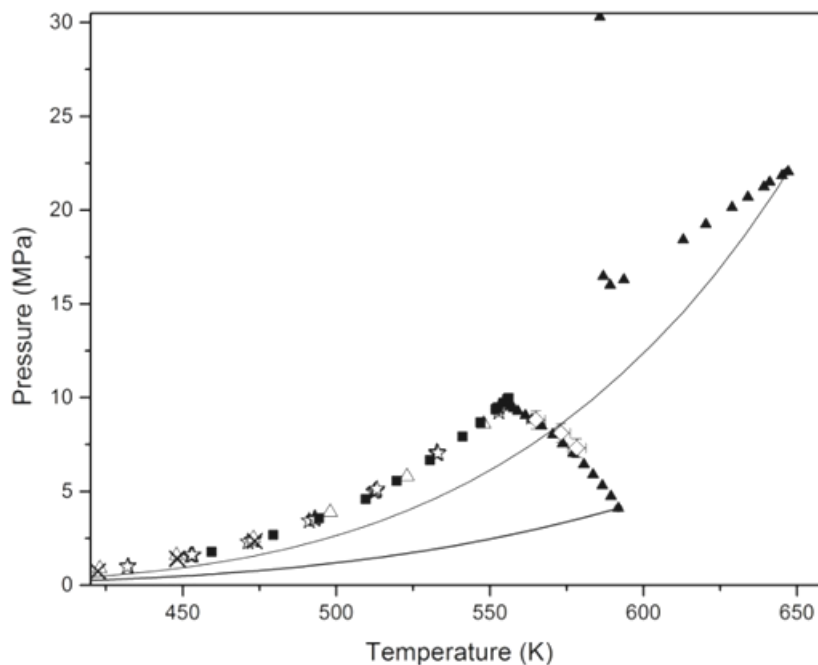


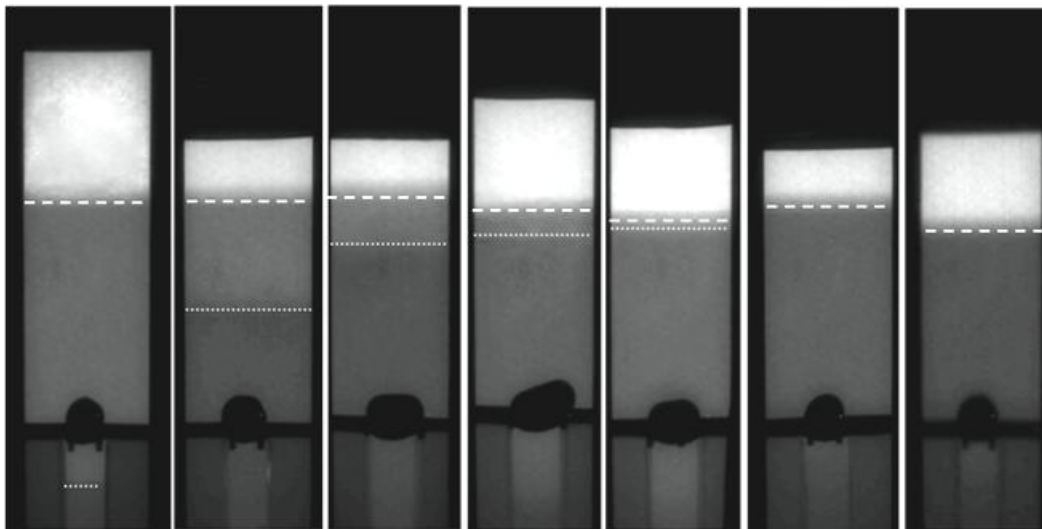
Figure 2.6. Pressure-temperature projection for the toluene + water binary (Type IIIa). The solid curves (—) are the water and toluene vapor pressures [27]. The solid triangles, Brunner [19], (▲) and the open diamonds, this work, (◇) are points on the L=V critical locus. Solid squares, Brunner [19], (■), crosses, Anderson [28], (×), open triangles, Chandler [29], (△) and stars, this work, (☆) are LLV three-phase points.

2.2.3 Phase diagram construction

Phase diagrams for water + Athabasca bitumen were constructed using the synthetic method where the phase behaviors of mixtures with fixed composition were studied individually over broad ranges of temperature and pressure. The number of phases present at each experimental condition, their volume and relative density were determined by analyzing X-ray still images. Phase behavior boundaries were determined indirectly and pressure–temperature phase diagrams for a range of fixed compositions were prepared based on corrected compositions using the procedure noted above. Pressure–composition phase diagrams at fixed temperature were constructed as composites. At each temperature and for each composition probed, the focus in this work is on the LV/L and LLV/LL boundaries as this is where the phase diagrams are most complex, where the nature of the phase behavior type is most readily identified, and where industrial interest is greatest.

2.3 Results and discussion

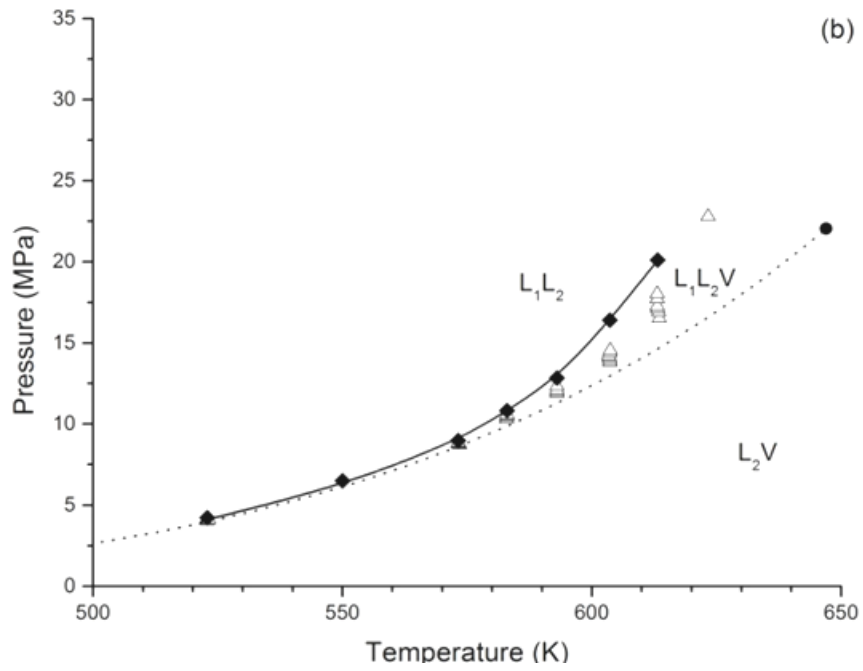
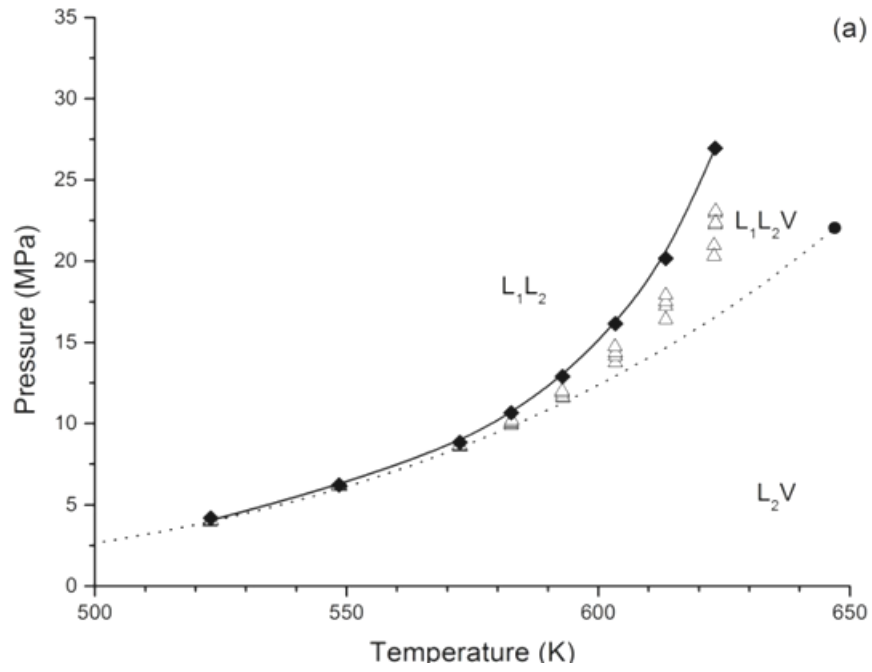
Athabasca bitumen + water mixtures present two specific phase behavior boundary measurement challenges. First, the physical and X-ray density [26] differences between water and bitumen differ little at room temperature. These differences increase at higher temperature. Detection of bitumen-rich liquid/water-rich liquid boundaries is difficult below 583 K but they become clearly visible at higher temperatures as illustrated in Figure 2.7. The water-rich phase designated L_1 in the phase diagrams is less dense than the bitumen-rich liquid designated L_2 . Second, bitumen is subject to thermal reactions that become significant over the time frame of phase behavior measurements above ~ 613 K [30]. As hydrocarbons with both lower and higher molar masses than originally present in the bitumen are generated, this tends to raise the pressure for the LLV/LL or LV/L transitions, thus broadening the range for LLV and LV behaviors. Further, the solubility of bitumen in water is low. As a consequence, detection of the L_1V to LLV phase behavior boundary adjacent to the water composition axis is infeasible, even at elevated temperatures. These effects restrict the composition and temperature ranges of the data presented. The foci for the measurements are temperatures from 523 K to 680 K and compositions from 10 to 100 wt % bitumen.

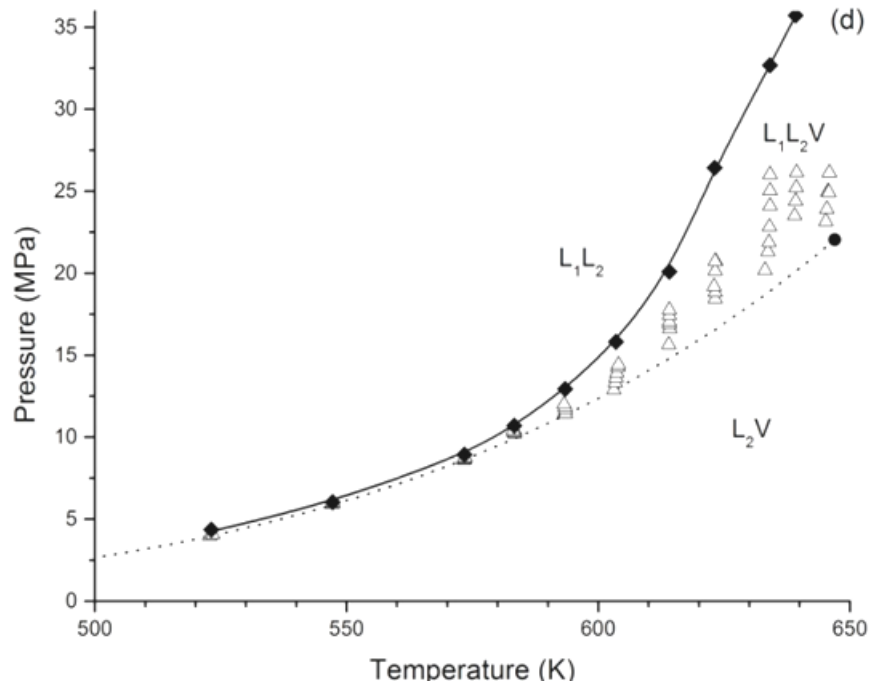
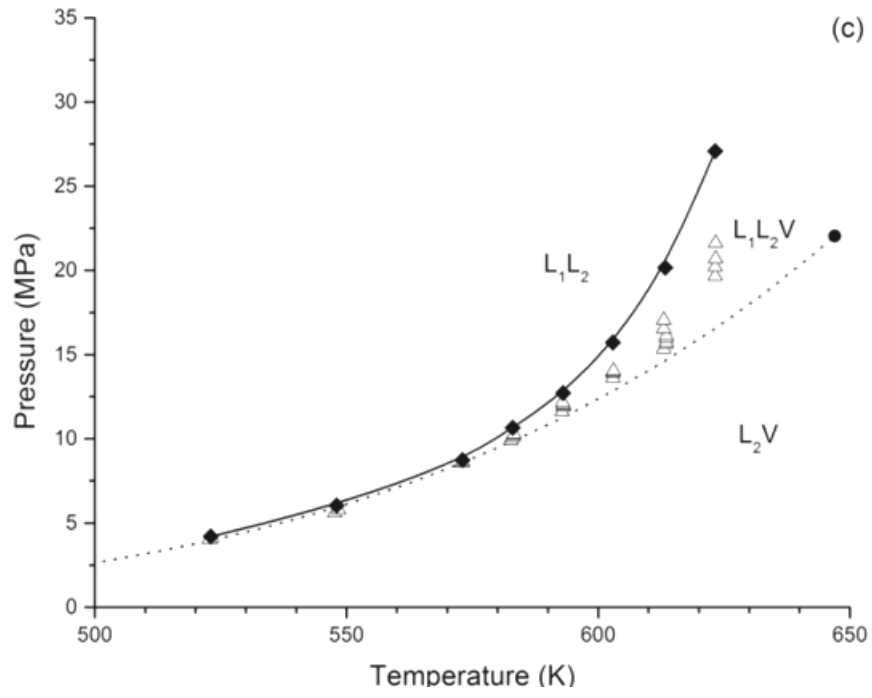


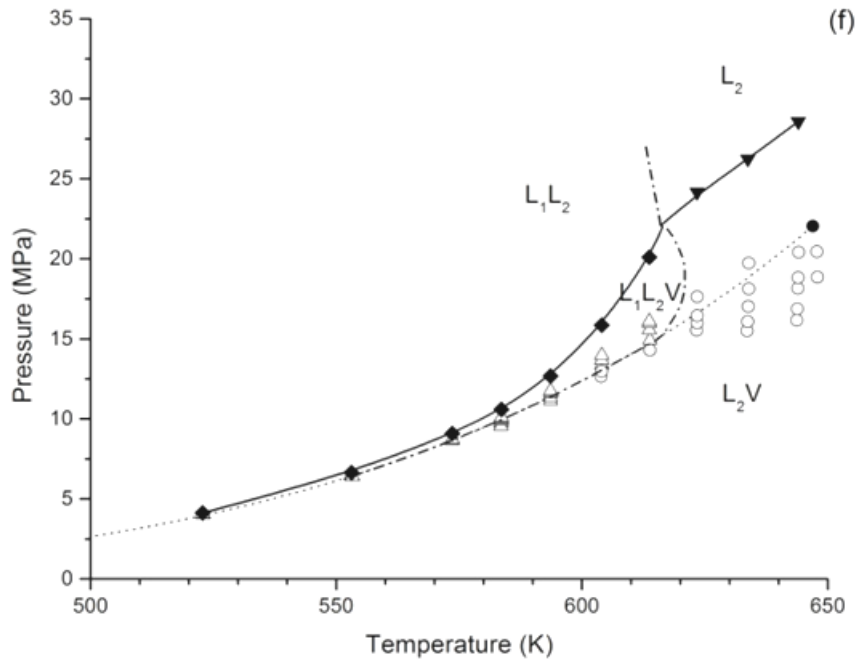
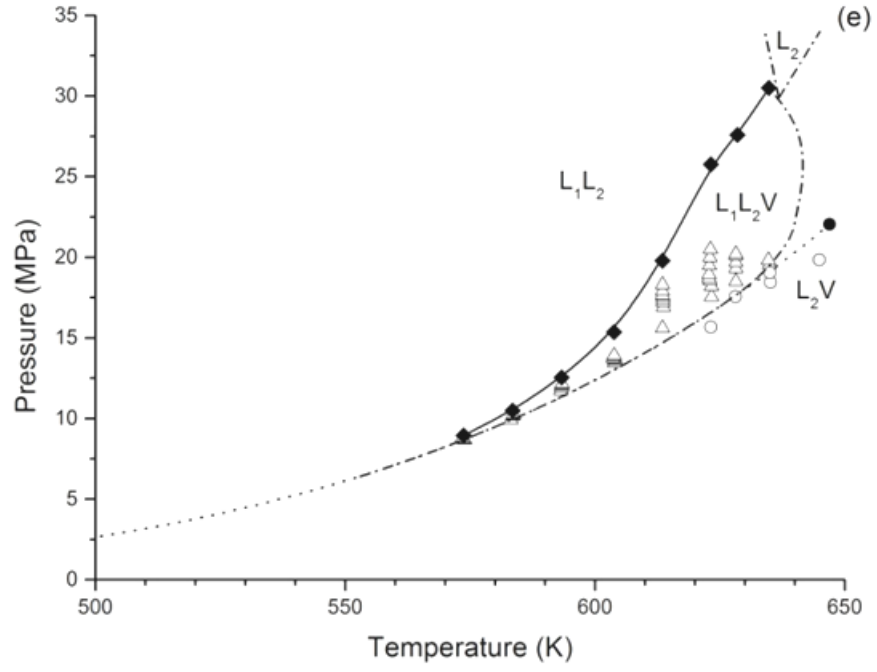
9.2 wt %	55.9 wt %	66.3 wt %	73.3 wt %	78.3 wt %	87.7 wt %	89.7 wt %
17.2 MPa	17.7 MPa	16.9 MPa	17.4 MPa	17.6 MPa	15.6 MPa	13.1 MPa

Figure 2.7. Typical x-ray images for Athabasca bitumen (AB) + water mixtures at 613.5 K. liquid/liquid(.....) and liquid/vapor (---) interfaces are shown in the images where present.

Pressure–temperature phase diagrams at fixed composition for Athabasca bitumen + water mixtures at 9.2, 55.9, 66.3, 73.3, 78.3, 87.7, 88.7 and 96.6 wt % Athabasca bitumen are shown in Figure 2.8a–h. Phase behavior observations and phase behavior boundary pressures are reported in Table 2.5. The vapor pressure curve for water is also shown in Figure 2.8a–h. Like water + pure hydrocarbon binary mixtures, LLV phase behavior arises in the Athabasca bitumen + water pseudo binary at or above the vapor pressure of water and the water vapor pressure provides a lower bound for possible LLV phase behavior. At room temperature, the mutual solubilities of water and hydrocarbons typically fall into the parts per million to parts per thousand range. At higher temperatures, the solubility of water in hydrocarbon liquids typically increases sharply while the solubility of large hydrocarbons in water remains low on a mass basis [31–34]. The phase diagrams for water + Athabasca bitumen reflect these effects. At 523 K and below, Athabasca bitumen + water mixtures exhibit LLV phase behavior for compositions ranging from 9.2 to 97 wt % bitumen over a narrow pressure range just above and well approximated by the vapor pressure of water. At higher temperatures, the pressure range for LLV phase behavior broadens but the lower pressure bound remains well approximated as the vapor pressure of water. Hydrocarbon-rich liquid + vapor (L_2V) phase behavior is observed below the LLV region, and a liquid–liquid region arises above the LLV region in all cases. As the critical temperature of water (647 K) is approached, there is no qualitative change in this behavior for mixtures comprising 9.2–73.3 wt % bitumen as shown in Figure 2.8a–d. For 78.3–96.6 wt % bitumen, Figure 2.8e–h, the LLV region was observed to possess an upper temperature bound that reflects the increasing solubility of water in the Athabasca bitumen and L_2V/L_2 phase behavior boundaries were identified at high temperatures for these compositions. The placement of L_2/LL phase behavior boundaries in Figure 2.8e–h is approximate. They were not observed experimentally. The absence of an observed LLV/ L_1V phase behavior transition at high temperature for 9.2 wt % bitumen, indicates that the solubility of bitumen in water remains less than 9.2 wt % at 620 K, where as the solubility of water in Athabasca bitumen is more than 13 wt % at the same temperature. Again, this asymmetric solubility behavior is consistent with the high-temperature behavior of typical hydrocarbon + water mixtures.







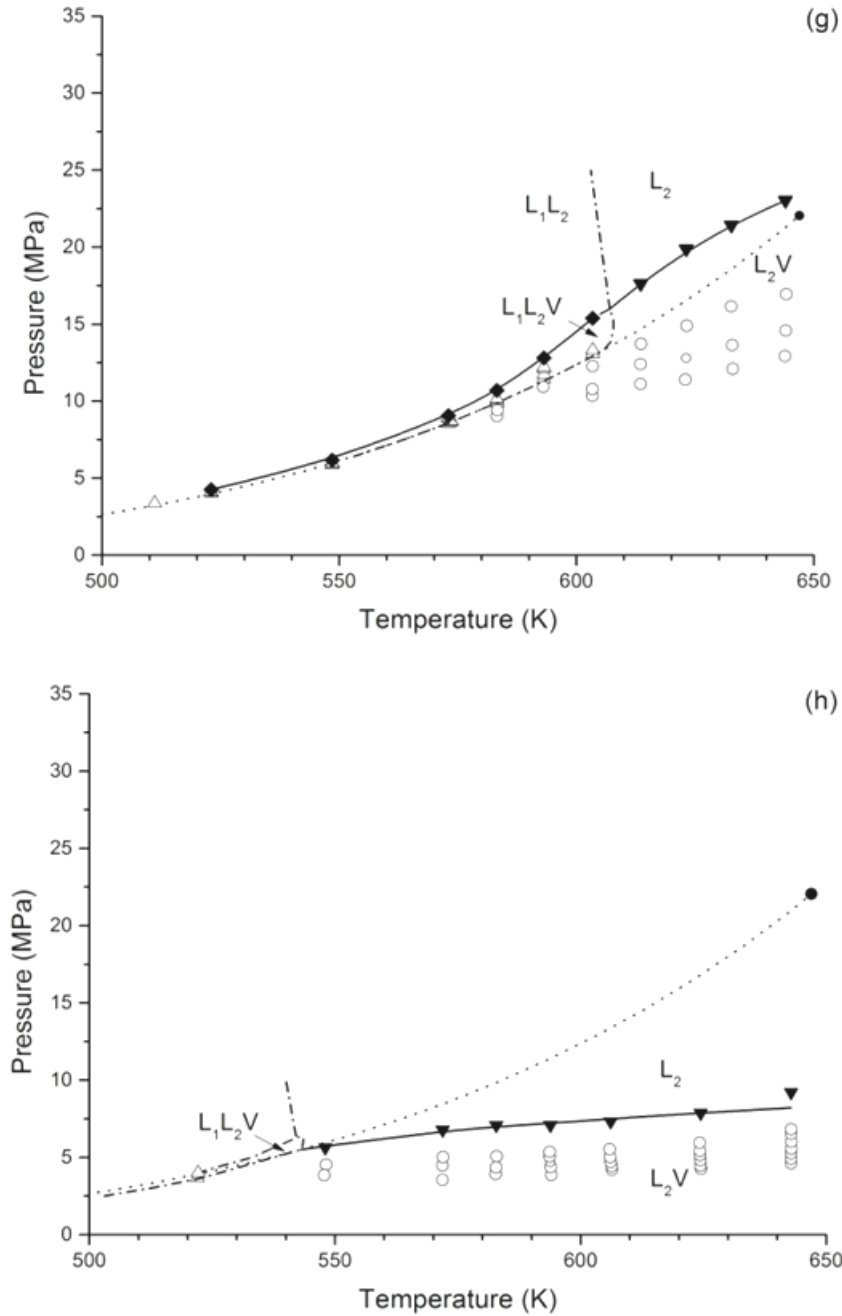
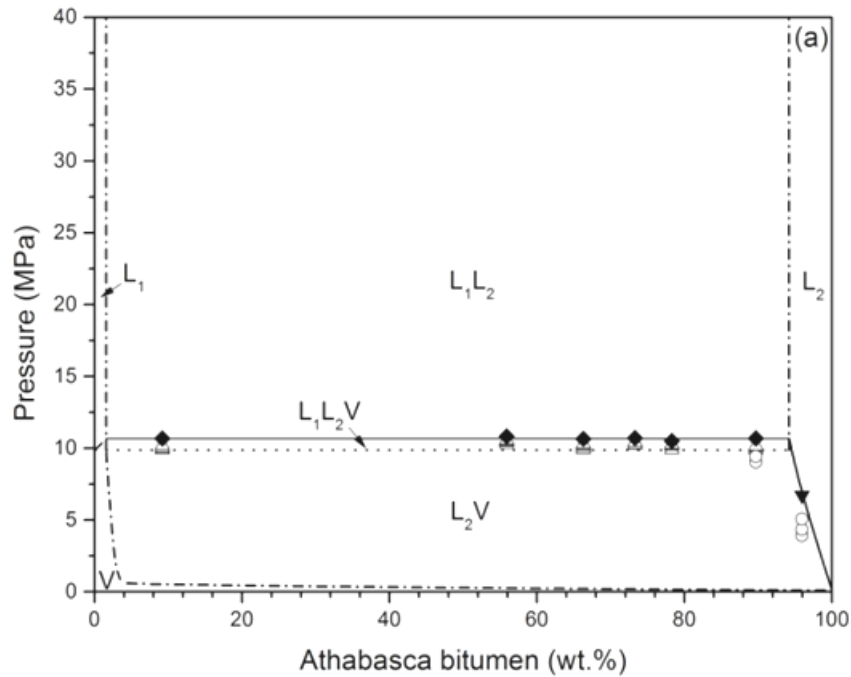


Figure 2.8. Pressure-temperature diagrams for Athabasca bitumen + water mixtures at fixed Athabasca bitumen wt %: a) 9.2 wt %, b) 55.9 wt %, c) 66.3 wt %, d) 73.3 wt %, e) 78.3 wt %, f) 87.7 wt %, g) 88.7 wt %, h) 96.6 wt %. The water vapor pressure curve is shown in each figure as a dotted curve (.....) terminating at a critical point designated with a solid circle (●). Liquid-vapor and liquid-liquid-vapor equilibrium data, are shown as open circles (○) and open triangles (△) respectively. Points on LV/L and LLV/LL boundaries are shown as solid squares (◆) and (▼), and solid curves (—) trace the LLV/LL and LV/L boundaries. Boundaries designated with a dash-dot lines (-.-) are illustrative and were not identified experimentally.

P – x phase diagrams at constant temperature, Figure 2.9a–c, were constructed as composites of the phase behavior observations and phase behavior boundaries presented in Figure 2.8a–h. Some parts of the phase diagrams at 583.2, 623.2 and 644 K, shown in Figure 2.9a–c respectively, are well-defined on this basis. Other parts of the diagrams are inferred from fragmentary data available, and from theory. The vapor pressure of water plays an important role in defining these diagrams. At 583.2 K, Figure 2.9a, the phase diagram is dominated by an L_2V region at low pressure and an LL region at high pressure. The LLV region is restricted to a well-defined 1 MPa wide band above the vapor pressure of water. The L_2V/L_2 phase behavior boundary is also well-defined. The other phase behavior boundaries (LL/ L_1 , LLV/ L_1V , L_2V/V , L_1V/V) are qualitative as the pressure–composition relationships for them are poorly defined. At 623.2 and 644 K, Figure 2.9b and c, the phase diagrams are qualitatively similar. The pressure range for the LLV region simply expands, and the composition range for the L_2 region broadens.



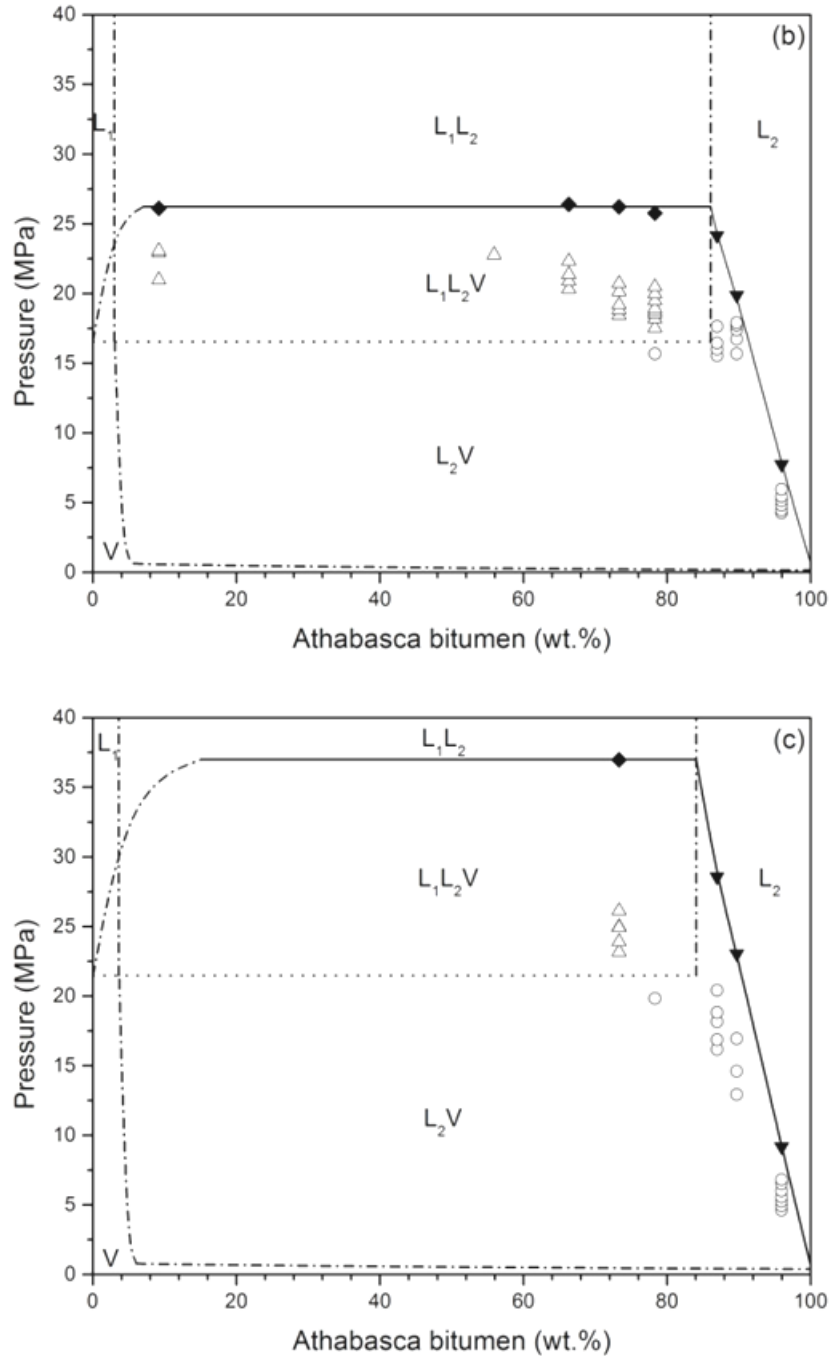


Figure 2.9. Pressure-composition diagrams for Athabasca bitumen + water at fixed temperature: a) 583.2 K, b) 623.2 K, c) 644 K. Measured liquid-vapor (○) and liquid-liquid-vapor (Δ) equilibrium data are shown. The vapor pressure of water obtained from [27]. Solid lines (—) show the LL/LLV and L_2V/L_2 boundaries where points on these boundaries are designated with (◆) and (▼), respectively, and the L_2V/LLV boundary defined by the vapor pressure of water (.....). Boundaries designated with a dash-dot lines (-.-) are illustrative and were not identified experimentally.

Table 2.5. LLV/LL and L₂V/L phase boundaries for Athabasca bitumen + water mixtures

AB (9.2 wt %) + water (90.8 wt %)		
T (K) ± 0.1	P (MPa) ± 0.07	Boundary
522.9	4.2	LLV/LL
548.4	6.2	LLV/LL
572.5	8.9	LLV/LL
582.8	10.7	LLV/LL
592.9	12.9	LLV/LL
603.4	16.2	LLV/LL
613.4*	20.2	LLV/LL
623.2*	27.0	LLV/LL

AB (55.9 wt %) + water (44.1 wt %)		
T (K) ± 0.1	P (MPa) ± 0.07	Boundary
522.9	4.2	LLV/LL
573.3	9.0	LLV/LL
583.0	10.8	LLV/LL
593.0	12.8	LLV/LL
603.6	16.2	LLV/LL
613.2	20.1	LLV/LL

AB (66.3 wt %) + water (33.7 wt %)		
T (K) ± 0.1	P (MPa) ± 0.07	Boundary
523.0	4.2	LLV/LL
548.0	6.0	LLV/LL
573.0	8.7	LLV/LL
583.0	10.7	LLV/LL
593.0	12.7	LLV/LL
602.9	15.7	LLV/LL
613.3	20.2	LLV/LL
623.2*	27.1	LLV/LL

AB (73.3 wt %) + water (26.7 wt %)

T (K) \pm 0.1	P (MPa) \pm 0.07	Boundary
523.1	4.4	LLV/LL
548.2	6.1	LLV/LL
573.4	8.7	LLV/LL
583.3	10.7	LLV/LL
593.2	12.9	LLV/LL
603.6	15.8	LLV/LL
613.5	20.1	LLV/LL
623.1	26.4	LLV/LL
633.9	32.7	LLV/LL
639.2	35.7	LLV/LL

AB (78.3 wt %) + water (21.7 wt %)

T (K) \pm 0.1	P (MPa) \pm 0.07	Boundary
573.2	9.0	LLV/LL
583.3	10.7	LLV/LL
593.3	12.5	LLV/LL
603.9	15.4	LLV/LL
613.5	20.1	LLV/LL
623.0	25.8	LLV/LL
628.5	27.6	LLV/LL
634.0	28.3	LLV/LL

AB (87.7 wt %) + water (12.3 wt %)

T (K) \pm 0.1	P (MPa) \pm 0.07	Boundary
522.9	4.1	LLV/LL
553.2	6.7	LLV/LL
573.6	9.1	LLV/LL
583.2	10.6	LLV/LL
593.3	12.7	LLV/LL
603.7	15.9	LLV/LL
613.6	20.1	LLV/LL
623.4	24.2	LV/L

633.8	26.2	LV/L
643.9	28.6	LV/L

AB (89.7 wt %) + water (10.3 wt %)

T (K) \pm 0.1	P (MPa) \pm 0.07	Boundary
523.0	4.2	LLV/LV
548.3	6.2	LLV/LV
573.0	9.1	LLV/LV
583.2	10.7	LLV/LV
593.1	12.8	LLV/LV
603.4	15.4	LLV/LV
613.5	17.6	LV/L
623.1	19.9	LV/L
633.6	21.4	LV/L
644.0	23.0	LV/L

AB (96.6 wt %) + water (3.4 wt %)

T (K) \pm 0.1	P (MPa) \pm 0.07	Boundary
522.1	4.3	LLV/LL
548.0	5.6	LV/L
572.9	6.8	LV/L
582.8	7.2	LV/L
593.1	7.1	LV/L
603.7	7.3	LV/L
623.4	7.8	LV/L
642.8	9.2	LV/L

*- Values were reduced to reflect the average experiment times at each temperature.

Water + hydrocarbon binary mixtures exhibit Type II, Type IIIa, or Type IIIb phase behavior as illustrated in Figure 2.1. For water + heavy hydrocarbon binaries, Type II and Type IIIb phase behavior are observed [18,19]. These latter phase behavior types are readily distinguished. For Type II phase behavior to arise, the L_1 and L_2 compositions approach one another, and converge at an upper critical end point ($L_1 = L_2 + V$) remote from the critical point of the lighter component. For Type IIIb phase behavior to arise, the

L_1 and L_2 phases possess differing compositions up to a K-point ($L_1 = V + L_2$) near the critical point of lighter component. L_1 and L_2 do not become critically identical. From Figure 2.9a and b, the composition difference between saturated L_1 and L_2 phases is large and changes slowly with temperature. The difference exceeds 90 wt % Athabasca bitumen at 583.2 K (Figure 2.9a) and exceeds 80 wt % Athabasca bitumen at 623.2 K (Figure 2.9b). Further, LLV phase behavior is observed at 644 K (Figure 2.9c), just below the critical temperature of water (647 K), where the mass fraction of Athabasca bitumen in the L_2 phase exceeds 80 wt %. Thus the presence of an upper critical end point ($L_1 = L_2 + V$) is improbable. As the L_1 and V phases possess nominally similar water rich compositions, and the experimental condition is within 3 K of the critical temperature of water, a K-point is probable. Thus even though a K-point ($L_1 = V + L_2$) was not observed the phase behavior of Athabasca bitumen + water mixtures is consistent with Type IIIb phase behavior. A pressure–temperature projection and a series of pressure–composition diagrams at fixed temperature corresponding to this case are shown in Figure 2.10. A rapid succession of phase diagrams is anticipated as the critical temperature of water is approached and exceeded.

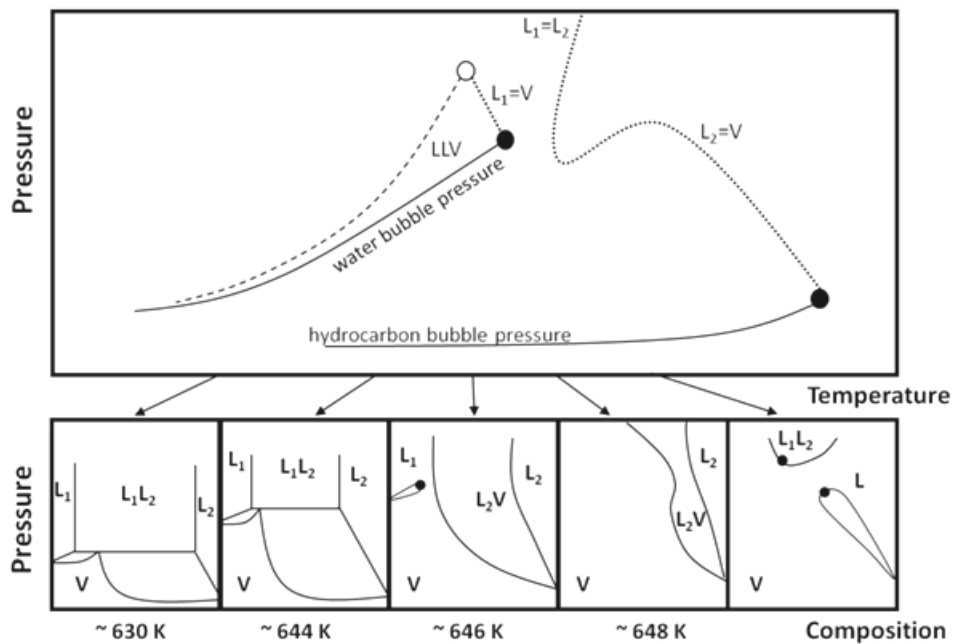


Figure 2.10. Schematic pressure–temperature projection and pressure–composition at fixed temperature phase diagrams for the Athabasca bitumen + water pseudo binary mixture. Pure component vapor pressure curves (—), liquid–gas ($L=V$) and liquid–liquid ($L=L$) critical loci (.....), liquid–liquid vapor curve (---), $L=V$ and $L=L$ critical points (●) and K-point (○).

Thermal reaction of Athabasca bitumen was detected as an increase in pressure with time at fixed volume and temperature, as shown in Figure 2.11. Reported pressures and hence phase behavior boundaries were not corrected for this effect, except as noted in Table 2.5. Based on the duration of experiments (about one hour at each temperature) and the rate of pressure rise at fixed temperature, L_2V/L and LLV/LL boundaries are over estimated by at most 1% at 613 K and 16% at 644 K. Experiments were not conducted at higher temperatures, in part because of the impact of thermal reaction on outcomes, and in part because water was corroding the interior surfaces of the view cell. While these effects are not insignificant, they are not expected to affect the phase behavior type designation for the Athabasca bitumen + water mixture.

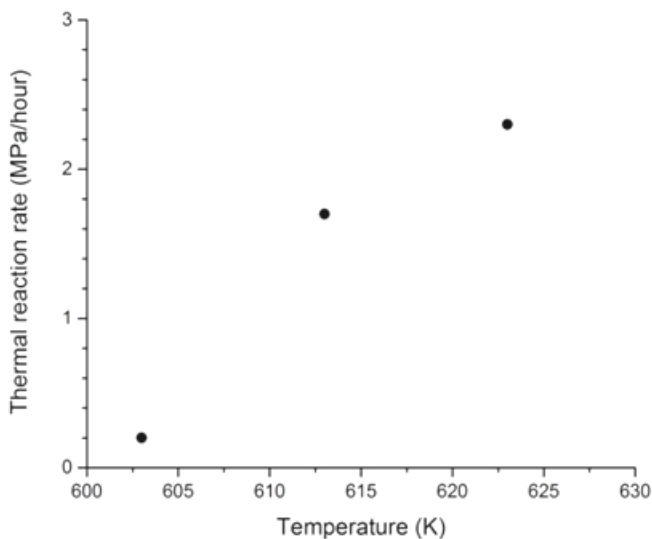


Figure 2.11. Thermal reaction rates for 9.2 (●) and 66.3 (○) wt % Athabasca bitumen + water mixtures.

Upcoming contributions will address the solubility of water in the bitumen-rich liquid phase, volume of mixing and the impact of diluent addition on the phase behavior of bitumen + water mixtures.

2.4 Conclusion

The phase behavior of Athabasca bitumen + water mixtures was investigated from, 9.2 to 96.6 wt % Athabasca bitumen, over the temperature interval 522.1–644 K, and the pressure interval 4.2–35.7 MPa. The apparatus and procedures were validated using known properties of pure fluids and binary mixtures where reported phase boundary

temperatures, pressures, and compositions were reproduced to within 0.5 K, 0.2 MPa, 0.1 wt % respectively for water + toluene and water + 1-methylnaphthalene binary mixtures from 453 to over 573 K. Pressure–temperature at fixed composition and pressure–composition at fixed temperature phase diagrams were prepared for the Athabasca bitumen + water pseudo binary mixture. Based on the composition difference between the water-rich and the Athabasca bitumen-rich liquid phases, the trend in this difference with temperature, and the observation of LLV phase behavior adjacent to the critical point of water, the phase behavior designation Type IIIb according to the van Konynenburg and Scott classification scheme is assigned to the mixture. Thermal reaction of Athabasca bitumen impacts the phase boundary pressures at temperatures exceeding 620 K but does not appear to impact the phase behavior type designation for the mixture.

2.5 References

- [1] A. Kruse, E. Dinjus, Hot compressed water as reaction medium and reactant-2. Degradation reactions, *Journal of Supercritical Fluids* 41 (2007) 361–379.
- [2] A. Kruse, E. Dinjus, Hot compressed water as reaction medium and reactant – properties and synthesis reactions, *Journal of Supercritical Fluids* 39 (2007) 362–380.
- [3] L.-n. Han, R. Zhang, J.-c. Bi, Upgrading of coal-tar pitch in supercritical water, *Journal of Fuel Chemistry and Technology* 36 (2008) 1–5.
- [4] T. Sato, T. Adschiri, K. Arai, G.L. Rempel, F.T.T. Ng, Upgrading of asphalt with and without partial oxidation in supercritical water, *Fuel* 82 (2003) 1231–1239.
- [5] L.N. Han, R. Zhang, J.C. Bi, Experimental investigation of high-temperature coal tar upgrading in supercritical water, *Fuel Processing Technology* 90 (2009) 292–300.
- [6] Z.M. Cheng, Y. Ding, L.Q. Zhao, P.Q. Yuan, W.K. Yuan, Effects of supercritical water in vacuum residue upgrading, *Energy and Fuels* 23 (2009) 3178–3183.
- [7] M. Morimoto, Y. Sugimoto, Y. Saotome, S. Sato, T. Takanohashi, Effect of supercritical water on upgrading reaction of oil sand bitumen, *The Journal of Supercritical Fluids* 55 (2010) 223–231.
- [8] M. Watanabe, S.-n. Kato, S. Ishizeki, H. Inomata, R.L. Smith Jr., Heavy oil upgrading in the presence of high density water: basic study, *The Journal of Supercritical Fluids* 53 (2010) 48–52.

- [9] W. Wahyudiono, T. Shiraishi, M. Sasaki, M. Goto, Bitumen upgrading under solvothermal/hydrothermal conditions, *Research on Chemical Intermediates* 37 (2011) 375–381.
- [10] K. Arai, T. Adschiri, Importance of phase equilibria for understanding supercritical fluid environments, *Fluid Phase Equilibria* 158–160 (1999) 673–684.
- [11] T.W. De Loos, A.J.M. Wijen, G.A.M. Diepen, Phase equilibria and critical phenomena in fluid (propane + water) at high pressures and temperatures, *The Journal of Chemical Thermodynamics* 12 (1980) 193–204.
- [12] T.W. De Loos, W.G. Penders, R.N. Lichtenthaler, Phase equilibria and critical phenomena in fluid (n-hexane + water) at high pressures and temperatures, *The Journal of Chemical Thermodynamics* 14 (1982) 83–91.
- [13] T.W. De Loos, J.H. van Dorp, R.N. Lichtenthaler, Phase equilibria and critical phenomena in fluid (n-alkane + water) systems at high pressures and temperatures, *Fluid Phase Equilibria* 10 (1983) 279–287.
- [14] T. Yiling, T. Michelberger, E.U. Franck, High-pressure phase equilibria and critical curves of (water + n-butane) and (water + n-hexane) at temperatures to 700 K and pressures to 300 MPa, *The Journal of Chemical Thermodynamics* 23 (1991) 105–112.
- [15] Q. Wang, K.-C. Chao, Vapor–liquid and liquid–liquid equilibria and critical states of water + n-decane mixtures, *Fluid Phase Equilibria* 59 (1990) 207–215.
- [16] R.L. Stevenson, D.S. LaBracio, T.A. Beaton, M.C. Thies, Fluid phase equilibria and critical phenomena for the dodecane–water and squalane–water systems at elevated temperatures and pressures, *Fluid Phase Equilibria* 93 (1994) 317–336.
- [17] S.P. Christensen, M.E. Paulaitis, Phase equilibria for tetralin–water and 1-methylnaphthalene–water mixtures at elevated temperatures and pressures, *Fluid Phase Equilibria* 71 (1992) 63–83.
- [18] E. Brunner, Fluid mixtures at high pressures IX. Phase separation and critical phenomena in 23 (n-alkane + water) mixtures, *The Journal of Chemical Thermodynamics* 22 (1990) 335–353.
- [19] E. Brunner, M.C. Thies, G.M. Schneider, Fluid mixtures at high pressures: phase behavior and critical phenomena for binary mixtures of water with aromatic hydrocarbons, *The Journal of Supercritical Fluids* 39 (2006) 160–173.
- [20] P.H. Vankonynenburg, R.L. Scott, Critical lines and phase-equilibria in binary vanderwaals mixtures, *Philosophical Transactions of the Royal Society of London. Series A. Mathematical Physical and Engineering Sciences* 298 (1980) 495–540.

- [21] A. Bazyleva, M. Fulem, M. Becerra, B. Zhao, J.M. Shaw, Phase behavior of Athabasca bitumen, *Journal of Chemical and Engineering Data* 56 (2011) 3242–3253.
- [22] M.R. Gray, P. Jokuty, H. Yeniova, L. Nazarewycz, S.E. Wanke, U. Achia, A. Krzywicki, E.C. Sanford, O.K.Y. Sy, The relationship between chemical-structure and reactivity of Alberta bitumens and heavy oils, *Canadian Journal of Chemical Engineering* 69 (1991) 833–843.
- [23] O.P. Strausz, E.M. Lown, A. Morales-Izquierdo, N. Kazmi, D.S. Montgomery, J.D. Payzant, J. Murgich, Chemical composition of Athabasca bitumen: the distill-able aromatic fraction, *Energy and Fuels* 25 (2011) 4552–4579.
- [24] X.Y. Zou, X.H. Zhang, J.M. Shaw, Phase behavior of Athabasca vacuum bottoms plus n-alkane mixtures, *SPE Production and Operation* 22 (2007) 265–272.
- [25] X.H. Zhang, *The Impact of Multiphase Behavior on Coke Deposition in Heavy Oil Hydroprocessing Catalysts*, University of Alberta, Edmonton, 2006.
- [26] S.J. Abedi, H.Y. Cai, S. Seyfaie, J.M. Shaw, Simultaneous phase behaviour, elemental composition and density measurement using X-ray imaging, *Fluid Phase Equilibria* 158 (1999) 775–781.
- [27] E.W. Lemmon, M.O. McLinden, D.G. Friend, Thermophysical properties of fluid systems, in: P.J. Linstrom, W.G. Mallard (Eds.), *NIST Chemistry WebBook*, NIST Standard Reference Database Number 69, National Institute of Standards and Technology, Gaithersburg MD, 2012.
- [28] F.E. Anderson, J.M. Prausnitz, Mutual solubilities and vapor-pressures for binary and ternary aqueous systems containing benzene, toluene, meta-xylene, thiophene and pyridine in the region 100–200 °C, *Fluid Phase Equilibria* 32 (1986) 63–76.
- [29] K. Chandler, B. Eason, C.L. Liotta, C.A. Eckert, Phase equilibria for binary aqueous systems from a near-critical water reaction apparatus, *Industrial and Engineering Chemistry Research* 37 (1998) 3515–3518.
- [30] H.Y. Cai, J.M. Shaw, K.H. Chung, Hydrogen solubility measurements in heavy oil and bitumen cuts, *Fuel* 80 (2001) 1055–1063.
- [31] I.G. Economou, J.L. Heidman, C. Tsonopoulos, G.M. Wilson, Mutual solubilities of hydrocarbons and water.3. 1-hexene, 1-octene C-10-C-12 hydrocarbons, *AIChE Journal* 43 (1997) 535–546.
- [32] J.L. Heidman, C. Tsonopoulos, C.J. Brady, G.M. Wilson, High-temperature mutual solubilities of hydrocarbons and water. 2. Ethylbenzene, ethylcyclohexane, and normal-octane, *AIChE Journal* 31 (1985) 376–384.

- [33] C. Tsonopoulos, Thermodynamic analysis of the mutual solubilities of hydrocarbons and water, *Fluid Phase Equilibria* 186 (2001) 185–206.
- [34] C. Tsonopoulos, Thermodynamic analysis of the mutual solubilities of normal alkanes and water, *Fluid Phase Equilibria* 156 (1999) 21–33.
- [35] D.-Y. Peng, D.B. Robinson, A new two-constant equation of state, *Industrial and Engineering Chemistry Fundamentals* 15 (1976) 59–64.

Chapter 3. Volume of mixing and solubility of water in Athabasca bitumen at high temperature and pressure¹

3.1 Introduction

The Phase behavior, mutual solubility and other physical property data for water + hydrocarbon mixtures are necessary for the development, design and optimization of a variety of high temperature industrial processes such as bitumen production and upgrading (Chapter 2, [1]). The properties of mixtures of water + Athabasca bitumen and other heavy hydrocarbons are of growing interest because water, at high temperature, provides a reaction medium for upgrading heavy hydrocarbons [2-10] that may prove to be preferred over conventional hydrocarbon based ones. In addition to upgrading applications, the solubility and volume of mixing of water in heavy hydrocarbon resources are essential to the development of production models for oil and bitumen production processes such as the Steam Assisted Gravity Drainage (SAGD) method where net water consumption, and water recycling present both environmental and economic challenges [11]. This study was also motivated by the potential to reduce the overall cost of production of finished products in the future by merging aspects of fluid composition and operating conditions for in situ production and upgrading processes. For example, water is already used in production and the solvent properties and solubility of water in the near-critical region make it an efficient medium for carrying out chemical reactions, and the changes of water solubility with temperature and pressure may facilitate subsequent water-hydrocarbon separation and water reuse.

The thermophysical properties and phase behavior of water-hydrocarbon mixtures at high-temperature have received limited attention and there are few benchmark data sets available to underpin industrial process design, development or optimization. Data are available for a limited number of pure hydrocarbon + water and hydrocarbon mixture + water cases. Maczynski et al. [12-23] reviewed and critically compiled the published data for mutual solubilities of C₅-C₃₆ hydrocarbons + water/seawater mixtures. Their compilation provides a comprehensive collection of mutual binary solubility data over a broad range of temperatures. Brown et al. [24] provide solubility data for binary mixtures

¹ This chapter with minor modifications has been published in the journal of Fluid Phase Equilibria: M. J. Amani, M. R. Gray, and J. M. Shaw, *Fluid Phase Equilibria*, DOI: 10.1016/j.fluid.2013.07.021.

of water with acetophenone, anisole, 1-octanol and toluene in the temperature range of 370 K to 550 K. Tsionopoulos et. al [25-30] measured and correlated mutual solubility data for hydrocarbon + water binaries under three phase liquid-liquid-vapor equilibrium conditions up to their upper critical end points (UCEP) where for example, the phase compositions of both liquid phases for homologous series of alkanes, alkyl cyclohexanes, 1-alkenes, and alkyl benzenes at high temperatures are reported [30]. Chandler [31] reported the mutual solubilities of toluene + water and benzene + water up to 473 K along the LLV three-phase curve up to a pressure of 17.2 MPa. Anderson et al. [32] investigated the mutual solubilities and vapor pressures for four binary and one ternary aqueous mixture. Leet et al. [33] studied the mutual solubilities of water and six polycyclic aromatic hydrocarbons including N-, O-, and S-containing polycyclic aromatics at high temperatures. Neely et al. [34] measured the mutual hydrocarbon–water liquid-liquid equilibrium data for mixtures comprising the benzene, toluene, and 3-methylpentane in a temperature range from ambient temperature up to 500 K. Brunner [35, 36] studied the phase behavior and critical phenomena of water + n -alkanes binary mixtures (up to n-eicosane) and water + aromatic compounds at pressures and temperatures exceeding the critical point of water. Phase equilibrium measurements for water + tetralin and 1-methylnaphthalene, up to 673.2 K, are also available [37]. Phase equilibrium data for reservoir fluids, including water, are very scarce. De Hemptinne et al. [38] investigated the phase equilibria of petroleum fractions + water mixtures and Pedersen [39] reported equilibrium compositions, three-phase equilibrium pressure and temperatures for water + petroleum reservoir fluids up to 473 K.

High-temperature experimental phase density and excess volume data for hydrocarbon + water mixtures are limited to a few studies. Abdulagatov et al. [40-45] conducted measurements for water + n-pentane to n-octane, and water + benzene at temperatures near the critical point of water and report liquid phase thermodynamic properties and partial molar volumes. Furutaka et al. [46-50] measured compositions and densities of hydrocarbon-rich phases at equilibrium for water + benzene, toluene, ethylbenzene, n-hexane and n-decane mixtures in the vicinity of the upper end critical point of these mixtures using infrared spectroscopy. Their work focused on unsaturated hydrocarbon-rich phases at pressures above the LLV three-phase curve. They report large and positive volumes of mixing for hydrocarbon-rich liquids. Hnedkovsky et al. [51, 52] present phase density and partial molar volume data of hydrocarbons at infinite dilution for water-rich

liquid phases where the hydrocarbons include benzene, toluene, and cresols over the temperature interval 298.15 to 573.15 K.

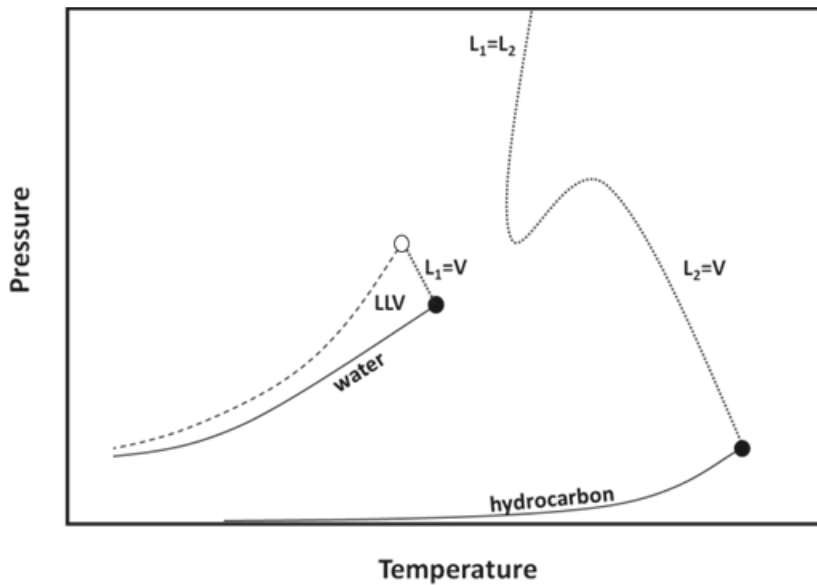


Figure 3.1. Type IIIb pressure-temperature projection for water + hydrocarbon binary mixtures. (●) critical points for the water and the hydrocarbon, and (○) the UCEP for the mixture. (.....) and (---) are the critical locus and LLV three-phase curve respectively and (—) denotes vapor/bubble pressure curves (Chapter 2).

In our prior work we showed that the Athabasca bitumen + water pseudo binary mixture exhibits Type IIIb phase behavior (Chapter 2) according to the naming scheme of van Konynenburg and Scott [53]. Type IIIb phase behavior occurs because for this hydrocarbon + water mixture the hydrocarbon critical temperature is much higher than the critical temperature of water [35, 36]. The key characteristics of Type IIIb phase behavior are illustrated in Figure 3.1. The LLV three-phase equilibrium curve extends from low temperature up to the vicinity of the critical point of water where it is intersected by the liquid-vapor critical locus extending from the critical point of water. This intersection, the upper critical point (UCEP), is where the water-rich liquid and vapor phases become critically identical. Above the UCEP temperature a maximum of two phases arise in the phase diagram. This phase behavior contrasts with the behavior of typical hydrocarbon + water mixtures, available in the literature, which exhibit Type II or Type IIIa phase behavior as discussed previously in Chapter 2. For Type IIIa phase behavior, the hydrocarbon-rich phase becomes critically identical to the vapor phase at the upper critical end point. At low temperatures, the properties of Type IIIa and Type

IIIb binary mixtures differ little but they are expected to diverge at high temperatures. The high temperature properties of the hydrocarbon-rich liquid phase are the focus of the current study where phase compositions, and excess volumes for model hydrocarbon + water mixtures are used to benchmark measurements for water + Athabasca bitumen mixtures and to place them in a broader context.

3.2 Experiments and methodology

d Athabasca bitumen, provided by Syncrude Canada Ltd, Alberta, Canada, was produced by a commercial froth treatment process. SARA analysis for Athabasca bitumen is presented in Chapter 2 and [54]. The properties of used water, toluene and 1-methylnaphthalene are described in Chapter 2.

A schematic of the X-ray view cell is shown in Figure 3.2. Detailed descriptions of the apparatus and operating procedures, along with illustrative applications have been reported in a series of recent publications [55-57]. In brief, the view cell consists of a beryllium cylinder with an approximate total internal volume of 200 cm³. The upper end cap includes a variable volume bellows and the view cell volume is controlled by back pressuring the bellows using high-pressure nitrogen. The cell is equipped with a magnet stirrer resting on the fixed lower end cap, and feed lines allow for both gas and liquid injection and air removal once the cell is assembled. More details can be find in Chapter 2. In this work, the cell volume was carefully calibrated and digital images were processed to identify interface elevations and hence phase volumes. This approach was found to be more accurate than calibrating transmitted x-ray intensity with phase density. The experimental approach, and calibration and operation procedures were validated by reproducing published experimental and recommended water, 1-methylnaphthalene, and water + toluene and water + 1-methylnaphthalene binary mixtures properties.

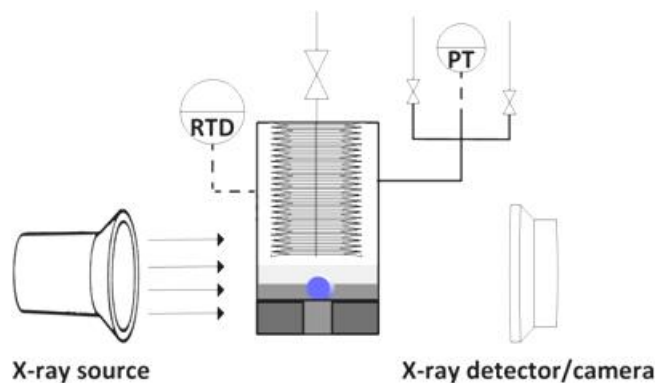


Figure 3.2. The X-ray view cell schematic. The view-cell is equipped with a variable volume bellows and a magnetic stirrer.

3.2.1 Water solubility measurement validation

Reliable measurement of mutual solubilities is challenging at elevated temperatures and pressures, and analysis of the phase compositions at equilibrium is subject to large errors [32]. To avoid the difficulties associated with sampling and subsequent analysis, experimentally measured points on the LV-L boundary that are close to the LLV boundary are extrapolated linearly to the experimentally identified LLV three phase pressure as illustrated in Figure 3.3a (mass basis) and Figure 3.3b (mole basis) for water + tetralin at 573.2 K [37]. These pressure-composition (at fixed temperature) diagrams are typical for Type II and Type III phase behaviors at temperatures below the UCEP and the approach, illustrated on both a mole and a mass basis, is akin to Luks' conjugate pair approach [58] for phase boundary identification. Here, points on the hydrocarbon-rich LV-L boundary are extrapolated to the intersection with the LL-LLV boundary. The composition at the point of intersection is the water-saturated hydrocarbon-rich liquid phase composition. This composition determines the maximum fraction or solubility of water in the hydrocarbon-rich phase. As high-temperature and high-pressure phase behavior measurements are time consuming, costly, and challenging, only a few LV-L transition points can be measured in practice. The difference between measured and extrapolated solubilities is minimized if LV-L transition data are available close to the solubility limit.

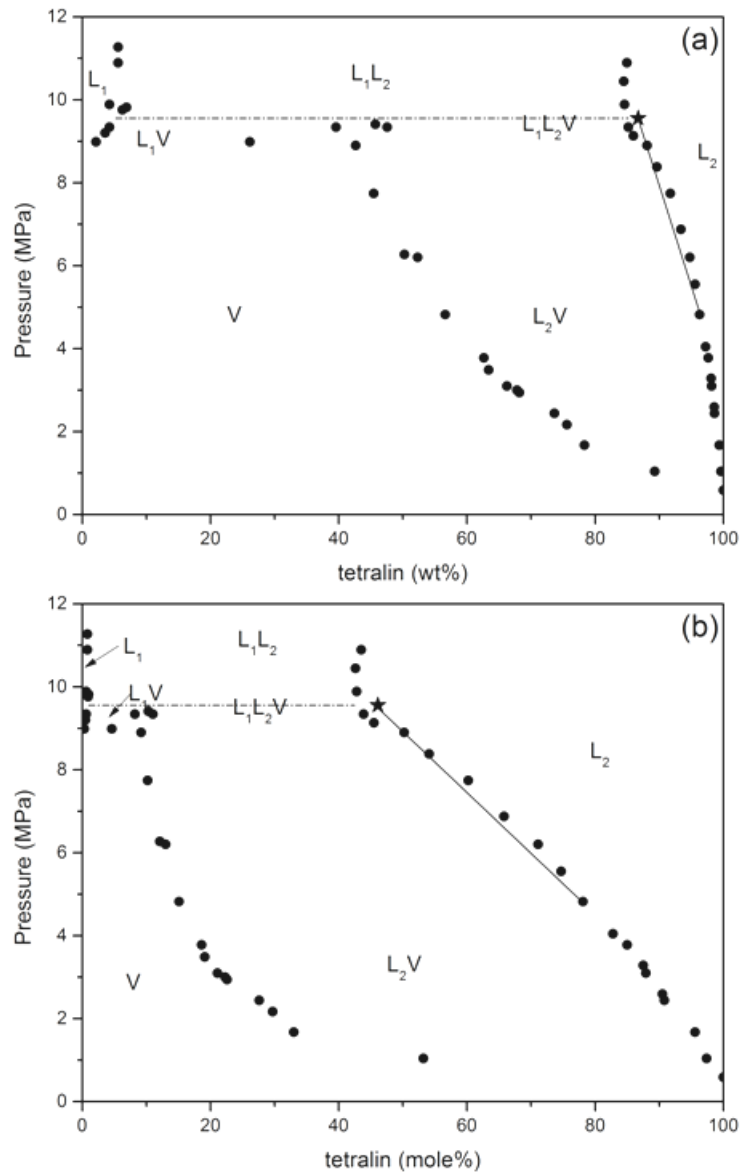


Figure 3.3. P-x diagrams for tetralin + water at 573.2 K: (a) mass-based and (b) mole-based. The experimental data (●) and the three-phase line (---) are from Christensen [37] and (★) is the estimated composition of the saturated tetralin-rich liquid.

This experimental approach was validated by reproducing water solubility in hydrocarbon-rich liquid data for the water + toluene and water + 1-methylnaphtalene binary mixtures. These experimental solubility results, based on as few as 2 LV-L transition points (including the pure hydrocarbon vapor pressure) per solubility measurement, are reported in Tables 3.1 and 3.2. The data, obtained in this manner, fall within the scatter of the literature data as shown in Figure 3.4. While precise measurement is unlikely, the quality of the results obtained using this indirect and non-

intrusive technique under extreme conditions vis-à-vis more complex approaches is encouraging from a technique development perspective. These validation results may also contribute to, but cannot resolve debates on the relative merits of compiled [21] versus measured experimental [26] data for water solubility in 1-methylnaphthalene at high temperature.

Table 3.1. Water solubility in toluene (wt %)

T (K)	wt %	# of LV-L points
513.1	7.5 ± 0.6	6
533.1	11.5 ± 1.3	4
553.2	19.0 ± 2.5	2

Table 3.2. Water solubility in 1-methylnaphthalene (wt %)

T (K)	wt %	# of LV-L points
533.3	5.7 ± 0.9	2
553.6	7.4 ± 1.4	2
573.2	13.6 ± 3.0	3

3.2.2 Liquid density measurement validation

As water was used to calibrate view-cell volume and the density of 1-methylnaphthalene is closer to that of bitumen + water mixtures than toluene, 1-methylnaphthalene was used for density measurement validation. The results are presented and compared to NIST recommended values [59] in Table 3.3. The two sets of values agree to within 5 kg/m^3 on average over the temperature interval 326.5 to 573.8 K. It is worth noting that the uncertainty of the NIST recommended values increases sharply with temperature, especially above 470 K. The uncertainty of the digital measurements reported here declines with increasing temperature, because the uncertainty is linked primarily to the height of an individual pixel (fixed) in a digital image divided by the number of pixels (proportional to volume which increasing with temperature). Thus the validation data reduce the uncertainty and improve the confidence limits for 1-methylnaphthalene liquid density measurements at high temperatures.

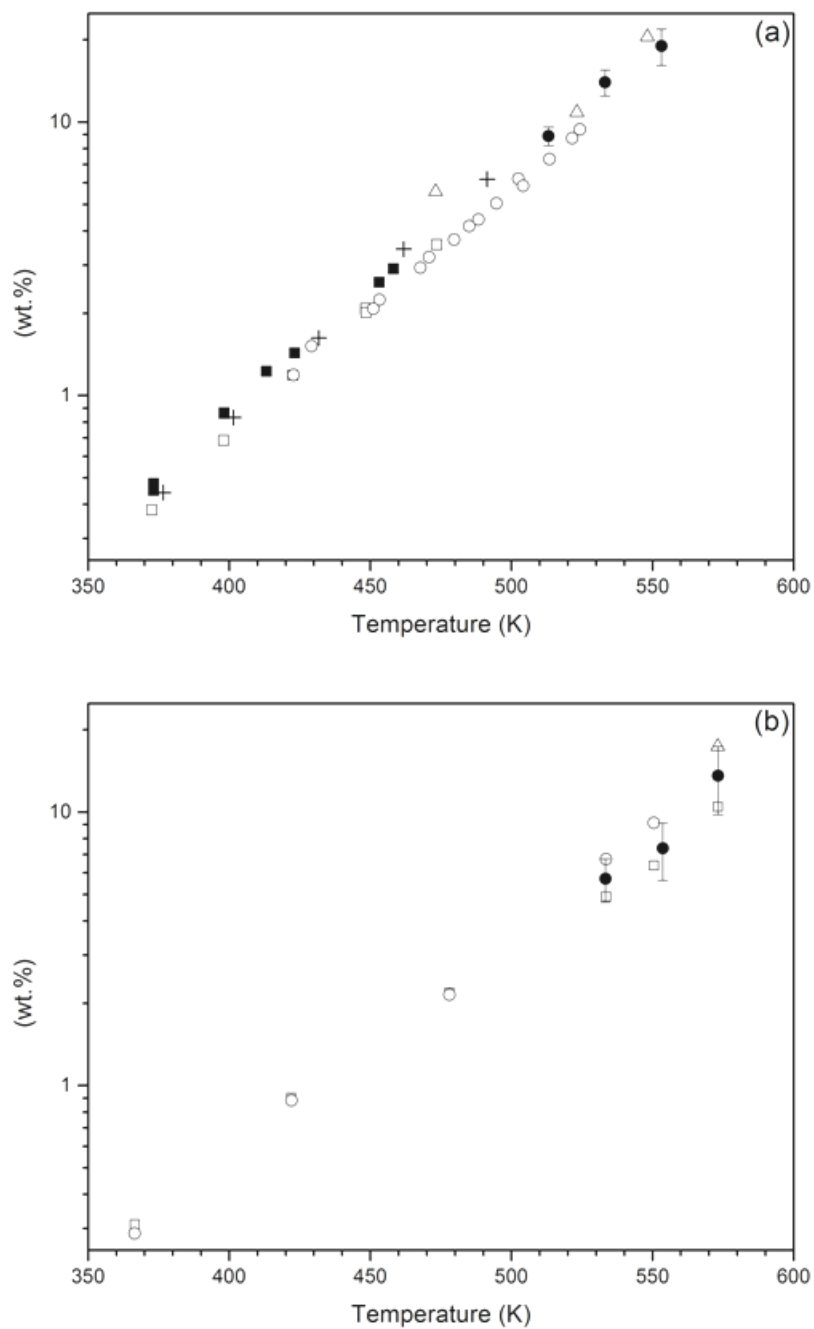


Figure 3.4. The solubility of water in: a) toluene (this work (●), Anderson et al. [32] (□), Brown et al. [24] (○), Chandler et al. [31] (Δ), Jou et al. [65] (■) and Neely et al. [34] (+)) and in b) 1-methylnaphthalene (this work (●), Economou et al. [26] (○), Christensen et al. [37] (Δ), and compilation of the former data by Shaw et al. [21] (□)).

Table 3.3. Saturated density of liquid 1-methylnaphthalene (kg/m³)

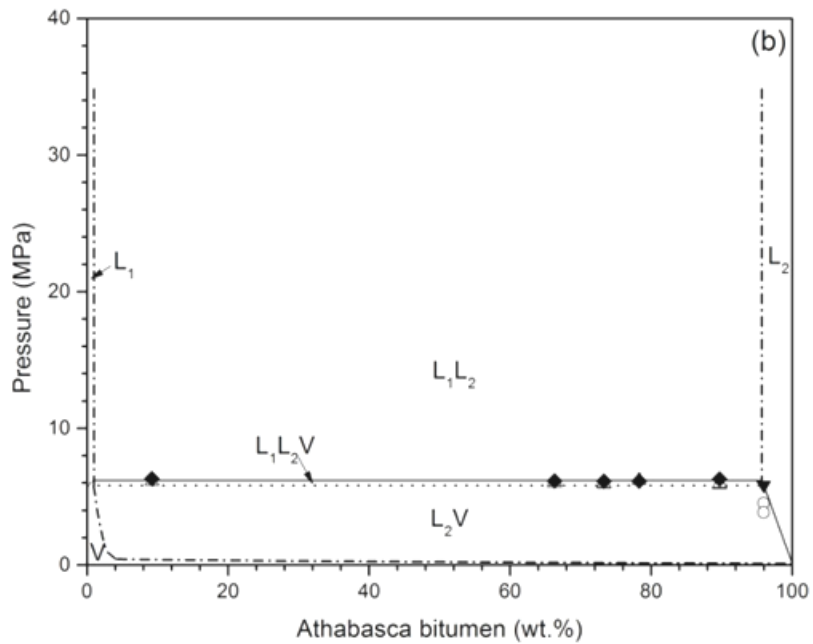
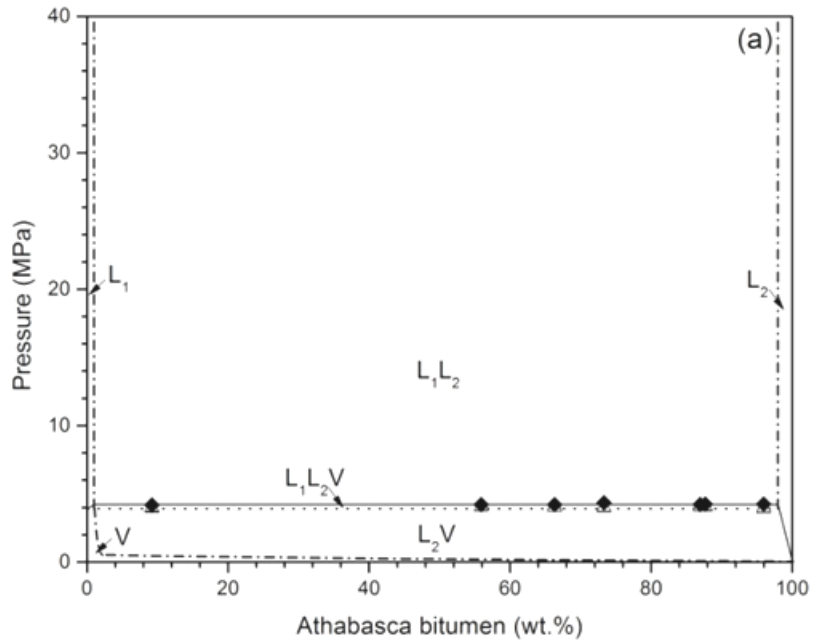
T (K)	This work	NIST [59]
326.5	1001 ± 13	994.3 ± 1.1
341.9	984 ± 13	982.7 ± 1.3
370.7	967 ± 12	961.4 ± 1.9
396.4	949 ± 12	942.4 ± 2.8
420.9	926 ± 11	924.2 ± 3.7
447.4	902 ± 11	903.9 ± 4.9
472.4	874 ± 10	884.1 ± 6.8
498.2	852 ± 9	863 ± 10
522.3	828 ± 9	841 ± 16
547.5	812 ± 8	817 ± 25
573.8	787 ± 8	790 ± 37

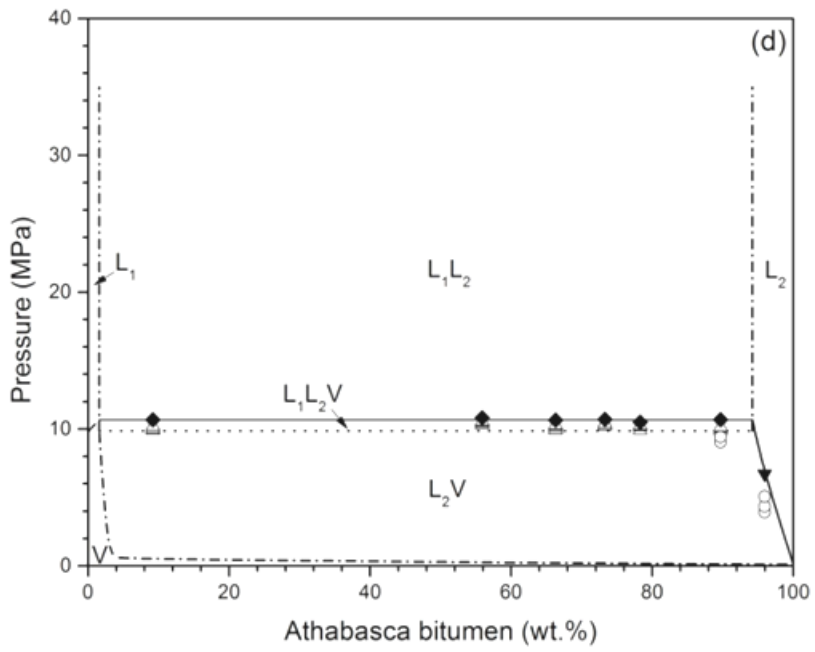
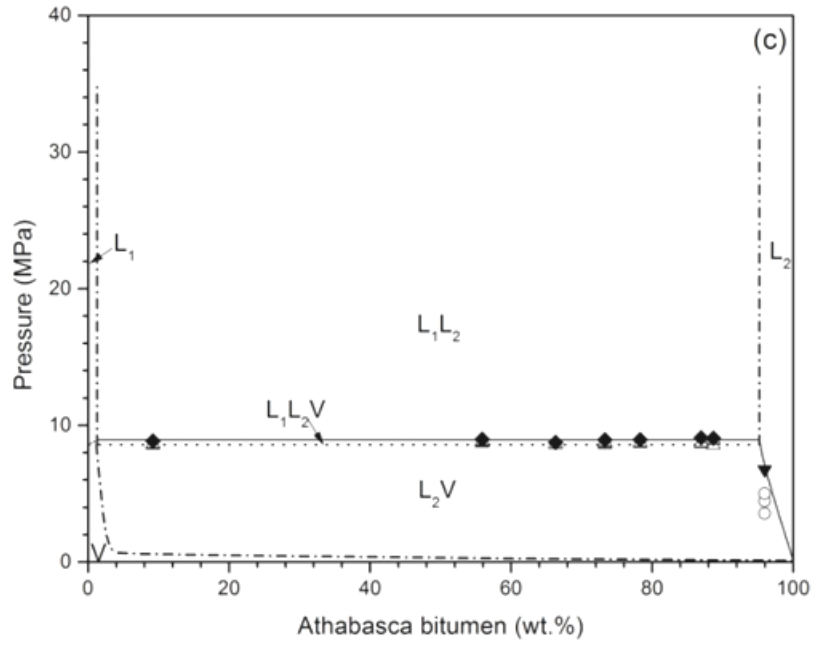
3.3 Results and discussion

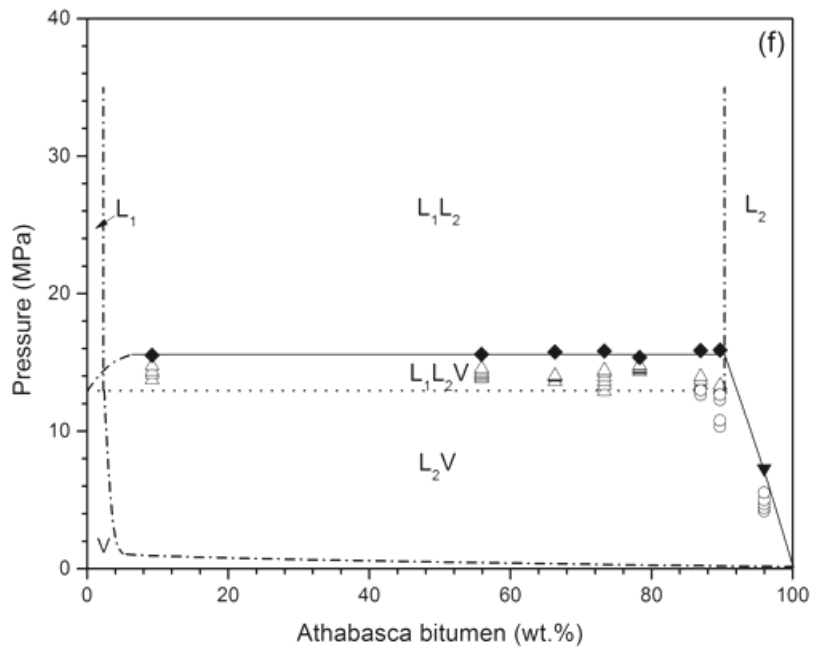
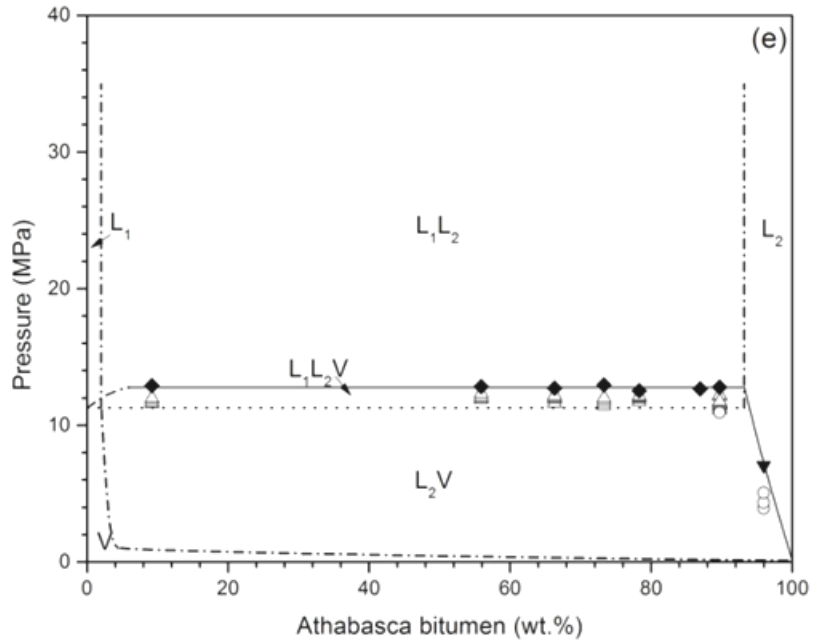
3.3.1 Solubility of water in bitumen

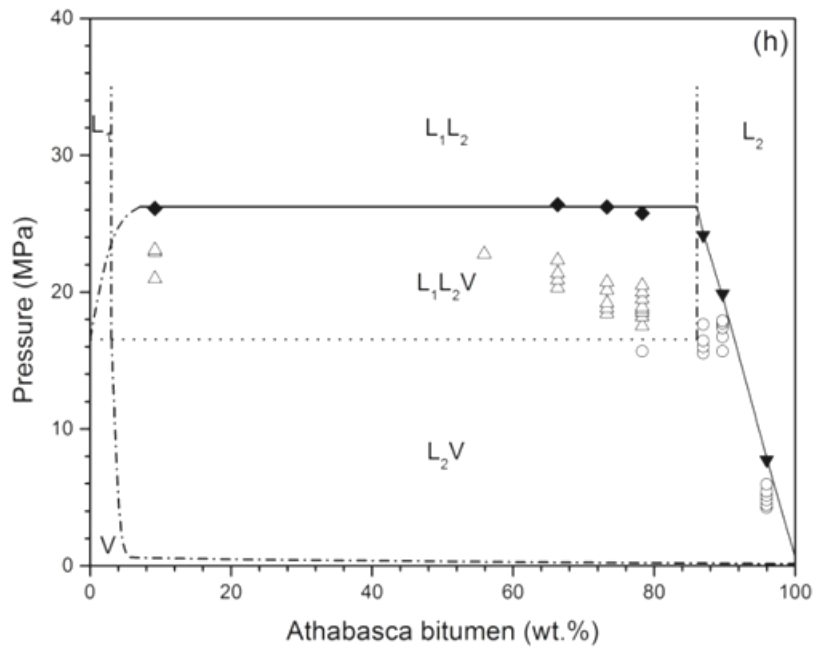
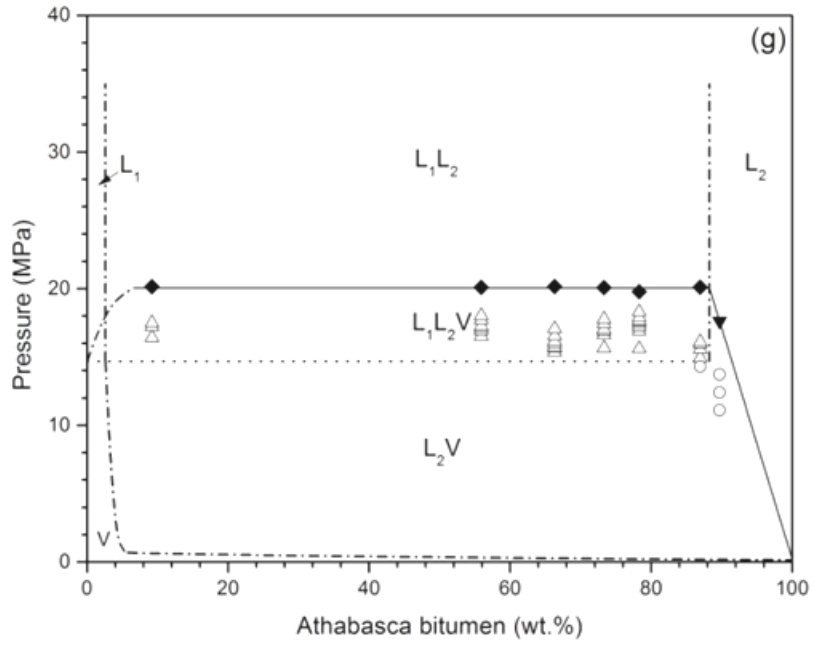
Pressure – composition diagrams at 523.0 K, 548.2 K, 573.1 K, 583.2 K, 593.1 K, 603.5 K, 613.4 K, 623.2 K, 633.8 K, 644.0 K for Athabasca bitumen + water mixtures, presented and described in detail in Chapter 2, are reproduced as Figures 3.5a-j so that the method for determining water solubility in bitumen is apparent. In Figures 3.5a-g, the solubility was determined from a minimum of five points defining the LLV-LL transition and two points defining the LV-L transition. On the scale of the Figures, the bubble pressure of the Athabasca bitumen is negligible. At higher temperatures, Figures 3.5h-j, there are fewer points defining the LLV-LL transition and more defining the LV-L transition. Above 600 K thermal degradation of Athabasca bitumen affects mixture composition and increases the apparent bubble pressure as a consequence of light hydrocarbon formation. Rates of pressure rise with time were measured and bubble pressures were found to be overestimated by approximately 1% at 613 K and 16% at 644 K based on the duration of experiments. Reported pressures were corrected for this effect. Solubility values for water in Athabasca bitumen, along with their uncertainty are reported in Table 3.4 and are shown in the context of available solubility data for water in

other pertinent pure and mixed hydrocarbons in Figure 3.6a. Water solubility in Athabasca bitumen is approximately one order of magnitude lower than in low molar mass hydrocarbons such as toluene irrespective of temperature.









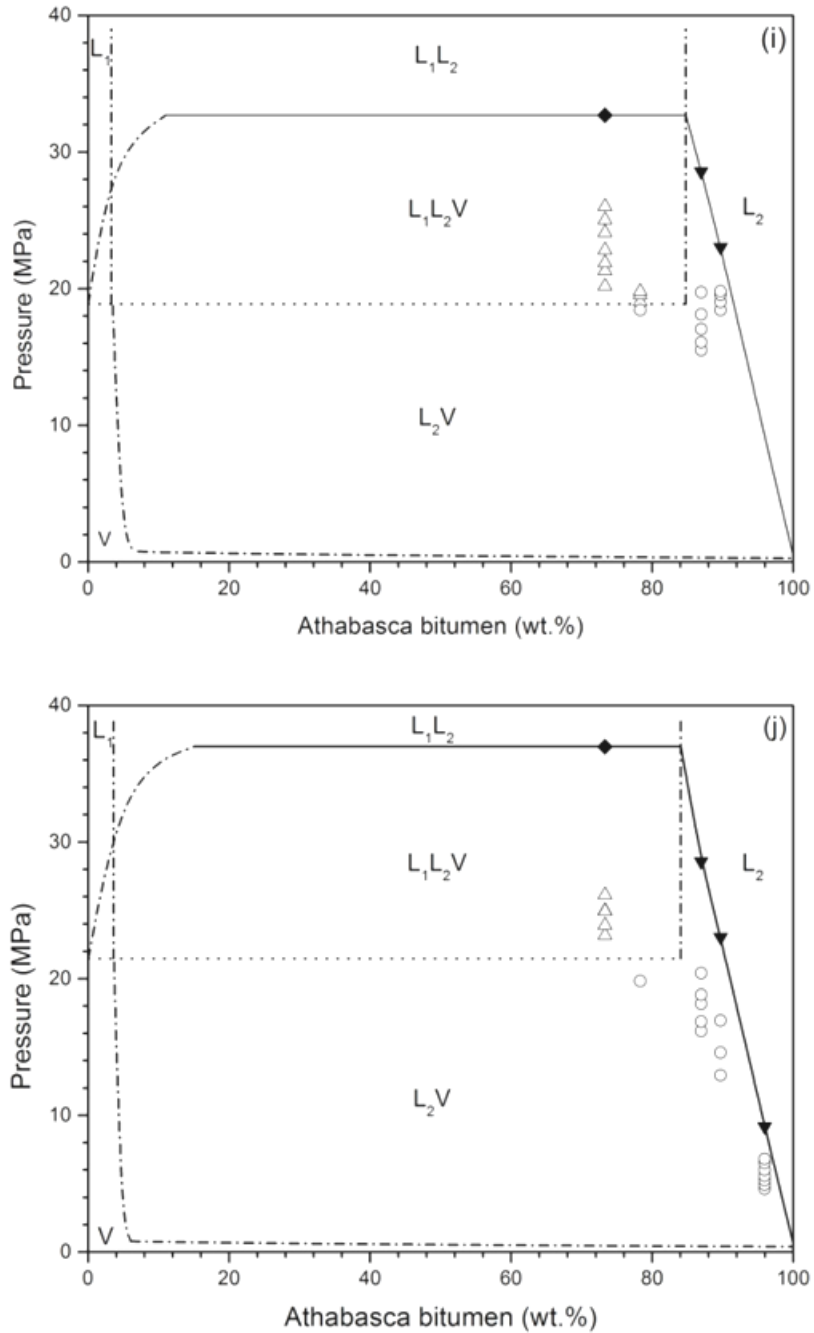


Figure 3.5. Pressure-composition diagrams for Athabasca bitumen + water at fixed temperature: (a) 523.0 K (b) 548.2 K, (c) 573.1 K, (d) 583.2 K, (e) 593.1 K, (f) 603.5 K, (g) 613.4 K, (h) 623.2 K, (i) 633.8 K, (j) 644. Measured liquid-vapor (○) and liquid-liquid-vapor (△) equilibrium data are shown. The vapor pressure of water obtained from [59]. Solid lines (—) show the LL/LLV and L_2V/L_2 boundaries where points on these boundaries are designated with (◆) and (▼), respectively, and the L_2V/LLV boundary defined by the vapor pressure of water (.....). Boundaries designated with a dash-dot lines (-.-) are illustrative and were not identified experimentally.

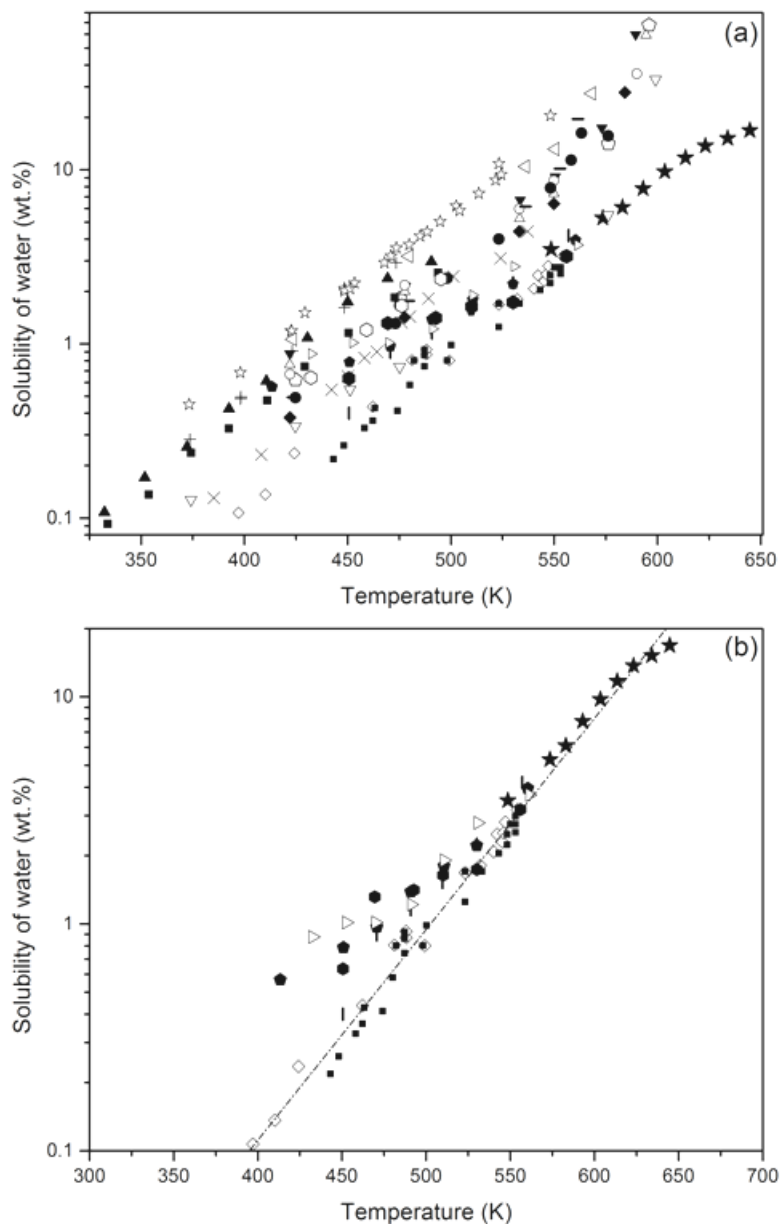


Figure 3.6. Solubility of water in Athabasca bitumen, this work (\star), and in other hydrocarbons: a) all available hydrocarbons; b) high molar mass compounds and heavy oils, and equation 3-1 (---). Symbols: toluene (\star) [24, 31, 32], ethylbenzene (\triangleleft) [27], m-xylene (+) [32], ethylcyclohexane (-) [27], n-octane (\square) [27], tetralin (\circ) [26], 1,2,3,4-Tetrahydroquinoline [33], thianaphthene (\blacktriangle) [33], cis-decalin (∇) [26], 1-butylcyclohexane (\blacklozenge) [26], decane (\bullet) [26], 1-methylnaphthalene (\blacktriangledown) [26], 1-ethylnaphthalene (\triangle) [26], 1,4-diisopropylbenzene (\circ) [26], 9,10-dihydrophenanthrene (\blacksquare) [33], naphtha (\circ , Mw = 147) [60], kerosene (\times , Mw = 173) [60], lubricating oil (\diamond , Mw = 425) [60], gross oil mixtures (\blacksquare , Mw = 425) [63], Coalinga crude oil (\circ , Mw = 439) [61], Huntington Beach crude oil (\bullet , Mw = 442) [61], Peace River crude oil (\bullet , Mw = 571) [61] Cat Canyon crude oil (\triangleright , Mw = 627) [61].

Table 3.4. Solubility of water in the bitumen-rich liquid phase.

T (K)	wt %	uncertainty (wt %)
548.2	3.7	1.1
573.1	5.3	1.5
583.2	6.2	1.8
593.1	7.7	2.2
603.5	8.8	2.2
613.4	11.3	1.2
623.2	13.5	1.1
633.8	15.2	1.4
644	16.9	1.5

Table 3.5. Density of Athabasca bitumen

T (K)	Density (kg/m ³)	uncertainty (kg/m ³)
377.2	986.6	9.5
399.8	976.7	9.3
422.8	963.7	9.0
446.9	943.8	8.6
472.0	929.7	8.4
492.3	917.9	8.2
513.4	906.5	8.0
533.4	895.3	7.8
552.6	881.7	7.6
571.3	871.1	7.4
594.2	855.6	7.1
603.5	850.6	7.0
614.0	840.8	6.9
624.2	833.5	6.8
633.8	824.0	6.6
643.5	814.8	6.5

The data in this work extend the existing water in hydrocarbon solubility data set for heavy hydrocarbon mixtures of industrial importance up to the critical point of water. The data are also well aligned with water solubility data in high-molar mass polynuclear aromatic compounds, lubricating oil [60], Coalinga crude oil, Huntington Beach crude oil and Peace River crude oil [61] where the data sets overlap or abut, as shown in Figure 3.6b. However, it would appear that from the temperature dependence of the solubilities reported in the work of Glandt and Chapman [60] that the low temperature solubilities for the fluids they measured are overstated. The temperature trends in their data do not align with other measurements.

From the perspective of process design and optimization, interpolation and extrapolation of water solubility in the hydrocarbon-rich liquid and hydrocarbon solubility in water-rich liquid are important topics. Both of these topics present significant challenges related to the quality and range of the underlying solubility data, the diversity of the underlying phase behaviors represented in the data sets, and hydrocarbon speciation. These challenges are addressed elsewhere [62] in detail. Here the log-linear behavior of water solubility in hydrocarbons, Figure 3.6a, on a mass basis is exploited to provide a first order estimate for water solubility in heavy hydrocarbons, including lubricating oil and Athabasca bitumen. Equation 3-1 tracks the low solubility limit of the experimental data. The coefficients appearing in equation 1 were regressed using water solubility data in Athabasca bitumen, gross oil mixture [63] and lubrication oil [60]:

$$m_w = A * e^{BT} \quad (3-1)$$

where m_w is the water mass fraction in the hydrocarbon-rich liquid phase, and T is temperature in K. The constants are $A = 2.019 * 10^{-07}$ and $B = 2.155 * 10^{-02}$ (1/K), and the average absolute relative deviation of the correlation relative to the data, 12.3%, falls within the uncertainty of the underlying data which ranges up to 30%.

3.3.2 Excess volume of the Athabasca bitumen-rich liquid phase

Measured density data for saturated Athabasca bitumen liquid, presented in Table 3.5, were regressed using the Rackett equation [64] :

$$\rho_{AB} = \exp \left[C * \left(1 - \frac{T}{D} \right)^E \right] \quad (3-2)$$

where ρ_{AB} is the density of Athabasca bitumen in kg/m^3 , $C = 1.586$, $D = 1.065 \cdot 10^3$, $E = 2.857 \cdot 10^{-1}$, $F = 5.493$ and T is absolute temperature in K to obtain smoothed density values. The average absolute deviation of equation 3-2 from the density data is 2.6 kg/m^3 . Excess volume values were then calculated on a mass basis from experimental phase density and composition data as:

$$\Delta V^E = \frac{1}{\rho} - \left(\frac{m_w}{\rho_w} + \frac{m_{AB}}{\rho_{AB}} \right) \quad (3-3)$$

where ΔV^E is the excess volume of the bitumen-rich liquid phase. m_w and m_{AB} are the mass fraction of water and Athabasca bitumen in the mixture, and ρ_w and ρ_{AB} are the smoothed saturated liquid densities obtained from NIST [59] for water and equation 3-2 for Athabasca bitumen. The saturated liquid densities were not corrected for pressure where the pressure is less than vapor pressure of water. The water is slightly less dense and the Athabasca bitumen slightly more dense at the pressures where the excess volumes are evaluated. As these trends compensate, the net impact on the excess volume calculations is expected to be small but the effect is variable and contributes to the uncertainty of the values. Thus the excess volume values reported in Table 3.6 must be viewed as approximate. However, the values are positive, as is expected for water + hydrocarbon mixtures.

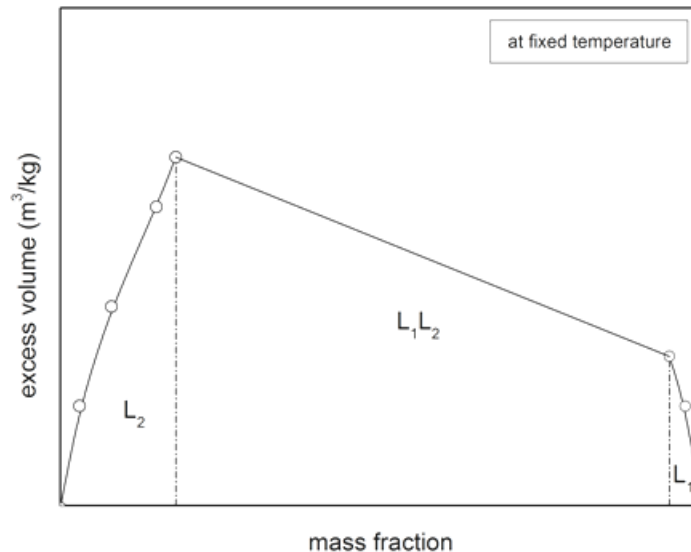


Figure 3.7. A typical volume of mixing for heavy hydrocarbon + water at temperatures lower than the upper critical end point.

For mixtures exhibiting liquid-liquid behavior, excess volume increases from zero to a maximum at the liquid-liquid boundary, is a linear function of composition in the two-phase region and then decreases to zero in the second single-phase liquid region, as shown in Figure 3.7. One way to interpret the excess volume measurements is suggested by Figure 3.7. If excess volume is treated as a linear function of composition within the single-phase region, each excess volume measurement can also be treated as an approximate measure of $\partial\Delta VE/\partial mw$. As the saturated composition is known, the excess volume for saturated liquid, with uncertainty estimates can be obtained, as shown in Figure 3.8. The excess volume at a water mass fraction less than the saturated value can be estimated as:

$$\Delta VE = mw *(A*T+B) \quad (3-4)$$

where

$$\partial\Delta VE/\partial mw = A*T + B \quad (3-5)$$

Again, mw is the mass fraction of water in the bitumen-rich phase, and T is in K. Constants $A = -1.63*10^{-5} \text{ (m}^3/\text{k.g.K)}$ and $B = 1.068*10^{-2} \text{ (m}^3/\text{k.g)}$ are calculated by linear regression.

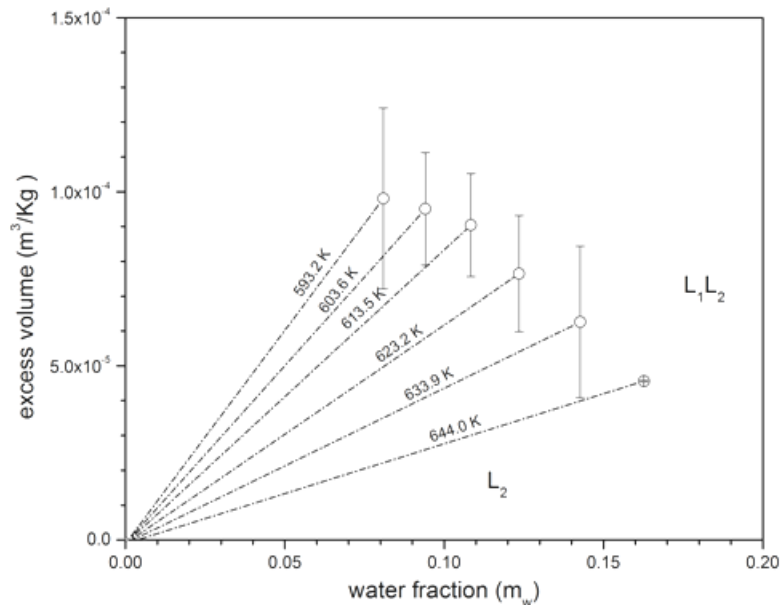


Figure 3.8. Excess volume (○) for the Athabasca bitumen-rich phase at saturation. The line segments, (-----) represent the excess volumes of unsaturated Athabasca bitumen. Temperature is a parameter.

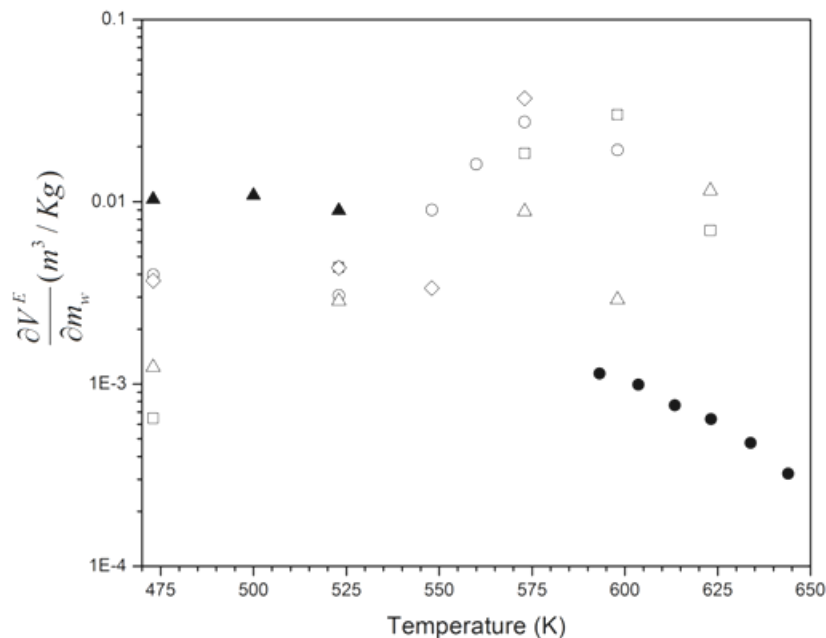


Figure 3.9. The derivative of excess volume with water mass fraction obtained by analyzing excess volume data for benzene (○) [46, 47], toluene (◻) [46, 49], ethylbenzene (△) [46, 49], n-hexane (▲) [50], n-decane (◇) [50], and for Athabasca bitumen (●) this work.

To place the behavior of water + Athabasca bitumen mixtures in a broader context, $\partial\Delta V^E/\partial m_w$ values for water in hydrocarbons were derived in a similar manner using excess volume measurements reported in the literature. Excess volumes for unsaturated water + benzene, toluene, ethylbenzene, n-hexane, and n-decane mixtures exhibiting Type IIIa phase behavior, are available at 10 MPa over a range of temperatures [48-50] near their respective upper critical end points. $\partial\Delta V^E/\partial m_w$ values for these mixtures are compared with those for water in Athabasca bitumen in Figure 3.9. The phase state associated with these data is a hydrocarbon-rich liquid (L_1) and according to literature [48-50], these hydrocarbon-rich phases approach their respective critical points (UCEP) within each data set. For the water + Athabasca bitumen pseudo binary mixture, which exhibits Type IIIb phase behavior, the reported derivative values are for L_2 , a hydrocarbon-rich liquid phase. This phase remains subcritical even as the water critical temperature is approached because the critical temperature of Athabasca bitumen is high relative to that of water. These phase state distinctions are important because the $\partial\Delta V^E/\partial m_w$ values in water + Athabasca bitumen mixtures are low compared to water + light hydrocarbon mixtures, and possess opposing trends with temperature as the critical temperature of water is approached.

Table 3.6. Bitumen-rich phase density and excess specific volume data

T (K)	P (MPa)	Water (wt %)	density of bitumen-rich liquid phase (kg/m ³)	ΔV^{excess} (m ³ /kg*10 ⁵)	$\Delta V^{\text{excess}}/\Delta \text{ water wt \%}$ (m ³ /kg *10 ⁶)
593.1	5.4	4.0	824.0	3.0	7.4
593.1	12.2	8.1	761.0	11.7	14.5
593.3	11.8	8.1	768.9	10.3	12.7
593.3	12.2	8.1	788.3	7.1	8.8
593.2	12.0	8.1	765.3	10.9	13.5
593.0	12.2	8.1	787.5	7.3	9.1
593.0	11.9	8.1	762.5	11.5	14.2
603.7	5.5	4.0	816.4	2.9	7.2
603.4	13.3	9.4	758.8	10.2	10.9
603.7	14.0	9.4	760.3	9.9	10.5
603.9	14.8	9.5	764.8	9.1	9.6
603.4	14.4	9.4	766.0	9.0	9.6
602.9	14.1	9.3	768.4	8.7	9.3
603.6	13.8	9.4	760.3	10.2	10.8
613.5	14.4	10.2	752.3	9.4	9.2
613.6	16.1	10.8	741.8	11.0	10.1
613.5	17.9	10.8	766.9	6.9	6.3
613.5	17.8	10.8	741.1	11.2	10.4
613.3	17.1	10.8	765.7	7.1	6.5
613.2	16.5	10.8	757.4	8.7	8.1
623.4	6.0	4.0	808.8	1.6	3.9
623.1	14.9	10.2	750.1	7.9	7.8
623.4	17.7	12.3	736.2	9.3	7.5
623.0	19.5	12.3	759.2	5.2	4.2
623.1	20.7	12.4	762.6	5.9	4.8
623.3	21.0	12.4	748.4	8.1	6.5
623.3	22.8	12.4	741.4	9.8	7.9
633.6	16.2	10.2	745.6	7.3	7.2
633.8	19.8	12.3	734.0	9.5	7.7
634.0	765.7	14.3	764.7	3.8	2.7
633.9	26.0	14.3	755.8	5.4	3.8
642.8	6.8	4.0	784.7	1.7	4.2
644.1	17.0	10.2	722.0	5.7	5.5
643.9	20.4	12.3	716.9	4.5	3.7
644.0	26.2	16.2	733.0	4.6	2.8

3.4 Conclusion

The solubility of water in Athabasca bitumen and the excess volume of the bitumen-rich liquid phase are reported over the temperature interval 593.2 to 644 K. The accuracy of the experimental methods and data were verified by reproducing phase diagrams and hydrocarbon-rich liquid compositions for water + toluene and water + 1-methylnaphthalene, and reproducing density measurements for 1-methylnaphthalene up to 573.8 K. The impacts of thermal degradation of Athabasca bitumen on measured values, particularly above 613 K, were mitigated but not eliminated by the experimental methods and procedures. The solubility of water in Athabasca bitumen increases with temperature. The reported values and the trend with temperature are in agreement with numerous data sets for comparable hydrocarbons but are at variance with values reported by Glant and Chapman [60] which appear to overestimate water solubility at lower temperatures. The excess volumes for the saturated sub-critical bitumen-rich liquid phase were found to be positive and the values were found to decrease with increasing temperature. Behavioral differences arising in Type IIIa and Type IIIb phase diagrams are delineated.

3.5 References

- [1] M.J. Amani, M.R. Gray, J.M. Shaw, Phase behavior of Athabasca bitumen +water mixtures at high temperature and pressure, *Journal of Supercritical Fluids* 77 (2013) 142–152.
- [2] T. Sato, T. Adschiri, K. Arai, G.L. Rempel, F.T.T. Ng, Upgrading of asphalt with and without partial oxidation in supercritical water, *Fuel* 82 (July) (2003) 1231–1239.
- [3] Z. Fang, T. Sato, R.L. Smith Jr., H. Inomata, K. Arai, J.A. Kozinski, Reaction chemistry and phase behavior of lignin in high-temperature and supercritical water, *Bioresource Technology* 99 (2008) 3424–3430.
- [4] M. Morimoto, Y. Sugimoto, Y. Saotome, S. Sato, T. Takanohashi, Effect of supercritical water on upgrading reaction of oil sand bitumen, *Journal of Supercritical Fluids* 55 (2010) 223–231.
- [5] M. Watanabe, S.-n. Kato, S. Ishizeki, H. Inomata, R.L. Smith Jr., Heavy oil upgrading in the presence of high density water: basic study, *Journal of Supercritical Fluids* 53 (2010) 48–52.

- [6] L.-N. Han, R. Zhang, J.-C. Bi, Upgrading of coal-tar pitch in supercritical water, *Journal of Fuel Chemistry and Technology* 36 (2008) 1–5.
- [7] L.N. Han, R. Zhang, J.C. Bi, Experimental investigation of high-temperature coal tar upgrading in supercritical water, *Fuel Processing Technology* 90 (February) (2009) 292–300.
- [8] Z.M. Cheng, Y. Ding, L.Q. Zhao, P.Q. Yuan, W.K. Yuan, Effects of supercritical water in vacuum residue upgrading, *Energy & Fuels* 23 (May–June) (2009) 3178–3183.
- [9] Z. Fang, R.L. Smith, H. Inomata, K. Arai, Phase behavior and reaction of polyethylene in supercritical water at pressures up to 2.6 GPa and temperatures up to 670 °C, *Journal of Supercritical Fluids* 16 (2000) 207–216.
- [10] W. Wahyudiono, T. Shiraishi, M. Sasaki, M. Goto, Bitumen upgrading under solvothermal/hydrothermal conditions, *Research on Chemical Intermediates* 37 (2011) 375–381.
- [11] J.G. Speight, *The Chemistry and Technology of Petroleum*, CRC Press, 2007.
- [12] A. Maczynski, D.G. Shaw, M. Goral, B. Wisniewska-Gocłowska, A. Skrzecz, Z. Maczynska, et al., IUPAC-NIST solubility data series. 81. Hydrocarbons with water and seawater—revised and updated part 1. C-5 hydrocarbons with water, *Journal of Physical and Chemical Reference Data* 34 (June) (2005) 441–476.
- [13] A. Maczynski, D.G. Shaw, M. Goral, B. Wisniewska-Gocłowska, A. Skrzecz, I. Owczarek, et al., IUPAC-NIST solubility data series. 81. Hydrocarbons with water and seawater—revised and updated. Part 2. Benzene with water and heavy water, *Journal of Physical and Chemical Reference Data* 34 (June) (2005) 477–552.
- [14] A. Maczynski, D.G. Shaw, M. Goral, B. Wisniewska-Gocłowska, A. Skrzecz, I. Owczarek, et al., IUPAC-NIST solubility data series. 81. Hydrocarbons with water and seawater—revised and updated. Part 3. C₆H₈–C₆H₁₂ hydrocarbons with water and heavy water, *Journal of Physical and Chemical Reference Data* 34 (June) (2005) 657–708.
- [15] A. Maczynski, D.G. Shaw, M. Goral, B. Wisniewska-Gocłowska, A. Skrzecz, I. Owczarek, et al., IUPAC-NIST solubility data series. 81. Hydrocarbons with water and seawater—revised and updated. Part 4. C₆H₁₄ hydrocarbons with water, *Journal of Physical and Chemical Reference Data* 34 (June) (2005) 709–753. 423
- [16] A. Maczynski, D.G. Shaw, M. Goral, B. Wisniewska-Gocłowska, A. Skrzecz, I. wczarek, et al., IUPAC-NIST solubility data series. 81. Hydrocarbons with water and seawater—revised and updated. Part 5. C-7 hydrocarbons with water and

- heavy water, *Journal of Physical and Chemical Reference Data* 34 (2005) 1399–1487.
- [17] D.G. Shaw, A. Maczynski, M. Goral, B. Wisniewska-Gocłowska, A. Skrzecz, I. Owczarek, et al., IUPAC-NIST solubility data series. 81. Hydrocarbons with water and seawater—revised and updated. Part 6. C₈H₈–C₈H₁₀ hydrocarbons with water, *Journal of Physical and Chemical Reference Data* 34 (2005) 1489–1553.
- [18] D.G. Shaw, A. Maczynski, M. Goral, B. Wisniewska-Gocłowska, A. Skrzecz, L. Owczarek, et al., IUPAC-NIST solubility data series. 81. Hydrocarbons with water and seawater revised and updated. Part 7. C₈H₁₂–C₈H₁₈ hydrocarbons with water, *Journal of Physical and Chemical Reference Data* 34 (December) (2005) 2261–2298.
- [19] D.G. Shaw, A. Maczynski, M. Goral, B. Wisniewska-Gocłowska, A. Skrzecz, I. Owczarek, et al., IUPAC-NIST solubility data series. 81. Hydrocarbons with water and seawater—revised and updated. Part 8. C-9 hydrocarbons with water, *Journal of Physical and Chemical Reference Data* 34 (December) (2005) 2299–2345.
- [20] D.G. Shaw, A. Maczynski, M. Goral, B. Wisniewska-Gocłowska, A. Skrzecz, I. Owczarek, et al., IUPAC-NIST solubility data series. 81. Hydrocarbons with water and seawater—revised and updated. Part 9. C-10 hydrocarbons with water, *Journal of Physical and Chemical Reference Data* 35 (March) (2006) 93–151.
- [21] D.G. Shaw, A. Maczynski, M. Goral, B. Wisniewska-Gocłowska, A. Skrzecz, I. Owczarek, et al., IUPAC-NIST solubility data series. 81. Hydrocarbons with water and seawater—revised and updated. Part 10. C-11 and C-12 hydrocarbons with water, *Journal of Physical and Chemical Reference Data* 35 (March) (2006) 153–203.
- [22] D.G. Shaw, A. Maczynski, M. Goral, B. Wisniewska-Gocłowska, A. Skrzecz, I. Owczarek, et al., IUPAC-NIST solubility data series. 81. Hydrocarbons with water and seawater—revised and updated. Part 11. C-13–C-36 hydrocarbons with water, *Journal of Physical and Chemical Reference Data* 35 (June) (2006) 687–784.
- [23] D.G. Shaw, A. Maczynski, G.T. Hefter, M. Kleinschmidt, D. Mackay, P.A. Meyers, et al., IUPAC-NIST solubility data series. 81. Hydrocarbons with water and seawater—revised and updated. Part 12. C-5–C-26 hydrocarbons with seawater, *Journal of Physical and Chemical Reference Data* 35 (June) (2006) 785–838.
- [24] J.S. Brown, J.P. Hallett, D. Bush, C.A. Eckert, Liquid–liquid equilibria for binary mixtures of water plus acetophenone, plus 1-octanol, plus anisole, and plus

- toluene from 370K to 550 K, *Journal of Chemical and Engineering Data* 45 (September–October) (2000) 846–850.
- [25] I.G. Economou, C. Tsonopoulos, Associating models and mixing rules in equations of state for water/hydrocarbon mixtures, *Chemical Engineering Science* 52 (February) (1997) 511–525.
- [26] I.G. Economou, J.L. Heidman, C. Tsonopoulos, G.M. Wilson, Mutual solubilities of hydrocarbons and water. 3. 1-Hexene, 1-octene, C-10–C-12 hydrocarbons, *Aiche Journal* 43 (February) (1997) 535–546.
- [27] J.L. Heidman, C. Tsonopoulos, C.J. Brady, G.M. Wilson, high-temperature mutual solubilities of hydrocarbons and water. 2. Ethylbenzene, ethylcyclohexane, and normal-octane, *Aiche Journal* 31 (1985) 376–384.
- [28] C. Tsonopoulos, G.M. Wilson, High-temperature mutual solubilities of hydrocarbons and water. 1. Benzene, cyclohexane and normal-hexane, *Aiche Journal* 29 (1983) 990–999.
- [29] C. Tsonopoulos, Thermodynamic analysis of the mutual solubilities of normal alkanes and water, *Fluid Phase Equilibria* 156 (March) (1999) 21–33.
- [30] C. Tsonopoulos, Thermodynamic analysis of the mutual solubilities of hydrocarbons and water, *Fluid Phase Equilibria* 186 (August) (2001) 185–206.
- [31] K. Chandler, B. Eason, C.L. Liotta, C.A. Eckert, Phase equilibria for binary aqueous systems from a near-critical water reaction apparatus, *Industrial & Engineering Chemistry Research* 37 (August) (1998) 3515–3518.
- [32] F.E. Anderson, J.M. Prausnitz, mutual solubilities and vapor-pressures for binary and ternary aqueous systems containing benzene, toluene, meta-xylene, thiophene and pyridine in the region 100–200 °C, *Fluid Phase Equilibria* 32 (December) (1986) 63–76.
- [33] W.A. Leet, H.M. Lin, K.C. Chao, Mutual solubilities in 6 binary-mixtures of water a heavy hydrocarbon or a derivative, *Journal of Chemical and Engineering Data* 32 (January) (1987) 37–40.
- [34] B.J. Neely, J. Wagner, R.L. Robinson, K.A.M. Gasem, Mutual solubility measurements of hydrocarbon–water systems containing benzene, toluene, and 3-methylpentane, *Journal of Chemical and Engineering Data* 53 (January) (2008) 165–174.
- [35] E. Brunner, Fluid mixtures at high pressures IX. Phase separation and critical phenomena in 23 (n-alkane + water) mixtures, *Journal of Chemical Thermodynamics* 22 (1990) 335–353.

- [36] E. Brunner, M.C. Thies, G.M. Schneider, Fluid mixtures at high pressures: phase behavior and critical phenomena for binary mixtures of water with aromatic hydrocarbons, *Journal of Supercritical Fluids* 39 (2006) 160–173.
- [37] S.P. Christensen, M.E. Paulaitis, Phase equilibria for tetralin–water and 1-methylnaphthalene–water mixtures at elevated temperatures and pressures, *Fluid Phase Equilibria* 71 (1992) 63–83.
- [38] J.C. de Hemptinne, A. Dhima, H. Zhou, The importance of water–hydrocarbon phase equilibria during reservoir production and drilling operations, *Revue De L Institut Francais Du Petrole* 53 (May–June) (1998) 283–302.
- [39] K.S. Pedersen, J. Milter, C.P. Rasmussen, Mutual solubility of water and a reservoir fluid at high temperatures and pressures: experimental and simulated data, *Fluid Phase Equilibria* 189 (2001) 85–97.
- [40] I.M. Abdulagatov, A.R. Bazaev, E.A. Bazaev, M.B. Saidakhmedova, A.E. Ramazanova, PVT_x measurements and partial molar volumes for water–hydrocarbon mixtures in the near-critical and supercritical conditions, *Fluid Phase Equilibria* 150–151 (1998) 537–547.
- [41] I.M. Abdulagatov, E.A. Bazaev, A.R. Bazaev, M.G. Rabezkii, PVT_x measurements for dilute water + n-hexane mixtures in the near-critical and supercritical regions, *Journal of Supercritical Fluids* 19 (2001) 219–237.
- [42] I.M. Abdulagatov, A.R. Bazaev, J.W. Magee, S.B. Kiselev, J.F. Ely, PVT_x measurements and crossover equation of state of pure n-hexane and dilute aqueous n-hexane solutions in the critical and supercritical regions, *Industrial and Engineering Chemistry Research* 44 (2005) 1967–1984.
- [43] A.R. Bazaev, I.M. Abdulagatov, J.W. Magee, E.A. Bazaev, A.E. Ramazanova, PVT_x measurements for H₂O+D₂O mixtures in the near-critical and supercritical regions, *Journal of Supercritical Fluids* 26 (2003) 115–128.
- [44] S.B. Kiselev, J.F. Ely, M. Abdulagatov, A.R. Bazaev, J.W. Magee, Equation of state and thermodynamic properties of pure toluene and dilute aqueous toluene solutions in the critical and supercritical regions, *Industrial and Engineering Chemistry Research* 41 (2002) 1000–1016.
- [45] M.G. Rabezkii, A.R. Bazaev, I.M. Abdulagatov, J.W. Magee, E.A. Bazaev, PVT_x measurements for water + toluene mixtures in the near-critical and supercritical regions, *Journal of Chemical and Engineering Data* 46 (2001) 1610–1618.
- [46] S. Furutaka, S. Ikawa, Infrared study of water–benzene mixtures at high temperatures and pressures in the two- and one-phase regions, *Journal of Chemical Physics* 113 (August) (2000) 1942–1949. 534

- [47] S. Furutaka, S. Ikawa, Infrared study of anomalous volume behavior of water–benzene mixtures in the vicinity of the critical region, *Journal of Chemical Physics* 117 (July) (2002) 1682–1685.
- [48] S. Furutaka, S. Ikawa, pi-hydrogen bonding between water and aromatic hydrocarbons at high temperatures and pressures, *Journal of Chemical Physics* 117 (July) (2002) 751–755.
- [49] S. Furutaka, S. Ikawa, Volume expansion behavior of water–hydrocarbon mixtures at high temperatures and pressures as studied by infrared spectroscopy, *Fluid Phase Equilibria* 217 (March) (2004) 181–188.
- [50] Y. Ishikawa, S. Arai, S. Furutaka, S. Ikawa, Anomalous volumetric behavior of water–hexane and water–decane mixtures in the vicinity of the critical region as studied by infrared spectroscopy, *Journal of Chemical Physics* 122 (May) (2005).
- [51] L. Hnedkovsky, S. Degrange, I. Cibulka, Partial molar volumes of organic solutes in water. I. O-, m-, and p-cresol at temperatures 298K to 573 K, *Journal of Chemical Thermodynamics* 30 (May) (1998) 557–569.
- [52] P. Hyncica, L. Hnedkovsky, I. Cibulka, Partial molar volumes of organic solutes in water. X. Benzene and toluene at temperatures from (298 to 573) K and at pressures up to 30 MPa, *Journal of Chemical Thermodynamics* 35 (December) (2003) 1905–1915.
- [53] P.H. Vankonynenburg, R.L. Scott, Critical lines and phase-equilibria in binary van der waals mixtures, *Philosophical Transactions of the Royal Society of London Series A: Mathematical Physical and Engineering Sciences* 298 (1980) 495–540.
- [54] A. Bazyleva, M. Fulem, M. Becerra, B. Zhao, J.M. Shaw, Phase behavior of Athabasca bitumen, *Journal of Chemical and Engineering Data* 56 (July) (2011) 3242–3253.
- [55] S.J. Abedi, H.Y. Cai, S. Seyfaie, J.M. Shaw, Simultaneous phase behaviour, elemental composition and density measurement using X-ray imaging, *Fluid Phase Equilibria* 158 (June) (1999) 775–781.
- [56] B. Zhao, J.M. Shaw, Composition and size distribution of coherent nanostructures in Athabasca bitumen and Maya crude oil, *Energy & Fuels* 21 (September–October) (2007) 2795–2804.
- [57] X.Y. Zou, X.H. Zhang, J.M. Shaw, Phase behavior of Athabasca vacuum bottoms plus n-alkane mixtures, *SPE Production&Operations* 22 (May) (2007) 265–272.
- [58] D.J. Fall, K.D. Luks, Liquid liquid vapor-phase equilibria of the binary-system carbon-dioxide + normal-tridecane, *Journal of Chemical and Engineering Data* 30 (1985) 276–279.

- [59] E.W. Lemmon, M.O. McLinden, D.G. Friend, Thermophysical properties of fluid systems, in: P.J. Linstrom, W.G. Mallard (Eds.), NIST Chemistry WebBook, NIST Standard Reference Database Number 69, National Institute of Standards and Technology, Gaithersburg, MD, 2012, <http://webbook.nist.gov>
- [60] J. Griswold, J.E. Kasch, Hydrocarbon–water solubilities at elevated temperatures and pressures, *Industrial and Engineering Chemistry* 34 (1942) 804–806.
- [61] C.A. Glandt, W.G. Chapman, Effect of water dissolution on oil viscosity, *SPE Reservoir Engineering* 10 (February) (1995) 59–64.
- [62] M.A. Satyro, J.M. Shaw, H.W. Yarranton, A practical method for the estimation of oil and water mutual solubilities, April, 2013 (in preparation).
- [63] W.L. Nelson, Solubility of water in oil, *Oil & Gas journal* (1956) 140.
- [64] H.G. Rackett, Calculation of bubble-point volumes of hydrocarbon mixtures, *Journal of Chemical and Engineering Data* 16 (1971) 308.
- [65] F.Y. Jou, A.E. Mather, Liquid–liquid equilibria for binary mixtures of water plus benzene, water plus toluene, and water plus p-xylene from 273K to 458 K, *Journal of Chemical and Engineering Data* 48 (May–June) (2003) 750–752. 588

Chapter 4. The phase behavior of Athabasca bitumen + toluene + water ternary mixtures¹

4.1 Introduction

Water plays a significant role in industrial processes at near ambient conditions, as a polar solvent, and as a non polar solvent under near critical conditions where the properties and property variation of near-critical and supercritical water are exploited [1, 2]. One of the demanding potential applications of water at elevated temperatures is in heavy oil/bitumen production and refining. The use of water in bitumen refining processes may provide a significant advantage over current practice due to the possible elimination of asphaltene precipitation and coke formation [3-10]. Water has the potential to be used as an effective solvent for controlling asphaltene aggregation and reactions. Many questions about the nature of bitumen/asphaltene behavior are still unanswered, and the economic impact of this uncertainty is significant. Detailed knowledge of the phase equilibria of water + bitumen and heavy oil mixtures near the critical point of water is a first step toward the development of potential process designs. This study is also motivated by the potential to reduce the overall cost of production of finished products in the future by merging aspects of fluid composition and operating conditions for in situ production and refining processes.

Water + hydrocarbon mixtures exhibit complex phase behaviors. Detection and prediction of their complex phase behaviors has been a research focus for decades and the phase behavior of water + numerous low molecular weight hydrocarbons have been assessed. However, experimental data for mixtures which include heavy hydrocarbons and industrially relevant mixtures (resids, boiling range cuts, SARA fractions) are sparse because phase behavior measurements for such mixtures is challenging due to opaqueness of the mixtures, the potential for emulsions to interfere with phase boundary measurements, thermal degradation of the hydrocarbons, and difficulties linked to sampling at high-temperatures and high-pressures. In prior work, the Athabasca bitumen + water pseudo binary mixture was shown to exhibit Type IIIb phase behavior [11, 12]

¹ This chapter with minor modifications has been accepted for publication in the journal of Fluid Phase Equilibria: M. J. Amani, M. R. Gray, and J. M. Shaw, "The phase behavior of Athabasca bitumen + toluene + water ternary mixtures", Fluid Phase Equilibria, January 2014.

according to van Konynenburg and Scott classification scheme [13], and the solubility of water in bitumen was measured. In this work, the focus is on impacts of solvent addition to bitumen mixtures containing water. Solvents typically possess low densities and low critical temperatures relative to water and bitumen, and higher water solubilities relative to bitumen. Significant changes in mixture phase behavior and water content in the hydrocarbon-rich liquid phase are anticipated.

4.1.1 Solubility of water in hydrocarbons

The phase behavior and mutual solubilities of toluene + water along the LLV three-phase curve up to the upper critical end point (UCEP) of the mixture have been investigated extensively [14-19]. At room temperature the solubility of water in toluene is negligible. With increasing temperature, the solubility increases by orders of magnitude, and the mixture becomes miscible at temperatures exceeding the UCEP. Maczynski et al. [20, 21] reviewed and critically compiled the published data for mutual solubilities of toluene and 1-methylnaphthalene + water binary mixtures published in the primary literature prior to 2003. As for multicomponent hydrocarbon mixtures, Anderson et al. [14] investigated the mutual solubilities and vapor pressures of benzene + pyridine + water ternary mixtures. Shimoyama and co-workers [22] studied the behavior of water + hexane + hexadecane, water + toluene + decane, and water + toluene + ethylbenzene ternary mixtures from 500 to 573 K. Few phase equilibrium data sets for industrial hydrocarbon fluids containing water are available. Nelson [23] reported approximate solubility data of water in mixtures such as jet fuels, kerosene and oils with molecular weights up to 425. Griswold [24] studied the solubility of water in three petroleum products including naphtha, kerosene and lubricating oil up to 553.2 K. Their results suggest that the solubility of water in petroleum fractions is largely independent of molecular weight of the oil. Pedersen et al. [25] reported equilibrium data for a few compositions for water + petroleum reservoir fluids up to 473 K and 100 MPa, while Glandt et al. [26] studied the effect of water dissolution on oil viscosity and reported solubility of water in four crude heavy oils. They concluded that sufficient water dissolves in crude oils at high temperatures (above 423 K) to reduce oil phase viscosity. They reported liquid–liquid and liquid–vapor phase equilibrium curves. There do not appear to be publicly available studies on phase diagrams or water solubility in the hydrocarbon-rich phase for water + hydrocarbon mixtures where the hydrocarbon mixture is itself asymmetric.

4.1.2 Phase behavior of hydrocarbon + water mixtures

Hydrocarbon + water binary mixtures exhibit Type II and Type III including both Type IIIa and Type IIIb phase behavior according to the van Konynenburg and Scott classification scheme Konynenburg [13] For Type II phase behavior, a continuous liquid-vapor critical curve starts from one of the pure component critical point and ends at the other pure component critical point. At low reduced temperatures, a second critical curve which represents the locus of liquid-liquid critical points. This critical curve intersects the three-phase line (LLV line) at an upper critical end point (UCEP). Type IIIa and Type IIIb [15] are frequently referred to as Type III phase behavior in the literature. The main difference between Type IIIa and Type IIIb is whether the three phase line that extends from low reduced temperature and pressure intersects the liquid-vapor critical locus close to the water critical point or the hydrocarbon critical point. Type IIIa corresponds to a wide variety of water + hydrocarbon binary mixtures where the molar mass of the hydrocarbon is low such as the lower n-alkanes [27] and for the smaller aromatics which possess lower critical temperatures than water [15]. Type II and Type IIIb phase behaviors tend to arise where the critical temperature of the hydrocarbon is greater than that of water. Water + 1-methyl-naphthalene and tetralin [28], and naphthalene and biphenyl [15] exhibit Type II behavior. Binary mixtures of water and n-alkanes with carbon numbers greater than 26 exhibit Type IIIb phase behavior [27]. Brunner [15, 27] observed phase behavior transitions among homologous series of n-alkanes and in ternary mixtures of water + decalin + tetralin. The Athabasca bitumen + water pseudo binary mixture also exhibits Type IIIb phase behavior as noted above (Chapter 2).

4.2 Experimental set-up and methodology

Athabasca bitumen [29], water, toluene and 1-methylnaphthalene were analyzed previously and characteristic properties are reported in Chapter 2. Bitumen and heavy hydrocarbons with high asphaltene contents are opaque to visible light, and their phase behavior is not readily observed using conventional phase detection methods. X-ray transmission tomography is an effective observation method [30] and it was used in this study to detect phase volumes and phase boundaries. The view cell comprised an x-ray transparent beryllium cylinder capped on top by a stainless steel bellows and on bottom by a fixed base plate. The intensity of the transmitted X-ray beam at fixed elevation is a function of the density and composition of phase present. More detailed descriptions of

the apparatus and operating procedures, along with illustrative applications, and result precision validation have been reported in Chapter 2 and 3. The calibration and operation procedures employed in this work were validated by reproducing published experimental and recommended water, 1-methylnaphthalene, and water + toluene and water + 1-methylnaphthalene binary mixtures properties and are reported in Chapter 2 and 3.

Careful calibration of x-ray intensity and the intensity difference between the water-rich and hydrocarbon-rich phases provides individual phase densities and information regarding the relative density of the two phases. From basic theory, the intensity of an x-ray beam transmitted through a layer of material with thickness x and density ρ is expressed as:

$$I = I_0 \exp(-\mu\rho x) \quad (4-1)$$

where I_0 is the initial X-ray intensity of the beam, and μ is the element specific mass attenuation coefficient. Mass attenuation coefficients for elements as a function of photon energy (keV) are available at NIST [31] and the mass attenuation coefficients for compounds or mixtures are obtained by summing element contributions:

$$\mu = \sum_i w_i \mu_i \quad (4-2)$$

where w_i is the weight fraction of the i^{th} atomic constituents of a compound.

The X-ray intensity difference between the water-rich and hydrocarbon-rich phases can be related to the density difference between coexisted phases. As the thickness of materials and the initial X-ray intensity are the same for both phases, the relation between transmitted X-ray intensity and density of phases at fixed elevation can be expressed as:

$$\alpha \ln \left(\frac{I_{hc}}{I_w} \right) = -\mu_w \rho_w + \mu_{hc} \rho_{hc} \quad (4-3)$$

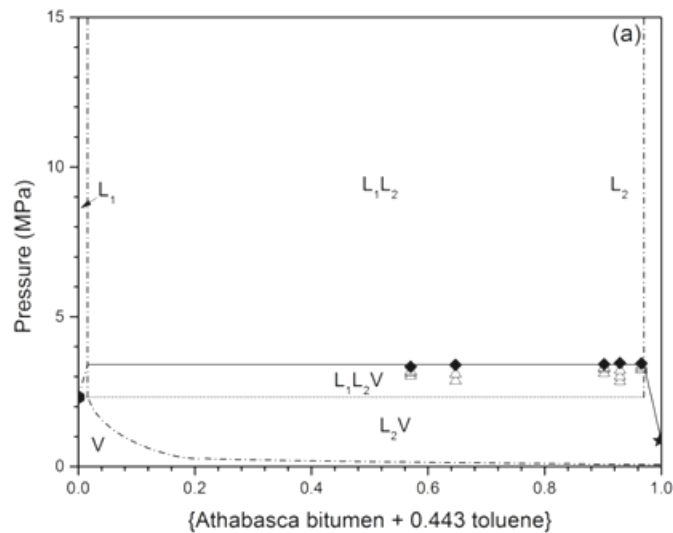
subscripts w and hc represent water and hydrocarbon-rich phase respectively. The coefficient α , a machine constant, known from the apparatus geometry and from calibration using a single-phase fluid, is needed because the distance from the point x-ray source to the detector varies with elevation within the cell. To improve the precision of the water-saturated hydrocarbon phase density measurements, the water-rich phase comprising essentially only water is used as an internal reference and the impact of water content on the X-ray attenuation coefficient of hydrocarbon-rich phase, a secondary

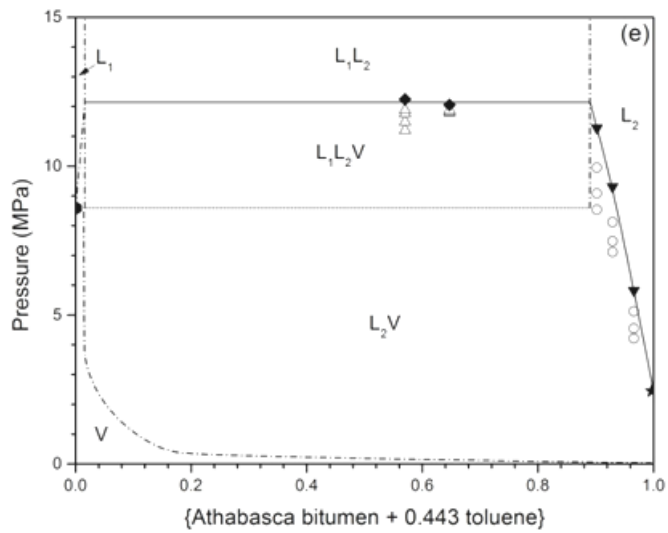
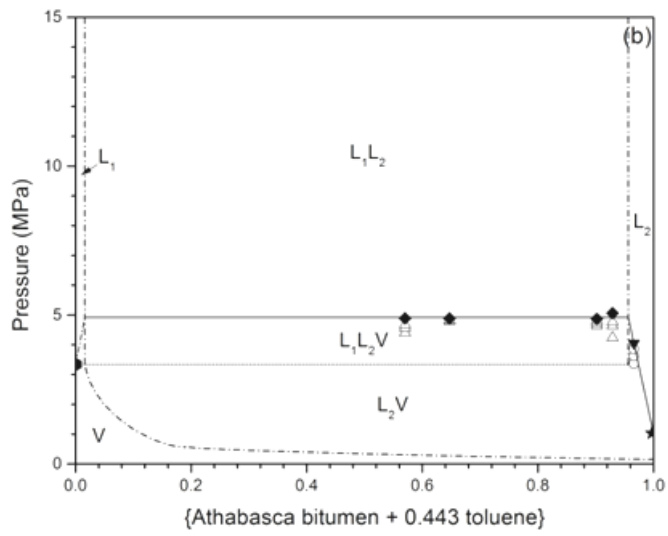
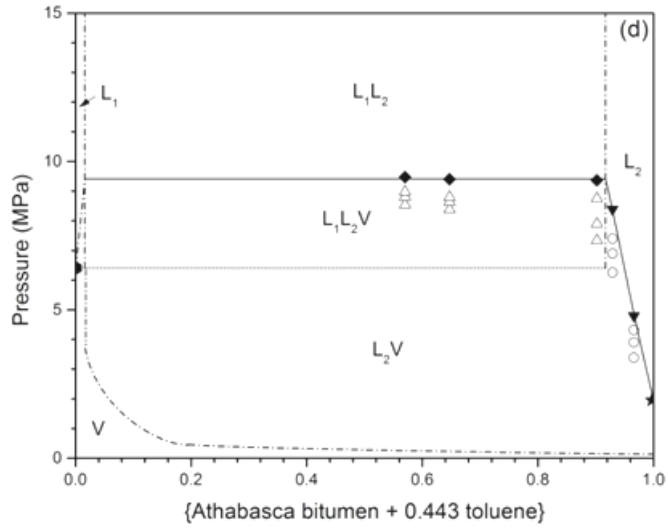
effect, is captured with equation 4-2. The water content in the hydrocarbon-rich phase is obtained from experimental data or from the literature, e.g.: toluene [20]. As water density is a precisely known function of temperature and pressure, and the mass attenuation coefficients are known accurately, the error of the hydrocarbon-rich liquid phase density measurements is small, as noted in the data tables even at high temperature and pressure.

4.3 Results and Discussion

4.3.1 Phase Diagrams for Bitumen + Toluene + Water Mixtures

To evaluate the impacts of solvent addition on bitumen + water mixture properties, phase equilibrium data for two $\{(1-w) \text{ Athabasca bitumen} + (w) \text{ toluene}\} + \text{water}$ mixtures with average weight fraction of $w = 0.443$ and 0.668 toluene were measured. Bubble pressure and other phase transition data for these mixtures are shown in Tables 4.1 and 4.2. P-x diagrams for these two mixtures over the temperature range 492.6 to 573.5 K are presented in Figures 4.1 and 4.2 respectively. While the bitumen rich phase is less dense than the water rich phase, density inversion is anticipated at higher temperatures. Consequently, the bitumen-rich phase is designated as L_2 in the phase diagrams and the water-rich liquid is designated as L_1 .





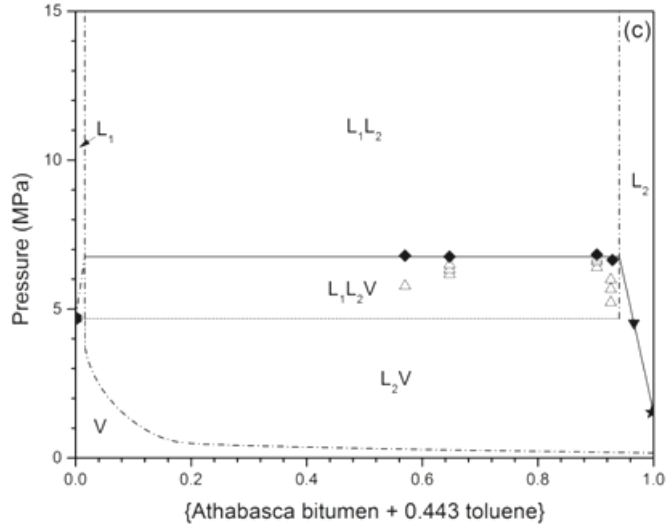
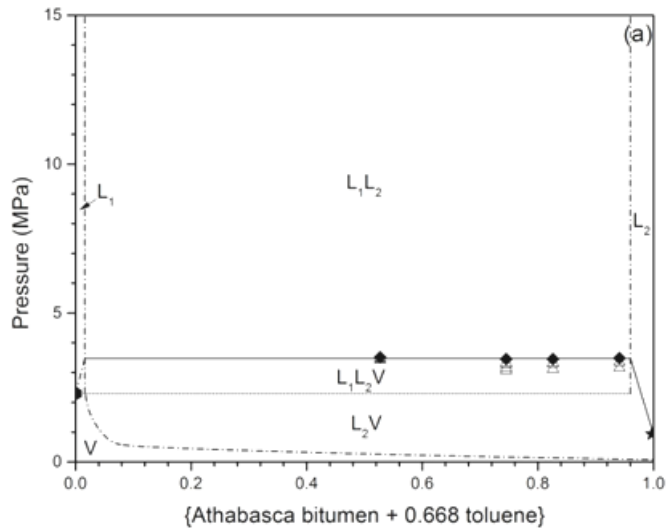
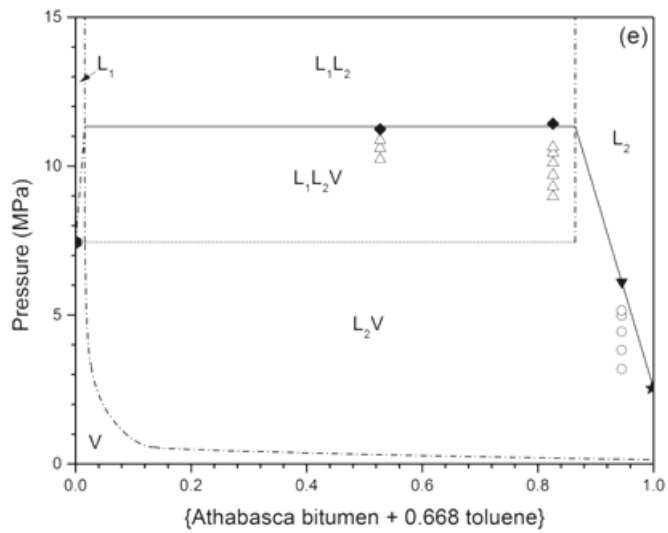
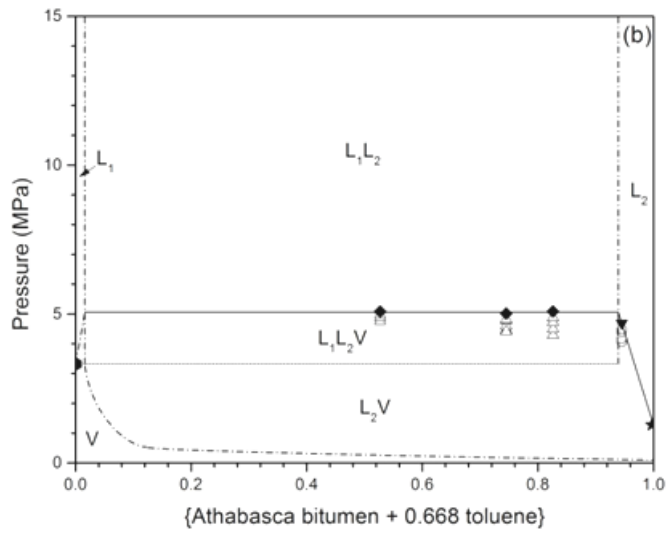
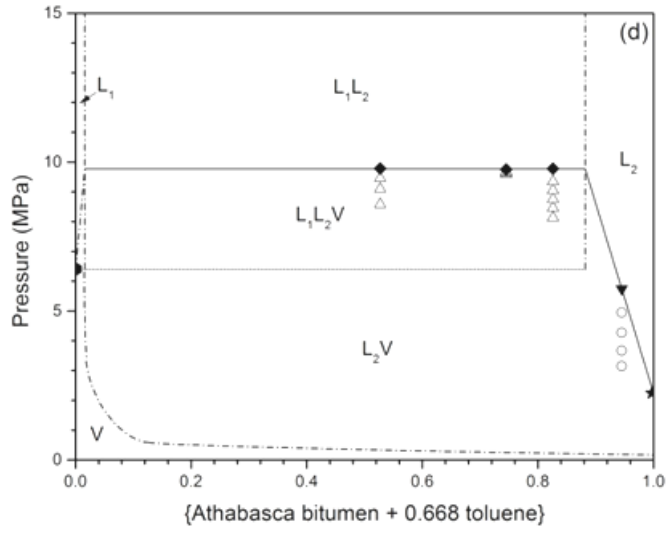


Figure 4.1. P-x diagrams of $\{(1-w) \text{ bitumen} + (w) \text{ toluene}\} + \text{water}$ mixture for $w=0.443$ wt fraction at 493.1 (a), 513.1 (b), 533.1 (c), 553.1 (d), 573.2 K (e). Measured liquid-vapor (○) and liquid-liquid-vapor (Δ) equilibrium data are shown. The vapor pressure of water (●) obtained from [32]. Solid lines (—) show the LLV/LL and L_2V/L_2 boundaries where points on these boundaries are designated with (◆) and (▼), respectively, and the LLV/ L_2V boundary defined by the vapor pressure of water (.....). Boundaries designated with a dash-dot lines (-.-) are illustrative and were not identified experimentally. Bubble pressure of Athabasca bitumen + 0.448 toluene (★) is also shown.





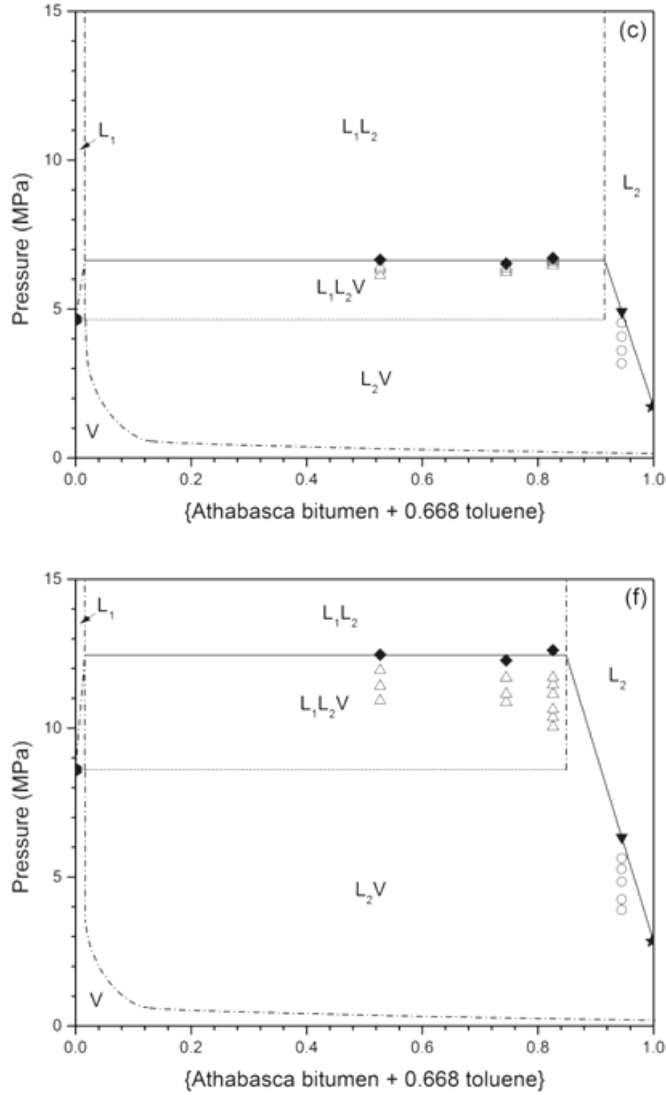


Figure 4.2. P-x diagrams of $\{(1-w) \text{ bitumen} + (w) \text{ toluene}\} + \text{water}$ mixture for $w=0.668$ wt fraction at 492.7 (a), 512.8 (b), 532.6 (c), 553.2 (d), 563.2 (e), 573.3 K (f). Measured liquid-vapor (○) and liquid-liquid-vapor (Δ) equilibrium data are shown. The vapor pressure of water (●) obtained from [32]. Solid lines (—) show the LLV/LL and L_2V/L_2 boundaries where points on these boundaries are designated with (◆) and (▼), respectively, and the LLV/ L_2V boundary defined by the vapor pressure of water (.....). Boundaries designated with a dash-dot lines (-.-) are illustrative and were not identified experimentally. Bubble pressure of Athabasca bitumen + 0.667 toluene (★) is also shown.

Water + pure hydrocarbon binary mixtures exhibit LLV phase behavior at pressures greater than the vapor pressure of pure water due to net repulsive interactions. Further, as the solubility of pure or mixed hydrocarbons in water is very low, the vapor pressure of water provides an approximate lower pressure limit for the LLV/ L_2V boundary. In

constructing the phase diagrams reported in Figures 4.1 and 4.2, and previously for Athabasca bitumen + water mixtures (Chapter 3), the vapor pressure curve for water is used as the lower pressure boundary of the LLV-phase region in the P-x diagrams. The LLV/LL, upper boundary of the LLV-phase region, and L₂V/L₂ boundaries are defined based on the LLV and LV equilibrium data points at fixed temperature and composition. The other boundaries are estimated based on phase behavior theory, and are illustrative. They were not observed experimentally.

Table 4.1. LLV/LL and L₂V/L₂ boundaries of {(1-w) bitumen + (w) toluene} + water mixtures at a weight fraction of w=0.443.

(a)-{Athabasca bitumen + 0.441 toluene }		
T (K) ±	P (MPa) ±	Boundary
0.1	0.07	
364.6	0.06	LV/L
395.2	0.13	LV/L
401.6	0.16	LV/L
412.6	0.18	LV/L
431.5	0.27	LV/L
452.1	0.46	LV/L
472.3	0.59	LV/L
492.0	0.85	LV/L
511.8	1.08	LV/L
532.1	1.46	LV/L
563.2	2.06	LV/L
573.2	2.30	LV/L

(b)-{Athabasca bitumen + 0.443 toluene } + 0.034 water		
T(K) ± 0.1	P (MPa) ± 0.07	Boundary
493.1	3.45	LLV/LL
513.1	4.06	LV/L
533.2	4.54	LV/L
553.2	4.80	LV/L
573.3	5.83	LV/L

(c)-{Athabasca bitumen + 0.441 toluene } + 0.071 water

T (K) ± 0.1	P (MPa) ± 0.07	Boundary
493.0	3.46	LLV/LL
513.1	5.07	LLV/LL
533.1	6.65	LLV/LL
553.2	8.40	LV/L
573.4	9.31	LV/L

(d)-{Athabasca bitumen + 0.442 toluene } + 0.098 water

T (K) ± 0.1	P (MPa) ± 0.07	Boundary
493.1	3.42	LLV/LL
513.1	4.87	LLV/LL
532.9	6.83	LLV/LL
553.0	9.37	LLV/LL
573.5	11.28	LV/L

(e)-{Athabasca bitumen + 0.448 toluene } + 0.353 water

T (K) ± 0.1	P (MPa) ± 0.07	Boundary
493.2	3.40	LLV/LL
513.1	4.88	LLV/LL
533.1	6.76	LLV/LL
553.2	9.40	LLV/LL
573.4	12.06	LLV/LL

(f)-{Athabasca bitumen 0.441 toluene } + 0.430 water

T (K) ± 0.1	P (MPa) ± 0.07	Boundary
493.2	3.34	LLV/LL
513.2	4.89	LLV/LL
552.9	9.30	LLV/LL
563.2	10.80	LLV/LL
572.9	12.24	LLV/LL

Table 4.2. LLV/LL and L₂V/L₂ boundaries of {(1-w) bitumen + (w) toluene} + water mixtures at a weight fraction of w=0.668.

(a)-{Athabasca bitumen + 0.670 toluene }

T (K) ±	P (MPa) ±	Boundary
0.1	0.07	
370.5	0.08	LV/L
383.2	0.10	LV/L
398.2	0.17	LV/L
422.4	0.28	LV/L
452.5	0.47	LV/L
472.4	0.71	LV/L
492.0	0.90	LV/L
512.6	1.29	LV/L
532.4	1.71	LV/L
552.5	2.22	LV/L
572.3	2.84	LV/L
592.9	3.41	LV/L

(b)-{Athabasca bitumen + 0.669 toluene } + 0.055 water

T(K) ± 0.1	P (MPa) ± 0.07	Boundary
492.7	3.49	LLV/LL
512.8	4.70	LV/L
532.8	4.92	LV/L
553.3	5.75	LV/L
563.3	6.11	LV/L
573.2	6.34	LV/L

(c)-{Athabasca bitumen + 0.668 toluene } + 0.174 water

T(K) ± 0.1	P (MPa) ± 0.07	Boundary
492.6	3.45	LLV/LL
512.9	5.09	LLV/LL
532.5	6.72	LLV/LL
553.3	9.79	LLV/LL
563.3	11.42	LLV/LL
573.4	12.62	LLV/LL

(d)-{Athabasca bitumen + 0.670 toluene } + 0.255 water

T (K) ± 0.1	P (MPa) ± 0.07	Boundary
492.8	3.45	LLV/LL
512.7	5.01	LLV/LL
532.5	6.53	LLV/LL
553.2	9.75	LLV/LL
573.2	12.27	LLV/LL

(e)-{Athabasca bitumen + 0.667 toluene } + 0.473 water

T (K) ± 0.1	P (MPa) ±	Boundary
	0.07	
492.6	3.52	LLV/LL
512.7	5.08	LLV/LL
532.9	6.66	LLV/LL
553.2	9.79	LLV/LL
563.1	11.24	LLV/LL
573.5	12.47	LLV/LL

4.3.2 Water solubility in bitumen + toluene mixtures at high temperatures

The solubility of water in the hydrocarbon-rich phase was identified from the intersection of the LLV/LL and the L₂V/L₂ phase behavior boundaries. The method was described and validated previously (Chapter 3). For example, at 573 K (Figure 4.1e), the water saturated {Athabasca bitumen + 0.443 toluene} mixture contains 0.05 weight fraction water. The solubility of water in {(1-w) bitumen +(w) toluene} mixtures are presented in Tables 4.3 a-b and shown in Figure 4.3 as functions of temperature. As expected, the solubility of water in the toluene + bitumen mixtures lies between the solubility of water in toluene and Athabasca bitumen. At temperatures remote from the critical point of toluene, the solubility of water in the toluene + Athabasca bitumen mixtures approaches the weight-averaged solubility of water in toluene and Athabasca bitumen:

$$S_{hc} = w \cdot S_{tol} + (1 - w) \cdot S_{bit} \quad (4-4)$$

where S_{hc} solubility of water in the mixture at a toluene weight fraction w . S_{tol} and S_{bit} are the solubility of water in toluene [32] and Athabasca bitumen (Chapter 3). At higher temperatures, the solubility of water in the toluene + Athabasca bitumen mixtures diverges from and is significantly lower than the weight-averaged solubility. This effect

arises because the solubility of water in toluene increases sharply as the UCEP of toluene + water binary, adjacent to the critical point of toluene, is approached. The toluene + bitumen mixtures remain remote from their joint critical region, yielding lower water solubility than the weighted average would suggest.

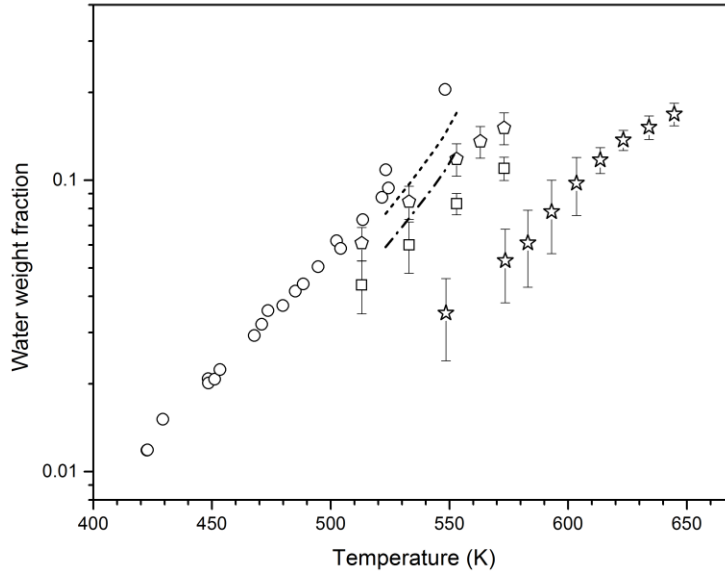


Figure 4.3. Solubility of water in $\{(1-w) \text{ bitumen} + (w) \text{ toluene}\}$ mixtures for $w = 0.0$ i.e.: Athabasca bitumen (\star) Chapter 3, $w=0.443$ (\square) and 0.668 (\circ), this work, and $w = 1.0$ i.e.: toluene (\circ) [14, 16-19]. Computed weight fraction averaged water solubilities in bitumen + toluene mixtures based on smoothed data: $w=0.443$ (---) and 0.668 (---) weight fraction (equation 4-4).

Table 4.3. Solubility of water in $\{(1-w) \text{ bitumen} + (w) \text{ toluene}\}$ blends at $w=0.443$ and 0.668 . Water solubility is reported in weight fraction.

(a)-{Athabasca bitumen + 0.443 toluene}

T (K) ± 0.1	P (MPa) ± 0.07	Water solubility	\pm Uncertainty
513.1	4.93	0.044	0.009
533.1	6.76	0.059	0.012
553.1	9.41	0.083	0.007
573.2	12.15	0.110	0.010

(b)-{Athabasca bitumen + 0.668 toluene }

T (K) ± 0.1	P (MPa) ± 0.07	Water solubility	±Uncertainty
512.8	5.06	0.061	0.008
532.6	6.64	0.084	0.011
553.2	9.78	0.118	0.015
563.2	11.33	0.138	0.017
573.3	12.45	0.151	0.019

4.3.3 Density of water-rich and hydrocarbon-rich liquid phases

Understanding the impacts of solvent addition on the volumetric behavior of bitumen + water mixtures is a key element in the development and design of bitumen production and refining processes. In general, the excess volume for hydrocarbon + water binaries is positive and Furutaka and co-workers [33, 34] observed large positive values for benzene, toluene, ethylbenzene, n-hexane and n-decane + water mixtures especially near their respective UCEPs. Density measurements obtained for toluene + water up to 553 K (Table 4.4) and 1-methylnaphthalene + water up to 573 K (Table 4.5) are consistent with this expectation as shown in Figures 4.4 and 4.5. For both cases the measured density is less than the density predicted on the basis of ideal mixing and the divergence increases as the UCEP is approached. For the ideal mixture density calculations, LLV/LL boundary pressure was used as the reference pressure for water. High quality smoothed density data are available at these pressures and temperatures, shown in Tables 4.4 and 4.5, for water and toluene [32]. High quality density values for 1-methylnaphthalene at the LLV/LL pressures are not available in the literature. The saturated liquid density was used instead. The impact of pressure on the density of 1-methylnaphthalene is expected to be small. The ideal mixing density of hydrocarbons + water is calculated as:

$$\rho_{\text{mixture}} = 1 / \left(\frac{w_1}{\rho_1} + \frac{w_2}{\rho_2} \right) \quad (4-5)$$

where w and ρ are the weight fraction and density and subscripts denote components.

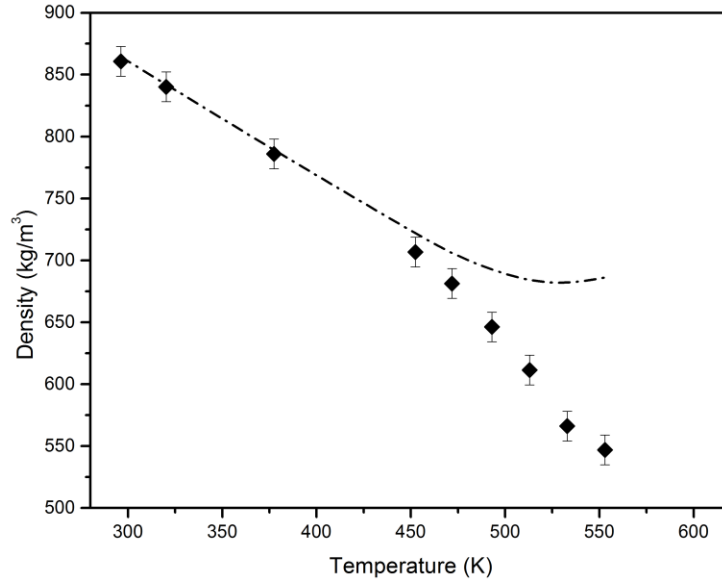


Figure 4.4. Experimental density of water-saturated toluene at the LLV/LL boundary pressure (\blacklozenge). The predicted density of the toluene-rich phase at the LL/LLV boundary pressure is based on water and toluene densities at the LLV/LL boundary pressure, and ideal mixing (equation 4-5) (— · —) using smoothed water solubility experimental data [20].

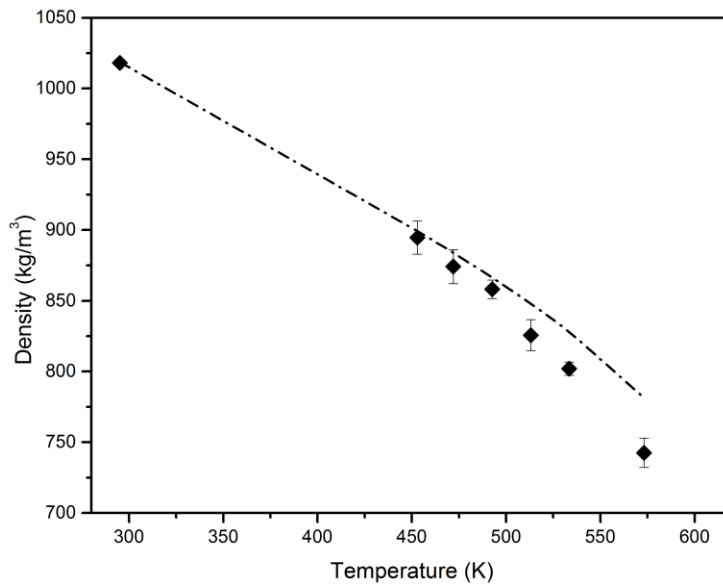


Figure 4.5. Experimental density of water saturated 1-methylnaphthalene at the LLV/LL boundary pressure (\blacklozenge). The predicted density of the 1-methylnaphthalene-rich liquid phase is based water density at the LLV/LL boundary pressure and 1 methylnaphthalene at its vapor pressure and ideal mixing equation 4-5 (— · —) using smoothed water solubility experimental data [21].

Table 4.4. Density of water-saturated toluene

T (K)	Water vapor pressure (MPa)	LLV/LL Boundary pressure (MPa)	Toluene density* (kg/m ³)	Water density* (kg/m ³)	Experimental density ± 12 (kg/m ³)	Predicted ideal mixing density* ± 6 (kg/m ³)
296.3	2.84*10 ⁻³	-	863.9	997.5	863	864.2
296.3	2.84*10 ⁻³	-	863.9	997.5	861	864.2
320.3	1.07*10 ⁻²	-	841.4	989.2	840	842.1
377.5	1.18*10 ⁻¹	-	785.6	955.2	786	788.8
452.4	9.86*10 ⁻¹	1.58	705.5	888.2	707	721.6
471.8	1.51	2.31	683.1	866.8	681	705.3
493.0	2.31	3.43	658.5	841.4	646	692.2
513.0	3.34	4.97	636.3	815.3	611	683.2
532.9	4.67	7.11	617.2	787.1	566	680.8
553.0	6.40	9.5	600.4	755.6	547	686.3

* The density of water [32] and toluene [32] at the LL/LLV pressure.

Table 4.5. Density of water-saturated 1-methylnaphthalene vs. predicted ideal mixing density.

T (K)	Water vapor pressure (MPa)	LLV/LL boundary pressure (MPa)	1-methylnaphthalene* density [56] (kg/m ³)	Water density* [56] (kg/m ³)	Experimental Density ± 12 (kg/m ³)	Predicted ideal mixing density* ± 6 (kg/m ³)
295.2	2.65*10 ⁻³	-	1018.6	997.5	1018	1019
453.0	9.98*10 ⁻¹	1.1	899.5	887.3	895	899
472.0	1.52	1.63	884.4	866.1	874	884
492.7	2.30	2.39	867.2	840.9	858	867
513.2	3.35	3.41	849.4	813.4	826	848
533.5	4.72	4.81	830.7	783.3	802	828
573.2	8.59	9.04	790.5	713.2	744	781

*Predicted ideal mixture density of the water-saturated 1-methylnaphthalene phase is calculated using the density of 1-methylnaphthalene [32] at its saturation pressure and water [32] at the LL/LLV boundary pressure (equation 4-5).

4.3.4 Density differences between the water-rich and hydrocarbon-rich liquid phases

For the water + toluene mixtures, the toluene-rich liquid phase is significantly less dense than the water-rich liquid phase over the range of conditions evaluated, while the water-rich liquid phase remains less dense than the 1-methylnaphtlene-rich liquid. These contrasting behaviors are both expected to arise in Athabasca bitumen + toluene + water mixtures because the density of Athabasca bitumen (1028 kg/m³ at 298K) is greater than but similar to that of water, while the density of toluene (862.3 kg/m³ at 298K) is less than the density of water at the same temperature. Further, the solubility of toluene in water at 298 K is negligible, so the impact of toluene on the water-rich phase density can be neglected. Thus the phase order in the view cell or in a separation vessel is a function of global composition at fixed temperature and due to differing temperature dependencies of the constituent and phase densities, a function of temperature at fixed composition. To a first approximation, the density of the hydrocarbon-rich phase can be computed using equation 4-5, at low temperatures. Explicit assumptions in equation 4-5 are that the volume of mixing for Athabasca bitumen and toluene is zero and the mutual solubility of water and hydrocarbons can be neglected. From Tables 4.6 and 4.7 this assumption based on the computed vs measured phase densities appears to be valid up to 500 K. The density values obtained can be compared with those of pure water from the literature [32]. Illustrative comparative calculations are shown in Figure 4.6 where phase density values computed using equation 4-5 for $w_{\text{tol}} = 0.170, 0.448$ and 0.667 weight fraction are compared to the density of saturated water. At $w_{\text{tol}} = 0.17$ there are two points of intersection between the hydrocarbon-rich and water-rich phase densities below 500 K. At these points the densities of the two phases are identical. The locus of phase inversion points, shown in Figure 4.7, constitute a boundary between compositions where the water rich phase is more or less dense than the hydrocarbon rich phase. Below $w_{\text{tol}} = 0.12$, the hydrocarbon-rich phase remains more dense than the water-rich phase. At higher weight fractions upper and lower phase inversion temperatures arise.

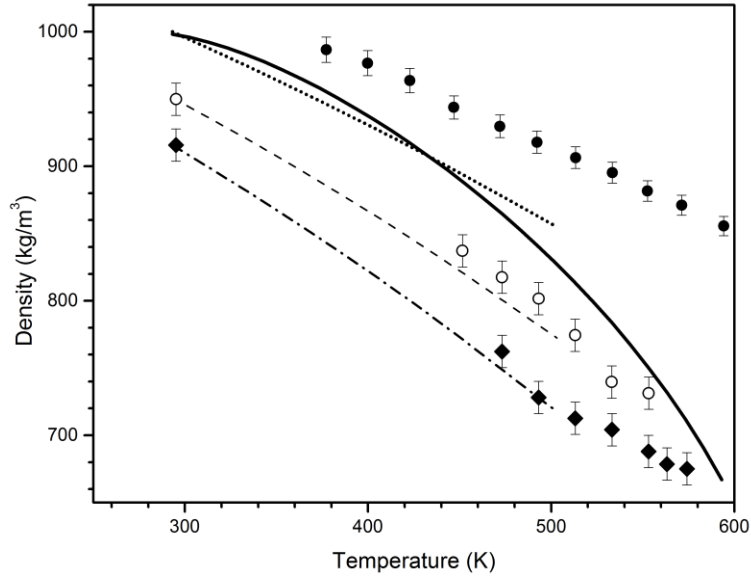


Figure 4.6. Computed density of saturated $\{(1-w) \text{ bitumen} + (w) \text{ toluene}\}$ mixtures at: $w = 0.170$ (.....), 0.448 (---), and 0.667 (-.-) weight fraction toluene at the LLV/LL boundary pressure (equation 4-5). Densities for Athabasca bitumen (●) Chapter 3, and water (—) [32] are shown for completeness. Experimental data for water saturated bitumen + toluene phase at $w = 0.448$ (○) and 0.667 (◆) are also shown.

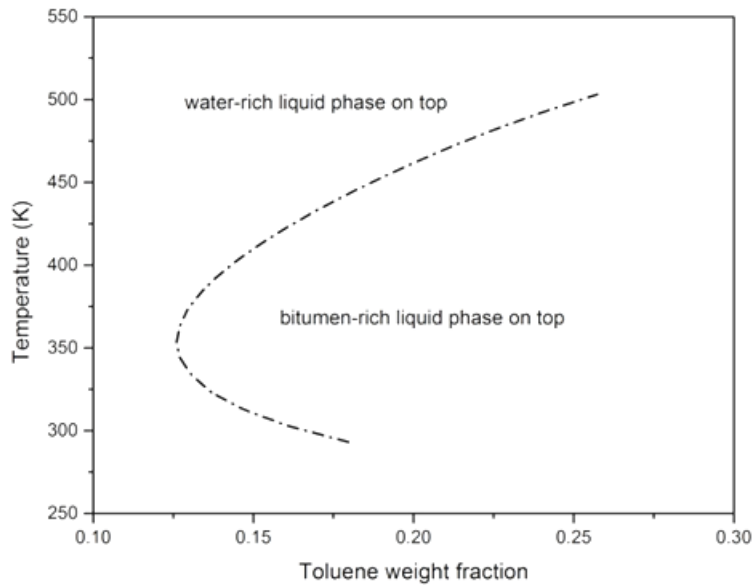


Figure 4.7. Approximate density inversion boundary for $\{(1-w) \text{ bitumen} + (w) \text{ toluene}\} + \text{water}$ (-.-) mixtures at the LLV/LL boundary pressure.

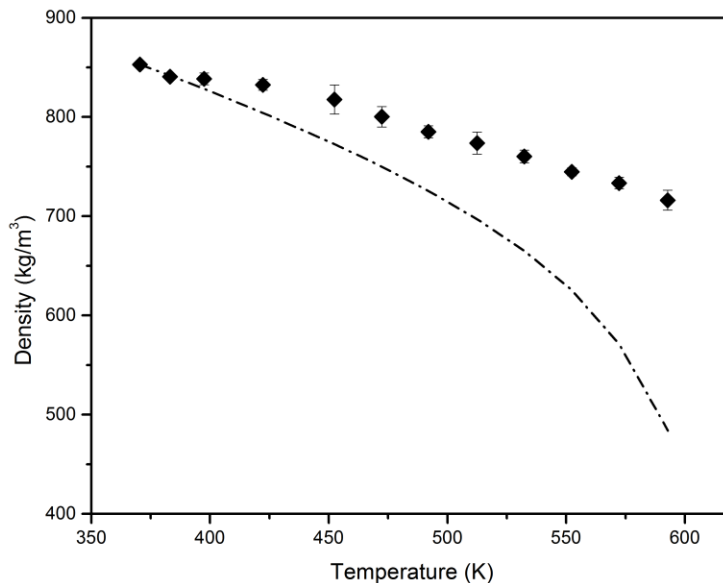


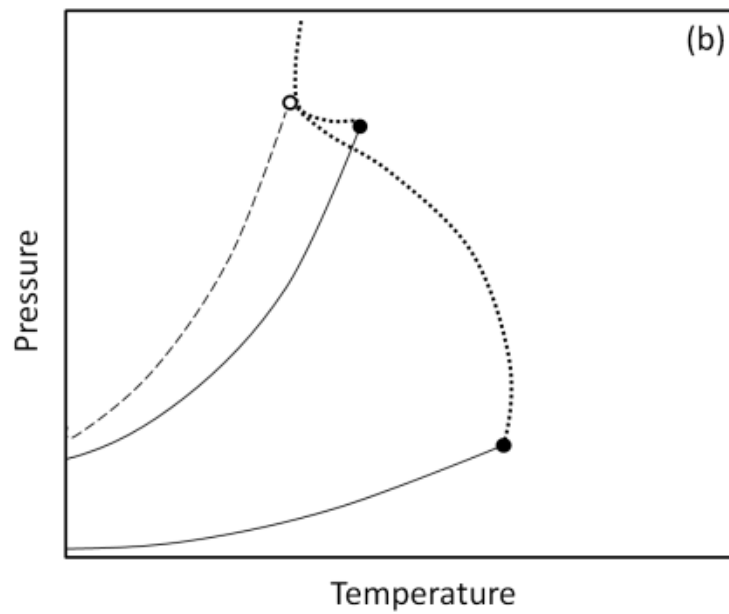
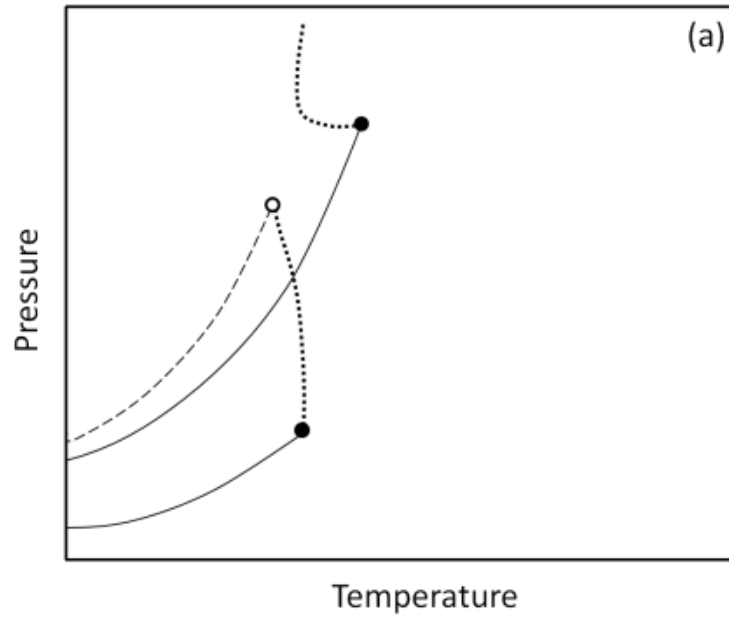
Figure 4.8. Experimental density of (1-w) Athabasca bitumen + (w) toluene at $w= 0.667$ vs temperature (\blacklozenge). The predicted density of toluene + bitumen mixtures at the saturation pressure based on ideal mixing (.-.-).

Above 500 K, the density of toluene decreases sharply in the approach to its critical temperature 591.8 K [15], and equation 4-5 no longer holds because measured densities for Athabasca bitumen + toluene pseudo binary mixtures diverge from ideality as shown in Figure 4.8 where the measured densities are significantly larger than the predicted ones. This effect arises because, even though the toluene on its own is nearing a critical point, the hydrocarbon mixture, comprising bitumen and toluene is remote from mixture critical point and consequently the measured mixture density is larger than expected based on ideal mixing. The larger experimental densities are also affected by toluene evaporation from bitumen phase at high temperatures.

4.3.5 Phase behavior type transition

If water + multicomponent hydrocarbon mixtures are treated as pseudo binary mixtures, the phase behavior type of the pseudo binary frequently undergoes a transition as the relative proportion of the hydrocarbons is altered. For example, Brunner [15] investigated the phase behavior of ternary mixtures of water + decalin + tetralin. For ternary mixtures of water + $\{(x)\text{decalin} + (1-x)\text{tetralin}\}$, by varying mole fraction x from $x= 0, 0.25, 0.5$ to 1 a transition from Type II to Type IIIa phase behavior was observed. The decalin + water binary exhibits Type IIIa phase behavior, while the tetralin + water binary exhibits

Type II phase behavior. As the mole fraction of tetralin increases the miscibility of these hydrocarbons in water increases. The transition in phase behavior type arises at approximately $x = 0.25$.



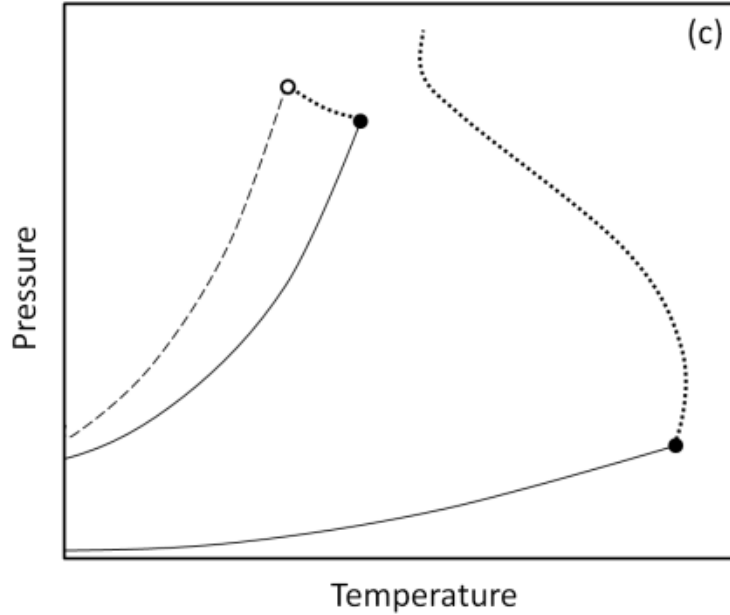


Figure 4.9. Schematic showing the transition from Type IIIa to Type IIIb phase behavior as the composition of bitumen in the bitumen + toluene + water mixtures increases, from Figure (a) to (c). The LLV curve (---), LV and LL critical locus (.....), the saturation curve of water and hydrocarbons (—) are shown. The upper critical end point of the mixture is represented by (O), while the critical point of water and hydrocarbons are represented by (●).

Table 4.6. Density of (1-w) bitumen + (w) toluene at w=0.667 weight fraction.

T (K)	Toluene pressure (MPa)	vapor	LV/L boundary pressure P (MPa)	Experimental Density ± 12 (kg/m ³)	Predicted density* ± 6 (kg/m ³)
370.5	$6.85 \cdot 10^{-2}$		0.06	853	851
383.2	$9.98 \cdot 10^{-2}$		0.13	839	840
398.2	$1.50 \cdot 10^{-1}$		0.16	836	826
422.4	$2.71 \cdot 10^{-1}$		0.18	829	802
452.5	$5.11 \cdot 10^{-1}$		0.27	812	771
472.4	$7.40 \cdot 10^{-1}$		0.46	792	748
492	1.03		0.59	775	723
512.6	1.43		0.85	762	695
532.4	1.91		1.08	746	663
552.5	2.51		1.46	728	623
572.3	3.24		2.06	716	568
592.9			2.3	696	481

*As the pressure is below the vapor pressure of toluene, the predicted ideal mixing density of the hydrocarbon-rich liquid phase is calculated using the density of Athabasca bitumen (Chapter 3) and toluene [32] at their respective saturation pressures (equation 4-5).

Table 4.7. Density of water saturated bitumen-rich phase for $\{(1-w) \text{ bitumen} + (w) \text{ toluene}\} + \text{water}$ mixtures at $w=0.448$ and 0.667 .

T (K)	LL/LLV boundary pressure (MPa)	Experimental density ± 12 (kg/m^3)	Predicted water-free bitumen + 0.448 toluene density* (kg/m^3)	Predicted water-saturated bitumen-rich phase density* ± 6 (kg/m^3)
295.2	-	949	949	949
451.6	1.7	836	820	820
473.2	2.53	818	800	801
493.2	3.40	802	780	781
513.1	4.88	775	761	763
533.1	6.76	742	743	745
553.3	9.40	736	728	730

T (K)	LL/LLV boundary pressure (MPa)	Experimental density ± 12 (kg/m^3)	Predicted water-free bitumen + 0.667 toluene density* (kg/m^3)	Predicted water-saturated bitumen-rich phase density* ± 6 (kg/m^3)
295.2	-	915	915	915
473.2	2.65	762	749	752
492.6	3.52	729	728	732
512.7	5.08	714	707	713
532.9	6.66	707	686	694
553.2	9.79	693	673	681
563.1	11.24	685	666	675
573.5	12.47	683	658	667

*- The density of pure toluene and water [32] is obtained at the LL/LLV boundary pressure, while density of Athabasca bitumen (Chapter 3) at its bubble pressure are used to evaluate the ideal mixture density at the LL/LLV boundary pressure.

The water + toluene binary mixture exhibits Type IIIa phase behavior [15], while the Athabasca bitumen + water pseudo-binary exhibits Type IIIb phase behavior (Chapter 2). These phase behavior types are indistinguishable at low temperatures but differ at high temperatures i.e., above the UCEP, where, in the present context, the water-rich liquid phase persists for Type IIIa phase behavior, Figure 4.9a, and the hydrocarbon-rich liquid phase persists for Type IIIb phase behavior, Figure 4.9c. Brunner [27] showed that at the transition, the LL critical locus intersects the UCEP of the LLV curve to create a tricritical end point, Figure 4.9b. In this preliminary study, limited to temperatures below

the critical point of toluene and the UCEP for the water + toluene binary mixture, the composition at the transition between Type IIIa and Type IIIb phase behavior could not be identified. Further the transition composition cannot be inferred from lower temperature phase order because phase inversion at high temperature, near the critical temperature of water, is anticipated. From a bitumen production, transport and refining process design and development perspective, phase order inversion in particular may be difficult to control, monitor or predict because the envisioned combinations of light hydrocarbons bitumen and water traverse broad ranges of temperature, pressure and composition that intersect critical conditions and phase behavior type transitions.

4.4 Conclusions

The experimental and computational results for toluene + Athabasca bitumen + water mixtures presented above illustrate key features of this pseudo ternary phase diagram and for low molar mass hydrocarbon + Athabasca bitumen + water mixtures more generally. Phase behavior transitions between Type IIIb and Type IIIa or Type II phase behavior according to the van Konynenburg and Scott classification scheme is a key feature of these ternary mixtures. Phase density inversions arise in these mixtures that change the order of the phases in view cells or separation equipment. From the perspective of phase density prediction, ideal mixing assumptions that break down at temperatures well below the critical temperature of low molar mass hydrocarbons in simple binary mixtures remain robust for multicomponent asymmetric ones within measurement and prediction error at high pressure. Finally, while toluene addition to mixtures of bitumen + water increases the solubility of water in hydrocarbon-rich phase at high temperature, the effect is less than expected on a mass basis where, data for water solubility in toluene and bitumen overlap.

4.5 References

- [1] A. Kruse and E. Dinjus, "Hot compressed water as reaction medium and reactant - Properties and synthesis reactions," *Journal of Supercritical Fluids*, vol. 39, pp. 362-380, Jan 2007.
- [2] A. Kruse and E. Dinjus, "Hot compressed water as reaction medium and reactant: 2. Degradation reactions," *The Journal of Supercritical Fluids*, vol. 41, pp. 361-379, 2007.
- [3] T. Adschiri, "Supercritical water up-grading of heavy oils," *Nihon Enerugi Gakkaishi/Journal of the Japan Institute of Energy*, vol. 88, pp. 172-175, 2009.

- [4] Z. M. Cheng, Y. Ding, L. Q. Zhao, P. Q. Yuan, and W. K. Yuan, "Effects of Supercritical Water in Vacuum Residue Upgrading," *Energy & Fuels*, vol. 23, pp. 3178-3183, May-Jun 2009.
- [5] L.-n. Han, R. Zhang, and J.-c. Bi, "Upgrading of coal-tar pitch in supercritical water," *Journal of Fuel Chemistry and Technology*, vol. 36, pp. 1-5, 2008.
- [6] J. D. McCollum and L. M. Quick, "Process for Upgrading a Hydrocarbon Fraction," USA Patent, 1979.
- [7] M. Morimoto, Y. Sugimoto, Y. Saotome, S. Sato, and T. Takanohashi, "Effect of supercritical water on upgrading reaction of oil sand bitumen," *The Journal of Supercritical Fluids*, vol. 55, pp. 223-231, 2010.
- [8] T. Sato, T. Adschiri, K. Arai, G. L. Rempel, and F. T. T. Ng, "Upgrading of asphalt with and without partial oxidation in supercritical water," *Fuel*, vol. 82, pp. 1231-1239, Jul 2003.
- [9] W. Wahyudiono, T. Shiraishi, M. Sasaki, and M. Goto, "Bitumen upgrading under solvothermal/hydrothermal conditions," *Research on Chemical Intermediates*, vol. 37, pp. 375-381, 2011.
- [10] M. Watanabe, S.-n. Kato, S. Ishizeki, H. Inomata, and R. L. Smith Jr, "Heavy oil upgrading in the presence of high density water: Basic study," *The Journal of Supercritical Fluids*, vol. 53, pp. 48-52, 2010.
- [11] M. J. Amani, M. R. Gray, and J. M. Shaw, "Phase behavior of Athabasca bitumen+water mixtures at high temperature and pressure," *The Journal of Supercritical Fluids*, vol. 77, pp. 142-152, 2013.
- [12] M. J. Amani, M. R. Gray, and J. M. Shaw, "Volume of mixing and solubility of water in Athabasca bitumen at high temperature and pressure," *fluid phase equilibria*, DOI: 10.1016/j.fluid.2013.07.021., 2013.
- [13] P. H. Vankonynenburg and R. L. Scott, "Critical Lines and Phase-Equilibria in Binary Vanderwaals Mixtures," *Philosophical Transactions of the Royal Society of London Series a-Mathematical Physical and Engineering Sciences*, vol. 298, pp. 495-540, 1980.
- [14] F. E. Anderson and J. M. Prausnitz, "Mutual solubilities and vapor-pressures for binary and ternary aqueous systems containing benzene, toluene, meta-xylene, thiophene and pyridine in the region 100-200-degrees-c," *Fluid Phase Equilibria*, vol. 32, pp. 63-76, Dec 1986.
- [15] E. Brunner, M. C. Thies, and G. M. Schneider, "Fluid mixtures at high pressures: Phase behavior and critical phenomena for binary mixtures of water with aromatic hydrocarbons," *The Journal of Supercritical Fluids*, vol. 39, pp. 160-173, 2006.
- [16] K. Chandler, B. Eason, C. L. Liotta, and C. A. Eckert, "Phase equilibria for binary aqueous systems from a near-critical water reaction apparatus," *Industrial & Engineering Chemistry Research*, vol. 37, pp. 3515-3518, Aug 1998.
- [17] J. S. Brown, J. P. Hallett, D. Bush, and C. A. Eckert, "Liquid-liquid equilibria for binary mixtures of water plus acetophenone, plus 1-octanol, plus anisole, and plus toluene from 370 K to 550 K," *Journal of Chemical and Engineering Data*, vol. 45, pp. 846-850, Sep-Oct 2000.

- [18] B. J. Neely, J. Wagner, R. L. Robinson, and K. A. M. Gasem, "Mutual solubility measurements of hydrocarbon-water systems containing benzene, toluene, and 3-methylpentane," *Journal of Chemical and Engineering Data*, vol. 53, pp. 165-174, Jan 2008.
- [19] F. Y. Jou and A. E. Mather, "Liquid-liquid equilibria for binary mixtures of water plus benzene, water plus toluene, and water plus p-xylene from 273 K to 458 K," *Journal of Chemical and Engineering Data*, vol. 48, pp. 750-752, May-Jun 2003.
- [20] A. Maczynski, D. G. Shaw, M. Goral, B. Wisniewska-Gocłowska, A. Skrzecz, I. Owczarek, et al., "IUPAC-NIST Solubility Data Series. 81. Hydrocarbons with water and seawater-revised and updated. Part 5. C-7 hydrocarbons with water and heavy water," *Journal of Physical and Chemical Reference Data*, vol. 34, pp. 1399-1487, 2005.
- [21] D. G. Shaw, A. Maczynski, M. Goral, B. Wisniewska-Gocłowska, A. Skrzecz, I. Owczarek, et al., "IUPAC-NIST solubility data series. 81. Hydrocarbons with water and seawater-revised and updated. Part 10. C-11 and C-12 hydrocarbons with water," *Journal of Physical and Chemical Reference Data*, vol. 35, pp. 153-203, Mar 2006.
- [22] Y. Shimoyama, M. Haruki, Y. Iwai, and Y. Arai, "Measurement and prediction of liquid-liquid equilibria for water + hexane + hexadecane, water + toluene + decane, and water + toluene + ethylbenzene ternary systems at high temperatures and pressures," *Journal of Chemical and Engineering Data*, vol. 47, pp. 1232-1236, 2002.
- [23] W. L. Nelson, "Solubility of water in oil," *oil & gas journal*, p. 140, April 1956.
- [24] J. Griswold and J. E. Kasch, "Hydrocarbon-water Solubilities at elevated temperatures and pressures," *Industrial and Engineering Chemistry*, vol. 34, pp. 804-806, 1942.
- [25] K. S. Pedersen, J. Milter, and C. P. Rasmussen, "Mutual solubility of water and a reservoir fluid at high temperatures and pressures: Experimental and simulated data," *Fluid Phase Equilibria*, vol. 189, pp. 85-97, 2001.
- [26] C. A. Glandt and W. G. Chapman, "Effect of water dissolution on oil viscosity," *Spe Reservoir Engineering*, vol. 10, pp. 59-64, Feb 1995.
- [27] E. Brunner, "Fluid mixtures at high pressures IX. Phase separation and critical phenomena in 23 (n-alkane + water) mixtures," *The Journal of Chemical Thermodynamics*, vol. 22, pp. 335-353, 1990.
- [28] S. P. Christensen and M. E. Paulaitis, "Phase equilibria for tetralin-water and 1-methylnaphthalene-water mixtures at elevated temperatures and pressures," *Fluid Phase Equilibria*, vol. 71, pp. 63-83, 1992.
- [29] A. Bazyleva, M. Fulem, M. Becerra, B. Zhao, and J. M. Shaw, "Phase Behavior of Athabasca Bitumen," *Journal of Chemical and Engineering Data*, vol. 56, pp. 3242-3253, Jul 2011.
- [30] S. J. Abedi, H. Y. Cai, S. Seyfaie, and J. M. Shaw, "Simultaneous phase behaviour, elemental composition and density measurement using X-ray imaging," *Fluid Phase Equilibria*, vol. 158, pp. 775-781, Jun 1999.

- [31] J. H. Hubbell and S. M. Seltzer, "Tables of x-ray mass attenuation coefficients and mass energy-absorption coefficients from 1 keV to 20 MeV for elements $Z = 1$ to 92 and 48 additional substances of dosimetric interest," ed: Radiation and Biomolecular Physics Division, PML, NIST, 2009.
- [32] E. W. Lemmon, M. O. McLinden, and D. G. Friend, "Thermophysical Properties of Fluid Systems," in NIST Chemistry WebBook, NIST Standard Reference Database Number 69, P. J. Linstrom and W. G. Mallard, Eds., ed Gaithersburg MD, <http://webbook.nist.gov>: National Institute of Standards and Technology, 2012.
- [33] S. Furutaka and S. Ikawa, "Volume expansion behavior of water-hydrocarbon mixtures at high temperatures and pressures as studied by infrared spectroscopy," *Fluid Phase Equilibria*, vol. 217, pp. 181-188, Mar 2004.
- [34] Y. Ishikawa, S. Arai, S. Furutaka, and S. Ikawa, "Anomalous volumetric behavior of water-hexane and water-decane mixtures in the vicinity of the critical region as studied by infrared spectroscopy," *Journal of Chemical Physics*, vol. 122, May 2005.

Chapter 5. Correlations for calculating the solubility of water in ill-defined hydrocarbons

5.1 Introduction

Thermodynamic data and accurate models for the properties of hydrocarbons mixtures containing water, including solubility, are often required to design unit operations, to develop processes for refining and production, and to perform environmental assessments. For ill-defined hydrocarbons such as Athabasca bitumen, examples include, hot water extraction processes (mined bitumen), in situ production processes such as SAGD, crude distillation towers, and refining more broadly. As water solubility in hydrocarbons and hydrocarbon solubility in water varies over four to six orders of magnitude with temperature variations from room temperature to the critical temperature of water ($T_c = 647.1 \text{ K}$), and the values are typically small, solubility measurement and correlation efforts encounter numerous challenges. Typically, water solubility in hydrocarbons can be estimated to within one order of magnitude, and hydrocarbon solubility in water to within two orders of magnitude over this temperature range using general-purpose correlations.

Solubility models for water + hydrocarbon mixtures fall into two categories. Some models attempt to estimate mutual solubilities, based on equations of state, activity models or correlations, while others focus on correlations for hydrocarbon solubility in water (outside the scope of this review) or on water solubility in hydrocarbons. These methods generally rely on fitting parameters to limited numbers of fluids or to specific homologous series, and calculation outcomes are sensitive to the choice of properties used in fluid characterization and to the uncertainties of these input properties. Due to the many experimental difficulties encountered, solubility data quality is also an issue. Care must be exercised in data selection for model training and testing. Maczynski et. al [1-12] provide detailed reviews of mutual solubility data for hydrocarbons and water published before 2003. This body of work is a key resource for work in this field.

There are a number of thermodynamics models including equation of state and empirical correlations that predict the mutual solubility of water and low molecular weight

hydrocarbons. De Hemptinne et. al [13] reviewed the available methods to describe mutual solubility of water and hydrocarbons. They noted that both aqueous and organic liquid phases cannot be described adequately with a single model and that different models for each phase are preferred. Kabadi et al. [14] proposed asymmetric mixing rules for water + hydrocarbon mixtures using Soave-Redlich-Kwong equation of state. Michel and co-workers [15] investigated the application of cubic equations of state in calculations of mutual solubilities of water and hydrocarbons. They stated the conventional mixing rules for cubic equation did not led to reliable results for practical applications. Soreide et al. [16] and Dhima et al. [17] also used two individual sets of binary interaction parameters for each aqueous phase and non-aqueous phase. They proposed a composition-based energy parameter for Peng-Robinson equation to consider impacts of the aqueous phase salinity. Haruki and co-workers [18-21] proposed an exponent-type mixing rule for the energy parameter in SRK equation. They adjusted the binary parameters to give most precise fits to the experimental data. Economou et al. [22] studied the application of Huron–Vidal mixing rule with PR equation on 1-hexene + water mixture. They stated Huron–Vidal mixing rule led to much better results comparing to conventional van der Waals mixing rules. Li et al. [23] coupled a modified Huron–Vidal mixing rule with the UNIFAC method to predict solubility and phase equilibria for light hydrocarbon-water. Yan et al. [24] applied the CPA model to estimate solubility of water in a hydrocarbon mixture containing C7+ components. Yaws [25-27] also developed simple empirical models to roughly estimate mutual solubility of hydrocarbons and water for three categories of hydrocarbons. These models illustrate the capability of equations of state to predict phase equilibria for a limited hydrocarbon + water binary mixtures. However these models can predict mutual solubilities of liquid phases qualitatively, but no general recommendation is proposed to extend these models for ill-defined heavy hydrocarbons + water mixtures. Estimation of properties based on these methods for reservoir fluids, in particular for ill-defined hydrocarbons where the oils are characterized using distillation curves, can be very poor. In a recent effort extend mutual solubility calculations to reservoir fluids, and distillation cuts, Satyro et al. [28] proposed a predictive NRTL-based approach to estimate mutual solubilities of hydrocarbons and water using hydrocarbon specific gravity and Watson-K factor as correlating parameters. Their general model was fit and evaluated using reliable mutual solubility data for pure hydrocarbons + water. For heavy hydrocarbons, their model diverges from the solubility

data, and they proposed a modified model for predicting the solubility of water in heavy hydrocarbons and reservoir fluids.

Empirical correlations are generally simpler than equation of state calculation approaches. They require fewer input parameters because they focus only on water solubility in the hydrocarbon phase. Tsonopoulos and co-workers [29-31] investigated the solubility of water in hydrocarbons at high temperatures, and analyzed available experimental solubility data from the perspective of prediction based on simple empirical correlations. The API handbook [32] suggests a few correlations to predict water solubility as a function of temperature and hydrogen to carbon ratio for pure and mixture hydrocarbons. As these models were developed based on the solubility of water in low molecular weight hydrocarbons, they do not predict reliable values for reservoir fluid + water mixtures at high temperature. These models also do not take the impact of pressure into account as they were developed to predict solubilities at the three-phase bubble pressure condition – the LL to LLV phase boundary. This is a major shortcoming that adversely affects process design calculations for hydrocarbon process effluent and refining alike.

The goal of this work is to develop predictive methods to estimate the solubility of water in ill-defined hydrocarbons at temperatures below and above the upper critical end point (UCEP) of heavy oil + water mixtures. The available experimental solubility data of water + pure hydrocarbons [1-12, 33, 34] and Athabasca bitumen (Chapter 3) [35] are used to regress two empirical models. The first model (Model A) is benchmarked against published solubility data of water in 10 heavy oil mixtures. *Model A* is correlated in terms of elemental hydrogen weight fraction and the average boiling temperature of the hydrocarbon. This correlation presents reliable water solubilities in ill-defined heavy hydrocarbons mixtures from room temperatures up to the UCEP of the mixtures. A second empirical model (Model B) intended to predict the solubility of water in heavy oil as a function of pressure at temperatures above the UCEP of mixtures comprising water + heavy hydrocarbons, is also discussed. The accuracy of these models is discussed in light of the thermal instability of the hydrocarbons at high temperatures, and the experimental inaccessibility of accurate measurements under these conditions.

5.2 Model development

5.2.1 Model A: solubility of water in hydrocarbons below the UCEP of hydrocarbon + water mixtures

Mixtures of water + light hydrocarbons, where the critical temperature of the hydrocarbons is less than the critical temperature of water exhibit Type IIIa phase behavior [36, 37]. Mixtures of water and heavy hydrocarbons, where the critical temperature of hydrocarbons are comparable to or exceed that of water, exhibit phase behavior Type II or IIIb [36-38]. All these binary mixtures show similar LLV behavior at low temperatures. LLV three-phase equilibrium extends from the SLLV four phase point (region) and extends to the UCEP where the light liquid phase becomes critically identical to the heavy liquid phase (TYPE II) or to a K-point where the light liquid becomes critically identical to the vapor (Type III). The distinction between Types IIIa and IIIb is that at high temperature the single liquid phase present in the phase diagram is water rich for Type IIIa and hydrocarbon rich for Type IIIb. The solubility of water in the hydrocarbon phase, for all cases, tends to be in the order of a few parts per million at room temperature, and the solubility increases sharply with temperature.

From basic thermodynamics [29], the solubility of a solute is related to the enthalpy of solution as:

$$\frac{\partial \ln(x_i)}{\partial(T)} = -\frac{\Delta h_i^{sol}}{RT^2} \quad (5-1)$$

where x_i is the mole fraction of solute (i), and Δh_i^{sol} is given by:

$$\Delta h_i^{sol} = \bar{h}_i - h_i \quad (5-2)$$

\bar{h}_i and h_i are respectively the enthalpy of solute (i) in solution and in a reference state typically a pure liquid. Over a narrow range of temperatures, the enthalpy of solution can be treated as a constant. For a wider range of temperatures, it is reasonable to assume that the enthalpy of solution varies linearly with temperature. Tsonopoulos and co-workers [29-31] made this assumption to correlate the solubility of hydrocarbons in water.

Treating Δh_w^{sol} as a linear function of temperature, equation 5-1 can be integrated for water as:

$$\ln(x_w) = \frac{A}{T} + B \ln(T) + C \quad (5-3)$$

where x_w is mole fraction of water. Equation 5-3 can be fitted to individual binary mixtures to predict water solubility over a broad range of temperatures.

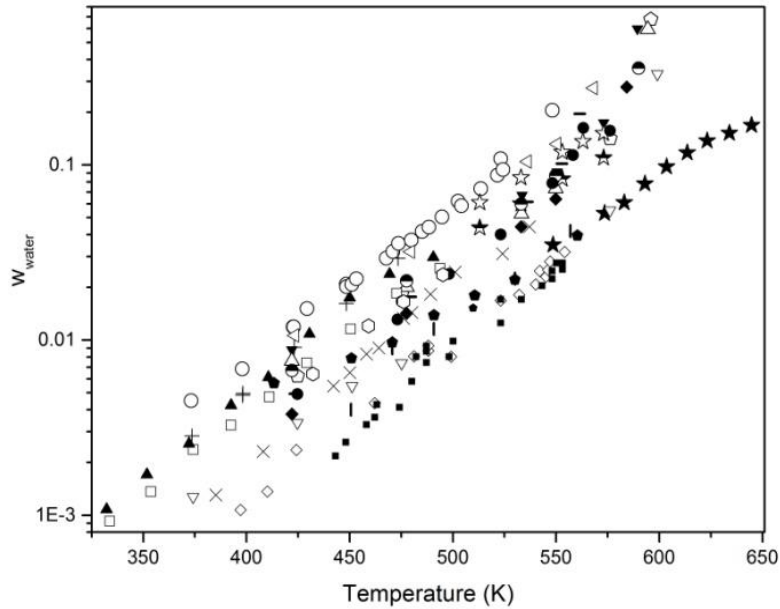


Figure 5.1. Solubility of water in pure hydrocarbons and reservoir fluids at temperatures above 373 K. Solubility of water in Athabasca bitumen (★) Chapter 3 [35], Athabasca bitumen + 0.443 toluene(★) Chapter 4 [50], Athabasca bitumen + 0.668 toluene (★) Chapter 4 [50], toluene (○) [5, 33, 34], ethylbenzene (◄) [6], m-xylene (+) [6], ethylcyclohexane (-) [7], tetralin (◊) [9], thianaphthene (▲) [52], cis-decalin (∇) [9], 1-butylcyclohexane (◆) [9], decane (●) [9], 1-methylnaphthalene (▼) [10], 1-ethylnaphthalene (Δ) [10], 1,4-diisopropylbenzene (⊙)[10], 9,10-dihydrophenanthrene (◻) [52], naphtha (○, Mw = 147) [47], kerosene(×,Mw = 173) [47], lubricating oil (◇, Mw = 425) [47], gross oil mixtures (■, Mw = 425) [46], Coalinga crude oil (l, Mw = 439) [48], Huntington Beach crude oil (●, Mw = 442) [48], Peace River crude oil (●, Mw = 571) [48] and Cat Canyon crude oil (▷, Mw = 627) [48].

In the case of bitumen and heavy oils, which are not well-characterized, measuring their properties including average molecular weight is challenging. Self-association of asphaltenic components may also impact the accuracy of these “molecular” measures. In this work, weight fraction is used to facilitate heavy oil applications. Figure 5.1 shows how saturated water weight fraction varies with temperature in diverse hydrocarbon + water mixtures including reservoir fluid and bitumen containing mixtures. Expressed in

this way, water solubility varies over one order of magnitude at any given temperature and the trends with temperature are comparable. These two features of the data have been exploited previously in the development of mixture specific or general correlations. The solubility of water in hydrocarbons decreases with increasing molecular size, and varies at fixed molar mass with the details of molecular structure. In this work, the normal boiling point (T_b) is used as a surrogate for molecular size, and hydrogen mass fraction (H_{wt}) as a surrogate for structure because these data are readily available for both pure compounds and mixtures. Satyro et al. (2013) used K_{Watson} (UOP factor) and specific gravity to develop their recent correlation. Yaws [25-27] used T_b and the API method [32] uses carbon to hydrogen to ratio to characterize the hydrocarbons.

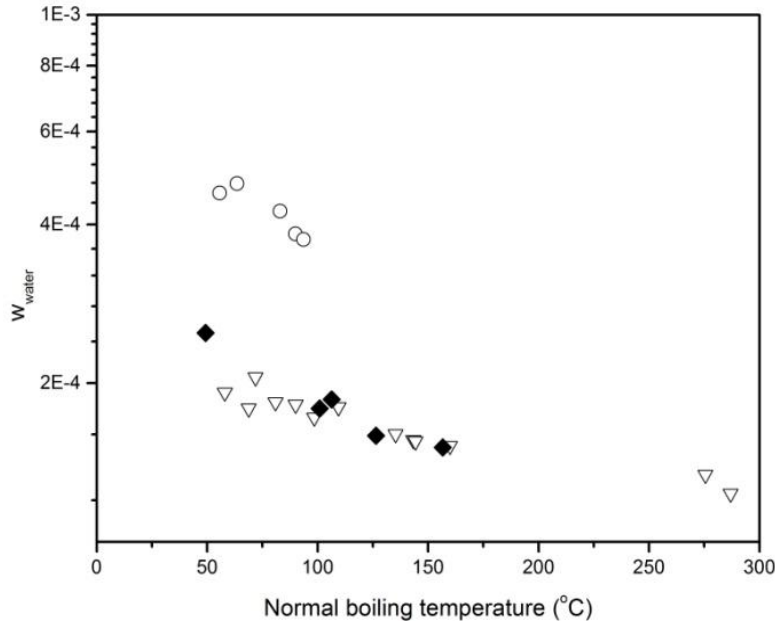


Figure 5.2. Solubility of water in paraffins (∇), olefins (\blacklozenge) and naphthenes (\circ) at 293.2 ± 1 K as a function of normal boiling point [1-12].

Figures 5.2 and 5.3 illustrate the dependence of water solubility in pure hydrocarbons at constant temperature to the hydrogen weight fraction (H_{wt}) and the boiling temperature (T_b) of hydrocarbons. The logarithm of water solubility varies linearly with H_{wt} and T_b of hydrocarbons at fixed temperature within each family of compounds. Thus, the coefficients of equation 5-3 can be expressed as linear functions of H_{wt} and T_b and *Model A* becomes:

$$\ln(w_w) = (a_1 T_b + b_1 H_{wt} + c_1) \frac{1}{T} + (a_2 T_b + b_2 H_{wt} + c_2) \ln(T) + (a_3 T_b + b_3 H_{wt} + c_3) \quad (5-4)$$

where w_w is the weight fraction of water in the hydrocarbon phase at saturation and T is absolute temperature in Kelvin. The mass fraction of water in the hydrocarbon phase at pressures less than the saturation pressure, well approximated by the water vapor pressure below 620 K, can be approximated by prorating the solubility value calculated based on the ratio of the water fugacity or pressure to the fugacity or pressure of water at saturation:

$$(w_w)_P = w_w \left(\frac{P}{P_{water}^{sat}} \right) \quad (5-5)$$

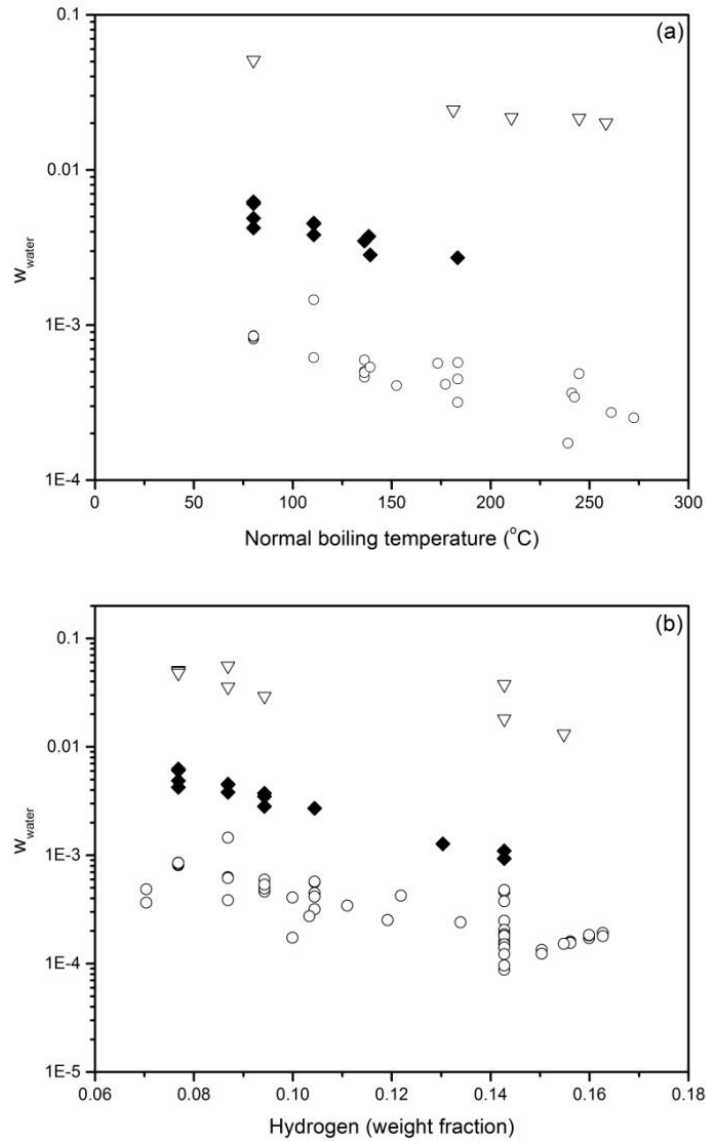


Figure 5.3. Solubility of water in aromatic hydrocarbons a) as a function of boiling temperature at 293.2 ± 1 K (○) and 373.2 (◆) and 477.6 (▽); b) as a function of hydrogen weight fraction 293.2 ± 1 K (○) and 373.2 (◆) and 473.2 (▽) [1-12].

5.2.2 Model B: solubility of water in hydrocarbon-rich liquids above the UCEP of hydrocarbon + water mixtures

Above the upper critical end point of a hydrocarbon + water mixture, the phase behavior Type of the mixture is a key starting point for the development a water solubility correlation method because a hydrocarbon-rich liquid phase may not be present. For mixtures exhibiting Types IIIa phase behavior, the liquid phase persisting at temperatures above the UCEP is water-rich. Examples include benzene, toluene and light n-alkanes + water mixtures. For mixtures exhibiting Type II phase behavior such as 1-methylnaphthalene, tetralin and naphthalene + water mixtures, either a hydrocarbon-rich phase or a water-rich phase persists at temperatures above the UCEP depending on the relative critical temperatures of the water and the hydrocarbon constituents. For water + hydrocarbon mixtures exhibiting Type IIIb phase behavior, the hydrocarbon-rich liquid phase persists above the UCEP. Examples of phase behavior Type IIIb phase behavior include water + large n-alkanes (C_{26} and above), water + indene, and water + heavy oils and bitumen. Correlation development must be restricted to cases where the high-temperature liquid phase is hydrocarbon-rich. For such cases, the UCEP approaches the critical temperature of water (647.1 K) and there is no water in hydrocarbon solubility data at these conditions in the literature. Fore knowledge regarding the phase behavior of the mixture is essential. Further, the vapor pressure of water is not available to provide a reliable reference condition for a correlation, and the important role of pressure must be approximated knowing that the properties of water, the dominant species in the vapor phase, are highly non-ideal. Finally, the hydrocarbon + water mixtures are reactive under these conditions.

With these caveats noted, Henry's law is a simple and effective model to relate solubility and pressure. The solubility of a solute in a liquid increases with increasing pressure. Henry's Law expresses the relationship between the solubility of a solute in mole fraction, x_i , and partial pressure of the solute in the gas phase, P_i :

$$P_i = Hx_i \quad (5-6)$$

where H is defined as the Henry constant. While equation 5-6 is strictly valid for sparingly soluble solutes where the gas phase may be treated as ideal, it is generally assumed that P_i/x_i remains constant, irrespective of pressure, at a fixed temperature. Within the precision of the hydrocarbon + water database, this assumption is justified, as illustrated in Figure 5.4 for bitumen + water mixtures, where the L_2V/L_2 pressure boundary varies linearly with water composition in the hydrocarbon-rich phase at 623.2, Figure 5.4a, and at 644 K, Figure 5.4b. As per the development of Model A, the correlation is developed on the basis of weight fraction, w_w , instead of mole fraction, x_w , and equation 5-6 becomes:

$$P_w = Kw_w \quad (5-7)$$

where K is a function of temperature and the partial pressure of water (P_w):

$$P_w = P - P_{\text{solvent}}^{\text{sat}} \quad (5-8)$$

where P is the total pressure of the mixture in MPa and $P_{\text{solvent}}^{\text{sat}}$ is the saturation pressure of bitumen (solvent). Below the critical temperature of water, K is readily expressed as a function of temperature in MPa by combining a water vapor pressure expression, such as the NIST water vapor pressure equation [56] with equation 5-4 to obtain:

$$\ln(K) = \ln(P_w^{\text{sat}}) - \ln(w_w) \quad (5-9)$$

Equation 5-9 is valid where the solubility of the hydrocarbon in liquid water is negligible. The water vapor pressure can be replaced by the three phase LLV to two phase LL boundary pressure if it is available. This latter modification requires solvent specific knowledge but levers the general expression for w_w (equation 5-4). It is not clear whether extrapolating equation 5-9, in modified or unmodified form, offers an advantage to following a solvent specific Van't Hoff construction as for Model A, where K can be expressed as:

$$\ln(K) = \frac{A'}{T} + B'\ln(T) + C' \quad (5-10)$$

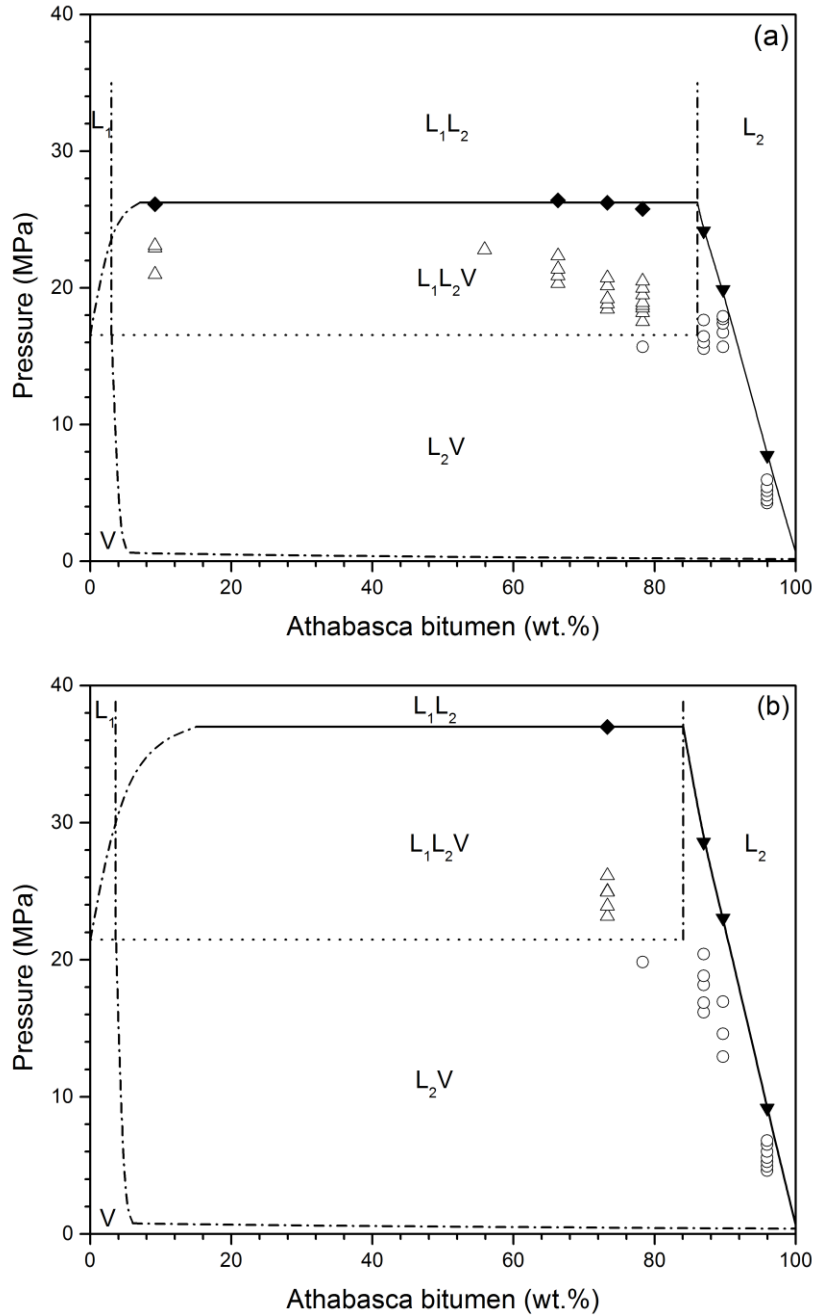


Figure 5.4. P-x diagrams of Athabasca bitumen + water (a) 623.2 K and (b) 644 K. Measured liquid-vapor (o) and liquid-liquid-vapor (Δ) equilibrium data are shown. The vapor pressure of water obtained from [39]. Solid lines (—) show the LL/LLV and L_2V/L_2 boundaries where points on these boundaries are designated with (\blacklozenge) and (\blacktriangledown), respectively, and the L_2V/LLV boundary defined by the vapor pressure of water (.....). Boundaries designated with a dash-dot lines (-.-) are illustrative and were not identified experimentally (Chapter 3).

Table 5.1. List of substances and their properties used fit parameters for *Model A* (equation 5-4)

Compound name	Formula	Mw	H_{wt}	T_b (°C)	T range (K)	No.	AARD (wt %)	References
2-Methyl-1,3-butadiene	C ₅ H ₈	68.1	0.1176	34.1	293.2-333.2	3	38.7	[1]
Cyclopentane	C ₅ H ₁₀	70.1	0.1427	49.3	273.2-313.2	5	11.6	[1]
2-Methyl-2-butene	C ₅ H ₁₀	70.1	0.1427	38.6	293.2-333.2	4	47.8	[1]
2-Methylbutane	C ₅ H ₁₂	72.1	0.1665	27.8	283.2-333.2	5	18.9	[1]
n-Pentane	C ₅ H ₁₂	72.1	0.1665	36.1	278.7-298.0	4	9.8	[1]
Benzene	C ₆ H ₆	78.1	0.0769	80.1	276.2-523.2	148	9.5	[2, 33, 34]
Cyclohexene	C ₆ H ₁₀	82.1	0.1219	83.0	293.2-313.2	3	26.5	[2]
1,5-Hexadiene	C ₆ H ₁₀	82.1	0.1219	59.5	286.2-293.2	2	74.1	[2]
Cyclohexane	C ₆ H ₁₂	84.2	0.1427	80.7	283.2-473.2	22	104	[3]
2,3-Dimethyl-1-butene	C ₆ H ₁₂	84.2	0.1427	55.6	303.2-303.2	1	53.6	[3]
1-Hexene	C ₆ H ₁₂	84.2	0.1427	63.5	293.2-420.4	4	32.7	[3]
Methylcyclopentane	C ₆ H ₁₂	84.2	0.1427	71.8	283.2-303.2	3	7.1	[3]
2,2-Dimethylbutane	C ₆ H ₁₄	86.2	0.1627	49.7	273.2-273.2	1	1.2	[3]
2,3-Dimethylbutane	C ₆ H ₁₄	86.2	0.1627	58.0	273.2-313.2	6	17.8	[4]
Hexane	C ₆ H ₁₄	86.2	0.1627	68.7	273.2-477.6	25	21.1	[4]
2-Methylpentane	C ₆ H ₁₄	86.2	0.1627	60.3	273.2-273.2	1	7.7	[4]
3-Methylpentane	C ₆ H ₁₄	86.2	0.1627	63.3	298.2-298.2	9	52.5	[4, 34]
1,3,5-Cycloheptatriene	C ₇ H ₈	92.1	0.0869	116.6	303.2-323.2	3	5.1	[5]
2,5-Norbornadiene	C ₇ H ₈	92.1	0.0869	90.0	293.2-323.2	3	70.8	[5]
Toluene	C ₇ H ₈	92.1	0.0869	110.6	273.2-548.2	90	10.0	[5, 33, 34]
Ethylcyclopentane	C ₇ H ₁₄	98.2	0.1427	106.3	283.2-303.2	3	5.5	[5]
1-Heptene	C ₇ H ₁₄	98.2	0.1427	93.6	293.2-303.2	2	49.5	[5]
Methylcyclohexane	C ₇ H ₁₄	98.2	0.1427	100.9	283.2-303.2	5	21.9	[5]
2,4-Dimethylpentane	C ₇ H ₁₆	100.2	0.1599	80.5	273.2-273.2	1	4.7	[5]
n-Heptane	C ₇ H ₁₆	100.2	0.1599	98.4	273.2-313.2	10	16.8	[5]
2-Methylhexane	C ₇ H ₁₆	100.2	0.1599	90.1	283.2-303.2	4	17.7	[5]
3-Methylhexane	C ₇ H ₁₆	100.2	0.1599	91.9	273.2-273.2	1	27.9	[5]
2,2,3-Trimethylbutane	C ₇ H ₁₆	100.2	0.1599	80.9	273.2-323.2	6	28.9	[5]
Styrene	C ₈ H ₈	104.1	0.0769	145.2	279.2-324.2	10	10.5	[6]

Ethylbenzene	C ₈ H ₁₀	106.2	0.0943	136.2	273.2-568.1	35	13.0	[6]
o-Xylene	C ₈ H ₁₀	106.2	0.0943	144.4	273.2-298.2	3	7.2	[6]
m-Xylene	C ₈ H ₁₀	106.2	0.0943	139.1	273.2-473.4	15	11.3	[6]
p-Xylene	C ₈ H ₁₀	106.2	0.0943	138.4	298.2-373.2	20	10.5	[6, 33]
1-Propenylcyclopentane	C ₈ H ₁₄	110.2	0.1272	121.3	298.2-298.2	1	46.5	[7]
1,7-Octadiene	C ₈ H ₁₄	110.2	0.1272	117.1	293.2-360.2	2	41.4	[7]
Ethylcyclohexane	C ₈ H ₁₆	112.2	0.1427	131.8	310.9-561.4	7	39.1	[7]
Isopropylcyclopentane	C ₈ H ₁₆	112.2	0.1427	126.4	283.2-303.2	3	16.6	[7]
1-Octene	C ₈ H ₁₆	112.2	0.1427	121.3	310.9-549.8	6	15.5	[7]
2,4-Dimethylhexane	C ₈ H ₁₈	114.2	0.1427	109.4	283.2-303.2	3	24.2	[7]
n-Octane	C ₈ H ₁₈	114.2	0.1427	125.7	298.2-298.2	12	46.1	[7]
2,2,4-Trimethylpentane	C ₈ H ₁₈	114.2	0.1578	99.2	273.2-550.4	5	23.9	[7]
2,3,4-Trimethylpentane	C ₈ H ₁₈	114.2	0.1578	113.5	273.2-298.2	2	51.8	[7]
Isopropylbenzene	C ₉ H ₁₂	120.2	0.0999	152.4	273.2-298.2	6	1.6	[8]
Butylcyclopentane	C ₉ H ₁₈	126.2	0.1427	156.6	273.2-323.2	3	14.1	[8]
2,6-Dimethylheptane	C ₉ H ₂₀	128.3	0.1561	135.2	283.2-303.2	5	22.9	[8]
2-Methyloctane	C ₉ H ₂₀	128.3	0.1561	143.3	283.2-323.2	3	11.5	[8]
3-Methyloctane	C ₉ H ₂₀	128.3	0.1561	144.2	283.2-303.2	3	11.3	[8]
Nonane	C ₉ H ₂₀	128.3	0.1561	150.8	283.2-303.2	1	22.7	[8]
2,2,5-Trimethylhexane	C ₉ H ₂₀	128.3	0.1561	124.1	298.2-298.2	2	37	[8]
1,2,3,4-Tetrahydronaphthalene	C ₁₀ H ₁₂	132.2	0.0908	207.6	273.2-298.2	4	38.2	[9]
Butylbenzene	C ₁₀ H ₁₄	134.2	0.1044	183.3	424.7-595.9	11	12.1	[9]
sec-Butylbenzene	C ₁₀ H ₁₄	134.2	0.1044	173.3	283.2-373.2	3	38.1	[9]
tert-Butylbenzene	C ₁₀ H ₁₄	134.2	0.1044	169.2	283.2-303.2	1	30	[9]
p-Cymene	C ₁₀ H ₁₄	134.2	0.1044	177.1	283.2-283.2	3	16.5	[9]
Diethylbenzene	C ₁₀ H ₁₄	134.2	0.1044	183.5	283.2-303.2	6	39.6	[9]
1,3-Diethylbenzene	C ₁₀ H ₁₄	134.2	0.1044	181.1	273.2-323.2	7	13.3	[9]
cis-Decalin	C ₁₀ H ₁₈	138.2	0.1303	195.8	310.9-582.5	6	91	[9]
1-Butylcyclohexane	C ₁₀ H ₂₀	140.3	0.1427	181.0	374.2-599.1	7	47.9	[9]
1-Decene	C ₁₀ H ₂₀	140.3	0.1427	170.6	310.9-584.3	3	6.7	[9]
Decane	C ₁₀ H ₂₂	142.3	0.1427	174.2	374.2-475.2	15	33.3	[9]

2,7-Dimethyloctane	C ₁₀ H ₂₂	142.3	0.1548	159.9	298.2-576.2	3	13	[9]
1-Methylnaphthalene	C ₁₁ H ₁₀	142.2	0.0704	244.7	283.2-303.2	13	25.3	[10]
2-Methylnaphthalene	C ₁₁ H ₁₀	142.2	0.0704	241.1	273.2-589.4	3	66.4	[10]
Hexylcyclopentane	C ₁₁ H ₂₂	154.3	0.1427	205.0	293.2-313.2	3	13.2	[10]
Unadecane	C ₁₁ H ₂₄	156.3	0.1537	195.9	283.2-303.2	2	25.4	[10]
1-Ethyl-naphthalene	C ₁₂ H ₁₂	156.2	0.0769	258.3	298.2-313.2	7	24.7	[10]
2-Allyl-1,3,5-trimethylbenzene	C ₁₂ H ₁₆	160.3	0.0999	239.1	366.5-594.4	3	81.3	[10]
1,4-Diisopropylbenzene	C ₁₂ H ₁₈	162.3	0.1110	210.5	293.2-313.2	7	14.7	[10]
2-Propyl-1,3,5-trimethylbenzene	C ₁₂ H ₁₈	162.3	0.1110	242.4	310.9-590.0	3	29.1	[10]
Dodecane	C ₁₂ H ₂₆	170.3	0.1528	216.3	293.2-313.2	2	25.9	[10]
(2-Ethylcyclopentyl)benzene	C ₁₃ H ₁₈	174.3	0.1034	261.0	298.2-313.2	3	26.8	[11]
Cyclopentyl-octane	C ₁₃ H ₂₆	182.3	0.1427	243.7	283.2-303.2	3	12.5	[11]
Tridecane	C ₁₃ H ₂₈	184.4	0.1521	235.5	283.2-303.2	2	27.4	[11]
1,4-Dicyclopentylbutane	C ₁₄ H ₂₆	194.4	0.1339	278.1	298.2-313.2	3	32.6	[11]
2,4,6-Trimethyl-2-phenylheptane	C ₁₆ H ₂₆	218.4	0.1192	272.4	283.2-303.2	3	15.0	[11]
7,8-Dimethyltetradecane	C ₁₆ H ₃₄	226.4	0.1503	275.5	293.2-323.2	4	34.3	[11]
Hexadecane	C ₁₆ H ₃₄	226.4	0.1503	286.9	293-323	4	32.0	[11]
Athabasca bitumen		550*	0.0970	511.0	548.2-644	9	18.4	[35]

* Estimated. See text for details.

Table 5.2. Parameters for *Model A* (equation 5-4).

Subscript	a	b	C
1	1.188×10^1	-3.914×10^4 (K)	2.933×10^3 (K)
2	2.758×10^{-2} (K ⁻¹)	-7.232×10^1	1.477×10^1
3	-1.998×10^{-1} (K ⁻¹)	5.202×10^2	-9.917×10^1

Table 5.3. Overview of *Model A* performance

<i>Model A</i>	compounds/mixtures	No. of points	AARD (wt %)	Deviation bias (wt %)
Training data set	78	663	19*	-0.5*
Test data set	13	122	---	---

*-Cyclohexane is not considered in calculations due to the large uncertainty among experimental data.

5.3 Results and discussion

5.3.1 Model A

5.3.1.1 Model A Fitting Results

The 9 universal parameters appearing in equation 5-4 (Model A) were determined by multi-variable linear regression between the input data (boiling point and hydrogen weight fraction) and the experimental solubility data summarized in Table 5.1. The molar mass of bitumen was estimated. The H_{wt} was measured and the boiling point was determined from simulated distillation. The coefficients are presented in Table 5.2 and the quality of fit to experimental data is summarized in Table 5.3. In this work, high quality data for solubility of water in hydrocarbons critically evaluated by Maczynski et al. [1-12] along with published data by Jou et al. [33], Neely et al. [34] and Chapter 3 [35], were selected to determine the fitting parameters. The uncertainty of these experimental data is only known approximately. The reported absolute relative error is 30%, on a mole fraction basis, for pure compounds and is 30 % on a weight fraction basis for Athabasca bitumen. This training data set comprises 663 data points for 77 individual pure compounds and Athabasca bitumen. The average absolute relative deviation (AARD) of the fitted correlation from the training data set is less than 18 mole % for the pure compounds and less than 19 wt % for the data set as a whole if the fitting results for cyclohexane are ignored. Further, the deviations are unbiased as noted in Table 5.3. The AARD values fall within the estimated measurement error and it could be argued that error is regressed by the correlation. It could equally be argued that the measurement error is over estimated on average. Concern over measurement error is however well founded and cyclohexane provides a clear example as illustrated in Figure 5.5, where the recommended solubility data for cyclohexane [3], regressed as part of the training data set, contrast with a second experimental data set [40] and values predicted by Model A. The AARD between *Model A* and the recommended data for cyclohexane is 112%, where as the AARD from the data by Burd [40], not regressed, is less than 12%. Other compounds with large AARD values include: 1,5-hexadiene, 2,5-norbornadiene, cis-decalin, 2-ethyl-1,3,5-trimethylbenzene and 2-allyl-1,3,5-trimethylbenzene as shown in Table 5.1. A parity plot, Figure 5.6, comparing the regressed water solubility values, Model A, with experimental data illustrates the quality of the fit over four orders of magnitude in water composition. One advantage of *Model A* vis-à-vis other correlations

for water solubility in hydrocarbons, appears to be the inclusion high temperature solubility data for a Type IIIb mixture in the training data set. Figure 5.7 illustrates that by including such high-temperature solubility data in the training data set, the resulting correlation does not diverge from measured solubility values at high temperature. By contrast, correlations that do not include high temperature solubility data in the training data set diverge significantly from solubility data at high temperatures.

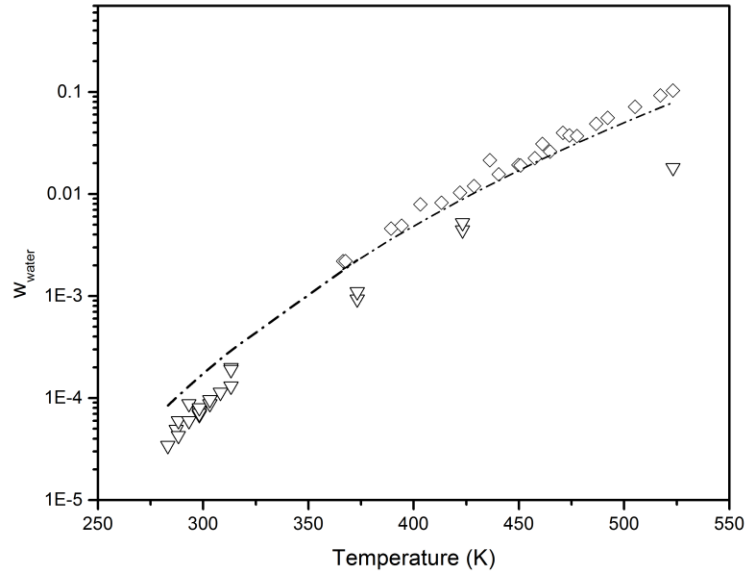


Figure 5.5. Calculated solubility of water in cyclohexane equation 5-4 (---), experimental data [40] (◆) and tentative experimental data [3] (▽).

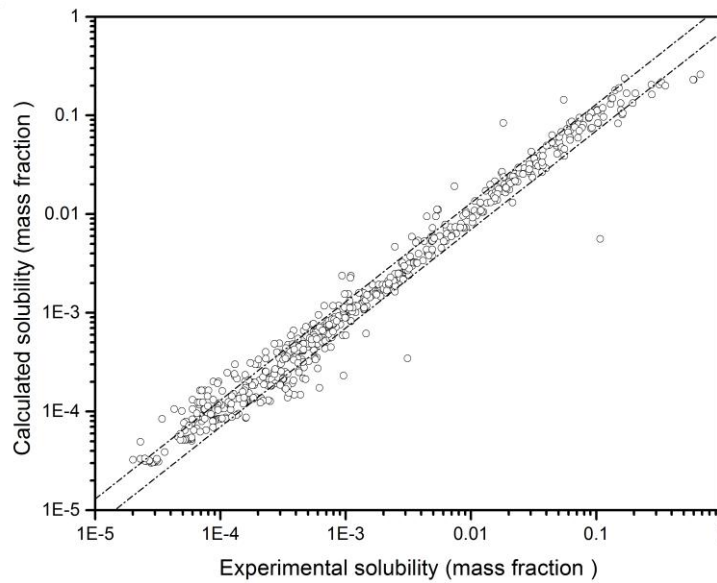


Figure 5.6. Error dispersion between calculated values for the solubility of water in pure hydrocarbons and Athabasca bitumen *Model A* (equation 5-4) and experimental data (Table 5.1). The $\pm 30\%$ deviations (---) are also shown.

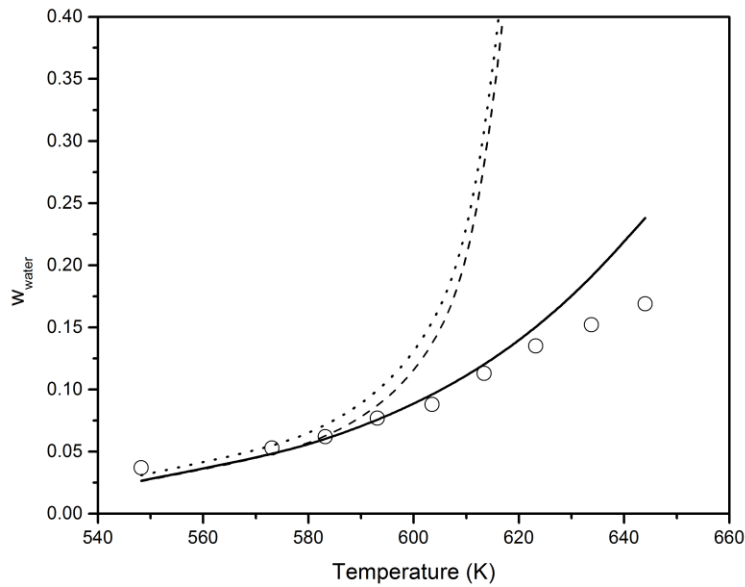


Figure 5.7. Calculated solubility of water in Athabasca bitumen (—) using: *Model A* (training set), (....) low temperature solubility model (test set) [28], (-.-) API recommended model (test set) [32] and experimental data (o) Chapter 3 [35].

5.3.1.2 *Model A* Testing and Evaluation

The predictive quality of *Model A* was evaluated by calculating water solubility values in 13 hydrocarbon mixtures including boiling cuts, reservoir fluids and heavy oil, and two highly asymmetric bitumen + solvent mixtures. These mixtures, their properties and the quality of the estimates are listed in Table 5.4, and the overall quality of the predictions is summarized in Table 5.3. Some illustrative examples are explored in detail below because fluid characterization is often incomplete and the input parameters molar average boiling point and hydrogen weight fraction must be estimated from available data or inferred.

Example 1: Water solubility prediction at low temperature

For this example, the performance of *Model A* is benchmarked against solubility of water in different types of gasoline [41, 42], kerosene and paraffinic oil [43] at low temperatures. The average normal boiling point and hydrogen weight fraction of these petroleum fractions are presented by Hibbard [42]. The predicted solubilities and experimental data are illustrated in Figures 5.8a-b. The large variation among water solubility values in different types of gasoline, Figure 5.8a, leads to a deviation, which is

clearly linked to uncertainty of the low temperature experimental data. As noted by Hibbard the average variation for all experimental data [41] is 136%, where as the average difference for experimental data at 323.2 K is 279%. A low-temperature NRTL based model appears to overestimate water solubility for this case. For kerosene and paraffinic oil, the average normal boiling points of the mixtures were estimated based on their initial and final boiling points [43] as 220 and 400 oC respectively. The hydrogen weight fractions were estimated using the Watson correlation [44, 45]. As shown in Figure 5.8b there is a good agreement between the predicted values and original data and a relatively small deviation for kerosene and paraffinic oil reflect this.

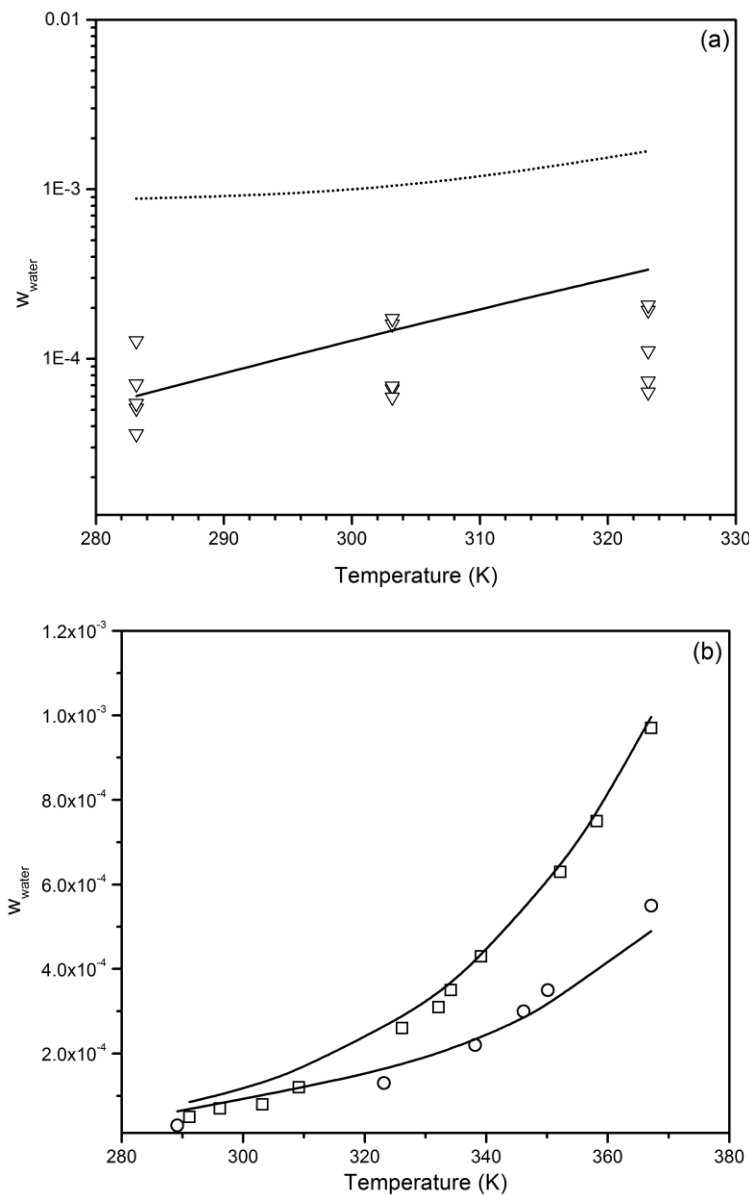
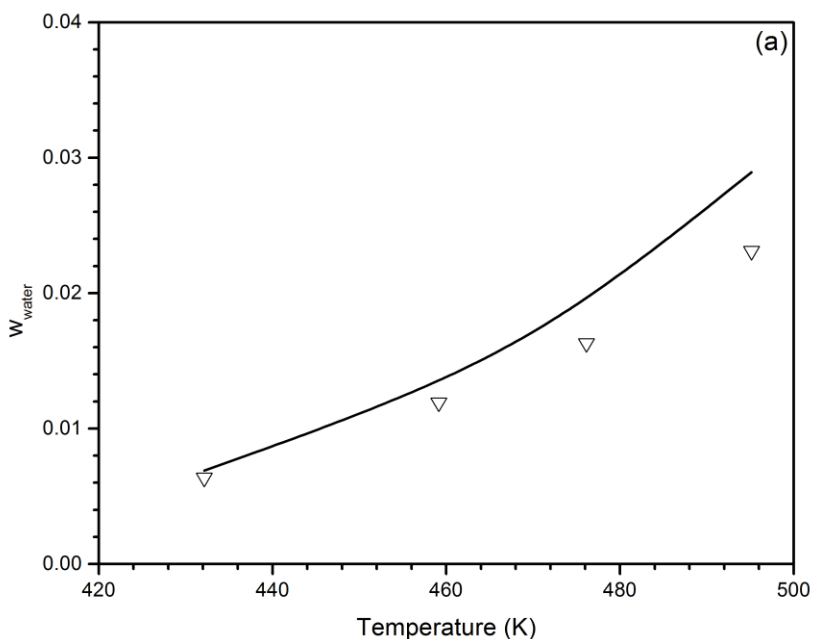
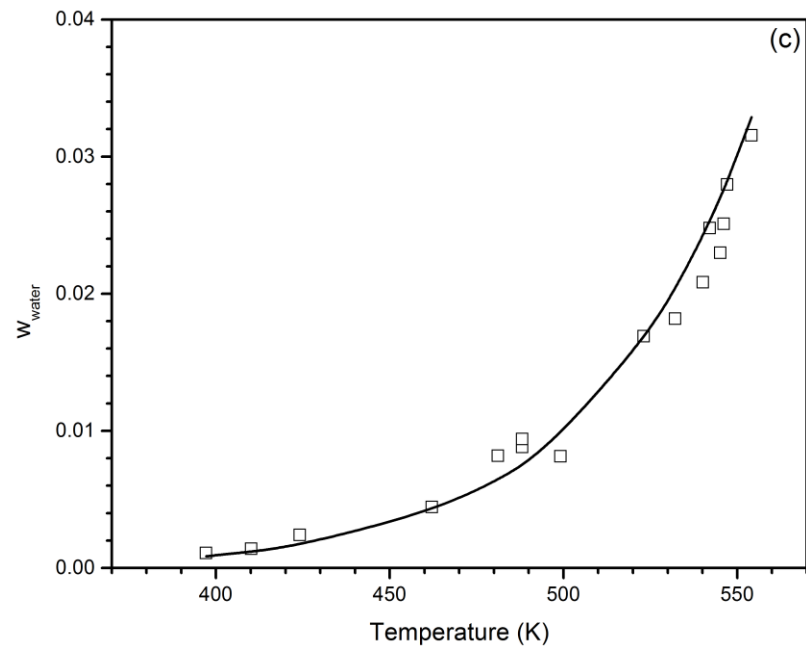
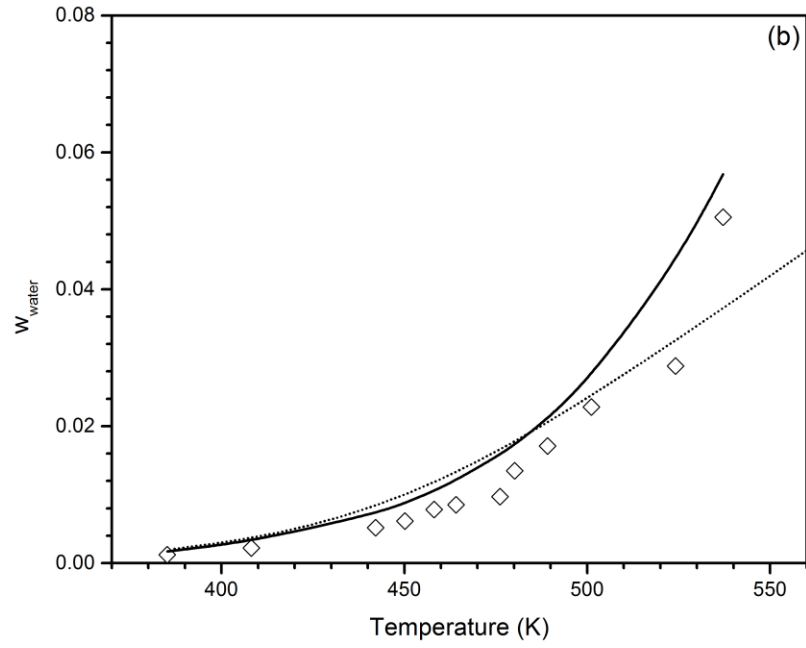


Figure 5.8. Calculated solubility of water in: (a) gasoline G10 - molecular weight 82 g/mole and an average boiling point 58.9 oC (∇) [41, 42], (b) kerosene (\square) and paraffinic oil (\circ) [43]. The predicted values using *Model A* (—) and a low-temperature NRTL based solubility model (.....) [28] are shown.

Example 2: Water solubility prediction in hydrocarbons with missing input data

This example concerns four petroleum fractions [46, 47]. The properties of naphtha, kerosene, lubricating oil and hydrocarbon fuels are presented in Table 5.4. In order to estimate water solubility values, hydrogen weight fraction and average boiling point of the mixtures are required. Naphtha and kerosene mainly comprise paraffinic hydrocarbons, so their hydrogen weight percent can be estimated by analogy with n-alkane molecules with similar molecular weights e.g. n-C12 and n-C13. In this work, the estimated hydrogen weight fractions by Hibbard [42] were used. The properties of the hydrocarbon fuel with average molecular weight 425 [46] were not reported, and the properties were considered to be the same as those of lubricating oil [47] with a similar molecular weight. The agreement between *Model A* and the experimental data is illustrated in Figure 5.9a-d. Computed results for an NRTL based model are available for kerosene [28] and these are also shown in Figure 5.9b. The AARD values are given in Table 5.4 for each of these cases. The impact of uncertainty in model input parameters on solubility outcomes is addressed explicitly below.





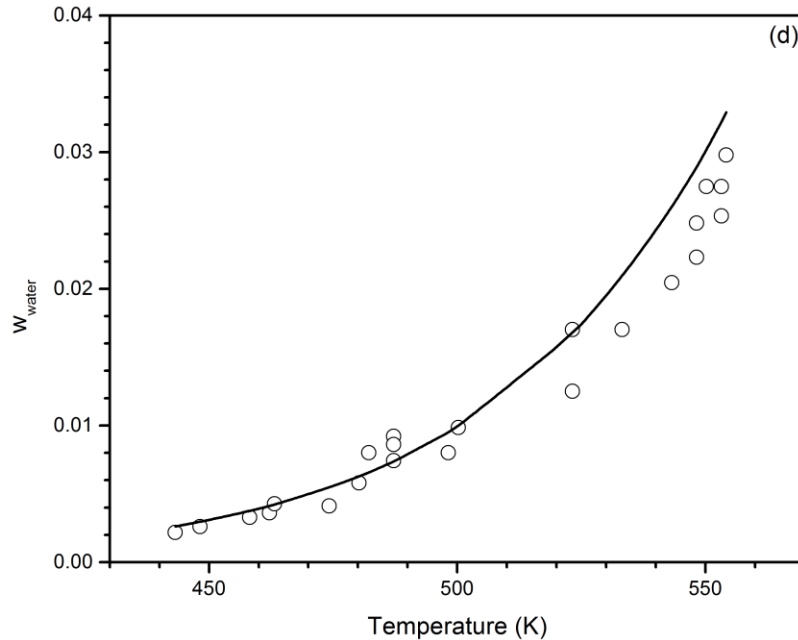
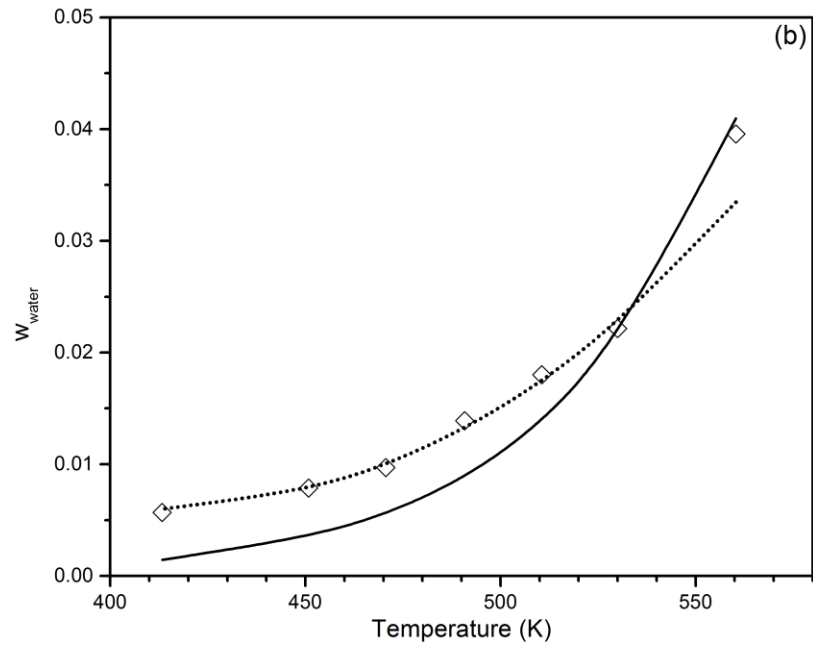
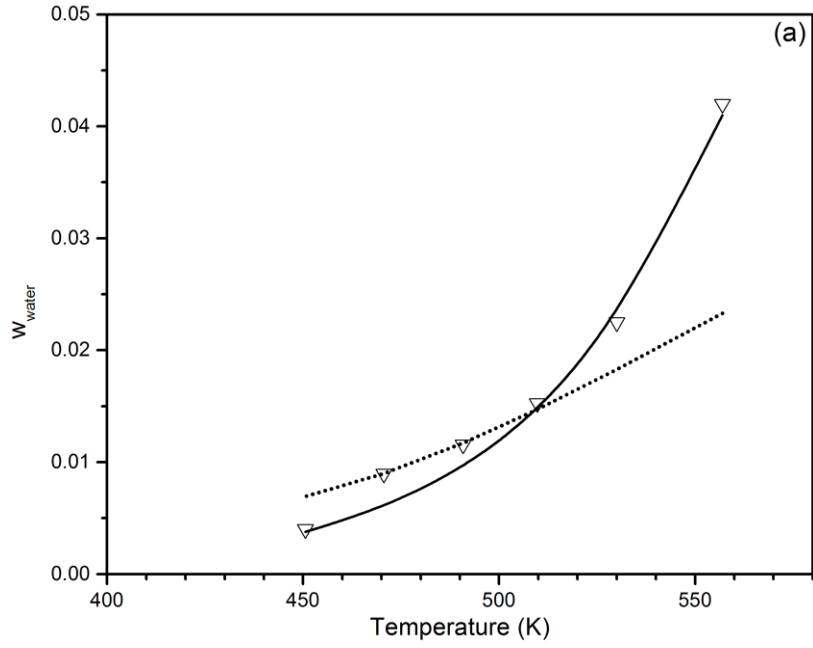


Figure 5.9. Solubility of water in hydrocarbons predicted by *Model A* (—) and (.....) low temperature solubility model (kerosene) [28] compared to experimental data: (a) naphtha (∇) [47], (b) kerosene (\diamond) [47], (c) lubricating oil (\square) [47] and (d) fuel mixtures (o) [46].

Example 3: Water solubility in ill-defined and asphaltenic reservoir fluids

In this example, the water solubility prediction results for four ill-defined heavy oils reported by Glandt et. al [48] are evaluated. The physical properties of Coalinga, Huntington Beach, Peace River, and Cat Canyon crude oils are summarized in Table 5.4. Elemental analyses for these heavy oils are not reported but hydrogen wt. fractions fall within a narrow range $\sim 0.10 \pm 0.01$. The hydrogen weight fractions for these crudes were estimated using the Watson correlation [44, 45] and are presented in Table 5.4. For Cat Canyon crude oil, which has a much larger molecular weight and aromatic carbon content than the other crudes, the hydrogen weight fraction appears to be overestimated by the Watson equation. The average boiling temperature values for these heavy oils were estimated using the Soreide model [49] recommended for heavy petroleum fractions. Predicted solubility values, Model A, are compared with experimental data for Coalinga, Huntington Beach, Peace River, Cat Canyon crude oils, and an NRTL based model fit to these data [28] in Figures 5.10a-d respectively. The experimental solubility data for Peace River (Figure 5.10c) and Cat Canyon (Figure 5.10d) possess unusual temperature trends compared to other hydrocarbons. It is likely that the solubility measurements for these mixtures are affected by water-in-oil emulsion formation at low lower temperatures.



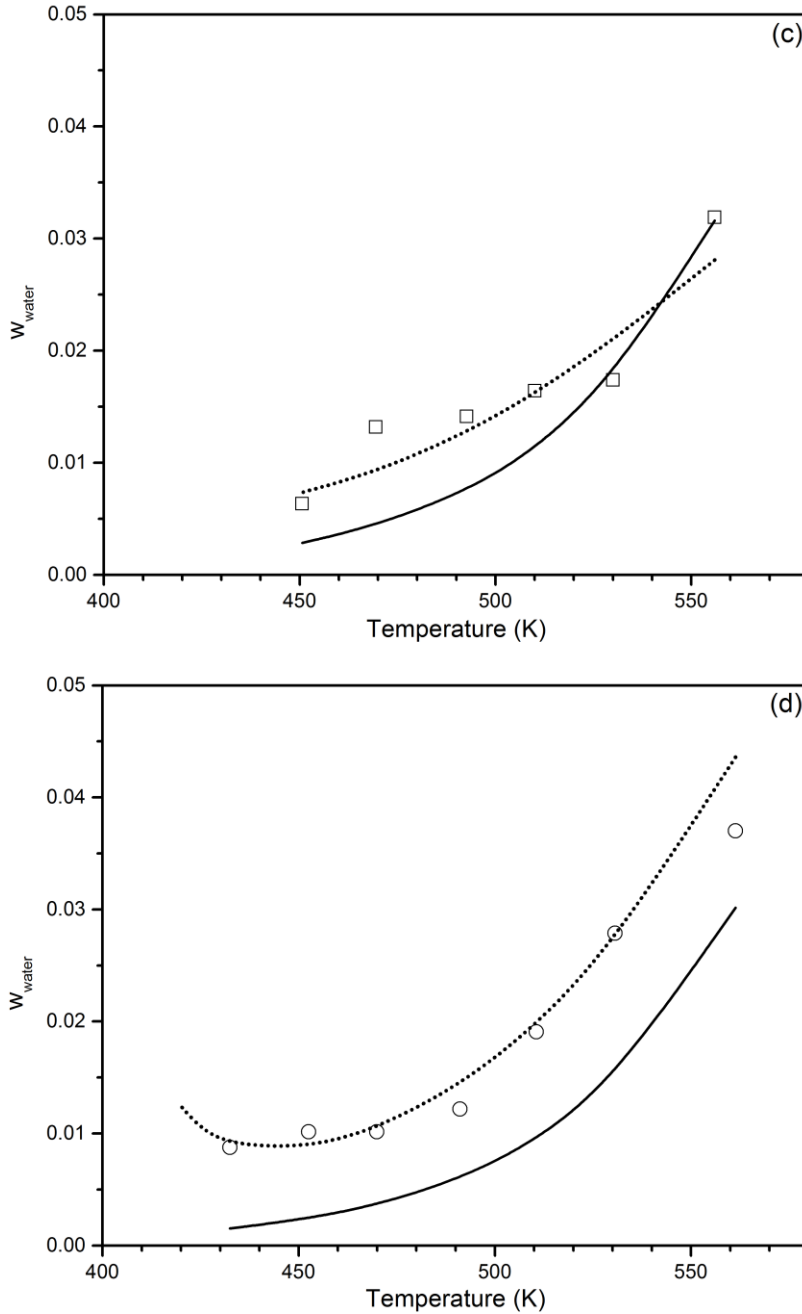


Figure 5.10. Predicted solubility of water in oils using *Model A* (—), fitted NRTL based solubility model (.....) [28], and the corresponding experimental data [48]: (a) Coalinga (∇), (b) Huntington Beach (\diamond), (c) Peace River (\square) and (d) Cat Canyon crude(\circ).

Example 4: Water solubility prediction in highly asymmetric mixtures

For this case, water solubility predictions for two Athabasca bitumen + toluene mixtures, comprising 44.3 wt % and 66.8 wt % toluene respectively are compared with experimental data (Chapter 4,[50]). While both Athabasca bitumen and toluene are part of the training data set, fluid characterization protocols for asymmetric mixtures can present

challenges. The required input physical properties of the Athabasca bitumen + toluene mixtures were calculated using the properties of Athabasca bitumen and toluene. The reported weight fractions of hydrogen, in Table 5.4, were obtained by mass balance and the nominal normal boiling points of the mixtures were obtained by first characterizing Athabasca bitumen using distillation curve data (ASTM D1160) and combining this with the toluene boiling point to calculate a molar average boiling temperature. A mean molar mass of 550 g/mole was assigned to Athabasca bitumen. The resulting molar average boiling points are present in Table 5.4. *Model A* and the data agree to within the error of the data and the uncertainty of the correlation as shown in Figure 5.11.

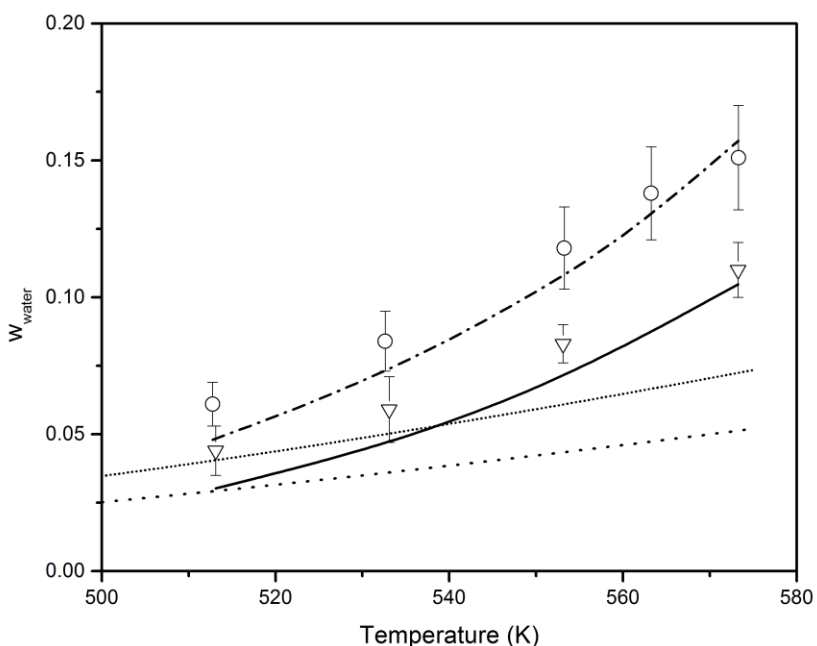


Figure 5.11. Predicted solubility of water in ((1-w) Athabasca bitumen + (w) toluene) + water. Model A: $w = 0.668$ (-.-) and 0.443 (—); NRTL based approach: $w = 0.668$ (.....) and 0.443 (-.-.-.-) [28, 51]. Experimental data in Chapter 4 $w = 0.668$ (∇) and 0.443 (\circ).

Water solubility values predicted using an NRTL based model [28], also shown in Figure 5.11, require careful fluid characterization, and extrapolation of a low temperature solubility correlation to obtain water solubility estimates for this case. The procedure, recommended by Dr. M. Satyro [28, 51] includes generating mutual solubilities for Athabasca bitumen and water from 513 to 573 K. The water in Athabasca bitumen was calculated using the high temperatures NRTL-based solubility model, while the Athabasca bitumen in water was calculated using the low temperature NRTL-based solubility model [28]. The generated values for Athabasca bitumen + water were then fit using the low-temperature NRTL model to obtain binary interaction parameters. The

water solubility values in Athabasca bitumen + toluene at high temperature were then calculated using the NRTL model. The predicted solubility values arising from this approach are biased (low) in this case but are acceptable because they fall within a factor of two of the measurements and comprise pure predictions. Toluene but not bitumen are in the training data set but there are no high temperature data in the training data set. The impact of the light solvent (toluene) on the solubility of water in the mixture is underestimated.

5.3.1.3 Impact of input parameter uncertainty on predicted water solubility outcomes.

As is clear from the illustrations above, fluid characterization, particularly for heavy oils and bitumen, is either incomplete or imprecise. However even rough estimates of input parameters leads to acceptable qualitative trends with temperature. Application of the model to heavy ill-defined mixtures is hampered because average boiling point is not well defined for such mixtures. Direct measurement of boiling point distributions of hydrocarbons can be performed up to 524 °C. Using simulated distillation techniques (Gas Chromatography) the measurements can be pushed higher by analogy, but not further than 700 °C. For example, 50 volume% of Athabasca bitumen possesses an atmospheric boiling point greater than 524 °C and the meaning is unclear. By contrast, fluid density at ambient conditions and hydrogen content have simple physical meanings. They can be measured accurately using low-cost experiments. The T_b approach while compatible with process simulators and equation of state calculation approaches, leads to the creation of pseudo-components that are unverifiable against experimental data. In the current work, the focus is to show the advantage of a new T_b based correlation vis-à-vis prior ones. Possible utilization of other input variables will be considered in future work.

The sensitivity of water solubility calculation outcomes to uncertainty in input parameters is an indication of the overall robustness of the calculations, which in this case must be reliable over broad ranges of temperature, and composition. The sensitivity of Model A to 10% variations in average normal boiling point and hydrogen weight fraction are illustrated in Figures 5.12a-b respectively for bitumen + toluene mixtures. The results are representative. The calculation outcomes fall within the range of the experimental measurement error, and are insensitive to such variations. This characteristic permits reliable water solubility estimates to be made, even when the inputs are uncertain because

10% uncertainties in elemental composition, and boiling point are large relative to measured or estimated values for these parameters even for asymmetric and ill-defined hydrocarbon mixtures.

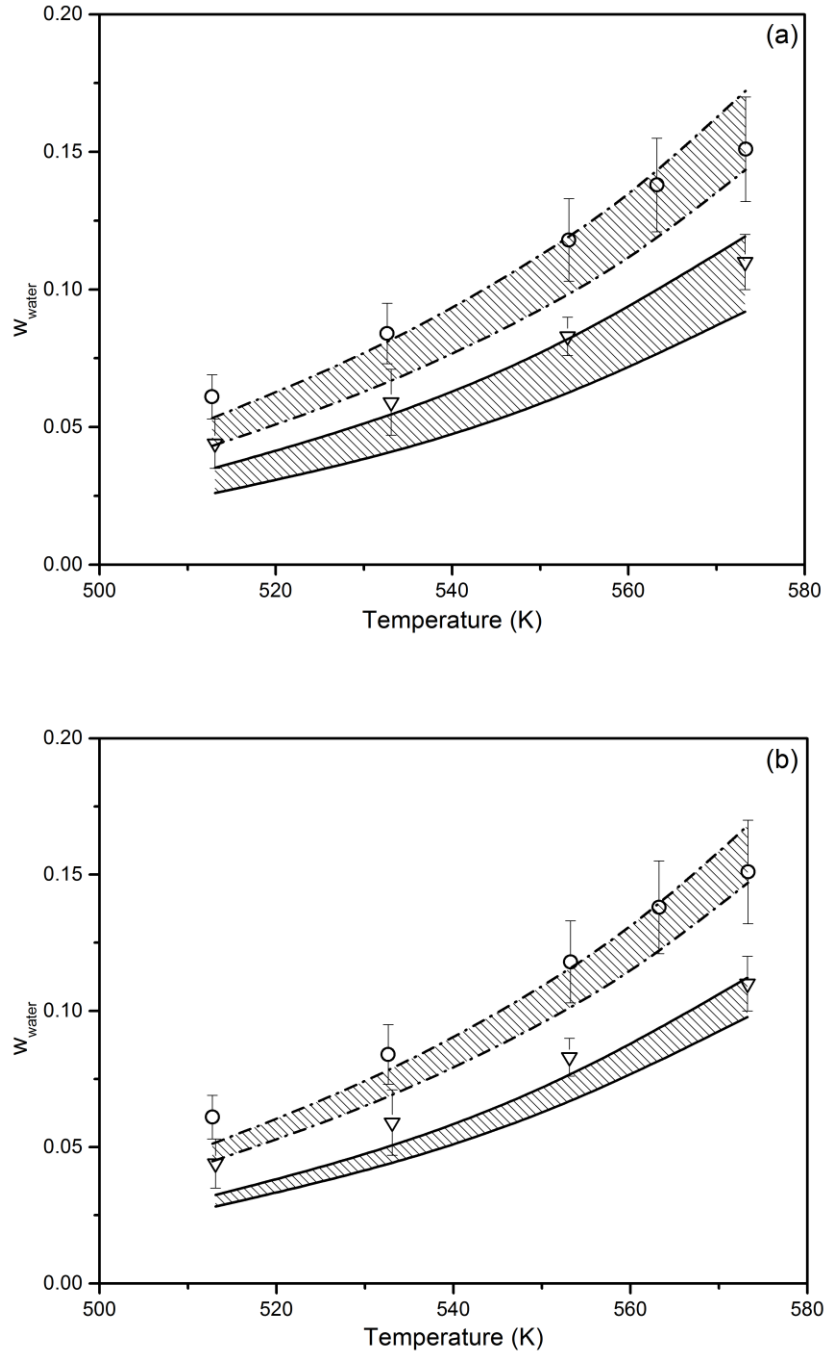


Figure 5.12. 10% variation in inputs (a) average normal boiling point and (b) hydrogen weight fraction. Predicted solubility of water in ((1-w) Athabasca bitumen + (w) toluene) + water: $w = 0.668$ (- -) and 0.443 (—) Model A, and experimental data in Chapter 4 $w = 0.668$ (∇) and 0.443 (o).

Table 5.4. Properties of heavy oils used to test Model A, and to obtain coefficients for Model B

Petroleum fractions	Mw	T_b (°C)	H_{wt}	T range (K)	No.	Method description	Ref
Gasoline	82	58.9	0.1561	283.2-323.2	3		[42]
	95	80.6	0.1554	283.2-323.2	3		[42]
	94	86.1	0.1460	283.2-323.2	3		[42]
	99	93.9	0.1496	283.2-323.2	3		[42]
	85	62.8	0.1554	283.2-323.2	3		[42]
Kerosene		220*	0.1419*	273.2-367.2	11		[43]
Paraffinic oil		400*	0.133*	289.2-367.2	6		[43]
Naphtha	147	172	0.1453*	432.2-495.2	4	Cloud point determination	[47]
Kerosene	173	226	0.1364*	385.2-537.2	12	Cloud point determination	[47]
Lubricating oil	425	445	0.1312*	397.2-554.2	15	Cloud point determination	[47]
Fuel oil	425	445*	0.1313*	443.2-554.2	23		[46]
Coalinga crude oil	439	458*	0.111*	450.6-557.0	6	Karl Fischer titration	[48]
Huntington crude oil	442	460*	0.102*	413.3-560.3	7	Karl Fischer titration	[48]
Peace River crude oil	571	517*	0.101*	450.6-556.0	6	Karl Fischer titration	[48]
Cat Canyon crude oil	627	556*	0.102*	432.5-561.3	7	Karl Fischer titration	[48]
Athabasca bitumen + 44.3% toluene		230*	0.0926	513.1-573.2	4	X-ray viewcell, P-x diagrams	[50]
Athabasca bitumen + 66.8% toluene		328*	0.0903	512.8-573.3	5	X-ray viewcell, P-x diagrams	[50]
Total				283.2-573.3	122		

*Estimated. See text for details.

5.3.2 Model B – Water Solubility in hydrocarbons above the UCEP

At fixed pressure, the solubility of water in hydrocarbons decreases with increasing temperatures. At higher temperatures, water becomes less polar and the solubility then increases. As the water critical temperature is approached, it becomes more volatile, and water solubility in hydrocarbons at fixed pressure again decreases. Further, the solubility of hydrocarbons in water increases sharply in the critical region. Consequently, the

temperature dependence of the mass based Henry like constant, K , is complex. Maxima and minima are observed as illustrated for Athabasca, in Figure 5.13 where the predicted K values based on the properties of Athabasca bitumen are compared with high temperature measurements. Because of the complexity of the temperature dependence and the minimum arising just below the critical temperature of water, *Model A* + the vapor pressure of water, diverges from the data in the critical region, because the hydrocarbon becomes sufficiently soluble in the water phase for the water vapor pressure and the LLV/LL boundary pressures to diverge, and this model is a poor basis for extrapolation to higher temperatures. This would appear to be a generalizable finding. Substitution of the LLV/LL boundary pressure for Athabasca bitumen + water pseudo binary mixture, from Table 5.5, improves the agreement with the data as the water critical point is approached and suggests a minimum value for $K=150$ MPa, and thus a maximum solubility, at ~ 620 K. Quadratic extrapolation of this model into the supercritical region, suggests that K values rise and at 700 K the estimate is $K=200$ MPa. However, extension of *Model A* in this way offers no advantages over direct regression of experimental K values because hydrocarbon specific data, only obtainable from solubility measurements at high temperature are required to extend the Model. Direct regression of the high-temperature water solubility and LLV/LL phase boundary data for Athabasca bitumen, presented in Table 5.5, yield a Van't Hoff type correlation for K , labeled Model B:

$$\ln(K) = 1.8532 \times 10^4 \times \frac{1}{T} + 3.2959 \times 10^1 \times \ln(T) - 2.3657 \times 10^2 \quad (5-11)$$

where K possesses the units (MPa) and T is in Kelvin. The extrapolated K values for water in Athabasca bitumen to temperatures as low as 450 K using *Model B* are in good agreement with *Model A* + LLV/LL boundary pressure and *Model A* + water vapor pressure, as shown in Figure 5.13. A minimum K value of 160 MPa is suggested at 560 K and extrapolation to 700 K suggests a value of 337 MPa.

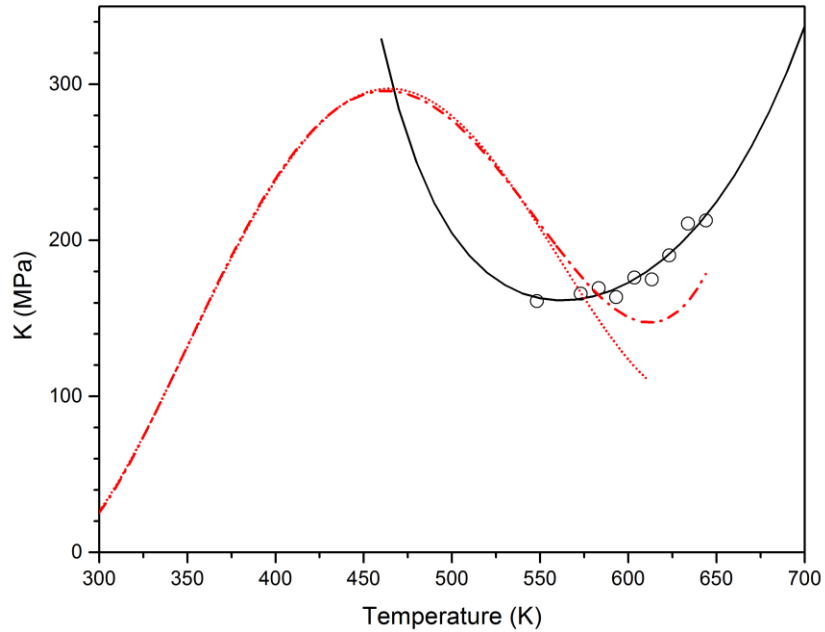


Figure 5.13. Estimating K for Athabasca bitumen (\circ) (evaluated based on equation 5-7 and 5-8) using *Model A* (equation 5-4) + the NIST water vapor pressure equation (.....) and the LLV/LL phase boundary pressure (---), and *Model B*, equation 5-11 (—).

As the data possess significant error, both *Model B* and the extended version of *Model A* fall within the range of the trend of the solubility and hence the trends in K values. Further, the extrapolated values to 700 K fall within the range of values found at lower temperatures where measurements are feasible. As the preferred conditions for surface upgrading of bitumen are ~ 700 K and a pressure of ~ 10 MPa, the results above are consistent with a water mass fraction in Athabasca bitumen under these conditions that is ~ 0.05 (extended *Model A*) and ~ 0.03 (*Model B*).

Table 5.5. Solubility of water in Athabasca bitumen Chapter 3 [35] and experimentally derived K values.

Temperature (K)	LLV/LL boundary pressure (MPa)	Water weight fraction (w_w)	Bubble pressure of bitumen	K (MPa/ w_w)
548.2	6.1	0.037	0.14	161.1
573.1	8.94	0.053	0.15	165.9
583.2	10.66	0.062	0.15	169.4
593.1	12.77	0.077	0.17	163.6
603.5	15.72	0.088	0.21	176.2
613.4	20.07	0.113	0.29	175.0
623.2	26.13	0.135	0.42	190.4
633.8	32.7	0.152	0.66	210.8
644	36.98	0.169	1.02	212.8

5.4 Conclusion

A simple empirical model to predict the solubility of water in ill-defined hydrocarbons below the UCEP of mixtures is developed. This model correlates water solubility in terms of average boiling point and hydrogen weight fraction of hydrocarbons. Critically evaluated solubility data of water in 77 pure hydrocarbons and one asphaltenic heavy oil, comprising 663 Individual data points, were used to fit nine universal parameters. The average deviation of the correlation from reference experimental data, 18 %, is less than the estimated uncertainty of the reference data. The reliability of model was evaluated against 13 petroleum samples including heavy asphaltenic oils in temperature range 283 to 573 K. The correlation is consistent with all Types of phase behavior arising for water + hydrocarbon mixtures including Type II, IIIa and IIIb phase behavior and it remains reliable from 273 K up to the UCEP of mixtures. Above the UCEP, two fluid-specific solubility modeling approaches, restricted to Type IIIb phase behavior, where the high temperature liquid phase is hydrocarbon-rich, were developed. As there are no data for water solubility in hydrocarbon-rich liquids above the critical temperature for water, the quality of the estimates could not be evaluated. However, the estimates are in close agreement and the extrapolated range of mass based Henry constant-like parameters obtained are consistent with values known to arise at lower temperatures.

5.5 References

- [1] A. Maczynski, D. G. Shaw, M. Goral, B. Wisniewska-Gocłowska, A. Skrzecz, Z. Maczynska, et al., "IUPAC-NIST solubility data series. 81. Hydrocarbons with water and seawater - Revised and updated part 1. C-5 hydrocarbons with water," *Journal of Physical and Chemical Reference Data*, vol. 34, pp. 441-476, Jun 2005.
- [2] A. Maczynski, D. G. Shaw, M. Goral, B. Wisniewska-Gocłowska, A. Skrzecz, I. Owczarek, et al., "IUPAC-NIST solubility data series. 81. Hydrocarbons with water and seawater - Revised and updated. Part 2. Benzene with water and heavy water," *Journal of Physical and Chemical Reference Data*, vol. 34, pp. 477-552, Jun 2005.
- [3] A. Maczynski, D. G. Shaw, M. Goral, B. Wisniewska-Gocłowska, A. Skrzecz, I. Owczarek, et al., "IUPAC-NIST solubility data series. 81. Hydrocarbons with water and seawater - Revised and updated. Part 3. C₆H₈-C₆H₁₂ hydrocarbons with water and heavy water," *Journal of Physical and Chemical Reference Data*, vol. 34, pp. 657-708, Jun 2005.

- [4] A. Maczynski, D. G. Shaw, M. Goral, B. Wisniewska-Gocłowska, A. Skrzecz, I. Owczarek, et al., "IUPAC-NIST solubility data series. 81. Hydrocarbons with water and seawater-revised and updated. Part 4. C₆H₁₄ hydrocarbons with water," *Journal of Physical and Chemical Reference Data*, vol. 34, pp. 709-753, Jun 2005.
- [5] A. Maczynski, D. G. Shaw, M. Goral, B. Wisniewska-Gocłowska, A. Skrzecz, I. Owczarek, et al., "IUPAC-NIST Solubility Data Series. 81. Hydrocarbons with water and seawater-revised and updated. Part 5. C-7 hydrocarbons with water and heavy water," *Journal of Physical and Chemical Reference Data*, vol. 34, pp. 1399-1487, 2005.
- [6] D. G. Shaw, A. Maczynski, M. Goral, B. Wisniewska-Gocłowska, A. Skrzecz, I. Owczarek, et al., "IUPAC-NIST Solubility Data Series. 81. Hydrocarbons with water and seawater-revised and updated. Part 6. C₈H₈-C₈H₁₀ hydrocarbons with water," *Journal of Physical and Chemical Reference Data*, vol. 34, pp. 1489-1553, 2005.
- [7] D. G. Shaw, A. Maczynski, M. Goral, B. Wisniewska-Gocłowska, A. Skrzecz, L. Owczarek, et al., "IUPAC-NIST solubility data series. 81. Hydrocarbons with water and seawater revised and updated. Part 7. C₈H₁₂-C₈H₁₈ hydrocarbons with water," *Journal of Physical and Chemical Reference Data*, vol. 34, pp. 2261-2298, Dec 2005.
- [8] D. G. Shaw, A. Maczynski, M. Goral, B. Wisniewska-Gocłowska, A. Skrzecz, I. Owczarek, et al., "IUPAC-NIST solubility data series. 81. Hydrocarbons with water and seawater - Revised and updated. Part 8. C-9 hydrocarbons with water," *Journal of Physical and Chemical Reference Data*, vol. 34, pp. 2299-2345, Dec 2005.
- [9] D. G. Shaw, A. Maczynski, M. Goral, B. Wisniewska-Gocłowska, A. Skrzecz, I. Owczarek, et al., "IUPAC-NIST solubility data series. 81. Hydrocarbons with water and seawater-revised and updated. Part 9. C-10 hydrocarbons with water," *Journal of Physical and Chemical Reference Data*, vol. 35, pp. 93-151, Mar 2006.
- [10] D. G. Shaw, A. Maczynski, M. Goral, B. Wisniewska-Gocłowska, A. Skrzecz, I. Owczarek, et al., "IUPAC-NIST solubility data series. 81. Hydrocarbons with water and seawater-revised and updated. Part 10. C-11 and C-12 hydrocarbons with water," *Journal of Physical and Chemical Reference Data*, vol. 35, pp. 153-203, Mar 2006.
- [11] D. G. Shaw, A. Maczynski, M. Goral, B. Wisniewska-Gocłowska, A. Skrzecz, I. Owczarek, et al., "IUPAC-NIST solubility data series. 81. Hydrocarbons with water and seawater-revised and updated. Part 11. C-13-C-36 hydrocarbons with water," *Journal of Physical and Chemical Reference Data*, vol. 35, pp. 687-784, Jun 2006.
- [12] D. G. Shaw, A. Maczynski, G. T. Hefter, M. Kleinschmidt, D. Mackay, P. A. Meyers, et al., "IUPAC-NIST solubility data series. 81. Hydrocarbons with water and seawater-revised and updated part 12. C-5-C-26 hydrocarbons with seawater," *Journal of Physical and Chemical Reference Data*, vol. 35, pp. 785-838, Jun 2006.

- [13] J.-C. de Hemptinne, J.-M. M. P. Ledanois, and A. Barreau, "Select Thermodynamic Models for Process Simulation - A Practical Guide Using a Three Steps Methodology," ed: Editions Technip.
- [14] V. N. Kabadi and R. P. Danner, "A modified soave-redlich-kwong equation of state for water hydrocarbon phase-equilibria," *Industrial & Engineering Chemistry Process Design and Development*, vol. 24, pp. 537-541, 1985.
- [15] S. Michel, H. H. Hooper, and J. M. Prausnitz, "Mutual solubilities of water and hydrocarbons from an equation of state - need for an unconventional mixing rule," *Fluid Phase Equilibria*, vol. 45, pp. 173-189, Apr 1989.
- [16] I. Soreide and C. H. Whitson, "Peng-Robinson predictions for hydrocarbons, CO₂, N₂, and H₂S with pure water and NaCl brine," *Fluid Phase Equilibria*, vol. 77, pp. 217-240, Sep 1992.
- [17] A. Dhima, J. C. de Hemptinne, and G. Moracchini, "Solubility of light hydrocarbons and their mixtures in pure water under high pressure," *Fluid Phase Equilibria*, vol. 145, pp. 129-150, Mar 1998.
- [18] H. Y. Shin, M. Haruki, K.-P. Yoo, Y. Iwai, and Y. Arai, "Phase behavior of water + hydrocarbon binary systems by using multi-fluid nonrandom lattice hydrogen bonding theory," *Fluid Phase Equilibria*, vol. 189, pp. 49-61, 2001.
- [19] M. Haruki, Y. Iwai, and Y. Arai, "Prediction of phase equilibria for the mixtures containing polar substances at high temperatures and pressures by group-contribution equation of state," *Fluid Phase Equilibria*, vol. 189, pp. 13-30, 2001.
- [20] M. Haruki, Y. Iwai, S. Nagao, and Y. Arai, "Measurement and correlation of liquid-liquid equilibria for water + aromatic hydrocarbon binary systems at high temperatures and pressures," *Journal of Chemical and Engineering Data*, vol. 46, pp. 950-953, 2001.
- [21] M. Haruki, Y. Iwai, S. Nagao, Y. Yahiro, and Y. Arai, "Measurement and correlation of phase equilibria for water + hydrocarbon systems near the critical temperature and pressure of water," *Industrial and Engineering Chemistry Research*, vol. 39, pp. 4516-4520, 2000.
- [22] I. G. Economou and C. Tsonopoulos, "Associating models and mixing rules in equations of state for water/hydrocarbon mixtures," *Chemical Engineering Science*, vol. 52, pp. 511-525, Feb 1997.
- [23] J. D. Li, I. Vanderbeken, S. Y. Ye, H. Carrier, and P. Xans, "Prediction of the solubility and gas-liquid equilibria for gas-water and light hydrocarbon-water systems at high temperatures and pressures with a group contribution equation of state," *Fluid Phase Equilibria*, vol. 131, pp. 107-118, May 1997.
- [24] W. Yan, G. M. Kontogeorgis, and E. H. Stenby, "Application of the CPA equation of state to reservoir fluids in presence of water and polar chemicals," *Fluid Phase Equilibria*, vol. 276, pp. 75-85, 2009.
- [25] C. L. Yaws and U. Yadav, "How temp. affects H₂O solubility in cycloalkanes," *Oil & Gas Journal*, vol. 110, pp. 96-+, Jan 2012.
- [26] C. L. Yaws, P. Rane, and V. Nigam, "Solubility of Water in Benzenes As a Function of Temperature," *Chemical Engineering*, vol. 118, pp. 42-46, Dec 2011.

- [27] C. L. Yaws and P. M. Rane, "How temp. affects H₂O solubility in alkanes," *Oil & Gas Journal*, vol. 108, pp. 130-133, Dec 2010.
- [28] M. A. Satyro, J. M. Shaw, and H. W. Yarranton, "A practical method for the estimation of oil and water mutual solubilities," vol. 355, pp. 12-25, 2013.
- [29] C. Tsonopoulos and G. M. Wilson, "high-temperature mutual solubilities of hydrocarbons and water .1. benzene, cyclohexane and normal-hexane," *Aiche Journal*, vol. 29, pp. 990-999, 1983.
- [30] J. L. Heidman, C. Tsonopoulos, C. J. Brady, and G. M. Wilson, "High-temperature mutual solubilities of hydrocarbons and water .2. Ethylbenzene, ethylcyclohexane, and normal-octane," *Aiche Journal*, vol. 31, pp. 376-384, 1985.
- [31] I. G. Economou, J. L. Heidman, C. Tsonopoulos, and G. M. Wilson, "Mutual solubilities of hydrocarbons and water .3. 1-hexene, 1-octene, C-10-C-12 hydrocarbons," *Aiche Journal*, vol. 43, pp. 535-546, Feb 1997.
- [32] *API Technical Data Book: Petroleum Refining*, 6th ed. vol. 2. Washington, D.C.: American Petroleum Institute, 1997.
- [33] F. Y. Jou and A. E. Mather, "Liquid-liquid equilibria for binary mixtures of water plus benzene, water plus toluene, and water plus p-xylene from 273 K to 458 K," *Journal of Chemical and Engineering Data*, vol. 48, pp. 750-752, May-Jun 2003.
- [34] B. J. Neely, J. Wagner, R. L. Robinson, and K. A. M. Gasem, "Mutual solubility measurements of hydrocarbon-water systems containing benzene, toluene, and 3-methylpentane," *Journal of Chemical and Engineering Data*, vol. 53, pp. 165-174, Jan 2008.
- [35] M. J. Amani, M. R. Gray, and J. M. Shaw, "Volume of mixing and solubility of water in Athabasca bitumen at high temperature and pressure," *fluid phase equilibria*, DOI: 10.1016/j.fluid.2013.07.021., 2013.
- [36] E. Brunner, M. C. Thies, and G. M. Schneider, "Fluid mixtures at high pressures: Phase behavior and critical phenomena for binary mixtures of water with aromatic hydrocarbons," *The Journal of Supercritical Fluids*, vol. 39, pp. 160-173, 2006.
- [37] E. Brunner, "Fluid mixtures at high pressures IX. Phase separation and critical phenomena in 23 (n-alkane + water) mixtures," *The Journal of Chemical Thermodynamics*, vol. 22, pp. 335-353, 1990.
- [38] M. J. Amani, M. R. Gray, and J. M. Shaw, "Phase behavior of Athabasca bitumen+water mixtures at high temperature and pressure," *The Journal of Supercritical Fluids*, vol. 77, pp. 142-152, 2013.
- [39] E. W. Lemmon, M. O. McLinden, and D. G. Friend, "Thermophysical Properties of Fluid Systems," in *NIST Chemistry WebBook*, NIST Standard Reference Database Number 69, P. J. Linstrom and W. G. Mallard, Eds., ed Gaithersburg MD, <http://webbook.nist.gov>: National Institute of Standards and Technology, 2012.
- [40] S. D. Burd, J. Braun, and W. G. Braun, vol. 48, ed: *Proc. Am. Pet. Inst., Div. Refin.*, 1968, p. 464.

- [41] E. W. Aldrich, "Solubility of water in aviation gasolines," *Industrial and Engineering Chemistry-Analytical Edition*, vol. 3, pp. 0348-0354, 1931.
- [42] R. R. Hibbard and R. L. Schalla, "Solubility of water in hydrocarbons," ed. Washington: National Advisory Committee for Aeronautics, 1952.
- [43] E. Groschuff, "Über die Löslichkeit von Wasser in Benzol, Petroleum, Paraffinöl," *Zeitschrift für Elektrochemie und angewandte physikalische Chemie*, vol. 17, pp. 348-354, 1911.
- [44] K. M. Watson, E. F. Nelson, and G. B. Murphy, "Characterization of petroleum fractions," *Industrial and Engineering Chemistry*, vol. 27, pp. 1460-1464, Jan 1935.
- [45] D. El-Hadi and M. Bezzina, "Improved empirical correlation for petroleum fraction composition quantitative prediction," *Fuel*, vol. 84, pp. 611-617, Mar 2005.
- [46] W. L. Nelson, "Solubility of water in oil," *oil & gas journal*, p. 140, April 1956.
- [47] J. Griswold and J. E. Kasch, "Hydrocarbon-water Solubilities at elevated temperatures and pressures," *Industrial and Engineering Chemistry*, vol. 34, pp. 804-806, 1942.
- [48] C. A. Glandt and W. G. Chapman, "Effect of water dissolution on oil viscosity," *Spe Reservoir Engineering*, vol. 10, pp. 59-64, Feb 1995.
- [49] I. Soreide, "improved phase behavior predictions of petroleum reservoir fluids from a cubic equation of state," ed: PhD thesis, the Norwegian Institute of technology, April 1989.
- [50] M. J. Amani, M. R. Gray, and J. M. Shaw, "The phase behavior of Athabasca bitumen + toluene + water ternary mixtures," ed: *Fluid Phase Equilibria*, (submitted on Nov 2013).
- [51] M. A. Satyro, "private communication," ed. Calgary, Oct 2013.
- [52] W. A. Leet, H. M. Lin, and K. C. Chao, "Mutual solubilities in 6 binary-mixtures of water + a heavy hydrocarbon or a derivative," *Journal of Chemical and Engineering Data*, vol. 32, pp. 37-40, Jan 1987.

Chapter 6. Conclusions and Remarks

The key conclusions, based on works performed in this research are as follows:

1- The X-ray apparatus capability was validated using known properties of pure fluids and binary mixtures of water + toluene and water + 1-methylnaphthalene binary mixtures. The available phase boundary temperatures and pressures, identified indirectly from 453 to over 573 K, were reproducible within 0.5 K, 0.2 MPa.

2- A new indirect and non-intrusive technique, applicable under extreme conditions, is developed to evaluate the phase boundary compositions of mixtures. The technique were validated by reproducing solubility of water in toluene and 1-methylnaphthalene up to 573 K with less than 25% error (wt %) comparing to literature data.

3- Phase diagrams for Athabasca bitumen + water were constructed using the synthetic method where the phase behaviors of mixtures with fixed composition were studied individually from 522.1 to 644 K and pressure up to 35.7 MPa. It was observed the LLV phase behavior can exist adjacent to the critical point of water. Based on the resulted P-x and PT diagrams, it was concluded that the phase behavior of the pseudo binary of Athabasca bitumen + water is Type IIIb according to the van Konynenburg and Scott classification scheme.

4- Bitumen at temperatures above 620 K tends to be thermally unstable. Thermal degradation of bitumen impacts the phase boundary pressure measurements, however the impacts on phase behavior Type alteration is negligible.

5- The solubility of water in Athabasca bitumen over the temperature interval 593.2 to 644 K was evaluated. Solubility of water in bitumen highly increases with temperature as that of water in other hydrocarbons do. The reported values and the trend with temperature are in agreement with numerous data sets for comparable hydrocarbons.

6- Athabasca bitumen + water have a positive volume of mixing in the interval 593.2 to 644 K similar to other hydrocarbons. The volume of expansion for bitumen-rich liquid is an order of magnitude less than other water-saturated light hydrocarbons where these compounds are close to their binary critical regions.

7- The mixture of Athabasca bitumen + toluene + water mixtures are studied for 0.443 and 66.8 weight fraction of toluene. Phase order inversion at fixed temperature with

increasing solvent mass fraction and with increasing temperature at fixed solvent mass fraction, and phase behavior type transitions are illustrated. These features of the phase diagrams for such mixtures complicate the evaluation of their phase behavior and impact possible industrial applications where phase order may be difficult to control, monitor or predict.

8- The solubility of water in mixtures of Athabasca bitumen + toluene at $w = 0.443$ and 66.8 weight fraction toluene were evaluated using the $L_2V/L_2 - LLV/LL$ boundary detection on pseudo binary P-x diagrams over the temperature interval 492.6 to 573.5 K. These results shows that toluene/solvent addition to mixture of bitumen + water increases the solubility of water in bitumen phase, however the effect is less than expected on a average mass basis where data for water solubility in toluene and bitumen overlap. This finding can open new direction to develop upgrading processes, where synthetic aromatic products are readily available to increase water solubility as required.

9- The density and excess volume of Athabasca bitumen + toluene + water at $w = 0.443$ and 66.8 weight fraction toluene were evaluated. From the perspective of phase density prediction ideal mixing assumptions that break down at temperatures well below the critical temperature of low molar mass hydrocarbons in simple binary mixtures remain robust for multicomponent asymmetric ones within measurement and prediction error at high pressure, however more experimental data are required.

10- Bitumen + toluene mixture exhibit non-ideal volumetric behavior at high temperature. The negative excess volume for bitumen + toluene is linked with non critical behavior of bitumen + toluene mixture while toluene goes through a critical phenomena at 591.8 K.

11- A new general empirical equation for water solubility in hydrocarbons is correlated in terms of average normal boiling point and elemental hydrogen weight fraction of hydrocarbons to estimate solubility of water in hydrocarbons below the UCEP. The average deviation of the proposed correlation from reference experimental data (AARD 18%) is less than uncertainty of the reference data. The correlation is consistent with all Types of phase behavior arise for water + hydrocarbon mixtures including Type II, IIIa and IIIb phase behavior which show LLV behavior below the UCEP. The reliability of the model is validated against water solubility data in 13 reservoir fluids and petroleum fractions in temperature range 283 to 573 K. The results were in good agreement both in

trends and values, although deviations from test data sets could not be assessed quantitatively due to uncertainty or unavailability of inputs.

12- A simple Henry's constant model is proposed to estimate the solubility of water in hydrocarbons at bitumen upgrading reactor conditions above the UCET of hydrocarbon + water mixtures. This model is restricted to heavy hydrocarbons + water mixtures which exhibit phase behavior Type IIIb. As there are no data for water solubility in hydrocarbon-rich liquids above the critical temperature for water, the quality of the estimates could not be evaluated. However, the estimates are in close agreement and the extrapolated range of mass based Henry constant-like parameters obtained are consistent with values known to arise at lower temperatures.

6.1 Future works and recommendations

Presenting reliable and accurate PVT data, phase diagrams, solubility data and density of hydrocarbon resource + water are essential step toward developing bitumen upgrading and production processes. The main objective of this work was to investigate the phase behavior and properties of bitumen liquid phase in presence of water at high temperatures. Single-phase bitumen liquid, where bitumen and water become miscible, was identified. In relation to this work, the nature of asphaltene aggregation in the liquid-liquid phase and single-phase regions should be followed up. The asphaltene aggregation study, which presents a number of hurdles, include the construction of a high-pressure and high-temperature cell suitable for use in a laboratory or synchrotron based SAXS apparatus or the development and implementation of some other optical method for detecting nanostructured particles in fluids.

To future investigations, solubility and PVT measurements at high temperatures over the critical point of water where bitumen undergoes upgrading reactions are necessary. The experimental data in supercritical region of water + hydrocarbons are currently not available in open literature. Further design and modifications are required to increase the capability of the X-ray view cell for such experiments.

Phase equilibrium measurements of n-alkanes + bitumen + water pseudo ternary mixtures is matter of interest due to their application is VAPEX and SAGD processes. Knowledge of thermophysical properties and aggregation of asphaltene with the nature of the phase behavior for these mixtures may open new directions to improve the current oil production processes.

The empirical solubility model presented in chapter 5 was developed to calculate solubility of water in complex heavy hydrocarbons where experimental measurements are exceedingly difficult due to containment and hydrocarbon thermal instability. The correlation inputs include T_b and $H_{wt\%}$. Limitations introduced by the ill-defined nature of T_b as a correlating parameter are also discussed. To circumvent this difficulty, a solubility model could be recast based on readily measured properties such as hydrocarbon density and hydrogen wt %. may prove more robust relative to composition and may prove to be easier to extrapolate to temperatures above the critical temperature of water.

Appendix 1. Standard Operating Procedures of the X-ray view cell

Scope

This standard operating procedure describes the methodology to follow when working with the view cell and highlights the main hazards involved.

The view cell is a device that permits on-line measurement of properties of organic fluids/water over a broad range of temperatures and pressures. Measurements, based on the use of x-ray video tomography, include phase behavior, phase density, phase volume, phase composition, mutual diffusion coefficients, gas solubility measurements, etc.

Hazard identification

Beryllium cell: beryllium and beryllium oxide are toxic especially as inhaled dusts or fine particles. They are also very corrosive to tissue. Beryllium/beryllium oxide surfaces should not be touched with bare hands, use disposable gloves (e.g., nitrile gloves). The cell is handled with care and it should be stored in a fume hood or the closed lead lined cabinet.

X-ray exposure: X-rays radiation increases the risk of cancer problems in those exposed. X rays are classified as a carcinogen by both the World Health Organization's International Agency and the U.S. government. The X-ray source is placed inside a thick well-protected lead chamber to prevent X-ray emission. After each disassembling, the lead chamber must undergo an X-ray leakage test. It is mandatory to perform an X-ray inspection once a year. The inspection is requested to the department of Environment, Health & Safety and it's performed by the Radiation Protection Officer. The records of the inspection are kept in the Lab Manager's office and a copy of the Registration Certificate (N° AX-016) is posted outside the lead lined cabinet is posted in the view cell.

H₂ leakage/release: hydrogen is used for leak testing. Hydrogen poses unique challenges due to its low-energy ignition, and wide range of combustible fuel-air mixtures. Hydrogen detector allow for rapid detection of hydrogen leaks to ensure that the hydrogen can be vented and the source of the leak tracked down. The portable hydrogen detector is placed on the view cell shelf. The sensitivity of detector can be adjusted by the tuner on the device.

High pressure cell: the view cell must undergo leakage tests before experiments. Leakage tests are done using pure hydrogen. Leakage is detected using a hydrogen detector. Pressure of the cell should be monitored for an hour to ensure proper sealing in the cell, pipes, connections, etc. The x-ray cabinet must be closed while the cell is being pressurized.

High temperature: the chamber must be closed while the cell temperature is high. After each experiment, the cell should be cooled slowly to room temperature and removed from the chamber. The electrical heaters must be handled wearing thick thermally insulated gloves.

Liquid nitrogen: at atmospheric pressure, liquid nitrogen boils at $-196\text{ }^{\circ}\text{C}$. Liquid nitrogen can cause sudden death of living tissue due to extreme cold exposure. Hand protection and goggles (not safety glasses) must be worn when dispensing and handling liquid nitrogen.

Chemical solvents: the solvents used include, but not limited to, toluene, THF, acetone. The MSDS for these solvents can be found in the MSDS Binder located in Lab 6-128. Care must be taken when working with solvents. For example, inhalation of toluene vapor can affect the central nervous system. Health issues have been reported at different concentration of toluene. At 50 ppm and higher concentration, sleepiness and headache are felt. As concentration goes over 100 ppm, irritation and severe dizziness happen. Over 500 ppm is very dangerous and causes mental disorder and confusion. Therefore, when working with organic solvents such as toluene, the work must be done under the fume hood. If this is not feasible, the use of respiratory mask is mandatory and other researchers working in the vicinity must be warned about. The respiratory masks can be found in lab 6-133 in a drawer labeled "Masks Respirators".

Water spill: water is used in the cooling system of the X-ray source. Water leakage from pipes/connections makes the lab floor slippery. It is also very dangerous if electricity cords/wires are on the floor.

Heavy portable cell: The loaded beryllium cell is heavy. A cart must be available to carry the beryllium cell between the fume hood and the lead lined cabinet.

Training required

Proper training should be taken before using the view cell. The training should be performed by the current research working in the unit.

Control/protective measures:

- The use of lab coat, disposables gloves, safety glasses and dosimeter is mandatory. The dosimeter can be obtained by contacting Shiraz Merali at 2-2724 (Shiraz.merali@ualberta.ca).
- When working with the beryllium cell gloves should be worn
- X-ray dosimeter must be worn while the X-ray source is in operation
- Safety goggles and thermal isolation gloves must be worn while working with liquid nitrogen
- Thick thermal isolation gloves must be used to handle the electrical heater or the view cell when they are hot
- Safety face shield should be worn while the cell is pressurized and the lead lined cabinet door is open. The safety glasses/goggles must be on when using the face shield.
- Safety gas mask should be used while disassembling the cell after high temperature experiments and when purging the pressurized lines to atmosphere

Emergency procedures

If there is an explosion or fire during an experiment, the following must be done:

- If it is safe, turn off the power to the electrical heaters and the x-ray source (X-ray Xylon equipment) to stand by position (~), as shown in Figure 1; otherwise depress the emergency electrical power shut down button
- Vacate the Lab and the building via nearest exit
- Pull down the nearest fire alarm
- Move to the designated evacuation area
- Meet emergency response crews to inform them about the situation

- Notify Dr. Shaw (780 999-3726), the lab manager, Mildred Becerra (780 940-6863) and Andree Koenig (2-5159)
- An incident report will have to be filed with the CME department's APO Sandra McFadyen.
- Phone Occupational Health and Safety immediately (Control Center 780 492 5555)



Figure 1. The x-ray control panel (XYLON panel). (0), (~) and (⚡) represent OFF, STANDBY and ON positions respectively.

Step by step procedure of the process

The standard procedure of experiments for Athabasca bitumen + water is described here. It should be noted that the current procedure explains how to inject liquid and solid samples. The procedure of loading the gas samples e.g. hydrogen and CO₂ can be found in other thesis [1].

1. Assembling of the view cell and injecting samples

The schematic configuration of the view cell is shown in Figure 2. Different parts are introduced and numbered in order of the assembled cell.

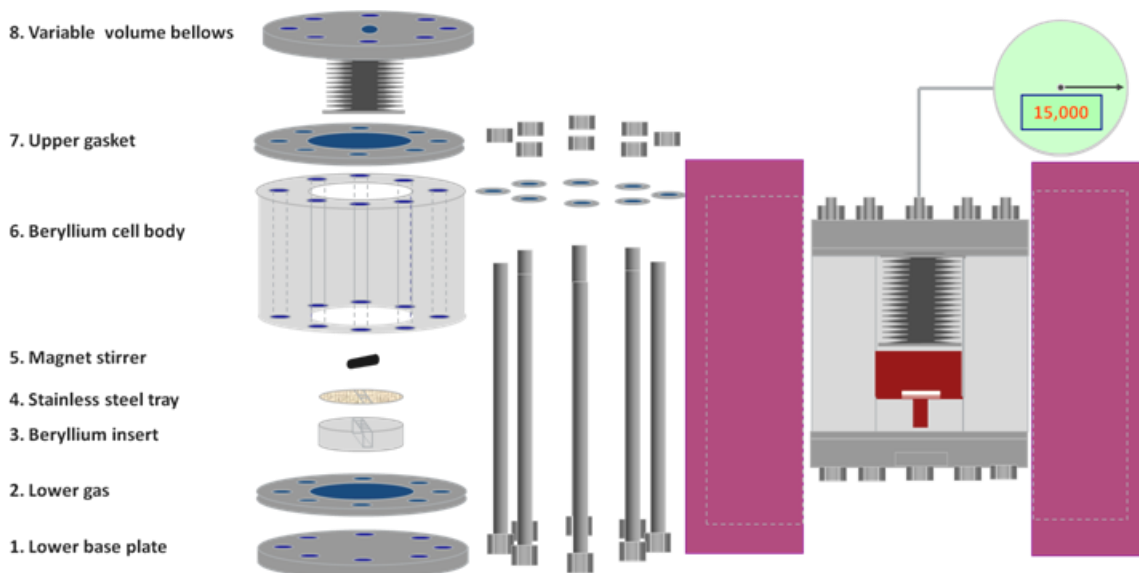


Figure 2. Schematic configuration of the view cell

- 1.1. Lab coat, gloves, and safety glasses must be worn while handling the beryllium cell.
- 1.2. The cell (6) and the variable-volume bellows (8) should have been placed in fume hood area after solvent rinsing. The rest of cell parts, placed on a designated lab cart should be rinsed by solvent (preferably toluene) and dried under fume hood . Both exterior and interior surfaces of the cell parts should be cleaned by toluene (any suitable solvent) and dried under the fume hood. The plastic electrical connectors attached to the beryllium cell, e.g. thermocouple plugs, are not resistant to chemical solvents and should not be exposed to chemicals.
- 1.3. Ensure the cell mount is securely screwed to the designated assembly by three screws. The stainless steel Lower Base Plate (1) of the cell sits on the cell mount, while eight bolts passes through the holes of the lower base plate
- 1.4. Place the beryllium insert on the lower base plate The beryllium insert (3) has a notch at the bottom, which aligns with a pin in the lower base plate
- 1.5. Place the stirrer support plate (4) on the beryllium insert, as shown in figure 2.



Figure 3. Correct position of the beryllium cell with respect to the cell mount

- 1.6. The channel of the beryllium insert should be aligned with the stamped mark **P** on the Cell Mount (Figure 3).
- 1.7. The lower gasket (2) sits on the Lower Base Plate. The same type of gaskets should be used for both lower and upper. The type of gaskets is selected depending on the materials and the experiment regime.
- 1.8. The beryllium cell body (6) is placed on the gasket covered the Lower Base Plate, while the beryllium insert is in aligned to stamped mark **P**. Align the sample tubing attached to the view cell with the stamped mark **P** (see configuration in Figure 3). The cell is aligned in a way that the sample tubing does not block the X-ray view path.
- 1.9. If any solid or viscous liquid sample present in the experiments, insert the samples before installing the upper gasket and the variable-volume bellows. If a

low viscosity liquid sample will be used, the cell assembly should be completed without sample addition; the liquid sample is added at a later stage.

- 1.10. Place the magnetic stirrer (5) in the view cell.
- 1.11. Place the gasket (7) at the top of the beryllium cell body.
- 1.12. Ensure upper gasket and top surface of the beryllium cell body are clean after sample addition, and mount the variable-volume bellows (8) on the upper gasket.

2. Tightening of the view cell

- 2.1. The eight bolts of the cell should be coated with thermal grease. Adding grease reduces the heating/cooling distortion effects. Important note: ungreased bolts and nuts can become severely stuck.
- 2.2. Install the eight nuts and the washer-spacers to the bolts, and firmly hand-tighten them before using . Correct configuration of washers is shown in Figure 4.
- 2.3. Tightening the nuts must be done in the specified sequence, 1 to 8, shown in Figure 5. The torque setting depends on the type of gaskets. For example, nickel carbon composite gaskets are used in Athabasca bitumen + water experiments. For these gaskets, the tightening should begin at 5 ft-lb set on torque wrench, and the torque must be increased in steps of 5 ft-lb until 45 ft-lb. For different types of gaskets, different settings must be used [1].
- 2.4. Tightly hold the bottom bolt with a suitable wrench, and fasten the nuts with the torque wrench in sequence based on a proper torque settings.
- 2.5. Install the VCR silver-plated gasket to the VCR fitting at the end of sampling tube. Notice: the sealing surface of the VCR gasket shouldn't be scratched.



Figure 4. Correct configuration of spacers

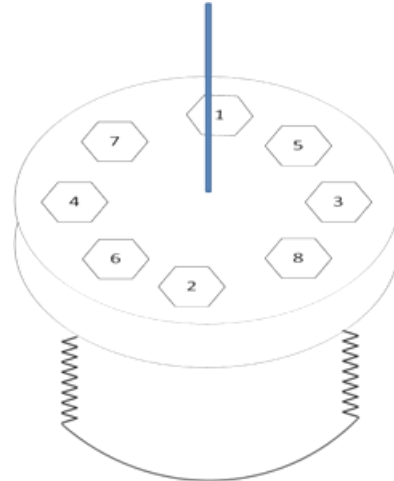


Figure 5. Bolt tightening order

3. Installation of the view cell inside the lead lined cabinet

- 3.1. Unscrew the three locking screws on the cell mount, and detach it from the designated assembly in the fume hood.
- 3.2. The assembled view cell is heavy. A lab cart is used to transfer it to the cabinet. The view cell has to be held and moved with two hands (one hand at the bottom of the assembly, the other on the eight bolts positioned at the other end of the structure). The sample tubing and thermometers are fragile and must not be touched or stressed. Place and align the channel on the cell mount with the X-ray source in the cabinet. The view cell must be placed in a direction that does not block the X-ray view path.
- 3.3. Recheck the VCR gasket at the end of the sample tubing of the view cell, see section 2.5.
- 3.4. Move the fork structure, attached to the “crane” assembly, to align with the top of the sample tubing of the view cell. The correct configuration of the beryllium cell and fork structure is shown in Figure 7.
- 3.5. Attach outlet line of the fork structure (lower VCR fittings) and sample tubing of the view cells. Hand-tighten it and then tighten with two wrenches to $\sim 1/8$ of a turn from the hand-tight position.

3.6. If the experiments are designed for a low viscosity liquid, the liquid samples must be injected to the view cell in this stage. To load the liquid samples follow these steps:

- Install a VCR gasket on the liquid injection tube (shown in Figure 6) and attach it to a syringe. Fill the syringe through the liquid injection tube with certain amount of the liquid sample. Connect the liquid injection tube on the syringe to the left sampling line of the fork structure and inject the sample into the cell gently.
- Detach syringe and re-attach sample line to fork structure
- Purge the sample lines into the view cell to ensure no liquid sample remains in the tubing (For details and safe operation see Sections 4 and 5). In order to prevent loss of sample, it is recommended to perform the purge process quickly. The elevation of the injected liquid sample in the beryllium cell (monitored by X-ray camera, for safe operation read Section 4 carefully) should be monitor before and after purge.
- Detach the syringe and follow Section 3.8.

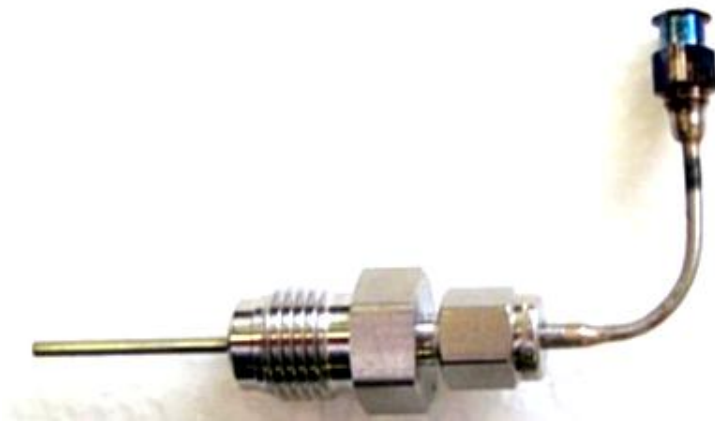


Figure 6. liquid injection tube to be attached to a syringe

3.7. Install another VCR silver-plated gasket on the hydrogen supplying tubing and attach it to the upper VCR fitting on the fork structure. Hand-tighten the VCR fitting and then tighten with two wrenches $\sim 1/8$ of a turn from the hand-tight position.


3.8. Attach the labeled thermocouple plugs and the RTD sensor plug to the beryllium cell.

3.9. Figure 7 shows the correct configuration of the view cell inside the cabinet.



Figure 7. Correct configuration of the view cell with respect to its base

4. Working with X-rays

- 4.1. The big and small water cooling system must properly work during X-ray source running. The big water cooling system is securely connected to the X-ray power source, to shut down X-ray in case of cooling water shortage.
- 4.2. Check the level of cooling fluid in both big and small water cooling systems. Top up cooling water using de-ionized water if required.
- 4.3. The x-ray source must be conditioned before each experiment (once a day). In order to condition the x-ray source, it must be blocked with the yellow lead brick to protect the camera against high power conditioning X-ray. Gloves must be used during this procedure – lead and beryllium surfaces are both toxic. The procedure for conditioning the x-ray source is as follows:
 - 4.3.1. Turn the x-ray control switch, on XYLON panel shown in Figure 1, to standby (~). Notice: because of safety concerns, the X-ray source does not work if the access door to the shielded chamber is not properly closed.
 - 4.3.2. Accept the default setting using the key pad. The default voltage for conditioning, 120 kV, is good to proceed.
 - 4.3.3. The time for conditioning is automatically set based on the given inactivity period. Enter the number of inactivity days of the x-ray source (Since last use) by the key pad, shown in Figure 1.
 - 4.3.4. Turn the control switch, on XYLON panel, to the on position (, Figure 1).
 - 4.3.5. The green safety light, next to the control switch, must be illuminated before running the X-ray source. If the green light is not on, re-check the access door to the chamber is closed, and cooling water level in the cooling systems is high enough.
 - 4.3.6. Press the black button (“I”, Figure 1) to run the x-ray source for conditioning. Remaining conditioning time begins to countdown on the screen. The X-ray source will be turned off automatically, once the x-ray source conditioning finishes.

4.3.7. The X-ray source is ready to use. You can run the X-ray source by pushing the black button. Suitable voltage and current parameters of the X-ray source depends on the samples inside the cell, while the Focus always must be 0.5. The voltage and current can be manipulate obtain the most clear liquid-liquid interface. The ideal values for Athabasca bitumen + CO₂ is given in table 1 [1].

Table 1. Ideal operational condition [1]

V (kV)	I (mA)	Focus
045.0	03.35	0.5

Important notice: after finishing working with the X-ray system, the cooling bath must be turned off manually 5-10 min after the x-ray source has been turned off.

5. Vacuum Operation (purging, cleaning)

- 5.1. Pressurize the air tubing, which operates the pneumatic solenoids (controlled by valves 4 and 8, Figure 8), up to 120 Psi. There is a safety mechanical mechanism on the solenoids to adjust the maximum allowed pressure.
- 5.2. Ensure thermal gloves and safety glasses are worn. Put the liquid nitrogen into the cold trap (in line before the vacuum pump), then put the cap on it and open the valves 10-13 on the inside panel (Figure 9) in order to make sure that all parts of tubing are under vacuum. Note: always valve 9 is closed.
- 5.3. Turn on the vacuum pump and give it ~ 5 minutes to stabilize.
- 5.4. First scroll the green N₂ switch (8) on the control panel quickly (Figure 8). The pressure on the bellows side decreases and bellows goes up (contracts) and return to its resting position. Monitor all bellows movements using the computer to prevent damage to the bellows and cell. If bellows shows a bizarre behavior, ensure all the valves are properly close/open and all connections are tightened.
- 5.5. Scroll switch (8) and (4) simultaneously for a very short period of time (to minimize sample lost) and make sure always the bellows is on its rest position. Repeat this step until the both cell and bellows are completely vacuumed (reached minimum pressure) and the bellows is on it resting position.

- 5.6. Close valve 11-13 (Figure 9) and monitor the pressure/temperature and bellows position changes for five minutes to ensure everything is OK. Pressure, temperature and bellows position must be remaining constant over time.

6. View cell leakage test using hydrogen

In this section, the sealing test of the view cell is discussed. If the view cell is not properly sealed, the view cell must be disassembled (Section 7) and all the procedures up to this point (Sections 1-4) should be repeated. Before proceeding make sure all connections are tightened and the X-ray source, monitoring system, data acquisition and monitoring (X-ray camera) software work properly. The view cell and connected tubing must be under vacuum before this procedure is conducted. Hydrogen is a combustible gas. Air must be eliminated from the system.

- 6.1. Ensure nitrogen and hydrogen support tubing's are not pressurized.
- 6.2. Correct configuration of valves is as follows: valves 1-9 must be completely closed and valves 10-12 must be open. Valve 13 remains close all the time (Figures 8-9).
- 6.3. Pressurize the nitrogen and hydrogen support tubing to a pressure around 200 Psi by turning clockwise the pressure regulator on both cylinders (Figure 10). Hydrogen cylinder is placed inside a gas cabinet.
- 6.4. Open the monitoring software on the computer and observe how bellows move when you change whether the pressure of cell or the bellows.
- 6.5. Pressurize the view cell by opening hydrogen valves (1-2) once. The bellows move up. Monitor the system on-line all the time. In order to prevent any damage caused by sudden movements of the bellows, both the cell and bellows should be pressurized gradually.
- 6.6. Pressurize the bellows by opening nitrogen valves (5-6). This step should be done until the bellows move back to its resting position or lower. Notice: the bellows never must touch the liquid surface.
- 6.7. Repeat steps 6.5 and 6.6 until the cell and bellows are pressurized ~ 150- 200 psi. Monitor the bellows position and all pressures; they should roughly remain unchanged by time. If the bellows unexpectedly moves or pressures change, then

cell leakage is serious. Find the leakage source as soon as possible and depressurize the cell. If the cell leaks, it must be reassembled.

- 6.8. In this step, the pressure of nitrogen and hydrogen support tubing's should increase to 800 psi.

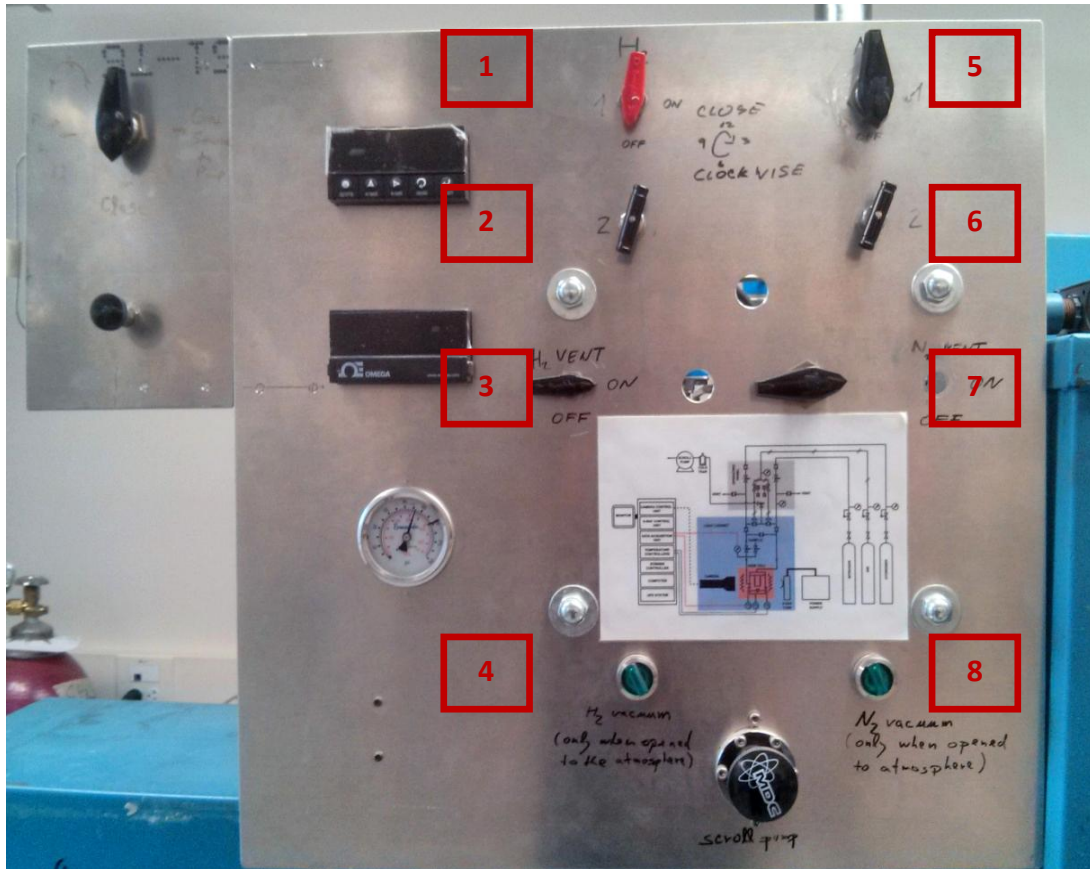


Figure 8. Valve configuration in View Cell Panel

- 6.9. Repeat steps 6.5 and 6.6 until the cell and bellows are pressurized ~ 700 psi. The pressure of nitrogen and hydrogen support tubing's should increase to 1500 psi.
- 6.10. Repeat steps 6.5 and 6.6 until the cell and bellows are pressurized ~ 1500 psi. Monitor the bellows position and all pressures and leave the cell for ~ 1 min.
- 6.11. Use Snoop® Liquid Leak Detector to check if the connections are been properly tightened. If leakage is spotted (bubbles are observed), use the appropriate wrench to tighten them.

- 6.12. Use the Hydrogen detector on the connections thoroughly to detect hydrogen leakage on the view cell tubing and gaskets. In case of serious leakage the cell must be reassembled.
- 6.13. Leave the view cell and bellows pressurized up to 1 hour and monitor pressure drops. If the pressure drops or bellows movement is significant, the cell must be reassembled.

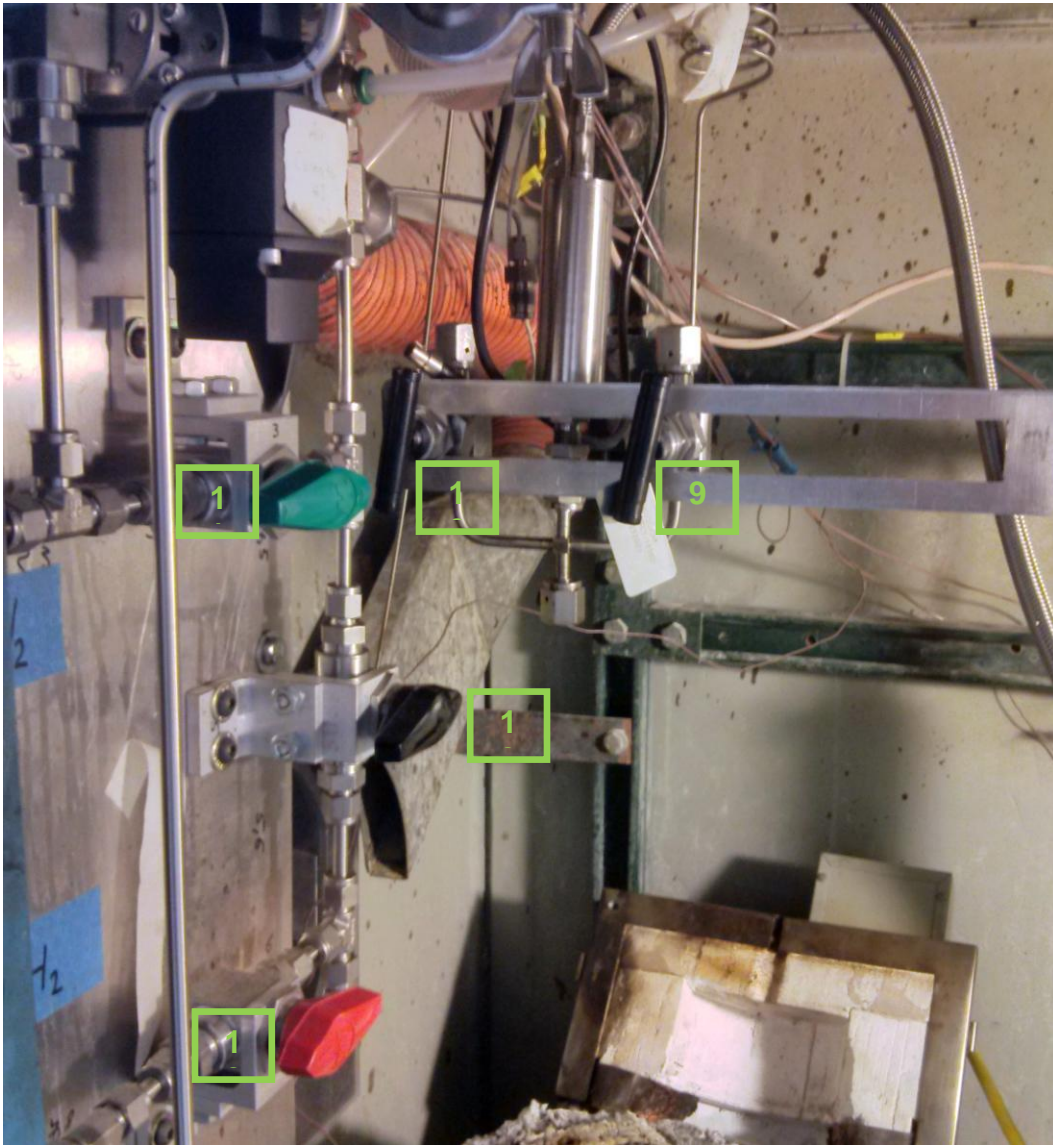


Figure 9. Valve configuration inside the cabinet

7. Running experiments

In this section, the procedure for experiments is explained. Before running an experiment, the cell should be purged with nitrogen to reduce air/oxygen in the cell. After venting, the cell must be vacuumed as explained in section 5 to remove inert gas from the cell.

- 7.1. Put the electrical heater jackets around the cell carefully. Ensure the electrical heater don't block the X-ray view.
- 7.2. Close valve 10 and isolate the view cell. Ensure valves 9-13 are closed.
- 7.3. Put a shield above electrical heaters to prevent burning of the plastic connectors.
- 7.4. Check elevation of sample and bellows inside the cell, all temperature/pressure parameters, and ensure all instruments work fine.
- 7.5. Turn on the magnet stirrer.
- 7.6. Turn on the heater controller. Set temperature to the desired value. Notice that temperature set point must increase gradually to prevent bellows damage. While temperature increases, keep the bellows in its rest position by nitrogen injection. See Section 6 for more details.
- 7.7. When the view cell reached the desired set point and pressure/temperature profile become steady, turn off the magnet stirrer. Try to keep the magnet stirrer in a direction that doesn't block the X-ray view. Take an image using the software. Save the image with the corresponding temperature and pressure.
- 7.8. Increase the pressure of the cell by injecting nitrogen into the bellows to reach a new equilibrium position. Turn on the magnet stirrer to reach equilibrium more quickly. Repeat Step 7.7 and 7.8 until all desired temperature/pressure condition are covered.

8. Post-experiment operation and cooling down view cell

- 8.1. Turn off the electrical heater.
- 8.2. Open N₂ valve (12) and ensure that the position of the other valves don't change.
- 8.3. Check the bellows position and ensure it is above its resting position by purging nitrogen from the bellows and quickly opening/closing nitrogen purging valve (8).

- 8.4. Wait a few minutes, typically 5-10 minutes, until the cell cools down a bit. Monitor the bellows elevation. It should not get below its resting position and never touch the liquid interface. If the bellows went down the resting the resting position, purge more nitrogen form bellows using valve (8). Repeat this step until the pressure of the reach near atmospheric pressure.
- 8.5. Open the hydrogen valves (9) and (10) inside the blue cabinet. Monitor the elevation of bellows again.
- 8.6. Open hydrogen purge valve (4) and then valve (8) in order to reach atmospheric pressure in both bellows and the cell. Notice: never purge the cell when the cell in pressurized at high temperatures; the sample will condense in the tubing and will block the purge system. If the purge system is blocked, the cell must isolated by closing the connecting valves and purge system must be disassembled and cleaned. Purging the cell is only recommended when the cell reached room temperature to prevent any unexpected gas accumulation in the cell.
- 8.7. Keep both valves (4) and (8) open until the cell cool down to room temperature.
- 8.8. Remove the electrical heater around the cell

9. Disassembling

- 9.1. Unplug thermo couple and transducer connectors carefully.
- 9.2. Open all VCR connections and detach the cell from the fork structure.
- 9.3. Move back the crane and make enough room to move out the cell.
- 9.4. Unscrew the cell mount. Ensure no wire or extension of cell is trapped or plugged inside the cell, and it can be moved easily.
- 9.5. Bring the lab cart near the blue cabinet and make enough room on cart. Put the view cell gently on the cart, handling it with both hands (as discussed in section 3.3).
- 9.6. The view cell should be securely mounted on the designated assembly by three screws inside the fume hood.
- 9.7. Use torque wrench and another wrench to lose the bolts and nuts as shown figure 4. Put the nuts in the box assigned for this.

- 9.8. Detach the bellows and place it on the designated structure securely (Figure 11). Wash it thoroughly with toluene under the fume hood.



Figure 11. Designated structure to protect the bellows cap.

- 9.9. Remove the liquid sample from the cell and detach the beryllium cell body. Notice: sample inside cell can be used for more detail analysis. A part of sample can be stored in a small container.
- 9.10. Remove and wash the beryllium insert, magnet stirrer and stirrer support plate with toluene. Keep them inside the fume hood to be completely dried.

Hazardous waste disposal procedures

- Organic waste such as toluene, crude oil, etc., must be disposed in the organic waste bottle located inside the fume hood. When the bottle is full, report to the lab manager (Mildred Becerra 2-9202) who will submit a request to the Environmental, Health and Safety Department – Hazardous Waste Disposal, for its disposal.
- Disposable syringes after use must be disposed in the plastic/needle container. When the container is full, report to the lab manager (Mildred Becerra 2-9202)

who will submit a request to the Environmental, Health and Safety Department – Hazardous Waste Disposal, for its disposal.

Equipment maintenance procedures

- Tools used in this unit must be placed back in the box tool assigned to the view cell
- After disassembling the view cell, all the view cell parts such as beryllium cell, bellows, fork structure, bolts, magnet, beryllium inert, stirrer support plate, etc., should be completely washed with toluene or another stronger organic solvent e.g., THF, under fume hood until they dry
- All pipes and connections must be checked for leakage by soap solution before each experiment. The loose connections must be tighten or replace in the case of serious leakage.
- The stainless steel bellows is fragile. It should be placed in its designated holder and kept in a safe area
- Beryllium cell must be kept under fume hood
- The piping system should be vented while the equipment is shut down
- Electrical equipment can be unplugged while the equipment is shut down

Reference:

[1] K. Khaleghi, "Experimental PVT Study of the Phase Behavior of CO₂ + Heavy Oil Mixtures," MSc., Chemical Engineering, University of Alberta, Edmonton, AB, Canada, 2011.

Appendix 2. Supplementary data

In This section, the detail data of PVT experimental measurements are provided. These data include initial inserted mass, pressure, temperature, density and volumes of coexisted liquid and vapor phases. The experimental data for aqueous mixture of toluene, 1-methylnaphthalene, Athabasca bitumen and Athabasca bitumen + toluene are presented. These data are very valuable for further research in developing thermodynamic models including equations of state.

Table 3.a. Toluene + water

Temperature (K)	Pressure (MPa)	Feed composition (toluene wt %)	Liquid phases volume ($m^3 \cdot 10^6$)	Vapor phase volume ($m^3 \cdot 10^6$)	Phases
493.0	3.43	40.7	67.6	26.8	LLV
493.0	3.53	83.0	88.5	14.9	LLV
493.2	3.58	86.5	114.8	9.9	LLV
493.2	3.52	88.4	85.3	15.6	LLV
493.1	3.57	90.3	84.1	16.4	LLV
493.2	3.57	92.5	81.4	19.1	LLV
493.1	1.05**	100.0			

Table 3.b. Toluene + water

Temperature (K)	Pressure (MPa)	Feed composition (toluene wt %)	Liquid phases volume ($m^3 \cdot 10^6$)	Vapor phase volume ($m^3 \cdot 10^6$)	Phases
512.8	5.04	83.0	92.4	13.3	LLV
513.1	5.03	86.5	120.3	9.0	LLV
513.3	5.13	88.4	89.7	17.1	LLV
513.1	5.12	90.3	87.1	19.6	LLV
513.1	4.31	92.5	82.9	47.2	LV
513.2	4.53	92.5	83.2	34.5	LV
513.2	4.75	92.5	84.1	20.0	LV
513.2	5.06*	92.5			LV/LLV
513.1	1.4**	100.0			

Table 3.c. Toluene + water

Temperature (K)	Pressure (MPa)	Feed composition (toluene wt %)	Liquid phases volume ($m^3 \cdot 10^6$)	Vapor phase volume ($m^3 \cdot 10^6$)	Phases
532.9	7.11	40.7	70.4	41.7	LLV
532.8	7.01	83.0	99.5	9.4	LLV
533.1	7.05	86.5	129.9	3.0	LLV
533.1	6.07	88.4	91.1	44.0	LV
533.3	6.38	88.4	92.2	30.8	LV

533.4	6.69	88.4	93.0	17.8	LV
533.3	7.10*	88.4			LV/LLV
532.8	6.03	90.3	89.8	40.3	LV
533.1	6.29	90.3	89.6	32.4	LV
533.2	6.61	90.3	91.3	15.6	LV
533.0	6.97*	90.3			LV/LLV
533.2	5.28	92.5	87.6	32.6	LV
533.1	5.51	92.5	87.4	25.4	LV
533.1	5.68	92.5	88.0	17.3	LV
533.1	6.14*	92.5			LV/LLV
533.1	1.93**	100.0			

Table 3.d. Toluene + water

Temperature (K)	Pressure (MPa)	Feed composition (toluene wt %)	Liquid phases volume ($m^3 \cdot 10^6$)	Vapor phase volume ($m^3 \cdot 10^6$)	Phases
553.2	9.49	40.7	73.1	30.5	LLV
553.0	9.04	83.0	100.1	36.8	LV
553.1	9.23	83.0	109.1	20.0	LV
553.1	9.26	83.0	110.3	14.4	LV
553.1	9.41*	83.0			LV/LLV
553.2	8.61	86.5	131.5	7.1	LV
553.3	8.94	86.5	133.5	3.6	LV
553.2	9.27*				LV/LLV
553.4	7.84	88.4	102.3	25.5	LV
553.4	8.12	88.4	102.0	18.2	LV
553.4	8.80*	88.4			LV/LLV
553.0	7.26	90.3	99.5	20.4	LV
553.0	7.53	90.3	100.8	13.0	LV
553.0	8.00*	90.3			LV/LLV
553.4	6.03	92.5	88.9	45.1	LV
553.4	6.62	92.5	89.3	31.9	LV
553.4	7.00	92.5	89.8	17.4	LV
553.4	7.18*	92.5			LV/LLV
553.2	2.53**	100.0			

Table 3.e. 1-methylnaphthalene + water

Temperature (K)	Solubility of water (wt %)	Error (%)
513.1	7.5	8.4
533.1	11.5	11.7
553.2	19.0	13.1

Table 4.a. 1-methylnaphthalene + water

Temperature (K)	Pressure (MPa)	Feed composition (1-MN wt %)	Liquid phases volume ($m^3 \cdot 10^6$)	Vapor phase volume ($m^3 \cdot 10^6$)	Phases
513.2	3.41	78.9	73.2	38.3	LLV
513.4	3.45	87.3	23.0	52.7	LLV
513.3	3.42	95.4	59.7	43.9	LLV
513.3	0.092**	100.0			

Table 4.b. 1-methylnaphthalene + water

Temperature (K)	Pressure (MPa)	Feed composition (1-MN wt %)	Liquid phases volume ($m^3 \cdot 10^6$)	Vapor phase volume ($m^3 \cdot 10^6$)	Phases
533.4	4.81	78.9	75.1	45.5	LLV
533.3	4.89	87.3	22.8	54.4	LLV
533.5	3.18	95.4	61.1	67.8	LV
533.3	3.27	95.4	61.1	61.7	LV
533.2	3.38	95.4	61.3	52.8	LV
533.3	3.46	95.4	61.5	41.9	LV
533.3	3.92*	95.4			LV/LLV
533.3	0.141**	100.0			

Table 4.c. 1-methylnaphthalene + water

Temperature (K)	Pressure (MPa)	Feed composition (1-MN wt %)	Liquid phases volume ($m^3 \cdot 10^6$)	Vapor phase volume ($m^3 \cdot 10^6$)	Phases
553.6	6.82	78.9	83.5	38.4	LLV
553.6	6.76	87.3	23.9	52.9	LLV
553.5	3.53	95.4	62.9	69.6	LV
553.7	3.57	95.4	63.1	65.6	LV
553.7	3.70	95.4	63.1	55.5	LV
553.5	3.73	95.4	63.6	50.5	LV
553.5	3.80	95.4	63.8	44.9	LV
553.6	4.30*	95.4			LV/LLV
553.6	0.209**	100.0			

Table 4.d. 1-methylnaphthalene + water

Temperature (K)	Pressure (MPa)	Feed composition (1-MN wt %)	Liquid phases volume ($m^3 \cdot 10^6$)	Vapor phase volume ($m^3 \cdot 10^6$)	Phases
573.2	9.05	78.9	83.5	38.4	LLV
573.2	5.45	87.3	22.0	92.6	LV
573.2	5.84	87.3	22.0	81.4	LV
573.2	6.16	87.3	22.1	72.7	LV
573.2	6.70	87.3	22.1	59.0	LV
573.1	7.23	87.3	22.5	44.8	LV
573.1	7.52	87.3	23.6	31.0	LV
573.2	8.70*	87.3			LV/LLV
573.3	4.16	96.3	65.0	69.9	LV

573.3	4.24	96.3	65.2	64.1	LV
573.2	4.30	96.3	65.2	59.6	LV
573.1	4.38	96.3	65.4	53.5	LV
573.2	4.49	96.3	65.4	45.9	LV
573.2	4.53	96.3	65.6	43.8	LV
573.2	5.13*	96.3			LV/LLV
573.2	0.298**	100.0			

Table 4.e. 1-methylnaphthalene + water

Temperature (K)	Solubility of water (wt %)	Error
533.3	5.70	15.3%
553.6	7.40	19.1%
573.2	13.60	21.8%

Table 5. Density of 1-methylnaphthalene

Temperature (K)	Experimental density, this work (Kg/m ³)	Uncertainty (Kg/m ³)	Reported density, NIST (Kg/m ³)	Reported Uncertainty (Kg/m ³)
326.5	1000.8	12.9	994.3	1.1
341.9	983.7	12.5	982.7	1.3
370.7	967.2	11.9	961.4	1.9
396.4	949.3	11.4	942.4	2.8
420.9	925.8	10.8	924.2	3.7
447.4	901.7	10.3	903.9	4.9
472.4	874.4	9.4	884.1	6.8
498.2	851.6	8.9	863.0	10.0
522.3	828.3	8.7	841.0	16.0
547.5	811.9	7.8	817.0	25.0
573.8	786.9	7.8	790.0	37.0

Table 6.a. LLV and LV phase equilibrium data for Athabasca bitumen + water mixtures

AB (9.2 wt %) + water /3.77 gr AB + 37.12 gr water						
Temperature (K)	Pressure (MPa)	Total volume (m ³ *10 ⁶)	AB phase volume (m ³ *10 ⁶)	Water phase volume (m ³ *10 ⁶)	Vapor phase volume (m ³ *10 ⁶)	Phases
522.8	3.9	59.1			74.4	LLV
523.0	4.0	59.4			60.7	LLV
523.0	4.0	59.6			46.3	LLV
548.5	6.1	60.8			74.0	LLV
548.4	6.2	61.0			59.9	LLV
548.3	6.2	61.3			49.7	LLV
572.6	8.6	62.3			74.2	LLV
572.5	8.6	63.0			59.2	LLV
572.4	8.7	63.8			48.5	LLV
582.8	9.9	63.3			75.8	LLV
582.8	10.0	63.8			65.4	LLV

582.8	10.1	64.7			58.1	LLV
582.9	10.2	65.0			46.1	LLV
593.0	11.6	64.2	3.8	60.4	71.1	LLV
592.9	11.7	64.9	3.8	61.1	68.0	LLV
592.8	11.9	65.4	3.8	61.5	55.2	LLV
592.8	12.0	66.0	3.9	62.1	49.0	LLV
603.4	13.7	63.2	3.8	59.4	85.7	LLV
603.4	14.1	63.3	3.7	59.6	74.7	LLV
603.4	14.4	64.2	3.8	60.4	64.0	LLV
603.3	14.8	65.4	3.9	61.5	51.0	LLV
613.4	16.4	63.0	3.7	59.3	74.9	LLV
613.5	17.2	63.2	3.9	59.3	61.3	LLV
613.4	17.5	64.0	3.9	60.1	52.9	LLV
623.0	2.4	768.0	3.8	58.5	64.9	LLV
623.2	2.4	738.0	3.8	56.6	62.7	LLV
623.3	2.4	760.0	3.8	56.5	65.9	LLV

Table 6.b. LLV and LV phase equilibrium data for Athabasca bitumen + water mixtures

AB (56.0 wt %) + water /23.2 gr AB +18.26 gr water							
Temperature (K)	Pressure (MPa)	Total volume ($m^3 \cdot 10^6$)	AB phase volume ($m^3 \cdot 10^6$)	Water phase volume ($m^3 \cdot 10^6$)	Vapor phase volume ($m^3 \cdot 10^6$)		Phases
522.9	4.0	40.8			105.4		LLV
522.7	4.1	41.1			90.4		LLV
522.8	4.1	41.3			71.4		LLV
523.0	4.1	41.5			72.2		LLV
523.2	4.1	41.1			59.4		LLV
573.5	8.7	39.8			100.6		LLV
573.2	8.8	39.8			89.2		LLV
573.2	8.8	40.5			72.3		LLV
573.2	8.8	41.0			67.1		LLV
573.2	8.9	41.3			54.7		LLV
582.9	10.3	36.7			104.1		LLV
582.9	10.5	40.0			89.0		LLV
583.0	10.5	40.1			72.8		LLV
583.0	10.6	41.1			56.8		LLV
593.0	11.9	39.3	33.3	5.9	101.5		LLV
593.0	12.0	41.3	33.2	8.1	87.7		LLV
593.0	12.1	42.7	32.8	9.8	70.2		LLV
593.0	12.3	43.0	33.0	10.0	54.9		LLV
603.5	14.1	64.5	33.7	30.8	66.0		LLV
603.4	14.2	65.5	33.7	31.9	60.0		LLV
603.6	14.4	65.7	33.9	31.9	56.9		LLV
603.7	14.6	66.4	33.7	32.7	51.3		LLV
613.5	16.5	62.0	32.3	29.7	84.0		LLV
613.4	16.9	61.3	33.2	28.1	77.3		LLV
613.2	17.1	62.2	34.5	27.6	71.4		LLV

613.1	17.3	63.2	35.4	27.8	66.6	LLV
613.1	17.7	64.4	35.2	29.1	56.5	LLV
613.1	18.0	65.5	35.4	30.2	49.5	LLV
623.3	22.8	39.6	35.7	3.9		LLV

Table 6.c. LLV and LV phase equilibrium data for Athabasca bitumen + water mixtures

AB (66.3 wt %) + water /37.64 gr AB +19.13 gr water							
Temperature (K)	Pressure (MPa)	Total volume (m ³ *10 ⁶)	AB phase volume (m ³ *10 ⁶)	Water phase volume (m ³ *10 ⁶)	Vapor phase volume (m ³ *10 ⁶)		Phases
523.2	4.1	62.0			49.3		LLV
522.7	4.0	62.2			80.7		LLV
547.6	5.6	63.8			80.8		LLV
548.4	5.8	63.8			48.2		LLV
572.9	8.6	64.9			68.8		LLV
573.0	8.6	65.0			57.9		LLV
573.0	8.6	65.2			50.0		LLV
583.0	10.1	65.4			76.4		LLV
583.2	10.2	65.9			64.5		LLV
583.2	10.3	66.0			53.2		LLV
583.2	10.3	66.4			46.5		LLV
593.0	11.9	66.0	51.8	14.2	70.5		LLV
593.1	12.0	66.2	51.8	14.4	64.1		LLV
593.0	12.1	66.2	52.0	14.2	55.7		LLV
592.9	12.2	66.0	51.8	14.2	46.8		LLV
602.9	13.6	69.6	52.8	16.8	73.4		LLV
602.9	13.9	69.1	53.3	15.8	67.2		LLV
602.9	14.0	69.3	53.8	15.4	60.5		LLV
613.0	15.4	68.1	54.0	14.1	77.1		LLV
613.5	15.6	68.1	54.4	13.7	73.1		LLV
613.5	15.8	68.1	54.9	13.2	70.5		LLV
613.5	16.0	67.4	55.2	12.2	63.2		LLV
613.5	16.2	68.1	56.2	11.9	56.2		LLV
613.0	16.6	67.9	54.9	13.0	50.7		LLV
613.0	17.1	67.1	56.2	10.8	50.8		LLV
623.2	19.5	60.8	57.4	3.4	67.6		LLV
623.3	20.0	62.5	57.4	5.1	62.9		LLV
623.3	21.0	63.7	57.4	6.3	53.7		LLV

Table 6.d. LLV and LV phase equilibrium data for Athabasca bitumen + water mixtures

AB (73.3 wt %) + water /39.68 gr AB +14.4 gr water						
Temperature (K)	Pressure (MPa)	Total volume (m ³ *10 ⁶)	AB phase volume (m ³ *10 ⁶)	Water phase volume (m ³ *10 ⁶)	Vapor phase volume (m ³ *10 ⁶)	Phases
522.8	4.0	61.6			67.2	LLV
523.2	4.1	61.6			51.8	LLV
548.1	5.9	62.3			73.1	LLV
548.2	6.0	62.7			58.2	LLV
573.3	8.6	62.8			80.0	LLV
573.4	8.6	63.0			68.2	LLV
573.4	8.7	63.7			56.4	LLV
573.5	8.7	64.0			48.5	LLV
583.4	10.2	68.0			68.9	LLV
583.3	10.3	68.7			56.7	LLV
583.4	10.4	68.5			46.5	LLV
593.1	11.4	69.0	55.9	13.1	80.3	LLV
593.3	11.4	69.4	56.1	13.3	74.8	LLV
593.3	11.7	69.4	56.4	13.0	70.7	LLV
593.2	11.8	69.7	56.2	13.5	57.6	LLV
603.5	13.6	67.8	56.7	11.2	70.6	LLV
603.5	13.9	67.7	56.8	10.8	68.3	LLV
603.5	14.3	68.3	57.2	11.2	52.3	LLV
603.6	14.4	68.9	57.2	11.7	46.7	LLV
613.5	17.1	67.0	59.9	7.1	63.3	LLV
613.5	17.5	67.2	59.9	7.3	55.7	LLV
613.5	17.8	67.3	60.0	7.3	48.1	LLV
623.0	19.2	64.1	58.4	5.8	74.3	LLV
623.2	20.2	64.1	58.4	5.8	64.6	LLV
623.3	20.7	64.3	58.9	5.4	58.6	LLV
633.1	20.2	62.2	60.4	1.9	91.2	LLV
633.7	21.3	62.2	60.4	1.9	85.7	LLV
633.9	21.9	62.4	60.6	1.9	82.1	LLV
634.0	22.8	62.2	60.6	1.7	74.7	LLV
634.1	24.1	62.4	60.9	1.5	64.9	LLV
634.1	25.1	62.6	61.1	1.5	58.5	LLV
634.1	26.0	62.6	61.2	1.4	52.2	LLV
639.0	23.5	62.8	60.7	2.0	76.4	LLV
639.2	24.4	63.6	60.9	2.7	70.1	LLV
639.3	25.2	63.1	61.2	1.9	65.2	LLV
639.4	26.2	63.1	61.4	1.7	59.9	LLV
643.9	23.2	65.0	64.3	0.7	64.3	LLV
644.1	23.9	65.1	64.5	0.7	59.3	LLV
644.1	25.0	65.1	64.5	0.7	51.9	LLV
644.0	25.0	65.5	64.5	1.0	51.3	LLV
644.0	26.2	65.8	64.6	1.2	44.0	LLV

Table 6.e. LLV and LV phase equilibrium data for Athabasca bitumen + water mixtures

AB (78.3 wt %) + water /42.74 gr AB +11.83 gr water						
Temperature (K)	Pressure (MPa)	Total volume (m ³ *10 ⁶)	AB phase volume (m ³ *10 ⁶)	Water phase volume (m ³ *10 ⁶)	Vapor phase volume (m ³ *10 ⁶)	Phases
573.2	8.7	61.5			77.3	LLV
573.2	8.7	61.8			62.1	LLV
573.1	8.8	62.2			52.0	LLV
583.3	10.2	64.0			62.1	LLV
583.3	10.2	64.4			53.1	LLV
583.3	10.3	64.5			45.2	LLV
593.3	12.0	66.1	58.8	7.3	69.7	LLV
593.3	12.0	65.8	58.7	7.1	61.0	LLV
593.4	12.1	66.3	59.0	7.3	51.4	LLV
593.4	12.2	67.3	59.0	8.3	45.0	LLV
604.0	14.5	63.8	61.0	2.7	70.4	LLV
604.0	14.6	64.4	61.2	3.2	63.8	LLV
603.6	14.6	65.1	61.4	3.7	57.0	LLV
603.8	14.8	66.0	61.5	4.4	50.2	LLV
613.5	16.9	62.2	61.3	0.8	82.8	LLV
613.6	17.2	62.2	61.3	0.8	76.6	LLV
613.6	17.4	62.3	62.2	0.2	71.2	LLV
613.6	17.6	62.0	61.5	0.5	67.2	LLV
613.5	17.7	63.0	61.8	1.2	62.2	LLV
613.5	17.9	63.0	62.5	0.5	56.0	LLV
613.5	18.3	63.0	62.2	0.8	48.0	LLV
623.2	16.5	63.0	63.0		86.6	LV
623.3	17.6	64.1	63.7	0.3	80.3	LLV
623.3	18.2	64.1	63.9	0.2	72.2	LLV
623.0	18.5	64.2	63.9	0.3	68.6	LLV
622.8	18.7	64.9	64.1	0.8	66.0	LLV
622.8	19.0	65.2	64.2	1.0	63.3	LLV
622.9	19.5	65.4	64.1	1.4	58.2	LLV
628.1	17.7	63.9	63.9		84.2	LV
628.2	18.5	64.1	63.9	0.2	76.8	LLV
628.2	19.3	64.2	63.9	0.3	69.6	LLV
628.2	19.7	64.4	64.1	0.3	66.3	LLV
628.2	20.1	64.6	64.1	0.5	62.9	LLV
628.2	20.2	64.7	64.2	0.5	61.8	LLV
634.1	18.5	64.7	64.7		82.0	LV
634.0	19.1	64.9	64.9		77.1	LV
633.9	19.6	65.0	64.7	0.3	73.0	LLV
633.9	19.8	65.5	65.2	0.3	70.4	LLV
644.9	19.9	62.8	62.8		78.0	LV

Table 6.f. LLV and LV phase equilibrium data for Athabasca bitumen + water mixtures

AB (87.7 wt %) + water /38.19 gr AB +5.35 gr water						
Temperature (K)	Pressure (MPa)	Total volume (m ³ *10 ⁶)	AB phase volume (m ³ *10 ⁶)	Water phase volume (m ³ *10 ⁶)	Vapor phase volume (m ³ *10 ⁶)	Phases
486.7	2.2	60.4			83.0	LLV
486.8	2.2	60.4			71.5	LLV
486.8	2.2	60.4			60.7	LLV
486.8	2.2	60.4			53.3	LLV
502.4	2.9	60.0			71.4	LLV
502.4	2.9	60.0			61.1	LLV
502.4	2.9	60.2			54.2	LLV
468.1	1.6	64.3			77.9	LLV
468.0	1.6	64.3			63.6	LLV
467.9	1.6	64.3			49.7	LLV
522.9	4.0	60.7			85.3	LLV
522.9	4.1	60.7			72.5	LLV
522.8	4.1	60.9			58.6	LLV
522.8	4.1	61.1			52.8	LLV
553.0	6.5	61.1			66.5	LLV
553.1	6.5	61.6			53.2	LLV
553.3	6.4	60.6			77.8	LLV
573.6	8.6	62.5			72.8	LLV
573.6	8.7	63.0			62.9	LLV
573.6	8.8	63.9			51.4	LLV
583.2	9.9	63.0			76.4	LLV
583.2	10.0	63.4			66.5	LLV
583.2	10.1	63.7			54.1	LLV
583.2	10.1	63.9			47.3	LLV
593.3	11.3	61.6	53.9	7.8	80.5	LLV
593.3	11.6	61.8	54.0	7.8	70.6	LLV
593.3	11.7	62.2	54.0	8.1	58.4	LLV
593.3	11.8	62.3	54.0	8.3	50.1	LLV
603.6	12.7	59.7	59.7		83.9	LV
603.7	13.0	59.9	59.9		78.9	LV
603.7	13.4	61.3	56.0	5.3	71.4	LLV
603.7	13.7	61.6	56.2	5.5	62.3	LLV
603.7	14.0	61.8	56.2	5.6	49.8	LLV
613.7	14.3	57.7	57.7		75.4	LV
613.7	14.9	59.2	57.0	2.1	66.9	LLV
613.6	15.6	59.5	57.4	2.1	59.7	LLV
613.6	16.0	59.5	57.4	2.1	55.4	LLV
613.6	16.1	59.7	57.6	2.1	52.4	LLV
623.4	16.0	59.2	59.2		68.2	LV
623.4	16.5	59.0	59.0		64.4	LV
623.4	17.7	59.0	59.0		54.6	LV
633.6	15.5	59.2	59.2		85.4	LV

633.7	16.1	59.3	59.3	79.5	LV
633.8	17.1	59.3	59.3	71.2	LV
633.9	18.1	59.3	59.3	62.5	LV
633.9	19.8	59.2	59.2	51.9	LV
643.9	18.2	60.2	60.2	67.5	LV
644.0	18.8	60.2	60.2	61.7	LV
644.1	20.4	60.2	60.2	52.8	LV

Table 6.g. LLV and LV phase equilibrium data for Athabasca bitumen + water mixtures

AB (89.7 wt %) + water /38.19 gr AB +4.35 gr water						
Temperature (K)	Pressure (MPa)	Total volume (m ³ *10 ⁶)	AB phase volume (m ³ *10 ⁶)	Water phase volume (m ³ *10 ⁶)	Vapor phase volume (m ³ *10 ⁶)	Phases
523.1	4.0	54.9			74.5	LLV
522.9	4.1	54.9			62.1	LLV
522.9	4.1	55.0			54.0	LLV
548.2	5.9	55.2			85.0	LLV
548.4	6.0	55.4			68.5	LLV
548.3	6.0	56.1			54.5	LLV
573.0	8.9	55.9			69.8	LLV
572.9	8.9	56.6			61.0	LLV
572.9	9.0	56.6			53.0	LLV
583.3	9.9	56.2	53.8	2.4	75.9	LLV
583.2	10.1	56.9	54.2	2.7	59.7	LLV
583.2	10.2	57.6	54.4	3.2	49.8	LLV
593.0	10.9	54.9	54.9	0.0	83.7	LV
593.1	11.5	56.2	54.5	1.7	72.2	LLV
593.1	11.8	56.4	54.5	1.9	67.5	LLV
593.1	12.1	56.6	54.5	2.0	60.7	LLV
593.1	12.2	56.7	54.5	2.2	50.8	LLV
603.3	10.3	55.5	55.5	0.0	90.3	LV
603.3	10.8	55.5	55.5	0.0	83.5	LV
603.4	12.3	55.7	55.5	0.2	63.1	LLV
603.4	13.1	56.1	55.5	0.5	46.9	LLV
603.4	13.3	56.4	55.5	0.8	41.5	LLV
613.6	14.4	56.6	56.6	0.0	52.9	LV
613.5	13.1	56.6	56.6	0.0	66.6	LV
613.5	11.8	56.2	56.2	0.0	86.8	LV
622.9	11.4	56.6	56.6	0.0	89.3	LV
623.1	12.8	56.6	56.6	0.0	72.3	LV
623.2	14.9	56.7	56.7	0.0	52.9	LV
633.7	12.1	56.9	56.9	0.0	87.9	LV
633.6	13.6	57.1	57.1	0.0	70.8	LV
633.35	16.2	57.1	57.1	0.0	50.0	LV
643.9	12.9	58.6	58.6	0.0	83.0	LV
644.1	14.6	58.8	58.8	0.0	67.6	LV
644.2	16.9	58.9	58.9	0.0	50.2	LV

Table 6.h. LLV and LV phase equilibrium data for Athabasca bitumen + water mixtures

AB (96.6 wt %) + water /42.74 gr AB +1.8 gr water						
Temperature (K)	Pressure (MPa)	Total volume (m ³ *10 ⁶)	AB phase volume (m ³ *10 ⁶)	Water phase volume (m ³ *10 ⁶)	Vapor phase volume (m ³ *10 ⁶)	Phases
522.0	3.7	47.7			75.5	LLV
522.1	4.0	48.0			53.7	LLV
548.0	4.5	48.9	48.9		57.8	LV
547.9	3.8	48.9	48.9		94.1	LV
572.9	3.6	49.2	49.2		97.5	LV
572.9	4.5	49.2	49.2		67.3	LV
573.0	5.0	49.4	49.4		54.0	LV
582.7	3.8	52.5	52.5		84.7	LV
582.8	4.2	52.3	52.3		72.4	LV
582.9	4.9	52.6	52.6		54.6	LV
593.2	3.9	53.5	53.5		94.5	LV
593.1	4.4	53.7	53.7		77.7	LV
593.0	4.7	53.9	53.9		67.9	LV
593.0	5.1	54.1	54.1		58.1	LV
593.0	5.4	54.1	54.1		51.6	LV
603.8	4.2	54.4	54.4		90.0	LV
603.8	4.4	54.4	54.4		79.0	LV
603.7	4.7	54.6	54.6		70.9	LV
603.6	5.0	54.4	54.4		62.8	LV
603.6	5.5	54.4	54.4		52.6	LV
623.4	4.3	54.9	54.9		92.8	LV
623.3	4.5	54.9	54.9		86.7	LV
623.3	4.8	55.1	55.1		76.9	LV
623.4	5.1	55.1	55.1		69.0	LV
623.4	5.4	55.1	55.1		61.6	LV
642.8	4.6	56.6	56.6		92.8	LV
642.8	4.9	56.6	56.6		85.1	LV
642.8	5.3	56.4	56.4		77.8	LV
642.9	5.6	56.8	56.8		70.8	LV
642.9	6.0	56.8	56.8		62.4	LV
642.8	6.5	56.6	56.6		54.8	LV

Table 7.a. LLV and LV phase equilibrium data for (Athabasca bitumen + 0.443 toluene)+ water mixtures

[AB + toluene (44.3 wt. %)] + water (43.0 wt.%) /21.99 gr AB + 17.31 gr toluene + 29.68 gr water				
Temperature (K)	Pressure (MPa)	Total liquid volume (m ³ *10 ⁶)	Vapor phase volume (m ³ *10 ⁶)	Phases
493.2	3.0	81.9	33.2	LLV
493.3	3.1	82.1	27.6	LLV
493.2	3.2	82.5	17.3	LLV
513.3	4.4	82.3	44.8	LLV
513.3	4.6	82.3	38.5	LLV

513.2	4.7	83.2	20.7	LLV
553.0	8.3	81.9	49.2	LLV
552.9	8.5	82.3	33.4	LLV
552.9	8.7	83.2	20.1	LLV
563.1	9.9	78.6	52.1	LLV
563.3	10.1	79.4	44.3	LLV
563.3	10.4	80.3	27.3	LLV
563.4	10.5	81.6	18.9	LLV
572.9	11.2	79.9	50.9	LLV
572.9	11.5	81.0	37.0	LLV
572.9	11.8	81.9	24.0	LLV
572.9	11.9	82.8	17.3	LLV

Table 7.b. LLV and LV phase equilibrium data for (Athabasca bitumen + 0.443 toluene)+ water mixtures

[AB + toluene (44.3 wt. %)] + water (35.3 wt.%) / 31.63 gr AB + 25.64 gr toluene + 31.28 gr water				
Temperature (K)	Pressure (MPa)	Total liquid volume (m ³ *10 ⁶)	Vapor phase volume (m ³ *10 ⁶)	Phases
493.2	2.9	105.1	31.8	LLV
493.2	3.1	104.5	18.1	LLV
513.1	4.8	106.5	20.3	LLV
513.1	4.8	106.3	12.5	LLV
533.1	6.2	107.4	25.3	LLV
533.2	6.3	107.4	20.1	LLV
533.1	6.5	107.4	11.4	LLV
553.3	8.4	109.6	24.9	LLV
553.3	8.6	110.0	19.9	LLV
553.2	8.8	110.0	14.5	LLV
563.7	9.8	110.6	21.0	LLV
563.8	10.0	110.9	17.3	LLV
563.8	10.2	111.1	11.2	LLV
573.5	11.9	107.4	26.8	LLV
573.4	12.0	108.2	18.7	LLV
573.4	12.0	111.3	6.6	LLV

Table 7.c. LLV and LV phase equilibrium data for (Athabasca bitumen + 0.443 toluene)+ water mixtures

[AB + toluene (44.3 wt. %)] + water (9.8 wt.%) / 30.59 gr AB + 24.27 gr toluene + 5.93 gr water				
Temperature (K)	Pressure (MPa)	Total liquid volume (m ³ *10 ⁶)	Vapor phase volume (m ³ *10 ⁶)	Phases
493.1	3.1	72.9	63.0	LLV
493.1	3.3	73.7	34.1	LLV
493.2	3.3	74.2	20.3	LLV
513.1	4.6	72.6	60.7	LLV
513.2	4.7	73.5	36.9	LLV
513.1	4.8	74.6	17.6	LLV
532.9	6.4	71.8	56.4	LLV
533.0	6.6	72.8	38.7	LLV

533.0	6.7	74.2	17.0	LLV
553.0	7.3	71.5	61.0	LLV
553.1	7.9	71.8	47.2	LLV
553.1	8.8	72.2	24.0	LLV
573.4	8.5	72.8	52.3	LLV
573.5	9.1	72.8	41.9	LLV
573.6	10.0	72.6	25.4	LLV

Table 7.d. LLV and LV phase equilibrium data for (Athabasca bitumen + 0.443 toluene)+ water mixtures

[AB + toluene (44.3 wt. %)] + water (7.1 wt.%) / 30.05 gr AB + 23.68 gr toluene + 4.13 gr water				
Temperature (K)	Pressure (MPa)	Total liquid volume (m ³ *10 ⁶)	Vapor phase volume (m ³ *10 ⁶)	Phases
493.0	2.8	69.5	60.9	LLV
493.0	3.0	69.7	46.4	LLV
493.0	3.2	70.2	24.3	LLV
513.1	4.2	68.8	67.3	LLV
513.1	4.6	69.7	41.3	LLV
513.2	4.8	70.8	21.4	LLV
533.0	5.2	69.0	56.7	LLV
533.2	5.7	69.3	41.7	LLV
533.3	6.0	70.1	25.7	LLV
553.2	6.3	67.7	61.4	LLV
553.3	6.9	68.0	42.3	LLV
553.3	7.4	68.4	28.7	LLV
573.4	7.1	69.7	46.4	LLV
573.4	7.5	69.9	38.1	LLV
573.5	8.1	70.2	25.1	LLV

Table 7.e. LLV and LV phase equilibrium data for (Athabasca bitumen + 0.443 toluene)+ water mixtures

[AB + toluene (44.3 wt. %)] + water (3.4 wt.%) / 30.53 gr AB + 22.79 gr toluene + 1.91 gr water				
Temperature (K)	Pressure (MPa)	Total liquid volume (m ³ *10 ⁶)	Vapor phase volume (m ³ *10 ⁶)	Phases
493.1	3.2	67.9	53.6	LLV
493.1	3.3	68.0	40.4	LLV
493.2	3.4	68.6	17.7	LLV
513.1	3.4	67.1	59.4	LLV
513.1	3.6	68.0	35.7	LLV
513.2	3.9	69.1	17.6	LLV
533.2	2.8	67.1	50.0	LLV
533.2	3.2	67.5	36.3	LLV
533.3	3.5	68.2	17.8	LLV
553.2	3.4	65.5	54.8	LLV
553.2	3.9	65.8	37.4	LLV
553.3	4.3	66.2	18.1	LLV
573.3	4.2	67.5	40.9	LLV
573.3	4.6	67.7	33.3	LLV

573.4 5.1 68.0 17.8 LLV

Table 8.a. LLV and LV phase equilibrium data for (Athabasca bitumen + 0.668 toluene)+ water mixtures

[AB + toluene (66.8 wt. %)] + water (47.3 wt.%) / 11.10 gr AB + 22.25 gr toluene + 29.98 gr water				
Temperature (K)	Pressure (MPa)	Total liquid volume (m ³ *10 ⁶)	Vapor phase volume (m ³ *10 ⁶)	Phases
492.6	3.4	74.8	47.1	LLV
492.7	3.5	75.7	29.8	LLV
492.5	3.5	75.9	19.0	LLV
512.7	4.8	75.7	48.6	LLV
512.8	4.9	76.5	31.1	LLV
512.8	5.0	77.2	16.4	LLV
532.9	6.3	77.2	28.1	LLV
532.9	6.4	78.3	17.2	LLV
553.1	8.6	72.4	60.3	LLV
553.2	9.1	72.4	44.1	LLV
553.3	9.5	73.0	20.7	LLV
563.0	10.2	69.9	57.4	LLV
563.2	10.6	70.8	42.7	LLV
563.3	10.9	71.9	20.6	LLV
573.5	10.9	67.3	67.8	LLV
573.5	11.4	67.3	46.9	LLV
573.7	11.9	67.7	23.0	LLV

Table 8.b. LLV and LV phase equilibrium data for (Athabasca bitumen + 0.668 toluene)+ water mixtures

[AB + toluene (66.8 wt. %)] + water (25.4 wt.%) / 11.31 gr AB + 22.95 gr toluene + 11.70 gr water				
Temperature (K)	Pressure (MPa)	Total liquid volume (m ³ *10 ⁶)	Vapor phase volume (m ³ *10 ⁶)	Phases
492.8	3.1	53.9	80.2	LLV
492.8	3.2	54.3	72.6	LLV
492.9	3.3	55.2	48.0	LLV
493.0	3.3	56.3	24.3	LLV
512.8	4.5	53.4	78.0	LLV
512.8	4.6	54.3	63.6	LLV
512.8	4.8	55.8	36.2	LLV
512.8	4.8	56.1	24.4	LLV
512.7	4.4	54.3	68.7	LLV
532.6	6.2	52.1	71.6	LLV
532.6	6.3	54.8	42.9	LLV
532.5	6.4	56.3	24.2	LLV
553.2	9.6	49.3	74.9	LLV
553.3	9.7	49.2	56.0	LLV
553.3	9.7	52.8	29.9	LLV
573.1	10.9	42.7	74.2	LLV
573.1	11.2	42.7	65.4	LLV
573.3	11.7	44.9	40.5	LLV

573.3 11.7 49.9 26.5 LLV

Table 8.c. LLV and LV phase equilibrium data for (Athabasca bitumen + 0. 668 toluene)+ water mixtures

[AB + toluene (66.8 wt. %)] + water (17.4 wt.%) / 11.42 gr AB + 22.99 gr toluene + 7.26 gr water				
Temperature (K)	Pressure (MPa)	Total liquid volume (m ³ *10 ⁶)	Vapor phase volume (m ³ *10 ⁶)	Phases
492.6	3.1	48.1	78.6	LLV
492.6	3.3	49.5	41.7	LLV
492.6	3.3	50.4	28.1	LLV
512.9	4.3	47.3	76.4	LLV
512.9	4.5	47.9	66.2	LLV
512.9	4.7	48.8	42.6	LLV
512.9	4.9	50.4	23.5	LLV
532.5	6.5	41.5	90.6	LLV
532.5	6.6	44.9	69.3	LLV
532.5	6.6	48.6	36.7	LLV
532.6	6.7	49.9	24.0	LLV
553.4	8.1	39.6	94.2	LLV
553.3	8.5	39.8	80.7	LLV
553.3	8.8	40.2	68.0	LLV
553.3	9.1	41.8	50.4	LLV
553.4	9.4	45.7	24.9	LLV
563.5	9.0	37.4	97.9	LLV
563.2	9.3	38.0	84.1	LLV
563.3	9.7	38.3	68.8	LLV
563.3	10.1	39.1	52.8	LLV
563.4	10.4	39.6	37.9	LLV
563.5	10.6	40.0	27.7	LLV
573.2	10.1	37.8	78.3	LLV
573.4	10.4	38.0	69.1	LLV
573.5	10.6	38.3	61.3	LLV
573.5	11.2	38.5	46.0	LLV
573.5	11.5	38.9	35.0	LLV
573.5	11.7	39.6	27.8	LLV

Table 8.d. LLV and LV phase equilibrium data for (Athabasca bitumen + 0. 668 toluene)+ water mixtures

[AB + toluene (66.8 wt. %)] + water (5.5 wt.%) / 11.37 gr AB + 22.93 gr toluene + 1.99 gr water				
Temperature (K)	Pressure (MPa)	Total liquid volume (m ³ *10 ⁶)	Vapor phase volume (m ³ *10 ⁶)	Phases
492.7	3.2	48.1	78.6	LLV
492.7	3.3	49.5	32.8	LLV
492.7	3.4	50.4	25.4	LLV
512.8	4.1	49.0	71.5	LLV
512.8	4.2	50.4	60.7	LLV
512.8	4.4	51.4	37.9	LLV
512.8	4.5	51.2	22.6	LLV

532.8	3.2	50.3	78.4	LLV
532.8	3.6	51.7	58.2	LLV
532.8	4.1	52.6	36.1	LLV
532.8	4.5	52.5	22.3	LLV
553.3	3.2	50.3	70.3	LLV
553.3	3.7	51.7	56.4	LLV
553.3	4.3	52.6	39.6	LLV
553.4	5.0	52.5	21.9	LLV
563.2	3.2	50.3	73.1	LLV
563.3	3.8	51.7	54.9	LLV
563.3	4.4	52.6	41.8	LLV
563.3	5.0	52.5	30.0	LLV
563.4	5.2	53.4	22.3	LLV
573.2	3.9	50.3	86.6	LLV
573.2	4.3	51.7	72.5	LLV
573.2	4.8	52.6	53.4	LLV
573.3	5.3	52.5	37.7	LLV
573.3	5.6	53.4	25.1	LLV

Appendix 3. Image processing code in MATLAB

A sample image processing code using MATLAB image processing software is presented. The code may change with respect to the desired parameters of the images. The code is developed to detect liquid-liquid boundary, bellows position and average intensities of designated areas.

```
clc
clear all,
close all
hold on

Address='C:\Users\Farshad\Desktop\Zipped files\01 Copy May 9
2011\01 Copy May 9 2011\Nov 11 - Water 37wt%+ Bitumen
67wt%\1.1 247.8C.tif'

image001 = double(imread(Address));

imagesize=size(image001);
for i=1:imagesize(1)
    if i/2~=ceil(i/2)
        image((i/2+0.5),:)=image001(i,:);
    end
    %     if i/2==ceil(i/2)
    %         image((i/2),:)=image001(i,:);
    %     end
end
imagesize=size(image);
imageaverage = zeros(1,imagesize(2));

figure(1);
pcolor(image);
shading interp
colormap jet

%%%%%%%%%%%%%%%%%%%%%%%%%%%%%%%%%%%%%%%%%%%%%%%%%%%%%%%%%%%%%%%%%%%%%%%%
%%%%%%%%
% Beryllium insert average
% Swap horizontally from YBe1 to YBe2 along XBe1 to Xbe2
%%%%%%%%%%%%%%%%%%%%%%%%%%%%%%%%%%%%%%%%%%%%%%%%%%%%%%%%%%%%%%%%%%%%%%%%
%%%%%%%%
```

```

%%%                               Red Top
                                XBe2=202;
                                YBe2=78;
                                %-----%
                                %   Be1           %
                                %           Be1     %
                                %-----%
XBe1=64;
  YBe1=64;

hold on
rectangle('Position',[XBe1,YBe1,XBe2-XBe1,YBe2-
YBe1],'EdgeColor','r')

for x = XBe1:XBe2
    counter = 0; sum=0;
    for y = YBe1 : YBe2
        % swap horizontally
        if image(y,x)==0
            a=1;
        else
            sum = sum + image(y,x);
            counter=counter+1;
        end
    end
    IBemeanC(1,x+ XBe1+1) = sum/counter;
end
BemeanC0=mean(IBemeanC);
%%%%%%%%%%%%%%%%%%%%%%%%%%%%%%%%%%%%%%%%%%%%%%%%%%%%%%%%%%%%%%%%%%%%%%%%
%%%%%%%%%%%%%%%%%%%%%%%%%%%%%%%%%%%%%%%%%%%%%%%%%%%%%%%%%%%%%%%%%%%%%%%%
% Beryllium insert down average
% Swap horizontally from YBe1 to YBe2 along XBe1 to Xbe2
%%%%%%%%%%%%%%%%%%%%%%%%%%%%%%%%%%%%%%%%%%%%%%%%%%%%%%%%%%%%%%%%%%%%%%%%
%%%%%%%%%%%%%%%%%%%%%%%%%%%%%%%%%%%%%%%%%%%%%%%%%%%%%%%%%%%%%%%%%%%%%%%%

% %%%                               Red Down
                                XBed2=200;
                                YBed2=20;
                                %-----%
                                %   Be2           %
                                %           Be2     %
                                %-----%
XBed1=56;
  YBed1=6;

```



```

hold on
rectangle('Position',[XBed1,YBed1,XBed2-XBed1,YBed2-
YBed1],'EdgeColor','r')

for x = XBed1:XBed2
    counter = 0; sum=0;
    for y = YBed1 : YBed2
        % swap horizontally
        if image(y,x)==0
            a=1;
        else
            sum = sum + image(y,x);
            counter=counter+1;
        end
    end
    IBemeanCd(1,x- XBed1+1) = sum/counter;
end
BemeanCd0=mean(IBemeanCd);
%%%%%%%%%%%%%%%%%%%%%%%%%%%%%%%%%%%%%%%%%%%%%%%%%%%%%%%%%%%%%%%%%%%%%%%%
%%%%%%%%%%%%%%%%%%%%%%%%%%%%%%%%%%%%%%%%%%%%%%%%%%%%%%%%%%%%%%%%%%%%%%%%
% Phase detection (Edge)average
% Swap horizontally from YE1 to YE2 along XE1 to XE2
%%%%%%%%%%%%%%%%%%%%%%%%%%%%%%%%%%%%%%%%%%%%%%%%%%%%%%%%%%%%%%%%%%%%%%%%
%%%%%%%%%%%%%%%%%%%%%%%%%%%%%%%%%%%%%%%%%%%%%%%%%%%%%%%%%%%%%%%%%%%%%%%%

%%%           Green Box
                                XE2=imagesize(2);
                                YE2=117;

%-----%
%   Edge   %
%           Edge %
%-----%

XE1=1;
YE1=3 ;

hold on
rectangle('Position',[XE1,YE1,XE2-XE1,YE2-YE1],'EdgeColor',
'g')
title('string')
%pause

for x = XE1:XE2 % swap vertically 765
    counter = 0; sum=0;
    for y = YE1 :YE2%170
        % 260 to 290 for bolt_vol_calib

```

```

        % swap horizontally
        if image(y,x)==0
            a=1;
        else
            sum = sum + image(y,x);
            counter=counter+1;
        end
    end
    imageaverage(1,x- XE1+1) = sum/counter;
end

for i=XE1+1:XE2-1
    dimage(i)=(imageaverage(1,i+1)-imageaverage(1,i-1))/2;
end;

%%%%%%%%%%%%%%%%%%%%%%%%%%%%%%%%%%%%%%%%%%%%%%%%%%%%%%%%%%%%%%%%%%%%%%%%
%%%%%%%%
figure(2);
hold on
subplot(3,1,1),
plot(imageaverage,'black')
%axis([0 750 0 10])
subplot(3,1,3),
plot(dimage,'black')
%axis([0 750 -1 1])
subplot(3,1,2),
image001=image(YE1:YE2,XE1:XE2);
pcolor(image001);
shading interp
colormap gray

figure(3);
image=image.^2;
pcolor(image);
shading interp
colormap gray

```